An Investigation of Motions of Catamarans in Regular Waves

by

Chih-Chung Fang, B.Sc., M.Sc.

Submitted as a Thesis for the Degree of Doctor of Philosophy,

Department of Naval Architecture and Ocean Engineering, University of Glasgow.

March 1996

DECLARATION

Except where reference is made to the work of others, this thesis is believe to be original.

DEDICATION

To my parents and dear Bob Christison.

ACKNOWLEDGEMENTS

The author would like to express his sincere gratitude to all those people who have contributed to this research work. The following are acknowledged :

Professor D. Faulkner, Former Head of Department, for his help in making this research possible, especially with regard to obtaining financial support through the Overseas Research Student Awards scheme and a Postgraduate Scholarship from the University of Glasgow.

Professor N. Barltrop, Head of Department, for his kind encouragement at the final research stage.

Professor A. Incecik, Lloyd's Register Chair of Offshore Engineering, University of Newcastle, for his supervision, valuable advice and enthusiastic encouragement throughout this research.

Dr. H.S. Chan, for his excellent private discussions and the provision of the two-dimensional frequency domain motion program used in this work. The discussions which they had are instrumental to the success of this research work.

Mr. B. Reilly, for constructing the excellent experimental measurement system and warm friendship. Mr. D. Percival, for his helpful assistance to overcome several numerical difficulties during the experimental analyses. Mr. D.J. Sinclair, Mr. F. Sweeney, Mr. D. Nicolson and Mr. G. Dunning, for making the tank testing facilities available and their continuous help during the experiments.

Special thanks go to Mr. R.B. Christison, the late Chief Technician, who had served over 50 years at the University of Glasgow and was involved in setting up the Hydrodynamics Laboratory in the early sixties. His strong and kindly supports for foreign students are greatly appreciated. Through his inspiration, the author has been impressed by the characteristics of Scottish culture.

Finally the author would like to thank his parents for their continuous encouragement and support.

NOMENCLATURE

Symbols not included in the list below are only used at a specific place and are explained where they occur.

A_s	Area of cylinder section.
A_w	Area of waterplane.
A_y	First moment of waterplane area about y-axis.
A_{jk}	Hydrodynamic added mass in the j-th direction due to the k-th mode of motion; expressed in the system o-xyz.
B	Width of Towing Tank.
B_s	Breadth of a section at the waterline.
$B_w(x,t)$	Beam of each demi-hull at instantaneous draught.
B_{jk}	Hydrodynamic damping coefficient in the j-th direction due to the k-th mode of motion; expressed in the system o-xyz.
C_{jk}	Hydrostatic restoring coefficient in the j-th direction due to the k-th mode of motion; expressed in the system o-xyz.
F_{imp}	Hydrodynamic impulsive force.
F_j^{δ}	Hydrostatic restoring force in j-th direction.
F_j^{R}	Hydrodynamic reactive force in j-th direction.
F_j^{w}	Wave exciting force in j-th direction.
$\bar{F}_j^{D}$	Complex amplitude of diffraction force in j-th direction.
$\bar{F}_j^{K}$	Complex amplitude of Froude-Krylov force in j-th direction.
$\bar{F}_j^{w}$	Complex amplitude of wave exciting force in j-th direction.
$\lvert F_j \rvert$	Amplitude of wave exciting force in j-th direction.
$\lvert F'_j \rvert$	Non-dimensional wave exciting force in j-th direction.
F_n	Froude number $F_n = U/\sqrt{gL}$
$G(p;q)$	Green function.
GM_L	Longitudinal metacentric height.
GM_T	Transverse metacentric height.
$H(t)$	Unit step function.
I	Fluid domain interior of the body.
I_{jj}	Moment of inertia about the origin.
Im	Imaginary part of a complex quantity.
K	Encounter wave number.
L	Length between perpendiculars of the catamaran.

L_m	Maximum distance from y-axis.
LCG	Longitudinal distance of the centre of gravity.
M_{ij}	Element of mass matrix.
P	Fluid pressure.
PV	Principal-value of a integral.
R	Fluid domain exterior of the body.
$R(t)$	Ramp function.
Re	Real part of a complex quantity.
$S_B(\vec{x}',t)$	Wetted body surface in unsteady flow.
S_I	Undisturbed free surface interior of the body.
S_F	Undisturbed free surface exterior of the body.
$\overline{S}_B$	Wetted body surface in steady flow (mean wetted body surface).
S_∞	Control boundary surface at far-field.
T	Maximum time interval of simulation.
T_e	Encounter wave period.
U	Mean forward speed of the body.
$\vec{V}(\vec{x}_0,t)$	Velocity field of total fluid flow.
$\vec{V}_s(\vec{x},t)$	Local velocity of a point on the surface $S_B(\vec{x}',t)$.
$\vec{W}(\vec{x})$	Velocity field of steady flow.
a	Radius of a circular cylinder.
a_{jk}	Non-dimensional hydrodynamic coefficient of the added mass term in the j-th force equation due to motion in the k-th mode; expressed in the system o-xyz.
$\bar{a}_{jk}$	Sectional hydrodynamic coefficient of the added mass term in the j-th force equation due to motion in the k-th mode; expressed in the system o-xyz.
$\bar{a}_{fs}$	Free surface induced acceleration.
$\bar{a}_s$	Body acceleration at the body-fixed coordinate o-x'y'z'.
b_{jk}	Non-dimensional hydrodynamic coefficient of the damping term in the j-th force equation due to motion in the k-th mode; expressed in the system o-xyz.
$\bar{b}_{jk}$	Sectional hydrodynamic coefficient of the damping term in the j-th force equation due to motion in the k-th mode; expressed in the system o-xyz.
$d(x,t)$	Sectional instantaneous draught.
d_r	Hull separation between two bodies.
g	Gravitational constant.

h	Water depth.
	Distance from centre point of cylinder to the mean free surface.
i	$\sqrt{(-1)}$
k	Wave number.
k_n	Discrete wave number.
l	Minimum characteristic length.
$\bar{n}(n_1, n_2, n_3)$	Normal vector outward the boundary surface.
$o-x_0y_0z_0$	Space-fixed coordinate system.
$o-xyz$	Steady translating coordinate system.
$o-x'y'z'$	Body-fixed coordinate system.
p	Coordinates of a field point in the system o-xyz.
p_{BD}	Body induced pressure.
p_{fs}	Free surface induced pressure.
q	Coordinates of a source point in the system o-xyz.
$\bar{q}$	Coordinates of mirror image of the source with respect to the plane z=0 in the system o-xyz.
r	Horizontal radial distance away from the body.
$\vec{r}'(\vec{x}')$	Position vector of a fluid particle on the surface $S_B(\vec{x}', t)$.
t	A time variable.
$\vec{x}(x, y, z)$	Coordinates of a field point.
z_b	Vertical coordinate of the centre of buoyancy.
z_G	Vertical coordinate of the centre of gravity.
$\vec{\alpha}(\vec{x}, t)$	Local oscillatory displacement vector.
$\dot{\vec{\alpha}}(\vec{x}, t)$	Local velocity of a point on the surface $S_B(\vec{x}', t)$.
β	Angle of incident wave with x-axis (180^0 at head sea).
$\delta(t)$	Dirac delta function.
Φ	Total velocity potential of the flow field.
$\overline{\Phi}$	Velocity potential of steady flow.
$\tilde{\Phi}$	Velocity potential of unsteady flow.
$\overline{\phi}$	Steady perturbation potential.
$\phi_j^I; \phi_B^I$	Velocity potential inside the domain I.
$\phi_j^R; \phi_B^R$	Velocity potential of fluid flow in the fluid domain R.
ϕ_0	Incident wave potential per unit amplitude.
ϕ_B	Body potential.
ϕ_{fs}	Wave potential.
ϕ_j	Radiation wave potential per unit amplitude.
ϕ_7	Diffraction wave potential per unit amplitude.
μ	Dipole strength.

ρ	Density of fluid.
σ	Source strength.
ω	Wave encounter frequency.
ω_n	Discrete wave frequency.
ω_0	Incident wave frequency.
ω_r	Characteristic frequency.
$\xi_j(t)$	Motion response in j-th mode of motion.
$\bar{\xi}_j$	Complex amplitude response in j-th mode of motion.
$\lvert\xi_j\rvert$	Motion amplitude response in j-th mode of motion.
ζ	Exact free surface elevation.
ζ_0	Incident wave amplitude.
∇	Grad operator.
	Volume displacement of a catamaran.
∇^2	Laplace's operator.

CONTENTS

LIST OF FIGURES

LIST OF TABLES

SUMMARY

The aim of this research is to develop computational tools to predict the large amplitude motions of catamaran travelling with forward speed in waves. In this thesis, the results of theoretical and experimental investigations to predict the motions of catamarans in regular waves are presented. The motion problem of a catamaran trãvelling in waves has been formulated with the assumptions that the flow field is a potential flow. The solution of governing equations is determined by a set of initial-boundary conditions. In order to solve the motion problem, the exact boundary conditions have been simplified through linearisation by using the perturbation expansion technique. If the motion is steady and sinusoidal in time, the initial value problem can be precipitated out. Then, the initial-boundary value problem can be simplified to the boundary value problem.

Solutions of small amplitude motion problem of catamarans have been obtained by solving the two-dimensional Green function integral equations over the mean wetted body surface in the frequency domain. Numerical computations for three catamarans (ASR5061, Marintek and V-1 catamarans) travelling in the oblique waves have been carried out to compare with experimental measurements. For the low forward speed case, good comparisons between the calculated and experimental results have been obtained. When the forward speed increases, the linear frequency domain technique gives a gross overprediction of the motion responses for the heave and pitch modes at the resonance frequencies and the calculated resonance frequency is slightly higher than the experimental measurement. Generally better predictions are obtained in heave motions than in pitch motions.

By extending the linear frequency domain theory, a quasi-nonlinear time domain technique has been developed to investigate the large amplitude motions of the catamarans in regular waves. The nonlinearity of hydrodynamic forces included in this practical method comes from the variations of ship's submerged portion. These forces are obtained from a database generated by the linear frequency domain method at each time step. The coupled equations, heave and pitch, have been solved in the time domain by using the Runge-Kutta method with proper initial values. In order to investigate the nonlinear effects of large amplitude motions of the V-1 catamaran in the head sea condition, numerical results obtained from the linear and nonlinear strip methods have been compared with those obtained from a series of experiments carried out in the Towing Tank of the Hydrodynamics Laboratory at the University of

Glasgow. Based on the comparative studies, the numerical results obtained from the time domain program can provide better predictions for the large amplitude motions of catamarans than the linear frequency domain method. It is concluded that the nonlinear effects are significant when the model speeds and wave amplitudes increase. The peak values of large amplitude motions around the resonance frequencies as obtained from the nonlinear time domain predictions as well as from measurements are smaller than those obtained from the linear theory.

In order to solve the finite-amplitude initial value problem, the two-dimensional transient motion is treated as a series of impulse problems by satisfying the exact body boundary condition and the linearised free surface condition. The solution has been constructed by means of a spectral representation for the wave field and a distribution of simple sources on the instantaneous wetted body surface. Preliminary results for the linear radiation problems on a submerged circular cylinder in deep water and a floating rectangle have been carried out by using the linear and nonlinear time domain techniques. Excellent agreement between the calculated hydrodynamic coefficients and the analytical solutions given by Ogilvie (1963) has been found for the submerged circular cylinder in deep water. For the floating rectangle, the calculated damping coefficients are slightly higher than those obtained from the published experimental measurements by Vugts (1968).

CHAPTER 1
INTRODUCTION

Catamarans are the most accepted form of high speed crafts for passenger / vehicle transportation. Compared with other high speed crafts, they possess good transport efficiency at moderately high speeds. The more useable and rectangular shape of deck area is one of the desirable characteristics of catamarans and gives a good stability quality and consequently a small rate and angle of roll. However, if the relative motion between the wave and ship becomes large, the catamaran is vulnerable to wave impacts on the bottom of the cross-deck in severe sea conditions. It may cause speed reductions, local structural damage and transient hull vibrations. Thus, for optimal seakeeping performance of catamarans, the vertical motions should be minimised to avoid the hydrodynamic impacts on the cross-deck bottom. The first step to be taken is to investigate the seakeeping characteristics of catamarans and to develop proper design tools for naval architects.

The basic theory of motions of a ship in waves was first established by Froude (1861) and subsequently by Krylov (1896). Assuming the incident waves are not disturbed by the existence of body, the wave forces acting on the submerged body due to incident waves are named as the Froude-Krylov forces. Based on the assumptions of high characteristic frequency, Lewis (1929) introduced the added mass terms into the Froude-Krylov approach without considering the free surface effects. Haskind (1946) solved the velocity potential due to the ship motion by using the Green's identities and derived the necessary Green function. Moreover, the linearised problem was first separated into the diffraction and radiation problems and the resulting integral equation was solved by using a thin ship approximation. In order to solve the two-dimensional problems for free floating bodies without forward speed, Ursell (1949) first developed a multipole method to present the radiation potential for a heaving circular cylinder. A source distribution method was published by Frank (1967). The submerged ship shape is divided into a series of straight-line segments and the two-dimensional Green function is applied to represent the unknown velocity potential of unit strength. Then, the source strength will be determined by a set of boundary conditions.

The initial efforts on the hydrodynamic problems associated with catamarans were primarily devoted to minimise the resistance in the calm water. (e.g. Michel, 1961; Everest, 1968; Oving, 1985; Insel and Molland, 1991). Until the early 1970's, some fundamental studies to predict the hydrodynamic forces acting on twin-hull floating bodies were carried out by Ohkusu (1969), Wang & Wahab (1971) and Lee et al.

(1971). Since then, there has been a significant growth of interest in the concept of multi-hull ships. A series of systematic theoretical and experimental investigations of motions and sea loads of catamarans was carried out at the Naval Ship Research and Development Centre. An extensive experimental programme with ASR(submarine rescue ship) catamaran model was conducted by Wahab et al. (1971) to investigate the behaviour of the ASR model in a seaway. The full and model scale experimental programme conducted with *Hayes* catamaran were presented by Hadler et al. (1974). Lee et al. (1973) studied the twin-hull motion problems by using the strip method which was the extension of the approach developed by Salvesen et al. (1970). Based upon Chapman's (1975) high speed theory which was proposed to formulate a vertical surface-piercing plate motions in unsteady yaw and sway, Faltinsen et al. (1992) and Ohkusu & Wen (1995) reported a kind of pseudo three-dimensional theory to evaluate the motion responses of a catamaran at high Froude number. The three-dimensional translating and oscillating source technique was applied by Chan (1993) and Hudson et al. (1995) to predict the seakeeping performance of multi-hull ships. Kring & Sclavounos (1991) reported a three-dimensional Rankine panel method to investigate the wave patterns and motions for multi-hull ships travelling with forward speed through head seas. Most of these investigations are limited to the linear motions of catamarans in small amplitude waves. A limited amount of research and development efforts have been devoted to the field of large amplitude motion problem of twin-hull ships. A quasi-nonlinear time domain approach by using the hydrodynamic coefficients generated from the strip method was used by Arthur (1988) and Fang & Her (1995) to simulate the nonlinear motions of SWATH ships.

The aim of present research is to develop computational tools to investigate the motions of catamarans travelling in waves. Firstly, the small amplitude motions of a catamaran configuration in oblique waves have been predicted by the linear frequency domain program based on the two-dimensional Green function method. Then, a quasi-nonlinear time domain technique extending the strip method has been used to simulate the large amplitude motions of a catamaran in regular head waves with various wave amplitudes and forward speeds. A set of experiments has been designed and carried out by using a scale model of a catamaran to validate the computational tools and to understand the nonlinear behaviour of a catamaran travelling in large amplitude waves. Finally, some fundamental studies on the two-dimensional transient theory have been developed for solving the "body-exact" problem where the body boundary conditions are satisfied on the instantaneous wetted surface of the body whilst the linearised free surface boundary conditions are maintained. All these investigations are detailed in the following Chapters of this thesis as summarised below.

Chapter 2 presents the problem formulation of motions of a marine vehicle travelling in waves. Three different coordinate systems have been introduced to describe the flow field and motions of the twin-hull ship. The flow field is assumed as a potential flow. Therefore, the Laplace's equation can be set up to represent the flow field and the solution is determined by a set of initial-boundary conditions. The exact boundary conditions lead to a nonlinear problem which is very difficult to solve in analytical or numerical calculations. In order to solve the motion problem, the theoretical formulation is simplified through linearisation by using the perturbation expansion technique. The linearised free surface and body conditions require the assumption that the disturbance on the free surface due to the steady forward motion is small and can be neglected. In the steady-state oscillating motions, the initial-boundary value problem can be simplified to the boundary value problem.

In Chapter 3, a two-dimensional pulsating source potential technique has been stated to solve the unsteady velocity potential due to the incident, diffracted and radiated wave systems. Based on assumptions of the slender body and high-frequency oscillation motions, the two-dimensional frequency domain method is used to predict the small amplitude motions of catamarans in oblique waves. Numerical computations have been carried out to predict the linear motion responses of ASR5061, Marintek and V-1 catamarans travelling in waves and validated with experimental measurements. Results of these comparisons are discussed. For a twin-hull floating bodies, the negative added mass in the vertical plane motions and a set of discrete characteristic frequencies have been observed during the numerical investigation.

In Chapter 4, a practical method has been developed for predicting nonlinear ship responses in regular waves by extending the strip method. The nonlinearity of hydrodynamic forces included in this method comes from the time-varying ship's submerged portion. The sectional hydrodynamic forces are retrieved from a database generated by the linear frequency domain technique at each time step, and then integrated in the longitudinal direction of ship's hull to obtain the total hydrodynamic forces and moments acting on the ship. Due to the large variation of hydrodynamic forces in the shallow draught region, the linear interpolation method has been selected to calculate the time-varying hydrodynamic coefficients and wave exciting forces. The coupled equations, heave and pitch, are solved in the time domain by using the adaptive stepsize Runge-Kutta method with proper initial values. Validation of mathematical model has been carried out by comparing numerical results obtained from the linear frequency domain method and nonlinear time domain technique with the V-1 catamaran travelling in the head sea conditions. Time domain simulations have

been used to trace the nonlinear motion responses of V-1 catamaran with various wave amplitudes and forward speeds. Some parametric studies have been carried out to investigate the nonlinearity of large amplitude motions of the V-1 catamaran in waves.

In Chapter 5, the tests carried out with the V-1 catamaran model at the Hydrodynamics Laboratory of the University of Glasgow are presented to evaluate the nonlinear effects due to large amplitude motions of catamarans travelling in waves. These tests cover different speeds and wave heights at a wide range of wave frequencies. A measurement rig has been designed and tested to investigate the large amplitude motions of a fast craft. Results obtained from calm water tests have been compared with previous work (Incecik et al., 1991). Numerical computations for predicting the motion responses of V-1 catamaran in the head sea conditions have been obtained from the linear frequency domain and nonlinear time domain techniques which have been described in Chapters 3 and 4. Comparisons between these calculated results and the experimental measurements with three forward speeds and three wave amplitudes are presented to investigate the nonlinear motions of the V-1 catamaran travelling in regular waves. The impact phenomena of large amplitude motions have been observed from a set of consecutive photographs of the test model.

Chapter 6 presents a theoretical formulation of the transient motion problem in the time domain. Based on the assumptions of slender body and small wave slopes in the longitudinal direction, the three-dimensional boundary value problem is approximated by a set of two-dimensional initial value problems. The two-dimensional transient motion has been treated as a series of impulse problems by satisfying the exact body boundary condition and the linearised free surface condition. A spectral method which was first proposed by Chapman (1979) has been used to solve the finite-amplitude initial value problem. In the case of a linear motion problem, the hydrodynamic forces obtained in the time domain can be related to the hydrodynamic coefficients defined in the frequency domain through the Fourier transform technique. Numerical calculations for the linear radiation problem on a submerged circular cylinder in deep water and a floating rectangle have been carried by using the linear and nonlinear time domain methods. These calculated results have been compared with the results of published analytical predictions and experimental measurements. Some numerical instabilities have been observed during the calculation of the hydrodynamic forces of the floating rectangle in the captive mode. The reasons for these discrepancies are discussed.

Finally, a review of main conclusions is given in Chapter 7.

CHAPTER 2
PROBLEM FORMULATION

2.1 Introduction

The problem of determining a particular flow caused by the existence and forward motion of the catamaran ship travelling in waves is to find a proper velocity potential that is based on the assumptions of "Ideal Fluid" and determined by the initial-boundary value problem.

The flow field of this ideal fluid is known as "Potential Flow" or "Irrotational Flow". It means that the fluid is homogenous, incompressible and inviscid. Moreover, the surface tension is neglected. Based on these assumptions, there exists a gradient of scalar function Φ to represent the velocity field of an irrotational flow. Firstly, the differential equation such as Laplace's equation which describes the flow field will be set up. The solution of this differential equation will be determined by the initial-boundary conditions.

The exact formulation of the boundary conditions leads to the nonlinear free surface condition and the body boundary condition on an unsteady body surface. These two conditions make the problem mathematically intractable. Therefore, a theoretical formulation of the linear boundary value problem in steady and unsteady flows induced by forward and oscillating motions of the moving body will be presented through linearisation by using the perturbation expansion technique.

2.2 Coordinate systems

In order to describe flow fields and motions of a rigid body moving in a seaway, it is necessary to define frames of reference. In general, the geometrical configuration of the twin-hull ship is easily described in a coordinate system fixed in the body. However, the motion of the fluid is easily described in an inertial system fixed in the fluid. Therefore, three right-handed orthogonal coordinate systems as shown in figure 2.1 are required to define the motions of the catamaran and the relation between them will be discussed.

Firstly, a coordinate system $o-x_0y_0z_0$ is defined as the space-fixed system. The $o-x_0y_0$ plane coincides with the undisturbed free surface, the x_0-axis in the direction

of the body's forward velocity and the z_0-axis vertically upward. This system will be used to describe the free surface boundary condition.

Secondly, the steady-translating system o-xyz is defined which moves in the same direction and mean forward velocity, U, as the moving body. The x-axis is pointing upstream parallel to the longitudinal plane of the body and the z-axis is pointing vertically upward through the centre of gravity of the body with the origin in the plane of the mean free surface. The relation between the steady-translating system o-xyz and the space-fixed system $o-x_0y_0z_0$ can be shown by the linear transformation:

$$\vec{x} = (x, y, z) = (x_0 - Ut, y_0, z_0) \tag{2.1}$$

These two coordinate systems will coincide when the forward speed of the body is zero. The body motion responses, $\xi_j (j = 1,2,...6)$, in six degrees of freedom will be described by the steady-translating system o-xyz. Here $j = 1,2,3,4,5,6$ refer to surge, sway, heave, roll, pitch and yaw motions respectively as shown in figure 2.1.

Finally, the oscillatory and translating system o'-x'y'z' is defined which is the body-fixed frame and which is the best way to describe the body boundary condition on the wetted body surface. The oscillatory and translating system o'-x'y'z' fluctuates with respect to the steady-translating system o-xyz. Therefore, the local oscillatory displacement $\bar{\alpha}(\vec{x}, t)$ of a point on the body surface $S_B(\vec{x}', t)$ can be defined by

$$\bar{\alpha}(\vec{x}, t) = (\xi_1(t), \xi_2(t), \xi_3(t)) + (\xi_4(t), \xi_5(t), \xi_6(t)) \times \vec{r}'(\vec{x}') \tag{2.2}$$

where $\vec{r}'(\vec{x}')$ is the position vector of the point on the surface $S_B(\vec{x}', t)$ relative to the body-fixed frame o'-x'y'z'. $(\xi_1(t), \xi_2(t), \xi_3(t))$ and $(\xi_4(t), \xi_5(t), \xi_6(t))$ are the unsteady translational and rotational displacement vectors respectively. $\bar{\alpha}(\vec{x}, t)$ is equal to zero in a steady equilibrium state if the origin o' locates at the centre of gravity which is on the undisturbed free surface.

2.3 Formulation of the initial-boundary value problem

In order to formulate the problem of potential flow, the velocity potential has to satisfy the equation of continuity at every point in the flow field except singular points. Furthermore, based on assumptions of the homogeneous, incompressible and inviscid fluid, the velocity potential of the flow field , $\Phi(\vec{x}_0, t)$, which must satisfy the Laplace's

equation in the fluid domain is written as

$$\nabla^2\Phi(\bar{x}_0,t)=0 \tag{2.3}$$

In order to determine the solution of (2.3), an initial-boundary value problem has to be solved. The initial state of the system should be prescribed at some instant of time. Moreover, we assume the ocean is infinite in all horizontal directions and the boundaries enclosing the fluid domain consist of the free surface, the wetted body surface, the sea bed and a control surface at far-field. These conditions will be discussed in the following sections.

2.3.1 Free surface condition

The effects of the free surface must be expressed in terms of appropriate boundary condition on the free surface which is described by its elevation:

$$z_0=\zeta(x_0,y_0,t) \tag{2.4}$$

The kinematic and dynamic boundary conditions must be satisfied on the free surface. It means that a fluid particle at the surface always remains at the surface and the pressure on the free surface must be atmospheric and conform to Bernoulli's equation. Assuming that the fluid is ideal and the surface tension at the free surface is negligible, the kinematic and dynamic conditions can be written respectively as:

$$\frac{D}{Dt}(\zeta-z_0)=0 \tag{2.5}$$

$$\Phi_t+\frac{1}{2}|\nabla\Phi|^2+gz_0=0 \tag{2.6}$$

where g is the gravitational constant.

On the exact free surface $\zeta(x_0,y_0,t)$, the dynamic boundary condition (2.6) can be combined with the kinematic condition (2.5):

$$\Phi_{tt}+g\Phi_{z_0}+2\nabla\Phi\cdot\nabla\Phi_t+\frac{1}{2}\nabla\Phi\cdot\nabla(\nabla\Phi\cdot\nabla\Phi)=0 \quad \text{on } z_0=\zeta(x_0,y_0;t) \tag{2.7}$$

This free surface condition is nonlinear and difficult to solve it analytically because the elevation of the free surface is not known a priori. Based on the linearisation, we can employ the perturbation expansion to linearise the free surface condition to the first-order and use Taylor series expansion to transform the exact free surface $\zeta(x_0, y_0, t)$ to some known surface such as the undisturbed free surface (Chan, 1990). Moreover, the total velocity potential $\Phi(\bar{x}_0, t)$ can be expressed through linearisation in the following form:

$$\Phi(\bar{x}_0, t) = \overline{\Phi}(\bar{x}) + \tilde{\Phi}(\bar{x}, t) \tag{2.8}$$

where $\overline{\Phi}(\bar{x})$ and $\tilde{\Phi}(\bar{x}, t)$ denote steady and unsteady potential respectively.

If the disturbance on the free surface due to the steady forward motion is small, the unsteady velocity potential $\tilde{\Phi}$ is an order of magnitude greater than the steady velocity potential $\overline{\Phi}$. All terms associated with the steady velocity potential are of higher order and may be neglected in the first order free surface condition for the unsteady flow. It is assumed that the velocity field of the steady flow relative to the steady-translating frame o-xyz is:

$$\bar{W}(\bar{x}) = \nabla\overline{\Phi}(\bar{x}) = (-U, 0, 0) \tag{2.9}$$

Thus, the linearised free surface boundary condition can be obtained:

$$(\frac{\partial}{\partial t} - U\frac{\partial}{\partial x})^2 \tilde{\Phi} + g\tilde{\Phi}_z = 0 \qquad \text{at } z=0 \tag{2.10}$$

2.3.2 Body boundary condition

The kinematic body boundary condition implies that the fluid velocity component normal to the instantaneous wetted body surface $S_B(x', y', z', t)$ is equal to the velocity component of the surface normal to itself. Thus:

$$\vec{V} \bullet \vec{n} = \vec{V}_s \bullet \vec{n} \qquad \text{on } S_B(x', y', z', t) \tag{2.11}$$

where

$$\vec{V}(\bar{x}_0, t) = \nabla\Phi(\bar{x}_0, t) \tag{2.12}$$

and

$$\vec{V}_s(\vec{x},t) = \dot{\vec{\alpha}}(\vec{x},t) \tag{2.13}$$

$\vec{V}(\vec{x}_0,t)$ is the velocity field of the flow; $\vec{V}_s(\vec{x},t)$ is the local velocity of a point on the wetted body surface $S_B(x',y',z',t)$.

- This body boundary condition must be satisfied on the exact oscillating surface $S_B(x',y',z',t)$ at each time step. In the linearised problem, the body boundary condition can be expanded onto the steady surface $\overline{S}_B$ by using the perturbation series method. Then, the linearised body boundary condition is

$$\tilde{\Phi}_n = \left[\dot{\vec{\alpha}} + (\vec{W}\cdot\nabla)\vec{\alpha} - (\vec{\alpha}\cdot\nabla)\vec{W}\right]\cdot\vec{n} \qquad \text{on } S_B, \overline{S}_B \tag{2.14}$$

Furthermore, by linearisation, the unsteady velocity potential $\tilde{\Phi}(x,y,z,t)$ can be decomposed linearly into three components due to incident waves, diffraction waves and radiation waves. If the small amplitude incident waves are sinusoidal and harmonic in time with frequency of encounter ω, the unsteady velocity potential can be written as:

$$\tilde{\Phi}(x,y,z,t) = \left[\zeta_0(\phi_0 + \phi_7) + \sum_{j=1}^{6}\bar{\xi}_j\phi_j\right]e^{-i\omega t} \tag{2.15}$$

where ζ_0 is the incident wave amplitude; ϕ_0 is the incident wave potential; ϕ_7 is the diffraction wave potential; ϕ_j is the radiation wave potential in j-th mode of motion, and $\bar{\xi}_j$ is the complex amplitude of motion.

In the diffraction problem the body is assumed to be fixed with respect to the body-fixed frame o'-x'y'z' as $\vec{\alpha} = 0$ and $\bar{\xi}_j = 0$. Thus, on the body boundary of no oscillatory motion, equation (2.14) simply becomes:

$$\frac{\partial}{\partial n}(\phi_0 + \phi_7) = 0 \qquad \text{on } S_B, \overline{S}_B \tag{2.16}$$

The radiation problem occurs as if the flow field is produced by the forced oscillation of the body in j-th degree of freedom in the absence of incident waves such that $\zeta_0 = 0$. The linearised body boundary condition given by (2.14) is reduced to:

$$\frac{\partial \phi_j}{\partial n} = -i\omega n_j + m_j \qquad \text{j=1,2,...6 on } S_B, \overline{S}_B \qquad (2.17)$$

where the components n_j are defined as

$$\vec{n} = (n_1, n_2, n_3) \qquad (2.18)$$

$$\vec{r}' \times \vec{n} = (n_4, n_5, n_6) \qquad (2.19)$$

and the forward speed related coefficients m_j are

$$(m_1, m_2, m_3) = -(\vec{n} \cdot \nabla)\vec{W} \qquad (2.20)$$

$$(m_4, m_5, m_6) = -(\vec{n} \cdot \nabla)(\vec{r}' \times \vec{W}) \qquad (2.21)$$

These body conditions involve the steady velocity field. If the body is thin, slender or the mean forward speed is low, then, m_j term becomes:

$$\begin{aligned} &m_j = 0 && \text{j=1,2,3,4} \\ &m_5 = Un_3 \\ &m_6 = -Un_2 && (2.22) \end{aligned}$$

This assumption leads to a simple speed correction, due to the angle of attack in pitch and yaw motion, on the linearised body boundary condition.

2.3.3 Sea bed condition

The fluid particle on the bottom has zero velocity normal to the boundary because the sea bed is a stationary boundary. Thus,

$$\frac{\partial \Phi}{\partial n} = \frac{\partial \Phi}{\partial z} = 0 \qquad \text{on z=-h} \qquad (2.23)$$

where h is the depth of sea.

In this study, since the deepwater condition is assumed, the velocity potential Φ should satisfy the sea bed condition as:

$$\frac{\partial \Phi}{\partial z} = 0 \qquad \text{at } z \to -\infty \qquad (2.24)$$

2.3.4 Initial value problem

In the initial value problem, the displacement and velocity of the fluid and body are specified at some instant of time, $t = 0$. Therefore, the initial value of velocity potential must be prescribed:

$$\Phi(\bar{x}, 0) = f_1(\bar{x}) \qquad (2.25)$$

$$\Phi_t(\bar{x}, 0) = f_2(\bar{x}) \qquad (2.26)$$

where $f_1(\bar{x})$ and $f_2(\bar{x})$ are given functions at $t = 0$.

If the motion problem of a rigid body is the steady-state harmonic oscillations in time, the time dependence can be eliminated because the appropriate initial conditions were well prescribed. Then, the initial-boundary value problem can be further simplified to the boundary value problem for solving the solution of Laplace's equation.

2.3.5 Far field radiation condition

A radiation condition at infinity must be imposed upon the potential function in order to ensure a unique solution to the motion problem. This far field radiation condition assumes that the fluid motion produced by the steady oscillating body travels away from the body and vanishes at infinity on all sides. This type of radiation condition was firstly used in the study of acoustics by Sommerfeld (1949). The far field radiation condition of $\Phi(\bar{x}, t)$ can be represented as:

$$\lim_{r \to \infty} \sqrt{r} \left(\frac{\partial \Phi(\bar{x}, t)}{\partial r} - ik\Phi(\bar{x}, t) \right) = 0 \qquad (2.27)$$

where r is the horizontal radial distance away from the body; k is the wave number. It is difficult to define the far field radiation condition for the unsteady flow due to the forward and oscillatory motions of the body moving with constant speed in waves. An implicit far field radiation condition may be expressed as:

$$\lim_{r\to\infty}\sqrt{r}\Phi(\bar{x},t)=0 \tag{2.28}$$

Based on the assumption that $\Phi(\bar{x},t)$, $\Phi_t(\bar{x},t)$ and their first derivatives are uniformly bounded, the boundary condition at infinity as proved by Finkelstein (1957) states that the fluid motion vanishes everywhere for the initial value problem. If the solution begins with determining the velocity potential as an initial value problem, the far field radiation condition is not necessary.

2.4 Conclusions

Based on the potential theory, a theoretical formulation for the steady and unsteady forward motion problems has been presented. Due to the nonlinearities in the free surface and body conditions, the linearisation of boundary conditions has been introduced to simplify the mathematical complexity. Furthermore, it has been assumed that the steady perturbation potential is of higher order and can be neglected in the linearised free surface condition for the unsteady flow. The combined effects of oscillating frequency and forward speed will only be considered.

The linearised body boundary condition contains the convective effects of the steady velocity field due to the forward speed effects. If the body is thin and slender or the mean forward speed is low, the linearised body boundary condition will be further simplified to a simple speed correction on the pitch and yaw motions.

The position and velocity of system must be specified for the initial value problem in order to solve the arbitrary motion problem. The far field radiation condition is automatically satisfied in the initial value problem. Furthermore, if the motion of a rigid body is considered in the steady-state time-harmonic motion, the initial-boundary value problem can be further simplified to the boundary value problem because all transients will die out.

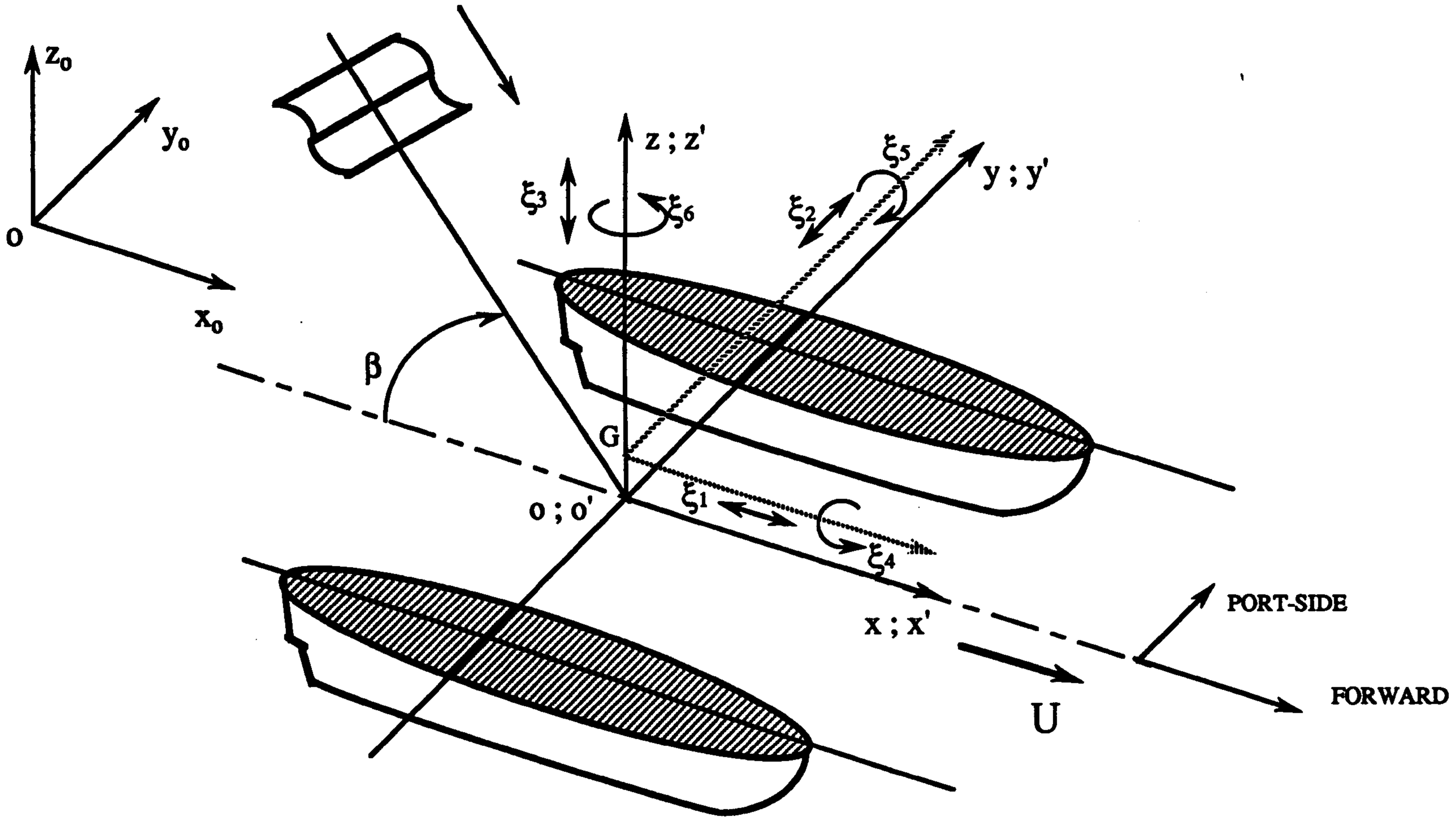

Figure 2.1: Coordinate systems of Twin-Hull Ship

CHAPTER 3
SMALL AMPLITUDE MOTIONS OF CATAMARANS IN WAVES

3.1 Introduction

It has been demonstrated that linear ship-motion theories can solve many seakeeping problems related to the average performance of a ship with good accuracy. The strip theory has been recognised as the most practical tool for predicting motions and loads of ships and ocean platforms utilised for various activities in deep and shallow ocean environments. This theory was first developed to compute the heave and pitch motions of a ship in head sea condition by Korvin-Kroukovsky (1955). Subsequently, the original strip theory has been improved by a number of investigators. Ursell (1962) and Newman & Tuck (1964) derived the long wave slender body theory and Ogilvie & Tuck (1969) and Salvesen et al. (1970) derived the short wave strip theory. However, these theories are based on the assumptions of potential flow, slender ship and small amplitude motions. (Motion amplitudes are assumed to be small compared to the transverse dimensions of the ship.)

Fundamental studies to formulate the hydrodynamic forces acting on catamarans started in the early 1970's (Ohkusu, 1969, Wang and Wahab, 1971). A study on the behaviour of an ASR catamaran in waves was presented by Wahab et al. (1971). The motions in waves and wave-induced forces and moments acting on the cross-deck structure in waves of various directions for several hull separations were investigated by means of the model tests of two asymmetric catamarans. Based on the theory developed by Salvesen et al. (1970), the strip method was extended by Lee et al. (1973) to predict the coupled heave and pitch motions of catamarans in head seas. The theoretical predictions were compared with the experimental results of three different catamaran models. Correlations between theoretical values and experimental results indicated that the motion amplitudes were overestimated. Some discrepancies were believed to be caused by viscous and forward speed effects. After one year, Hadler et al. (1974) presented a report for the experiments of USNS *Hayes*. It was the first ocean-going catamaran of the U.S. Navy. The paper highlighted the model development and full-scale trial programmes conducted on *Hayes*. Recently, there are further published research studies for investigating the small amplitude motion problem of catamarans in waves, such as Chapman's (1975) type pseudo three-dimensional theory by Faltinsen et al. (1992), Ohkusu and Wen (1995); Ranking panel method by Kring and Sclavounos (1991) and three-dimensional translating pulsating Green function method by Chan (1993), Hudson et al. (1995). Although the three-

dimensional method is a more accurate technique than the two-dimensional technique for the calculation of the motions of twin hulls, the computation time for the three-dimensional method is significantly higher than for the two-dimensional method.

In this Chapter, a two-dimensional linearised method based on the potential flow theory is used to predict the motion performance of catamarans in waves. In order to validate this method, the numerical results have been compared with experimental values obtained for three different catamarans. The experimental values of an ASR catamaran with hull separation/beam = 1.58 in 180^0 heading at Froude number = 0.31 and the motion responses of Marintek catamaran model in 90^0 and 135^0 wave headings at Froude number =0.49 have been compared with calculations based on the two-dimensional potential theory. For the third catamaran model (V-1 catamaran model), the existence of characteristic frequencies of the hydrodynamic forces on the twin hulls is discussed and the motion response values measured in the head sea condition have been compared with the results obtained from two-dimensional linear theory.

3.2 Theoretical formulation based on the two-dimensional Green function

The problem of linear ship motion is formulated in terms of the potential flow theory. Therefore, the fluid is assumed to be homogeneous, incompressible and inviscid. By assuming that the motions are steady in a moving coordinate system and are sinusoidal in time, the initial value problem can be precipitated out. Moreover, the amplitude of incident wave is small compared with the wave length and the dimensions of the body's cross section. Then, the exact boundary value problem can be further simplified through linearisation as described in Chapter 2.

Based on the linearisation, the total potential, Φ, can be separated into the steady potential, $\overline{\Phi}$, and the unsteady potential, $\tilde{\Phi}$. Furthermore, the steady velocity potential, $\overline{\Phi}$, can be divided into the uniform stream and the steady perturbation potential $\overline{\phi}(x,y,z)$:

$$\begin{aligned}\Phi(x,y,z,t) &= \overline{\Phi}(x,y,z)+\tilde{\Phi}(x,y,z,t)\\ &= (-Ux+\overline{\phi}(x,y,z))+\tilde{\Phi}(x,y,z,t)\end{aligned} \tag{3.1}$$

The unsteady potential, $\tilde{\Phi}$, can be decomposed linearly into separate components due to the incident waves, diffraction waves and radiation waves. Then, it can be written as

$$\tilde{\Phi}(x,y,z,t) = \left[\zeta_0(\phi_0 + \phi_7) + \sum_{j=1}^{6} \bar{\xi}_j \phi_j \right] e^{-i\omega t} \qquad (3.2)$$

where ϕ_0 is the incident wave potential of amplitude, ζ_0, ϕ_7 is the diffraction wave potential and ϕ_j is the radiation wave potential in j-th mode of motion. The body is assumed to be rigid and to oscillate in six degrees of freedom about its mean position with encounter frequency ω and complex amplitudes $\bar{\xi}_j$ (j=1,2,...6). Here j=1,2,3,4,5,6 refer to surge, sway, heave, roll, pitch, and yaw modes of motion respectively.

The incident wave potential of unit amplitude which satisfies the Laplace's equation and the linearised free surface boundary condition can be described as

$$\phi_0 = -i\frac{g}{\omega_0} e^{kz + ik(x\cos\beta + y\sin\beta)} \qquad (3.3)$$

with the wave number k is given by the dispersion relation

$$k = \frac{\omega_0^2}{g} \qquad (3.4)$$

and the frequency of encounter is

$$\omega = |\omega_0 - Uk\cos\beta| \qquad (3.5)$$

where ω_0 is a wave frequency; and β is an angle of incidence with the x-axis (180^0 at head sea). It is understood that the real part is to be taken in all expressions.

With the basic linear assumption, the diffraction wave potential ϕ_7 and the radiation wave potential ϕ_j, in the j-th mode of motion, must satisfy the following linearised boundary conditions:

Laplace's equation in the fluid domain

$$\nabla^2\phi_j = 0; \qquad j=1,2,...7 \qquad (3.6)$$

the linearised free-surface condition

$$(i\omega + U\partial/\partial x)^2 \phi_j + g\frac{\partial \phi_j}{\partial z} = 0 \qquad \text{j=1,2,...7 at } z\text{=0;} \tag{3.7}$$

the kinematic body boundary condition

$$\frac{\partial \phi_j}{\partial n} = -i\omega n_j + m_j \qquad \text{j=1,2,...6 on } S_B; \tag{3.8}$$

and

$$\frac{\partial \phi_7}{\partial n} = -\frac{\partial \phi_0}{\partial n} \qquad \text{on } S_B; \tag{3.9}$$

the kinematic boundary condition on the ocean floor

$$\frac{\partial \phi_j}{\partial n} = 0 \qquad \text{j=1,2,...7 at } z \to -\infty; \tag{3.10}$$

where g is acceleration due to gravity; n_j is the generalised direction cosine with $\vec{n} = (n_1, n_2, n_3)$ and $\vec{r}' \times \vec{n} = (n_4, n_5, n_6)$; $\vec{n}$ is a unit normal vector outward to the mean wetted body surface and $\vec{r}'$ is a position vector of a point on the mean wetted body surface; $(m_1, m_2, m_3) = -(\vec{n} \cdot \nabla)\vec{W}$ and $(m_4, m_5, m_6) = -(\vec{n} \cdot \nabla)(\vec{r}' \times \vec{W})$; and $\vec{W}$ is a steady velocity field. If the body is slender, the steady perturbation potential due to forward motion is negligible in the unsteady flow. Then $m_j = 0$ for j=1,2,3,4; $m_5 = Un_3$ and $m_6 = -Un_2$, which are used in the present study.

For the two-dimensional method, a high-frequency assumption is made that the frequency of oscillation ω is much higher than the differential operator $U\partial/\partial x$ in the free surface boundary condition which reduces to

$$-\omega^2 \phi_j + g\frac{\partial \phi_j}{\partial z} = 0 \tag{3.11}$$

This free surface boundary condition (3.11) for the ship body oscillation at forward speed requires that the wave length is approximately of the same order as the ship beam. This is a very critical assumption and it makes the theory somewhat questionable in the low frequency range since the forward speed effects on the free surface are not included.

Under these assumptions, the three dimensional Laplace's equation and boundary conditions can be reduced to the two-dimensional problems by using strip theory. A two-dimensional pulsating source potential technique is developed to solve the unsteady velocity potential due to the incident, diffracted and radiated wave systems.

The two-dimensional Green function method is an integral equation used in solving a linearised boundary value problem. The formulation of the Green function method is based on Green's second identity to define a velocity potential using a Green function on the boundary of the fluid domain. It will be shown from Green's theorem that ϕ_j may be constructed from a source distribution along the underwater surface of a floating body and its image. Figure 3.1 shows the fluid domain for the twin-hull bodies. The y axis is taken to coincide with the undisturbed free surface and the z axis is directed vertically upward. The origin is taken at the midpoint between twin hulls. S_B is the surface of the body below the y axis. The y axis is divided into S_I interior to the body and S_F on either side. The lower half-plane, z<0, is divided into two regions: R exterior to the body and bounded by S_F, S_B and S_∞; and I interior to the body and bounded by S_I and S_B. Let the body potential in these two regions be ϕ_j^R and ϕ_j^I.

Quasi-analytic methods are usually applied in the form of a surface integral derived from Green's theorem. Let

$$G(p,t;q) = G(y,z;\eta,\zeta)e^{-i\omega t} \tag{3.12}$$

where

$p = y + iz$:field point
$q = \eta + i\zeta$:source point

A two-dimensional Green's function which satisfies the linearised boundary conditions is given by Wehausen et al. (1960) and defined as:

$$G(p;q) = \mathrm{Re}\left\{\log(p-q) - \log(p-\bar{q}) + 2PV\int_0^\infty \frac{e^{-i\nu(p-\bar{q})}}{K-\nu}d\nu\right\} - 2\pi i\,\mathrm{Re}\left\{e^{-iK(p-\bar{q})}\right\} \tag{3.13}$$

where

$\bar{q} = \eta - i\zeta$:image source point

$$K = \frac{\omega^2}{g} \text{ : encounter wave number} \tag{3.14}$$

From Green's second identity :

$$\int_{S_B} (\phi_j \frac{\partial G}{\partial n_q} - G \frac{\partial \phi_j}{\partial n_q}) dl = \iint_{R+I} \nabla \cdot (\phi_j \nabla G - G \nabla \phi_j) ds$$
$$= \iint_{R+I} (\phi_j \nabla^2 G - G \nabla^2 \phi_j) ds \tag{3.15}$$

where $\partial / \partial n_q$ is the normal derivative with respect to the source point q and the normal vector $\bar{n}$ is pointing into the fluid domain R.

Since ϕ_j and G are the solutions of Laplace's equation except at a singular point in the fluid domain I and R, the equation (3.15) can be reduced to

$$\int_{S_B} (\phi_j \frac{\partial G}{\partial n_q} - G \frac{\partial \phi_j}{\partial n_q}) dl = 0 \qquad \text{in fluid domain (R and I)} \tag{3.16}$$

This integral along the body contour S_B has three different characteristics which depend on the position of the field point p relative to the source point q.

Firstly, the field point p is outside the fluid domain R. Since the source point q never coincides with the field point p, equation (3.16) is valid.

Furthermore, if the field point p lies inside the fluid domain R but not on the boundary S_B, concurrence of the field point p and source point may occur. When $p = q$, the singularity of the Green function G makes equation (3.16) invalid. This difficulty can be circumvented by surrounding the source point by a small circle of radius ε with contour S_ε whose origin is at p. Then $S_B + S_\varepsilon$ is a closed contour surrounding the fluid domain R but exterior to S_ε. Thus, equation (3.16) can be replaced by

$$\int_{S_\varepsilon + S_B} (\phi_j^R(q) \frac{\partial G(p;q)}{\partial n_q} - G(p,q) \frac{\partial \phi_j^R(q)}{\partial n_q}) dl = 0 \quad p \text{ inside R} \tag{3.17}$$

Then

$$\int_{S_\varepsilon}(\phi_j^R(q)\frac{\partial G(p;q)}{\partial n_q}-G(p,q)\frac{\partial \phi_j^R(q)}{\partial n_q})dl+\int_{S_B}(\phi_j^R(q)\frac{\partial G(p;q)}{\partial n_q}-G(p,q)\frac{\partial \phi_j^R(q)}{\partial n_q})dl=0 \tag{3.18}$$

Using Gauss's theorem, the following results can be obtained from equation (3.18):

$$\int_{S_\varepsilon}(G(p,q)\frac{\partial \phi_j^R(q)}{\partial n_q})dl=\int_{S_\varepsilon}G(p;q)(n_q\cdot\nabla)\phi_j^R(q)dl=\iint_{R_\varepsilon}G(p;q)\nabla^2\phi_j^R(q)ds=0 \tag{3.19}$$

Then, equation (3.18) can be reduced to

$$\int_{S_B}(\phi_j^R(q)\frac{\partial G(p;q)}{\partial n_q}-G(p,q)\frac{\partial \phi_j^R(q)}{\partial n_q})dl=\lim_{\varepsilon\to 0}\int_{S_\varepsilon}-(\phi_j^R(q)\frac{\partial G(p;q)}{\partial n_q})dl$$

$$=-\lim_{\varepsilon\to 0}[2\pi\varepsilon\cdot\phi_j^R(p)\cdot\frac{1}{\varepsilon}]=-2\pi\phi_j^R(p) \qquad \text{for } p \text{ inside R.} \tag{3.20}$$

Finally, if the field point p lies on the boundary contour S_B, the contour S_ε is chosen to be a small semi-circle that the singularity can be avoided. Then, the factor of 2π in equation (3.20) becomes π, we can write

$$\int_{S_B}(\phi_j^R(q)\frac{\partial G(p;q)}{\partial n_q}-G(p,q)\frac{\partial \phi_j^R(q)}{\partial n_q})dl=-\pi\phi_j^R(p) \qquad \text{for } p \text{ on } S_B \tag{3.21}$$

Now we summarise the results given by equations (3.16), (3.20) and (3.21)

$$\int_{S_B}(\phi_j^R(q)\frac{\partial G(p;q)}{\partial n_q}-G(p;q)\frac{\partial \phi_j^R(q)}{\partial n_q})dl=\left\{\begin{matrix}0\\-\pi\phi_j^R(p)\\-2\pi\phi_j^R(p)\end{matrix}\right\}\ \text{for}\ \begin{matrix}p\notin R\\p\in S_B\\p\in R\end{matrix} \tag{3.22}$$

Also from Green's theorem, the representations for the interior domain I can be obtained. Let us define that ϕ_j^I is the interior potential inside the domain I described before. Thus

$$\int_{S_B}(\phi_j^I(q)\frac{\partial G(p;q)}{\partial n_q}-G(p;q)\frac{\partial \phi_j^I(q)}{\partial n_q})dl=\begin{Bmatrix}0\\ \pi\phi_j^I(p)\\ 2\pi\phi_j^I(p)\end{Bmatrix}\quad\text{for}\quad\begin{matrix}p\notin \mathrm{I}\\ p\in S_B\\ p\in \mathrm{I}\end{matrix}\tag{3.23}$$

Then from (3.22) and (3.23)

$$2\pi\phi_j^R(p)=\int_{S_B}(\phi_j^I(q)-\phi_j^R(q))\frac{\partial G(p;q)}{\partial n_q}dl$$
$$+\int_{S_B}(\frac{\partial \phi_j^R(q)}{\partial n_q}-\frac{\partial \phi_j^I(q)}{\partial n_q})G(p;q)dl\qquad\text{for } p \text{ in R, on } S_B\tag{3.24}$$

Similarly,

$$2\pi\phi_j^I(p)=\int_{S_B}(\phi_j^I(q)-\phi_j^R(q))\frac{\partial G(p;q)}{\partial n_q}dl$$
$$+\int_{S_B}(\frac{\partial \phi_j^R(q)}{\partial n_q}-\frac{\partial \phi_j^I(q)}{\partial n_q})G(p;q)dl\qquad\text{for } p \text{ in I}\tag{3.25}$$

Thus, the potential over the entire lower half-plane is equivalent to a source distribution over S_B and a dipole distribution over S_B. Then

$$\mu(q)=\phi_j^I(q)-\phi_j^R(q)\tag{3.26}$$

$$\sigma(q)=\frac{\partial \phi_j^R(q)}{\partial n_q}-\frac{\partial \phi_j^I(q)}{\partial n_q}\tag{3.27}$$

where $\mu(q)$ and $\sigma(q)$ can be interpreted as the dipole strength and the source strength respectively. The most common assumption is that the potential is continuous across the body, $\mu(q)$=0. The normal velocity is discontinuous across the body surface. If it is specified that

$$\phi_j^R(p)=\phi_j^I(p)\qquad\text{for } p \text{ on } S_B\tag{3.28}$$

and the velocity potential is of the form,

$$2\pi\phi_j(p)=\int_{S_B}\sigma(q)G(p;q)dl\tag{3.29}$$

which is equivalent to a source distribution of strength $\sigma(q)$ along S_B and its image is represented by Green's function defined in equation (3.13).

If we apply the linearised body condition (3.8) and (3.9), the unknown source strength $\sigma(q)$ can be determined. Thus

$$\pi\sigma(p)+\int_{S_B}\sigma(q)\frac{\partial G(p;q)}{\partial n_p}dl=2\pi\frac{\partial\phi_j(p)}{\partial n_p} \qquad \text{for } p \text{ on } S_B \tag{3.30}$$

The first term in the left hand side of equation (3.30) ensures the isolation of singularity for the validity of equation (3.15).

Once the source densities $\sigma(q)$ are known, the velocity potential $\phi_j(p)$ can be solved by (3.29). The hydrodynamic forces and moments can be obtained by substituting the known velocity potential into the linearised Bernoulli's equation and integrating the resultant formulation over the mean wetted body contour.

3.3 Hydrodynamic forces

The hydrodynamic forces can be obtained by integrating the hydrodynamic pressures in terms of the appropriate velocity potential and its derivatives over the mean wetted body surface $\overline{S}_B$. Under the linearisation procedure, the unsteady velocity potential can be decomposed into potentials due to incident waves, diffraction waves and radiation waves.

The hydrodynamic exciting forces F_j^W are the results of the pressure associated with the incident wave potential and diffraction potential due to the incident waves per unit amplitude and can be expressed in the form

$$\begin{aligned} F_j^W &= -\rho\iint_{\overline{S}_B} n_j(i\omega+U\frac{\partial}{\partial x})(\phi_0+\phi_7)dse^{-i\omega t} \\ &= \overline{F}_j^W e^{-i\omega t}=\left|F_j\right|e^{-i(\omega t+\varepsilon_j)} \qquad j=1,2,\ldots 6 \end{aligned} \tag{3.31}$$

where

$$\overline{F}_j^W=\overline{F}_{jR}^W+i\overline{F}_{jI}^W \tag{3.32}$$

$$|F_j| = \sqrt{\bar{F}_{jR}^{w2} + \bar{F}_{jI}^{w2}} \tag{3.33}$$

$$\varepsilon_j = \tan^{-1} \frac{-\bar{F}_{jI}^{w}}{\bar{F}_{jR}^{w}} \tag{3.34}$$

$\bar{F}_j^w$ and $|F_j|$ are the complex amplitude and amplitude of wave exciting forces, respectively. ε_j is the phase angle which is positive if the force leads the wave elevation at the origin of the coordinate.

The exciting forces F_j^W can be further decomposed into two components as the Froude-Krylov force and diffraction force. The Froude-Krylov force involves the incident wave potential only and corresponds to the force experienced by the body when the incident wave trains pass through it unaffected. Therefore the Froude-Krylov force is significant in the long wave or for a thin body in head waves with little scattering waves. The diffraction force becomes important in the short wave region or for a large body with a large frontal area exposed to the incident waves.

Under the assumption of a linear frequency response to harmonic excitation relationship, the solutions for the displacements from the mean position of the catamaran can be expressed by

$$\xi_k(t) = \bar{\xi}_k e^{-i\omega t} = |\xi_k| e^{-i(\omega t + \varepsilon_k)} \qquad \text{k=1,2,...6} \tag{3.35}$$

where

$$\bar{\xi}_k = \xi_{kR} + i\xi_{kI} \tag{3.36}$$

$$|\xi_k| = \sqrt{\xi_{kR}^{\ 2} + \xi_{kI}^{\ 2}} \tag{3.37}$$

$$\varepsilon_k = \tan^{-1} \frac{-\xi_{kI}}{\xi_{kR}} \tag{3.38}$$

$\bar{\xi}_k$ and $|\xi_k|$ are the complex amplitude and amplitude of motions, respectively; ε_k is the phase angle with respect to the wave crest. A positive phase angle of the motion response indicates that a motion reaches its positive maximum value before the crest of the undisturbed incoming regular wave passes the origin.

The hydrodynamic reactive forces in the j-th direction resulting from the motion ξ_k are obtained by

$$F_{jk}^R = -\rho \iint_{\bar{S}_B} n_j (i\omega + U\frac{\partial}{\partial x})\phi_k ds \bar{\xi}_k e^{-i\omega t} \qquad \text{j,k=1,2,...6} \qquad (3.39)$$

where j and k indicate the direction of the fluid reaction force and the mode of motion respectively.

On the other hand, the hydrodynamic reactive forces can be expressed in phase with the body acceleration and velocity, that is

$$F_{jk}^R = -(A_{jk}\ddot{\xi}_k(t) + B_{jk}\dot{\xi}_k(t)) = (\omega^2 A_{jk} + i\omega B_{jk})\bar{\xi}_k e^{-i\omega t} \qquad (3.40)$$

The coefficients A_{jk} and B_{jk} are real quantities which are functions of the body shape, the forward speed and the frequency of motion. As A_{jk} is associated with the body acceleration, it is normally called "Added Mass coefficient". The quantity B_{jk} is related to the velocity of the motion in the k-th mode and is called "Damping coefficient". The added mass and damping coefficients are given from (3.39) and (3.40)

$$A_{jk} = -\frac{\rho}{\omega^2}\mathrm{Re}\iint_{\bar{S}_B} n_j (i\omega + U\frac{\partial}{\partial x})\phi_k ds \qquad (3.41)$$

$$B_{jk} = -\frac{\rho}{\omega}\mathrm{Im}\iint_{\bar{S}_B} n_j (i\omega + U\frac{\partial}{\partial x})\phi_k ds \qquad (3.42)$$

The hydrostatic restoring forces are defined as the fluid forces to restore the body to its static equilibrium state when the body is displaced freely from the rest position. By using Gauss's theorem, the surface integral can be transformed to the volume integral in the form

$$F_j^\delta = \rho g \iint_{\bar{S}_B} z n_j ds = \rho g \iiint_{\delta V} n_j dV = -\rho g \iint_{A_w} dA_w \int_0^{z(\xi_3(t)+y\xi_4(t)-x\xi_5(t))+\cdots} n_j dz e^{-i\omega t}$$

$$= -\sum_{k=1}^{6} C_{jk}\bar{\xi}_k e^{-i\omega t} \qquad \text{j=1,2,...6} \qquad (3.43)$$

The quantity C_{jk} is called the hydrostatic restoring coefficient which is a function of the body geometry only and is independent of the motion ξ_k. With one longitudinal plane of symmetry, a motion in the longitudinal plane cannot produce any forces perpendicular to that plane. The hydrostatic coefficients C_{jk} are given by

$$C_{33} = \rho g A_w; C_{44} = \rho g \nabla GM_T; C_{55} = \rho g \nabla GM_L;$$

$$C_{35} = C_{53} = -\rho g A_y \qquad (3.44)$$

where A_w and A_y are the area and the first moment of the waterplane area at z=0 respectively; ∇ is the volume displacement of the catamaran; GM_T is the transverse metacentric height and GM_L is the longitudinal metacentric height above the origin.

3.4 Equations of motion

For dynamic equilibrium the total wave-induced forces must be equal to the mass inertia forces and the coupled linear equations of motion of the rigid body can be written as

$$\sum_{k=1}^{6}\left\{(M_{jk} + A_{jk})\ddot{\xi}_k(t) + B_{jk}\dot{\xi}_k(t) + C_{jk}\xi_k(t)\right\} = \zeta_0 F_j^W \qquad \text{j=1,2,...6} \qquad (3.45)$$

where $\ddot{\xi}_k$ and $\dot{\xi}_k$ are motion acceleration and velocity respectively; M_{jk} is the mass matrix; A_{jk} is the added mass; B_{jk} is the damping; and C_{jk} is the restoring coefficient. F_j^W is the wave exciting force;ζ_0 is the incident wave amplitude. The indices j and k indicate the direction of the fluid force and the mode of motion respectively.

It is assumed that the catamaran has one longitudinal plane of symmetry. The symmetry of the hull with respect to the longitudinal centre-plane of the twin-hull ship leads to decoupling of the vertical plane modes from the horizontal plane modes. Thus the equations of motion can be divided into surge-heave-pitch and sway-roll-yaw equations. The generalised mass matrix [M] of the ship whose centre of gravity is at (0,0, z_G) can be written as

$$[M] = \begin{bmatrix} M & 0 & 0 & 0 & Mz_G & 0 \\ 0 & M & 0 & -Mz_G & 0 & 0 \\ 0 & 0 & M & 0 & 0 & 0 \\ 0 & -Mz_G & 0 & I_{44} & 0 & -I_{46} \\ Mz_G & 0 & 0 & 0 & I_{55} & 0 \\ 0 & 0 & 0 & -I_{64} & 0 & I_{66} \end{bmatrix} \qquad (3.46)$$

where M is the mass of the ship, I_{jj} is the moment of inertia about the origin in the j-th mode of motion and I_{jk} is the cross-product of inertia about the origin.

Once the hydrodynamic forces as described in section 3.3 are determined by integration of the related radiation potential and the diffraction potential due to the incident wave, the linear motion responses of catamaran in regular waves can be obtained from equation (3.45).

3.5 Correlation studies

Based on the two-dimensional Green function, the formulation of the hydrodynamic forces on a catamaran and the resulting motion responses in regular waves has been described in the previous sections. The validation of the mathematical model was carried out by comparing numerical results obtained from the two-dimensional frequency domain program developed by Dr. H. S. Chan in 1993 with those obtained from experiments with three catamaran models. (ASR5061, 1971; Marintek, 1992; V-1 model, 1994)

3.5.1 Motion responses of the ASR5061 catamaran

The most comprehensive sea load measurements were carried out in the Naval Ship Research and Development Centre by Wahab et al. (1971) for the ASR5061 catamaran model advancing obliquely in deep water waves. The model 5061 represents the ASR at the end of the preliminary design stage. Tests were carried out for a range of regular waves, speeds, headings and hull separations with six degree freedom of motions. The demi-hull is asymmetrical forward and symmetrical aft as shown in figure 3.2. Some of the main particulars are given in Table 3.1. The ASR5061 catamaran was modelled by 21 sections and each contour was approximated by a number of straight-line segments, as shown in figure 3.3. In this correlation study, the experimental values of ASR model with hull separation/beam = 1.58, wave direction $\beta = 180^{o}$ and Froude number $F_n(=U/\sqrt{gL})$ =0.31 were compared with the theoretical results based on the two-dimensional method.

Figures 3.4 and 3.5 show the comparison of experimental data with the present theoretical results for the non-dimensional pitch and heave motions of the ASR5061 catamaran against the non-dimensional wave frequencies. Comparisons show that

there is a good correlation between the theoretical and experimental results except around the resonance regions. When the effects of viscous damping are not taken into account, the numerical results obtained from the two-dimensional potential theory are higher than experimental results at the resonance regions for both heave and pitch motions. Both experimental data and numerical results show a second peak in the pitch motion response curve. It may be caused by the interaction effects between the twin hulls.

3.5.2 Motion responses of the Marintek catamaran

Tests with the Marintek catamaran model were carried out in the Ocean Environment Laboratory of MARINTEK (Faltinsen et al., 1992). The demi-hull of this catamaran is round bottom, symmetrical with respect to the longitudinal vertical plane and had a transom stern as shown in figure 3.6. Table 3.2 gives the main particulars of the test model and figure 3.7 shows the segmentation of Marintek catamaran model for the numerical calculations. A free running model was used and measurements were carried out with 90^0 and 135^0 heading at F_n=0.49. The published non-dimensional heave and roll responses in regular beam waves and heave and pitch transfer functions in 135^0 oblique waves for the catamaran model have been compared with the numerical values obtained from the two-dimensional method as shown in figures 3.8 to 3.11.

In figure 3.8, the experimental roll motions are somewhat higher than the numerical results at certain frequencies and the resonance position of the experimental curve is slightly shifted towards the low frequency. For heave motion predictions in beam sea, the numerical results are in good agreement with the experimental values as shown in figure 3.9. Unfortunately, the published experimental data lack values at high wave frequencies to validate the numerically predicted transfer function values of heave motion around the resonance region.

Results for the non-dimensional pitch and heave motion responses in 135^0 heading are presented in figures 3.10 and 3.11. There are some discrepancies observed in the prediction of pitch motions at the lower wave frequencies. A good correlation between the numerically predicted and experimentally measured heave motion responses is obtained. However, the analytical results overpredict the values determined experimentally and the calculated heave and pitch resonance positions shift slightly towards the higher wave frequency region. Experimental errors may have occurred in

the autopilot system since it was not possible to keep the constant heading during these tests as discussed by the authors (Faltinsen et al., 1992).

3.5.3 Motion responses of the V-1 catamaran

Incecik et al. (1991) reported a series of experiments for the V.I.L. catamaran model with variable spacing between the demi-hull and the position of LCG. In this study, the V.I.L. catamaran model was modified to arrive at the V-1 model. The V-1 model was tested with a new measurement system to investigate the nonlinear effects of large amplitude motions in the Towing Tank of the Hydrodynamics Laboratory at the University of Glasgow. Details about the experimental work can be found in Chapter 5. In this Chapter, the experimental data of small incident wave amplitude, $\zeta_0 = 1.0cm$, have been used to validate the two-dimensional frequency domain method. The V-1 model is a high speed catamaran hull form. The demi-hull is of the planing type, featuring V-type section and cut-off transom stern as shown in figure 3.12. The principal dimensions of the V-1 catamaran are given in Table 3.3. The segmentation of the V-1 catamaran model is presented in figure 3.13.

The hydrodynamic forces in terms of added mass, damping coefficients and wave exciting forces at three different forward speeds are indicated in figures 3.14 to 3.28 and in the following non-dimensional forms :

- Added mass coefficient

$$
\begin{array}{lll}
a_{jk}: & A_{jk} / \rho\nabla & \text{j,k=1,2,3} \\
 & A_{jk} / \rho\nabla L & \text{j=1,2,3 : k=4,5,6} \\
 & & \text{k=1,2,3 : j=4,5,6} \\
 & A_{jk} / \rho\nabla L^2 & \text{j,k=4,5,6}
\end{array} \qquad (3.47)
$$

- Damping coefficient

$$
\begin{array}{lll}
b_{jk}: & B_{jk} / \rho\nabla\sqrt{g / L} & \text{j,k=1,2,3} \\
 & B_{jk} / \rho\nabla L\sqrt{g / L} & \text{j=1,2,3 : k=4,5,6} \\
 & & \text{k=1,2,3 : j=4,5,6} \\
 & B_{jk} / \rho\nabla L^2\sqrt{g / L} & \text{j,k=4,5,6}
\end{array} \qquad (3.48)
$$

- Wave exciting force

$$|F_j|: \quad \begin{cases} |F_j| L / \rho g \zeta_0 \nabla & \text{j=1,2,3} \\ |F_j| / \rho g \zeta_0 \nabla & \text{j=4,5,6} \end{cases} \qquad (3.49)$$

where g is acceleration due to gravity; ∇ is the volume displacement of the catamaran; L is the length between perpendiculars of the catamaran. These results are plotted against the non-dimensional frequency.

For a catamaran with port-starboard symmetry, the vertical plane motions (surge, heave and pitch) are affected by the symmetric interaction and the horizontal plane motions (sway, roll and yaw) by the antisymmetric interaction (Hudson et al., 1995). There exists a set of discrete characteristic frequencies at which the motion of the fluid between the twin bodies is strongly excited by the body oscillation (Wang and Wahab,1971). These frequencies closely correspond to the gravity wavelength for deep water which satisfies the following relation :

Symmetric interaction : $\omega_r = \sqrt{2n\pi g / d_r}$ for n=1,2,3... (3.50)

Antisymmetric interaction : $\omega_r = \sqrt{(2n-1)\pi g / d_r}$ for n=1,2,3... (3.51)

where d_r is the hull separation between two bodies. The characteristic frequencies derived from these equations are similar to the natural modes of the motion of fluid between two vertical walls of d_r apart, with no energy dissipation. These like the form of a standing wave between the hulls.

It should be noted that another resonance peak of hydrodynamic coefficient exists between $\omega = 0$ and the first characteristic frequency specified in equation (3.50) in the vertical plane motions. The large negative added mass is observed around $\omega\sqrt{L/g} = 3.05$ in the heave and pitch modes. For heaving motion of two-dimensional single bodies in a free surface, no negative heave added mass has been reported. Thus the existence of negative added mass for twin-hull bodies strongly suggests the effect of hydrodynamic interaction between the twin hulls. From equation (3.50), the first characteristic frequency of the vertical plane motion is at $\omega\sqrt{L/g} = 7.089$ for the V-1 catamaran. These abrupt discontinuities of results at characteristic frequencies can also be found from the numerical investigations as shown in figures 3.14 to 3.25. In the horizontal plane motions, the apparent discontinuity is observed around non-dimensional encounter frequency $\omega\sqrt{L/g} = 5.012$ from the hydrodynamic coefficient

curves of the V-1 catamaran. This is a kind of antisymmetric standing wave interaction and can be predicted by using the minimum distance between the hulls in equation (3.51). There are no any troughs observed among zero and first characteristic frequency in the antisymmetric interaction to the V-1 catamaran configuration.

The cross coupled hydrodynamic coefficients are well satisfied the Timman-Newman's (1962) symmetry relationships at the zero forward speed condition as found in hydrodynamic coefficient curves. Figures 3.26 to 3.28 show the wave exciting forces, moments and related phases of the V-1 catamaran in the head sea condition. The symmetric hydrodynamic interaction between twin hulls can also be found in the curves of wave exciting force and moment. The discontinuity of numerical results is very significant at $\omega_0\sqrt{L/g}=3.81$ (related to $\omega\sqrt{L/g}=7.089$) at Fn=0.226. Furthermore, the minor effects appear at $\omega_0\sqrt{L/g}=2.58$ when Froude Number is equal to 0.677.

Validations of the two-dimensional method by the model tests of V-1 catamaran are given in figures 3.29 to 3.34. In this study, the incident wave amplitude was chosen 1cm in order to eliminate the nonlinear effects. Experiments with three different forward speeds, Fn= 0.00, 0.226, 0.677, were carried out in the head sea condition to compare the measurements with theoretical results. Agreement between the experimental data and predictions based on the two-dimensional frequency domain theory for heave and pitch motions is good at zero speed. When the Froude number increases, the analytical method begins to overpredict peak values. The theoretically predicted position of resonance is higher compared to the experimental measurement when the forward speed increases. For the pitch motion predictions, the comparison shows some differences between the numerical results and experimental data in the low frequency region as shown in figures 3.32 and 3.34. The validation studies on the prediction of the small amplitude motions of V-1 catamaran in the head sea condition indicate that the resonance positions of both heave and pitch response curves shift to the lower wave frequency region and the peak amplitudes increase as the model speed increases. In general, phase angle predictions are in good agreement with experimental measurements except some minor discrepancies in the high frequency region. Better predictions are obtained in heave motions than in pitch motions by using the linear frequency domain method.

3.6 Conclusions

A two-dimensional potential theory based on Green's function for estimating the small amplitude motion of catamaran in the frequency domain has been presented. Numerical computations of motion response in oblique waves have been validated by experimental results of three catamarans.

The two-dimensional numerical method can provide reasonable predictions of motion responses of catamarans at low forward speed. Numerical calculations for the ASR5061 catamaran moving at Fn=0.31 in the head sea condition have been performed by using the linear frequency domain technique. It has been found that the theoretical results are in good agreement with the published experimental results except the amplitudes around the resonance region. A good comparison between the numerical predictions and published experimental measurements of Marintek model in heave and pitch modes at Fn=0.49 has been obtained. In the roll motions, the amplitude values predicted by the two-dimensional method are lower than the measured values and the position of resonance obtained from theory shifted to the higher frequency region.

Some interesting phenomena due to the effects of interactions between twin hulls have been found in the calculated hydrodynamic coefficients of the V-1 catamaran. The negative added mass and a set of discrete characteristic frequencies have been observed by using the two-dimensional method. The calculated cross coupled hydrodynamic coefficients agree very well with the Timman-Newman's symmetry relationship for the zero speed case. For the motion response predictions, the heave motions predicted by the two-dimensional method are better than the results for pitch mode. Moreover, it has been found that the phase angle results obtained from the two-dimensional technique are in a good agreement with the experimental measurements. The forward speed effects on the motion response of V-1 catamaran have been investigated by through theoretical and experimental observations. As the forward speed increases, the resonance positions of motion response curves in both heave and pitch modes shift slightly to the lower wave frequency region and the magnitudes of motion responses at resonance frequencies increase. This phenomenon is very important in the slamming problem.

Generally, the theoretical results give a gross overprediction of the motion responses at the resonance frequencies for the three catamarans. However, the

predictions can be improved by incorporating the viscous damping into the two-dimensional potential theory. Details can be found in Fang et al. (1996).

The linear frequency domain method can provide accurate predictions for the small amplitude motions of catamarans travelling in waves. However, the application of the method will be restricted to the prediction of small amplitude motions because of the linearised boundary value assumption. The motion problems are simplified if the motion of the body can be treated as a small perturbation about some mean position. The linearised approaches cannot be used to forecast some of the nonlinear responses of a ship even in moderate sea conditions. In order to solve the problem of large amplitude motions of a catamaran, one needs to develop a nonlinear time domain simulation technique. The author will develop such a technique in the next Chapter.

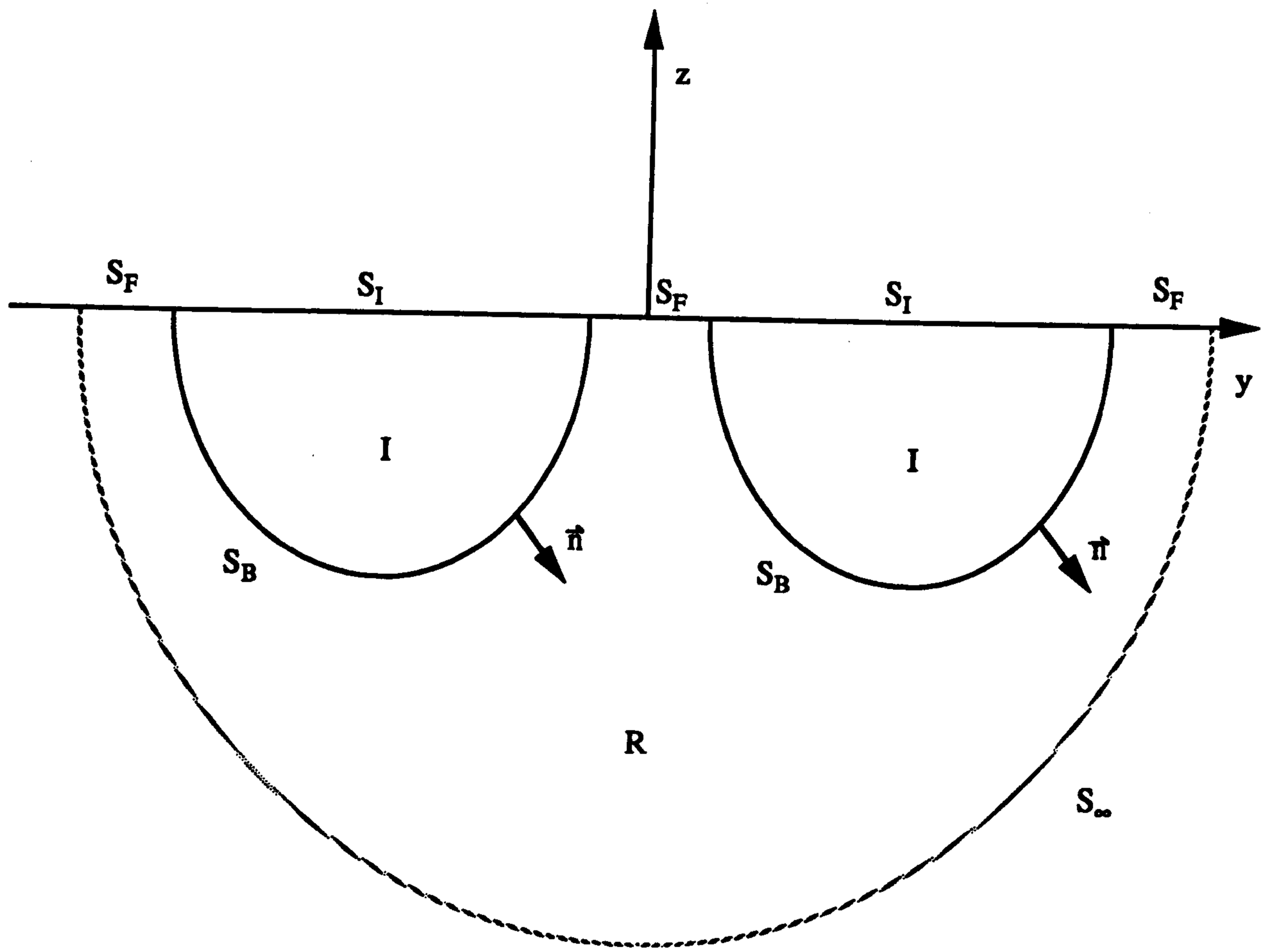

Figure 3.1 : Description of Boundary Value Problem for Twin -Hull Bodies

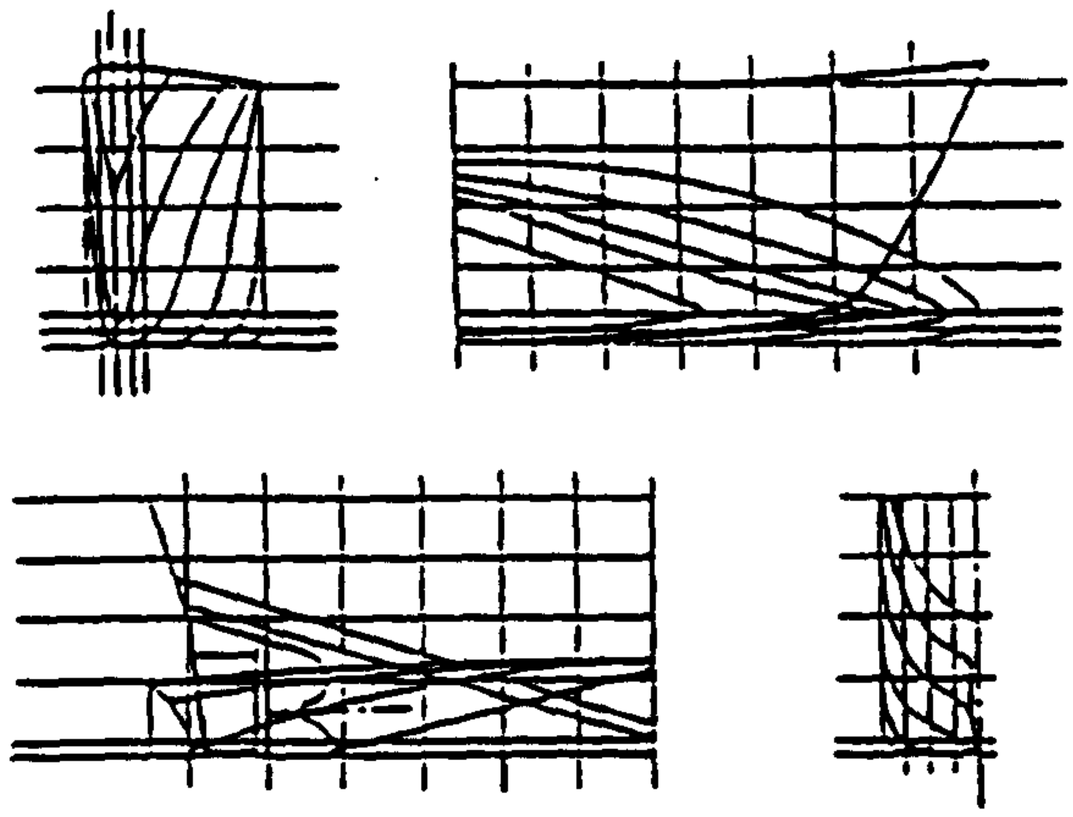

Figure 3.2: Body Plan of the ASR5061 Catamaran Model

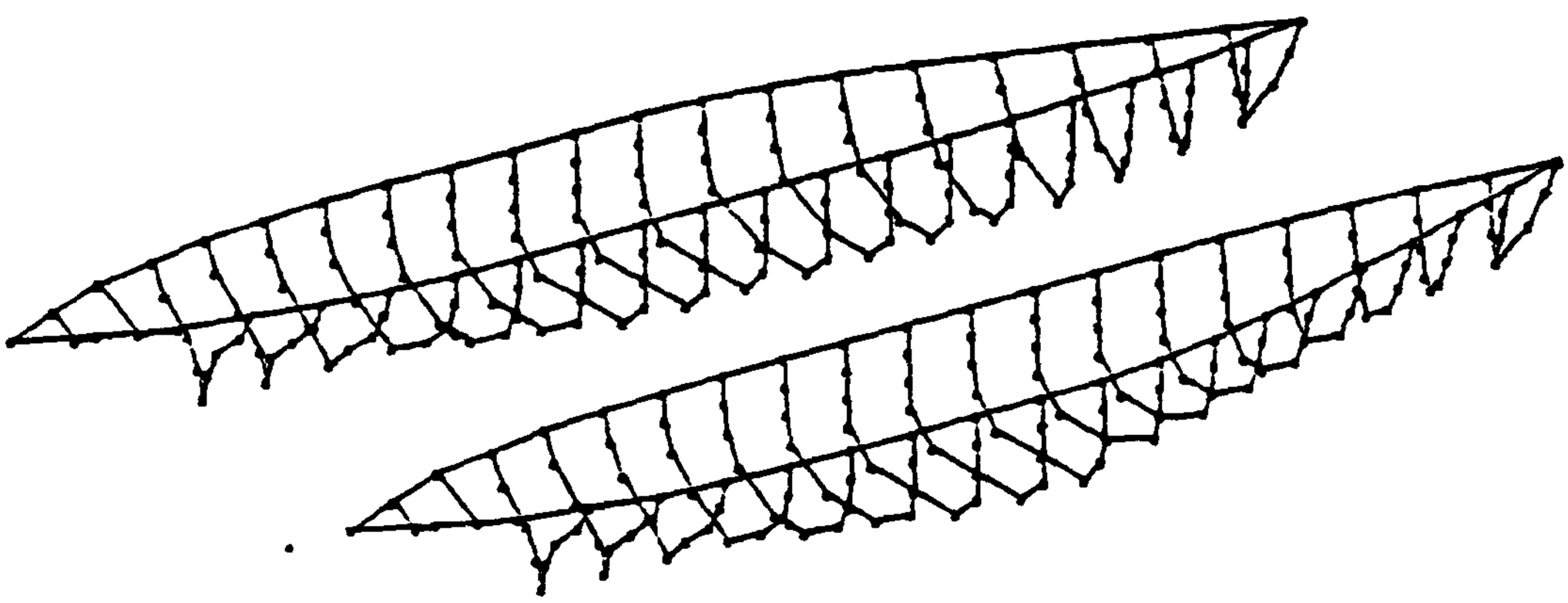

Figure 3.3: Segmentation of the ASR5061 Catamaran Model

Length between perpendiculars:	64.0m
Beam of twin-hull:	26.2m
Beam of demi-hull:	7.3m
Draught:	5.5m
Hull separation between two hulls:	11.6m
Hull centre-line spacing:	18.9m
Displacement:	2750 tons
LCG aft of F.P.:	32.16m
Vertical centre of gravity:	6.4m
Longitudinal radius of gyration:	16.0m
Transverse metacentric height:	17.98m
Calculated natural heaving frequency:	1.33rad/sec
Calculated natural pitching frequency:	1.27rad/sec

Table 3.1 : Main Particulars of the ASR5061 Catamaran Model

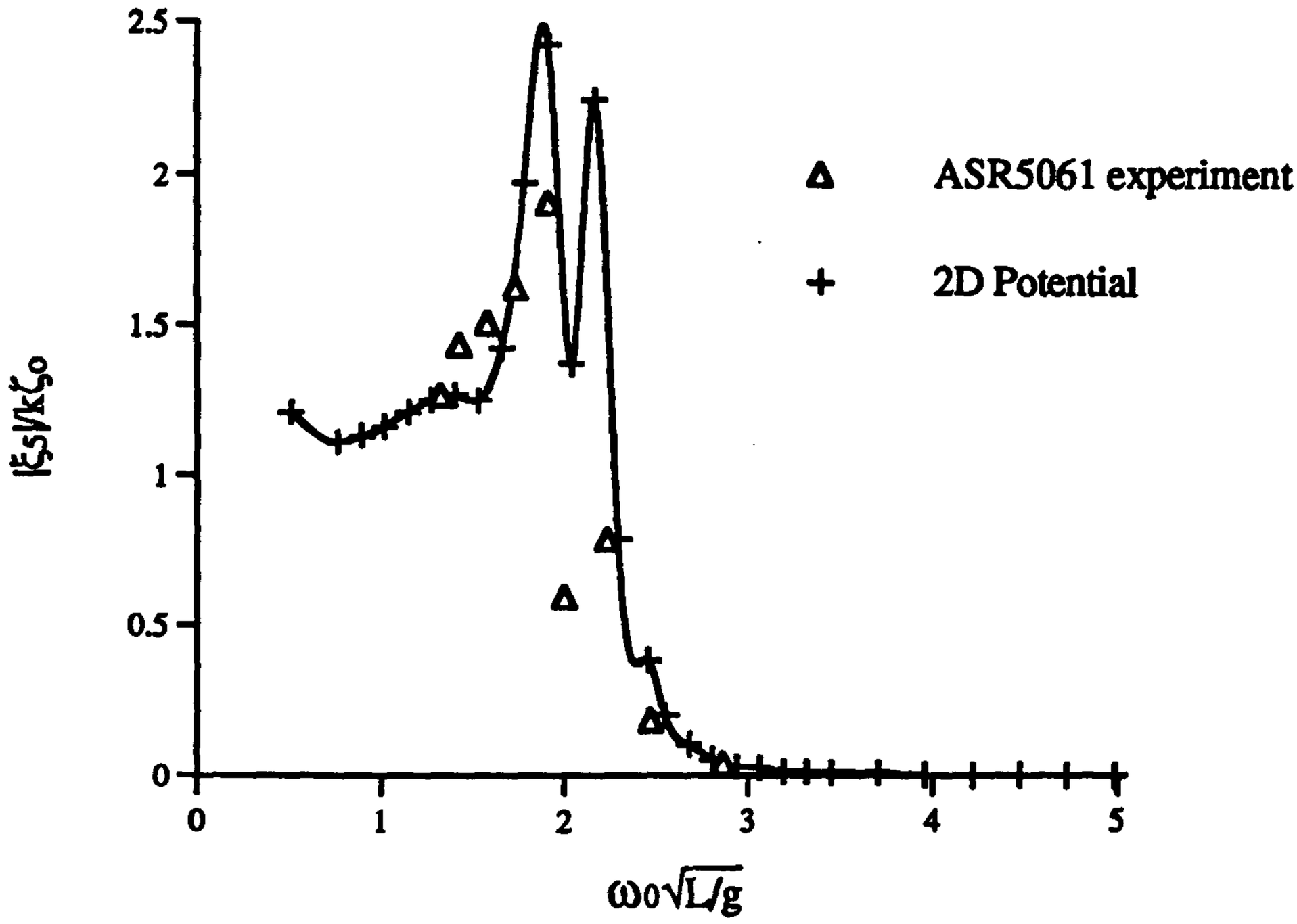

Figure 3.4 : Pitch Motion Response in 180 deg. heading for the ASR5061Catamaran at F_n=0.31.

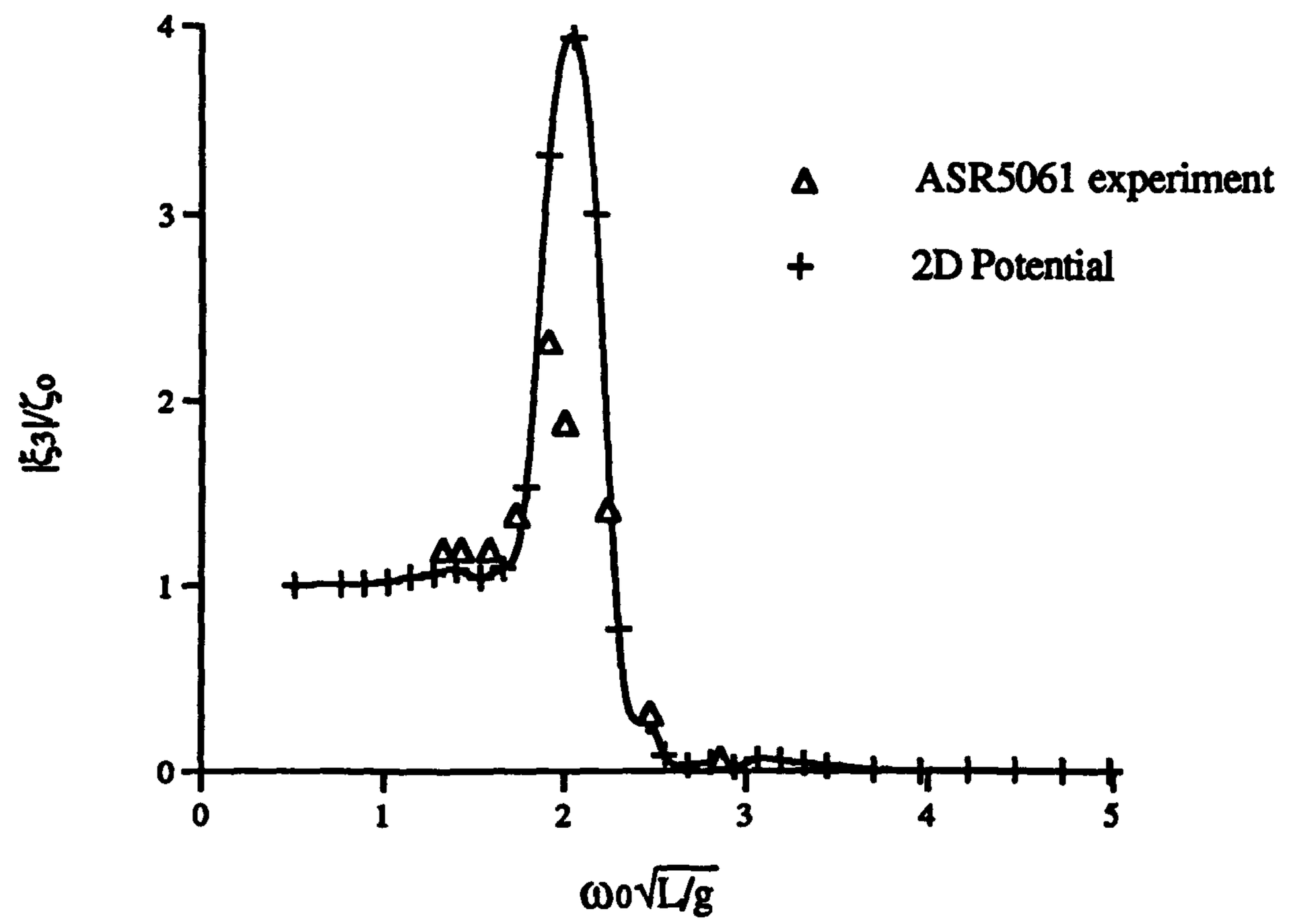

Figure 3.5 : Heave Motion Response in 180 deg. heading for the ASR5061 Catamaran at F_n=0.31.

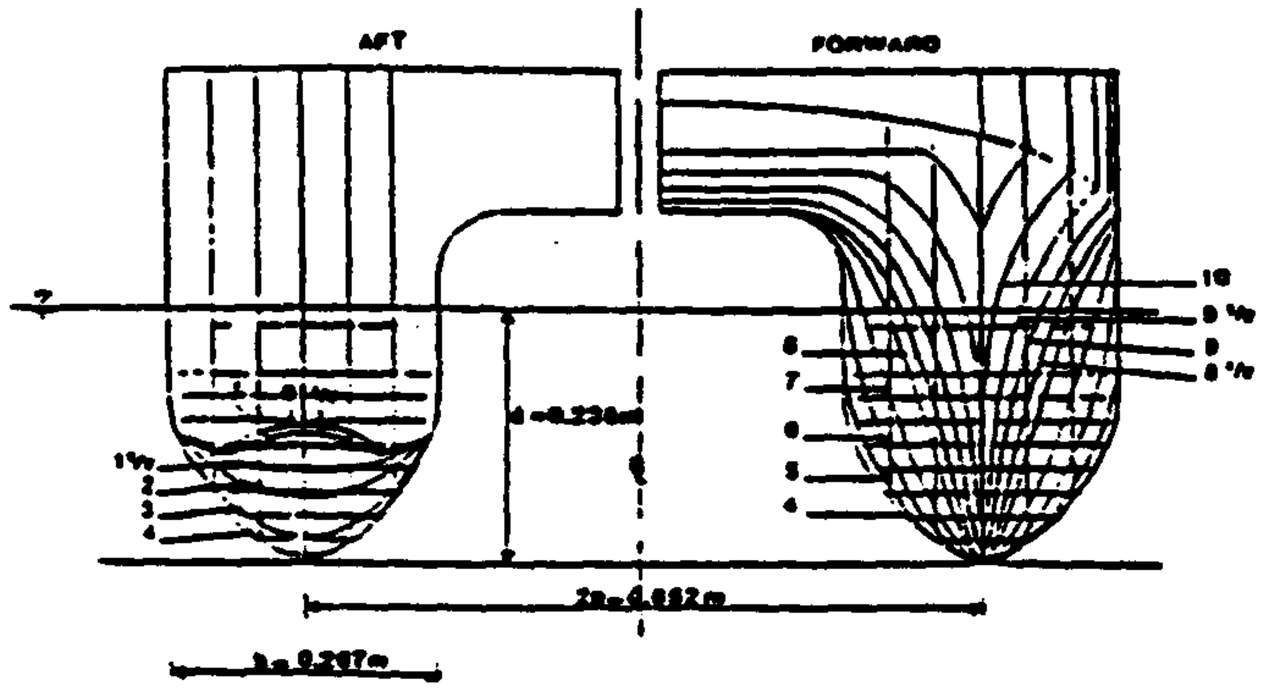

Figure 3.6: Body Plan of the Marintek Catamaran Model

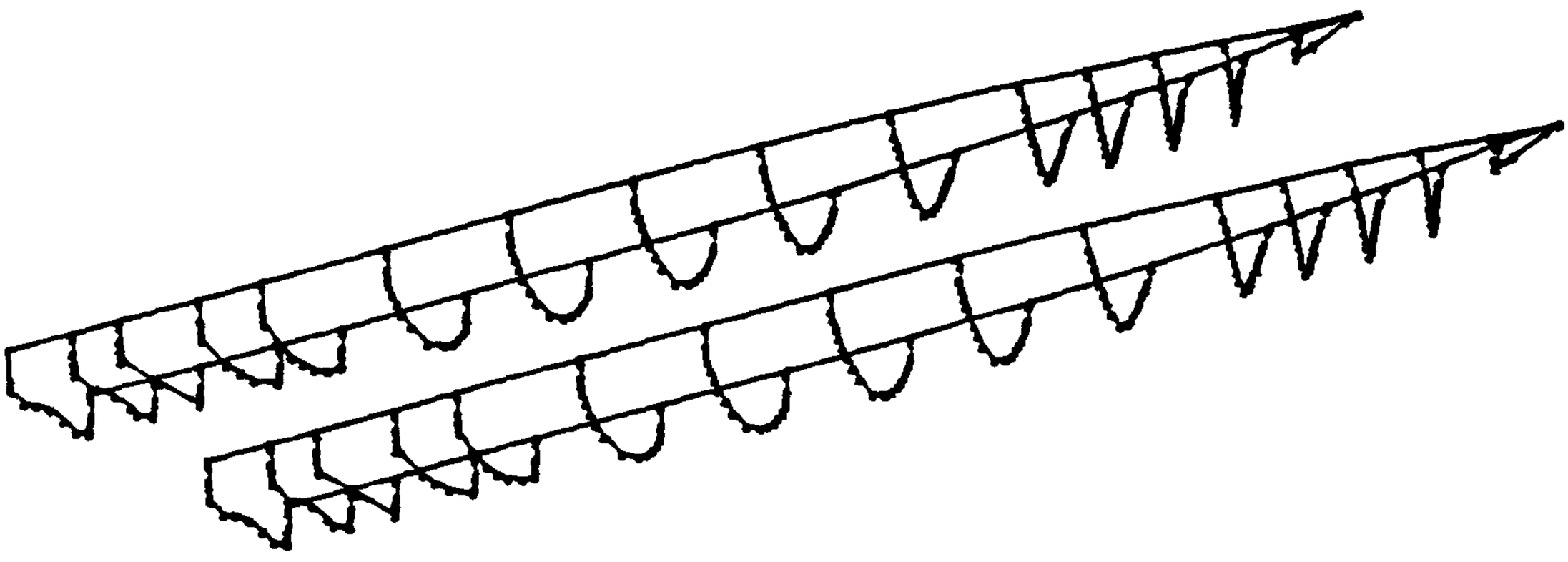

Figure 3.7: Segmentation of the Marintek Catamaran Model

Length between perpendiculars:	3.778m
Beam of twin-hull:	0.918m
Beam of demi-hull:	0.267m
Draught:	0.235m
Displacement:	0.257m^3
Hull centre-line spacing:	0.652m
LCG aft of amidships:	0.296m
VCG from base line:	0.332m
Transverse metacentric height:	0.556m
Radius of gyration (pitch):	0.981m
Radius of gyration (roll):	0.334m
Radius of gyration (yaw):	1.022m
Calculated natural heaving frequency:	7.00rad/sec
Calculated natural pitching frequency:	7.18rad/sec
Calculated natural rolling frequency:	8.87rad/sec

Table 3.2 : Main Particulars of the Marintek Catamaran Model

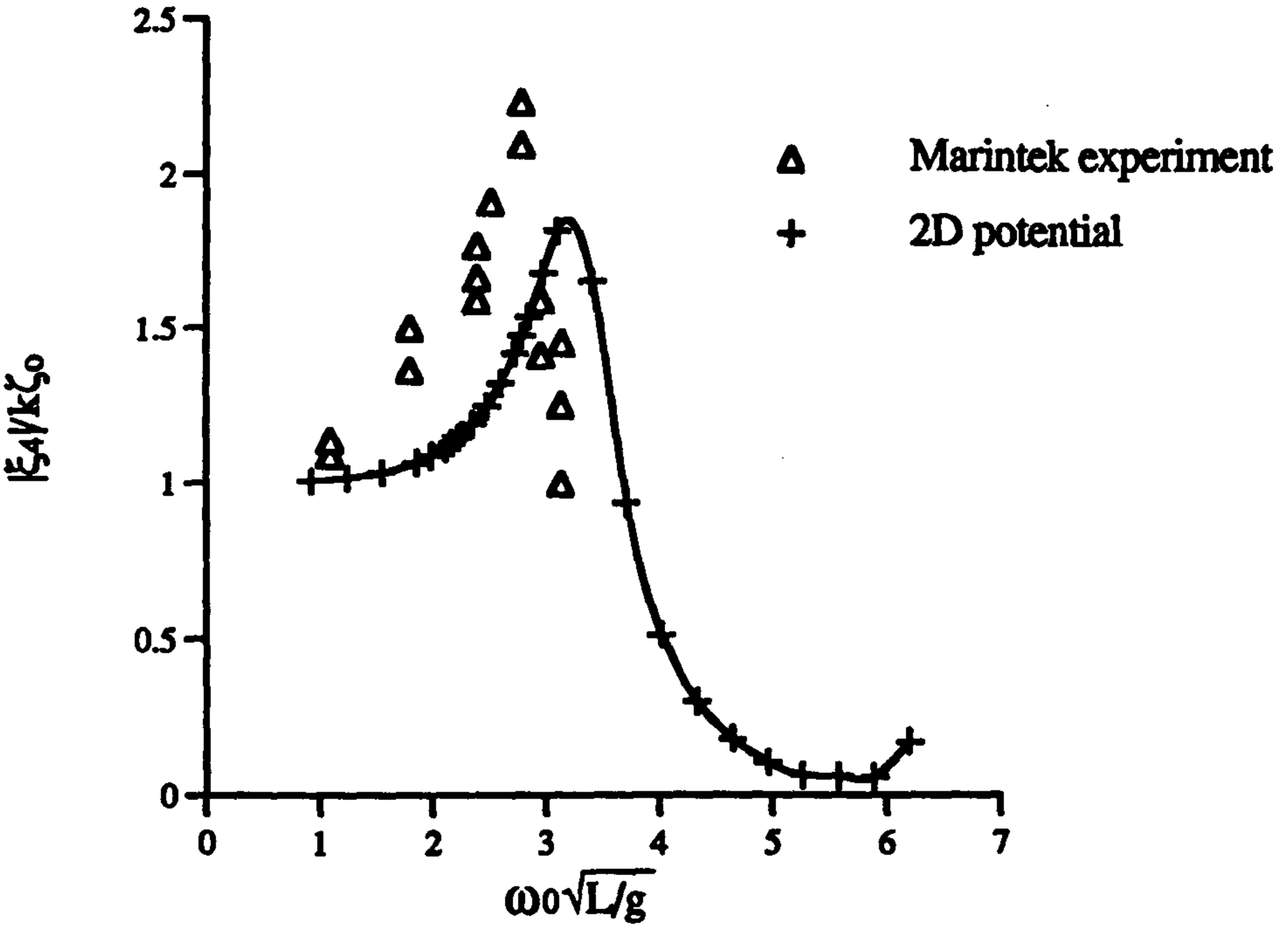

Figure 3.8 : Roll Motion Response in beam sea for the Marintek Catamaran at Fn=0.49

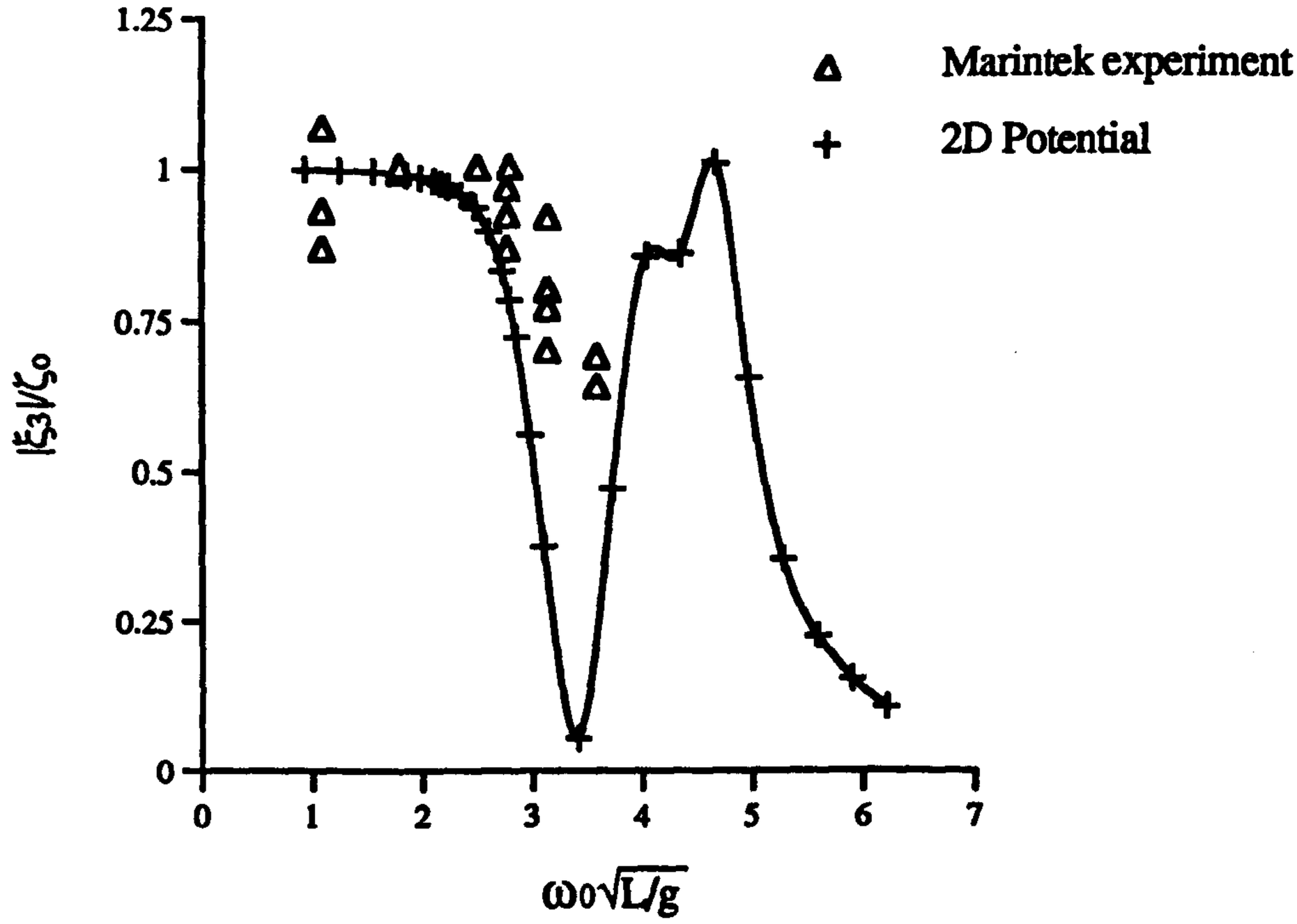

Figure 3.9 : Heave Motion Response in beam sea for the Marintek Catamaran at Fn=0.49

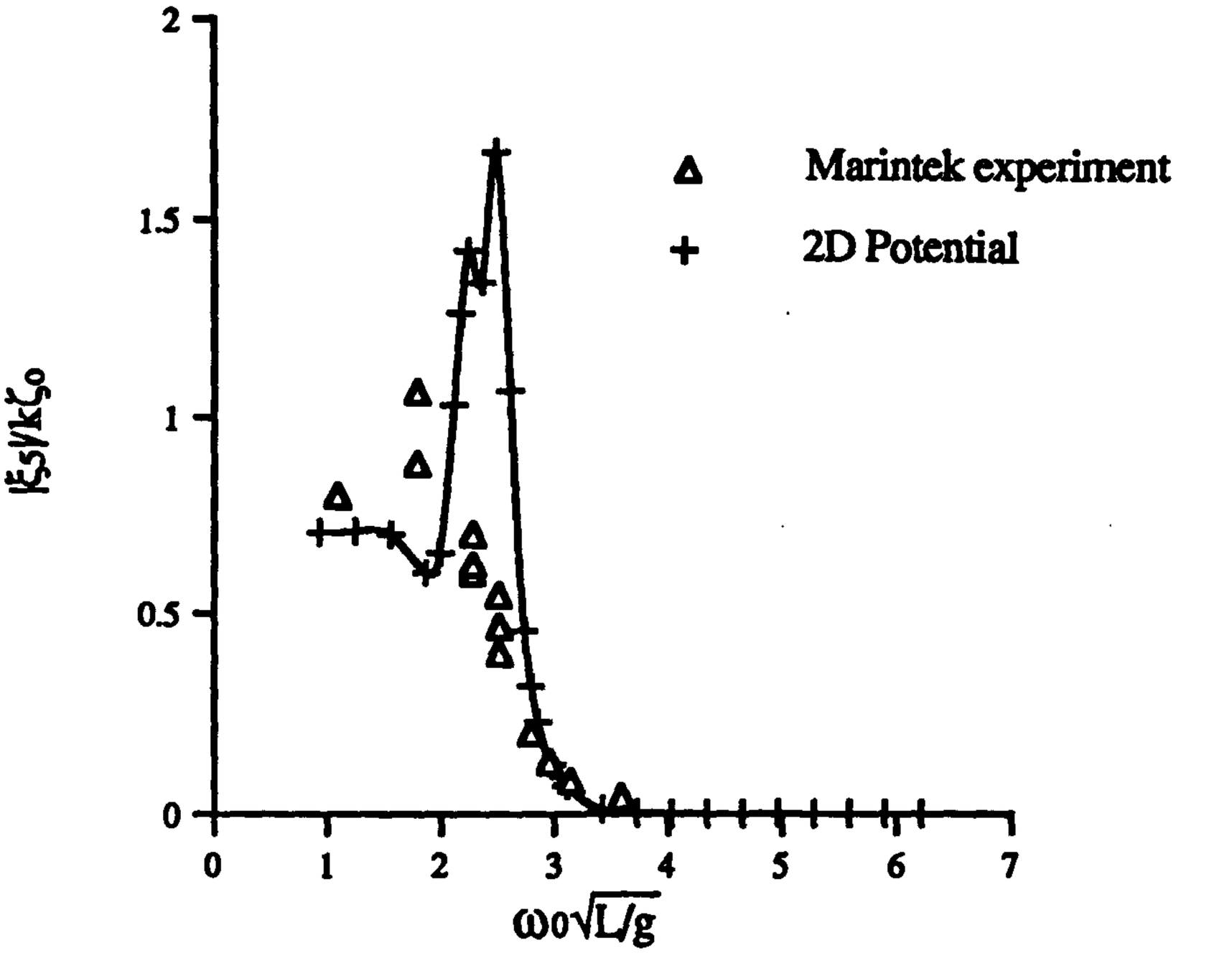

Figure 3.10 : Pitch Motion Response in 135 deg. heading for the Marintek Catamaran at F_n=0.49

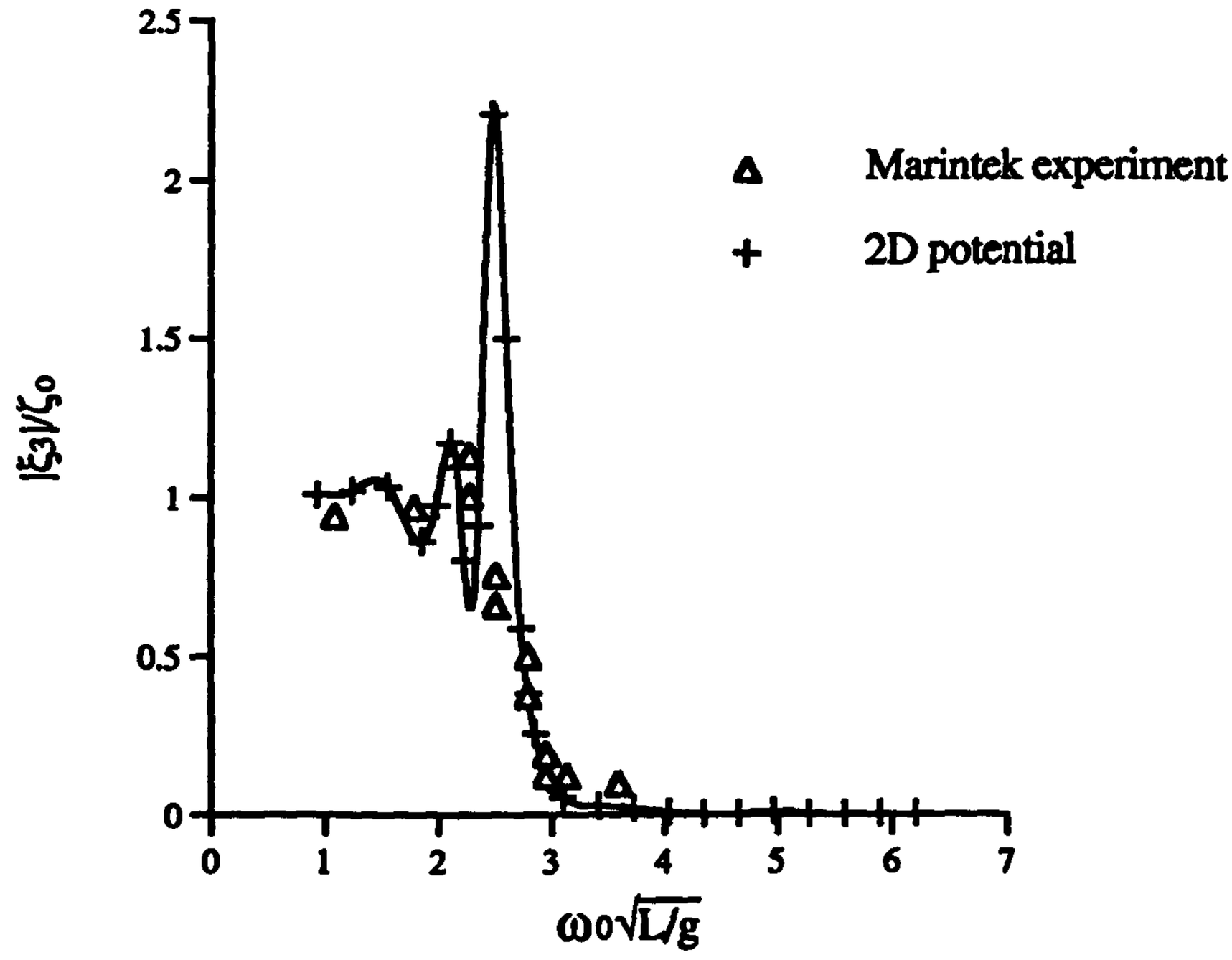

Figure 3.11 : Heave Motion Response in 135 deg. heading for the Marintek Catamaran at F_n=0.49

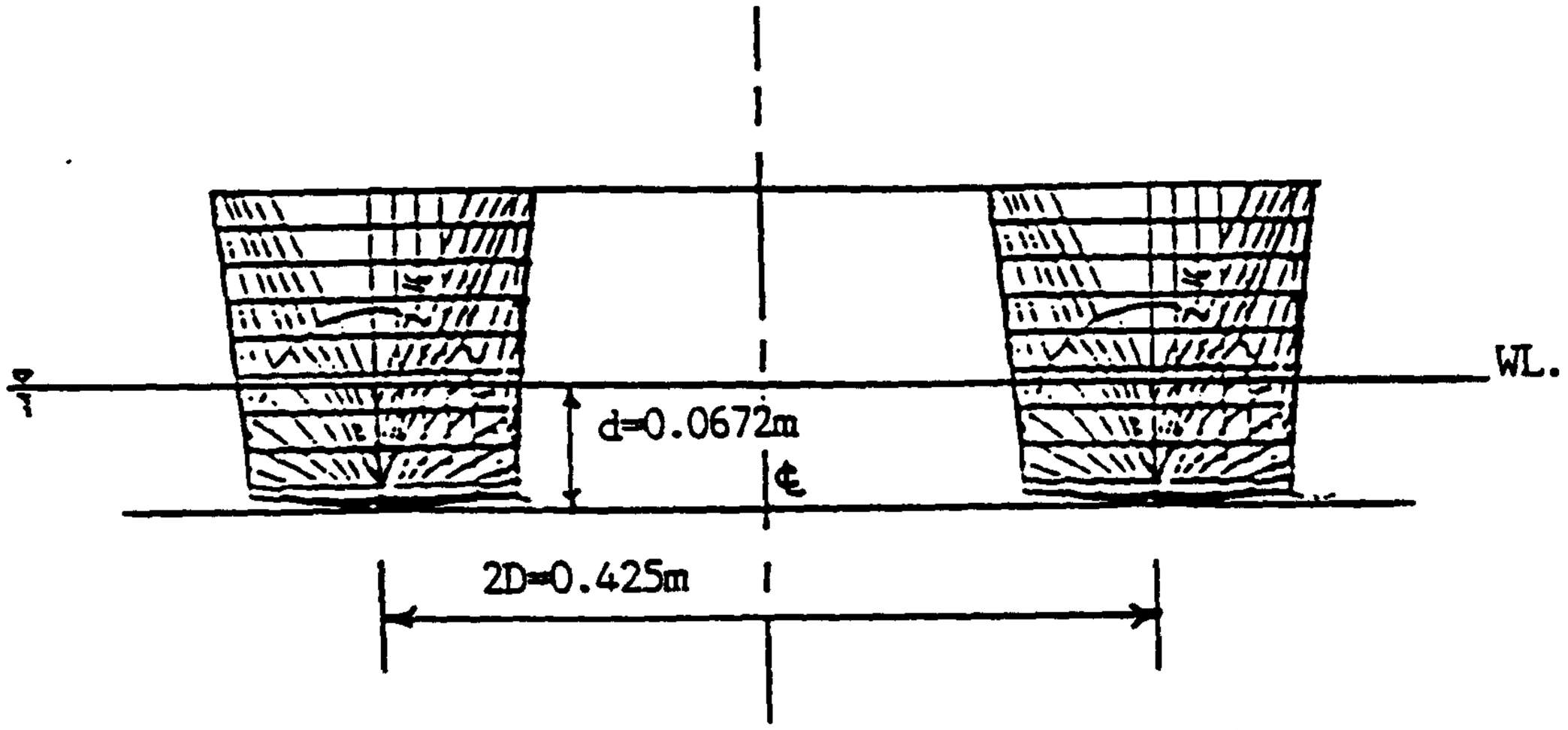

Figure 3.12: Body Plan of the V-1 Catamaran Model

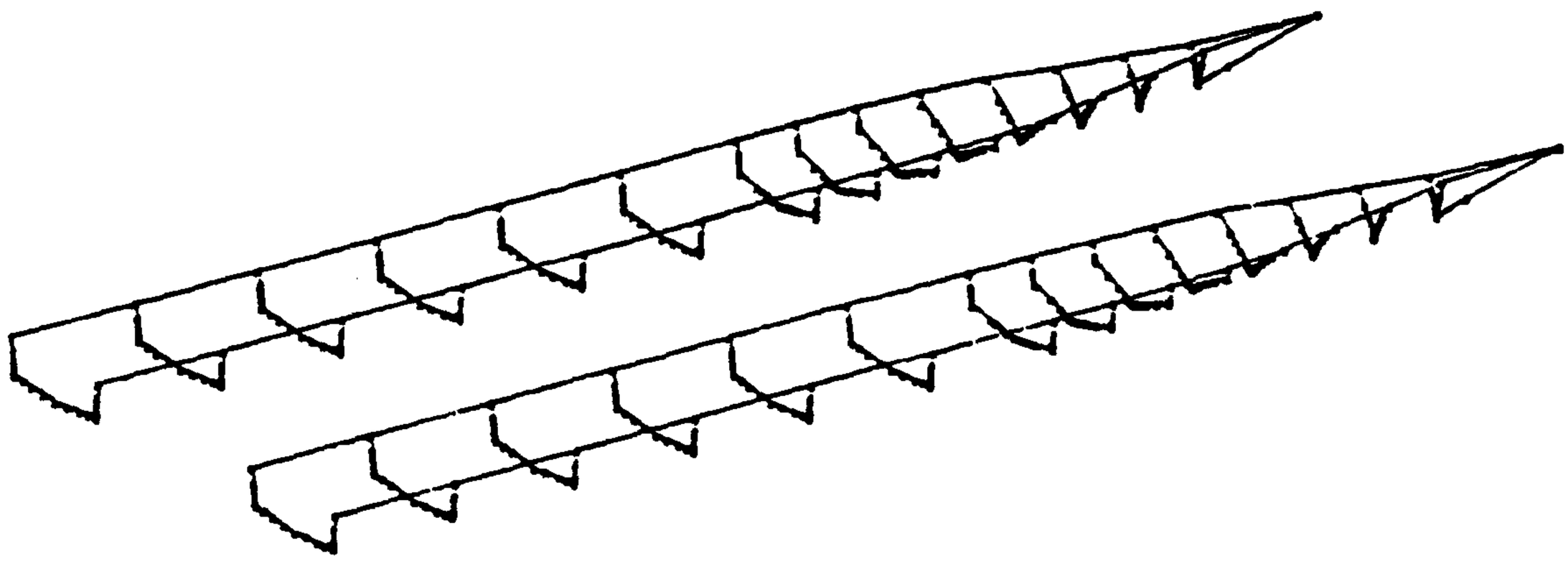

Figure 3.13: Segmentation of the V-1 Catamaran Model

Length between perpendiculars:	2.0m
Beam of twin-hull:	0.6m
Beam of demi-hull:	0.175m
Draught:	0.0672m
Displacement:	0.02847m^3
Hull centre-line spacing:	0.425m
LCG from transom stern:	0.80m
VCG from base line:	0.055m
Radius of gyration (pitch):	0.5138m
Radius of gyration (roll):	0.556m
Initial trim angle (bow down):	0.02deg
Calculated natural heaving frequency:	10.0rad/sec
Calculated natural pitching frequency:	8.20rad/sec

Table 3.3 : Main Particulars of the V-1 Catamaran Model

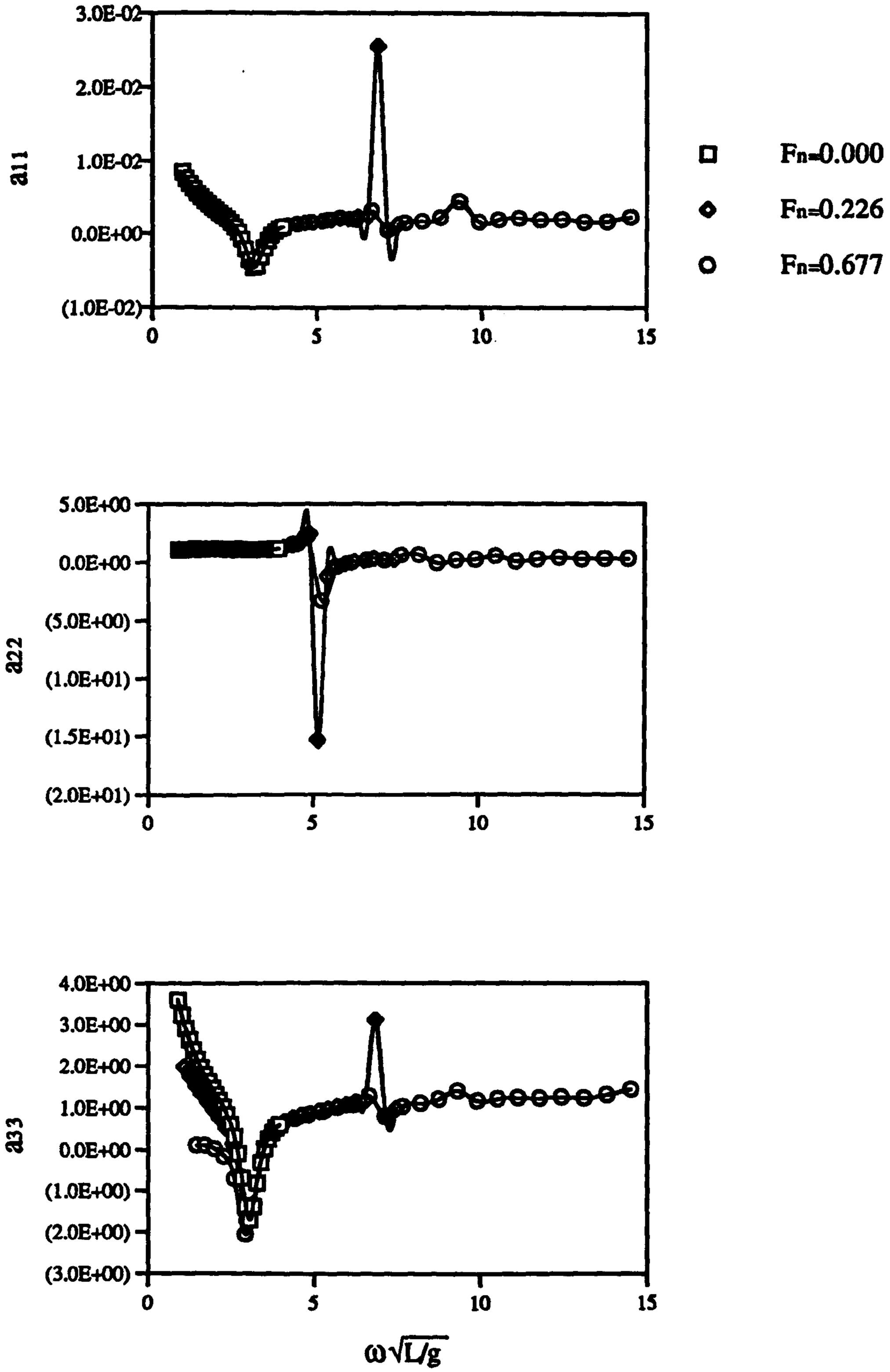

Figure 3.14 : Non-dimensional Added Mass Coefficients of the V-1 Catamaran at various Froude Numbers (Surge-Sway-Heave)

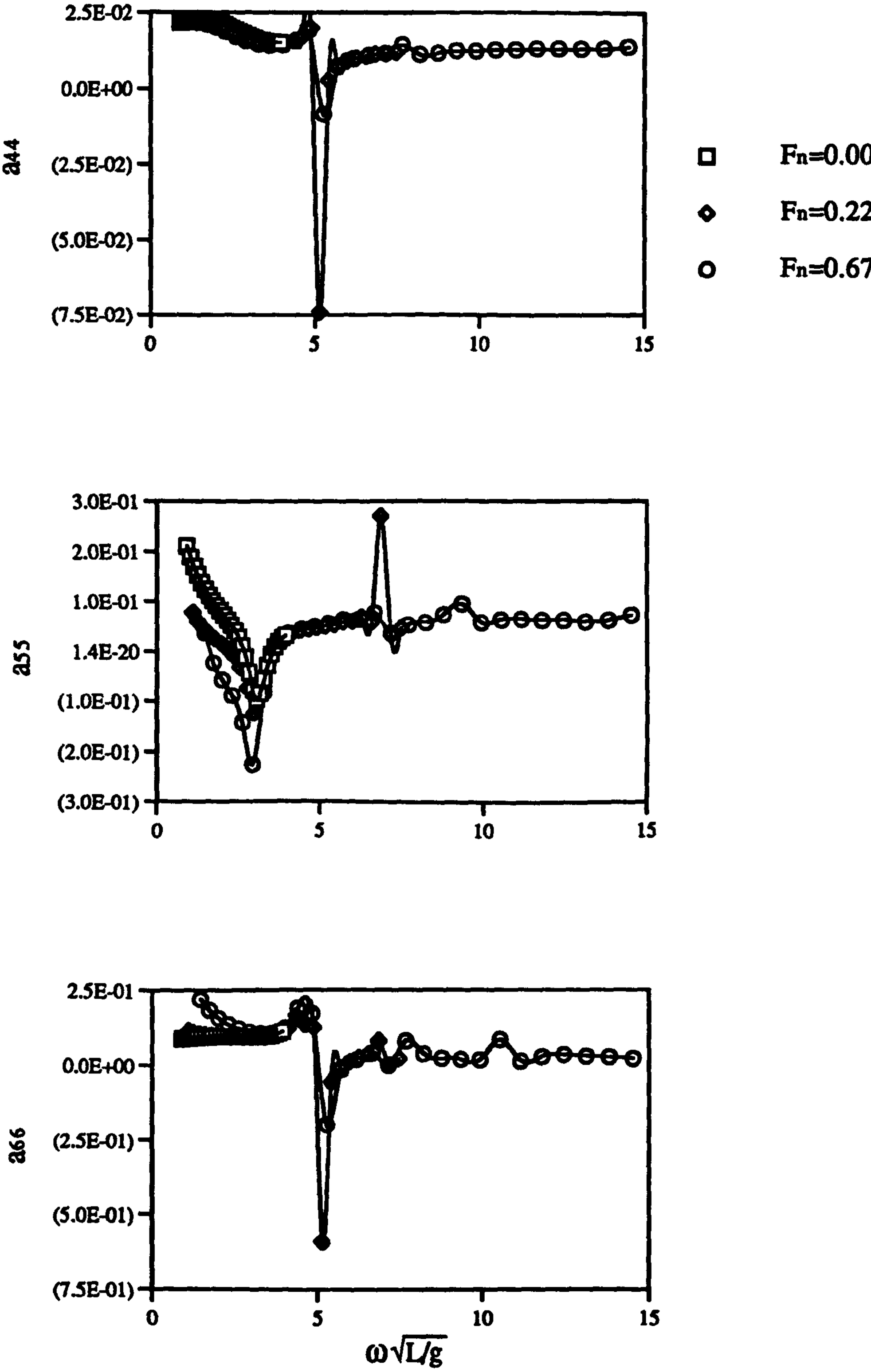

Figure 3.15 : Non-dimensional Added Mass Coefficients of the V-1 Catamaran at various Froude Numbers(Roll-Pitch-Yaw)

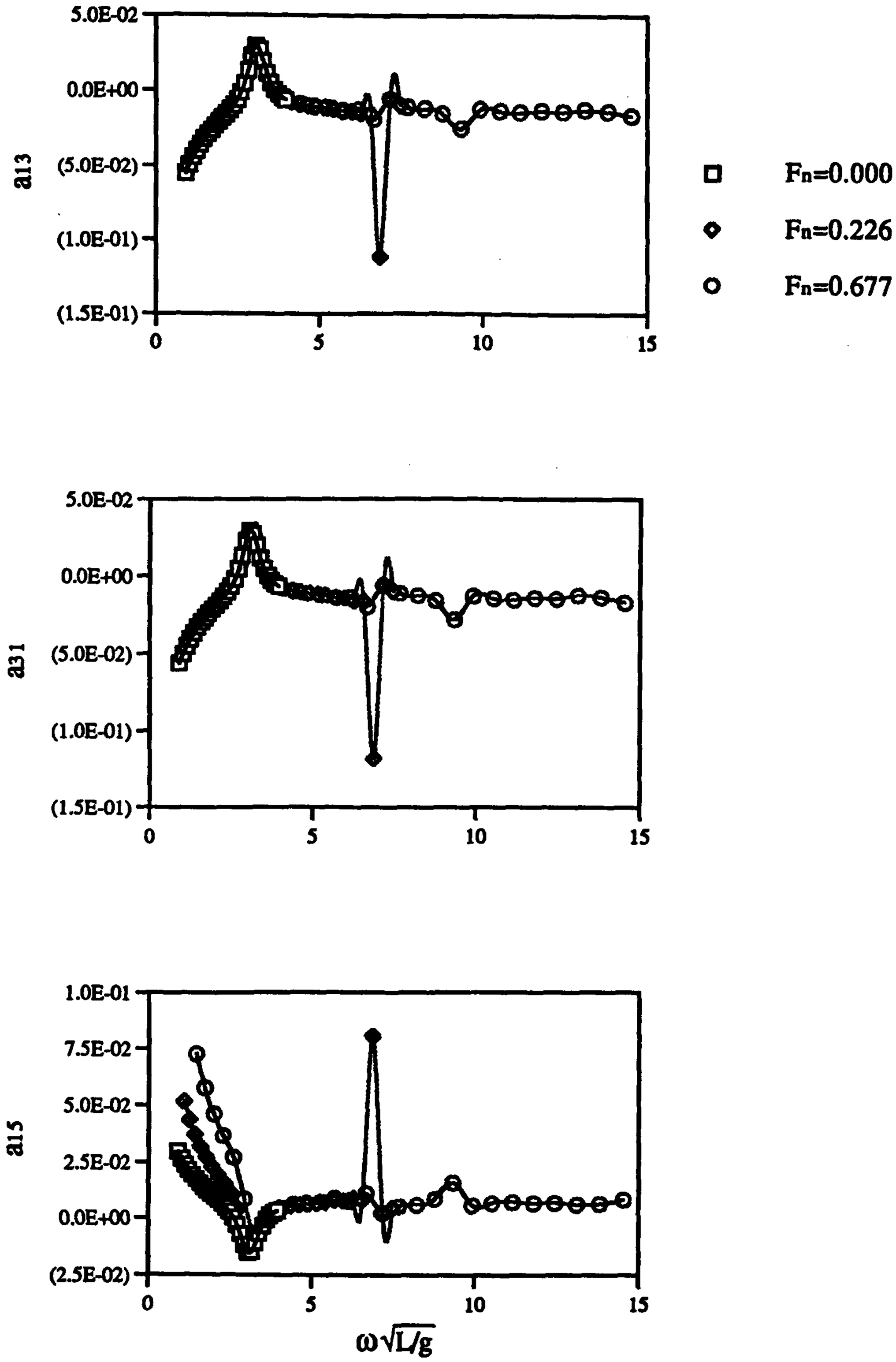

Figure 3.16 : Non-dimensional Coupled Added Mass Coefficients of the V-1 Catamaran at various Froude Numbers(Surge-Heave-Pitch)

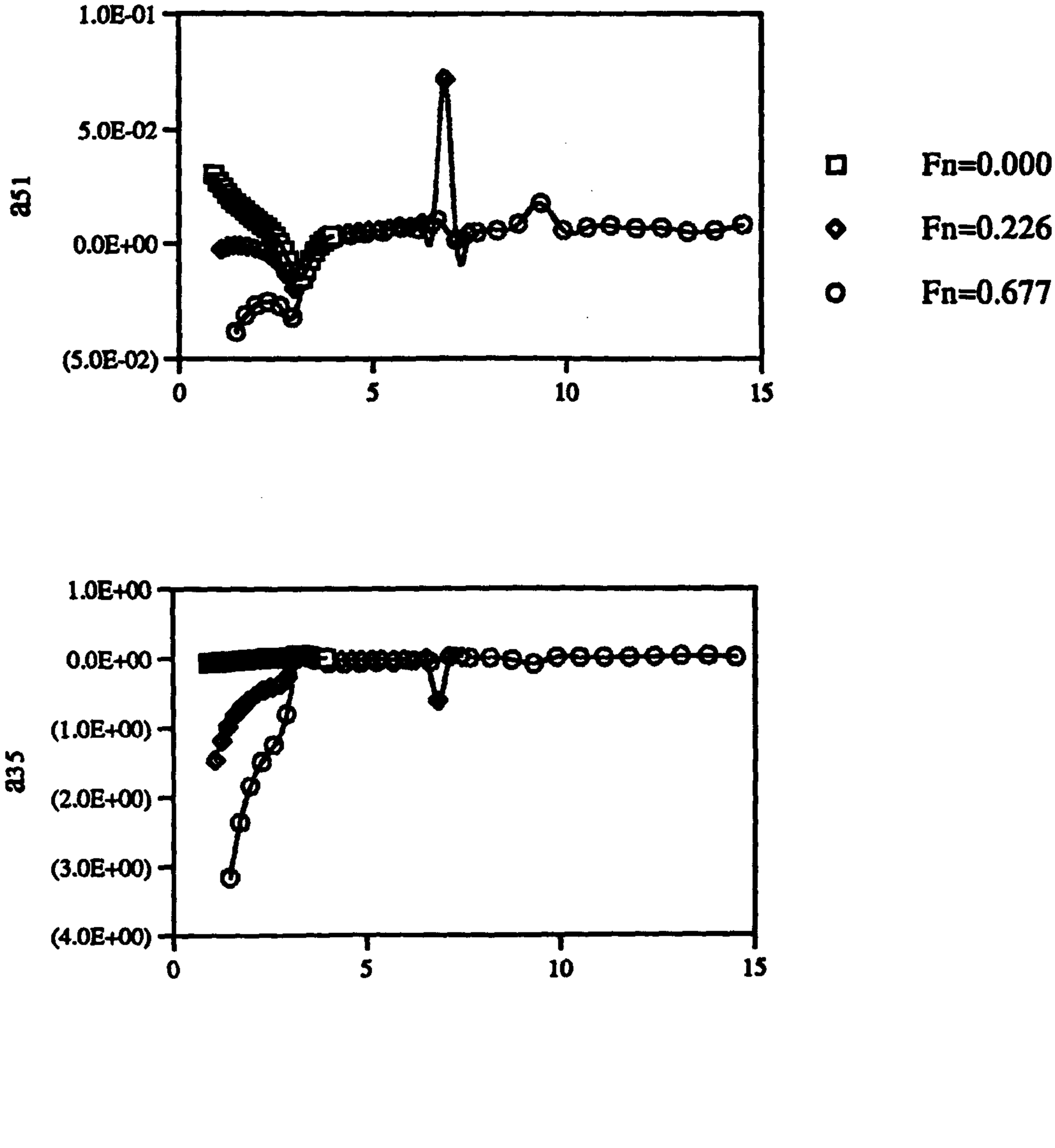

Figure 3.17 : Non-dimensional Coupled Added Mass Coefficients of the V-1 Catamaran at various Froude Numbers(Surge-Heave-Pitch)

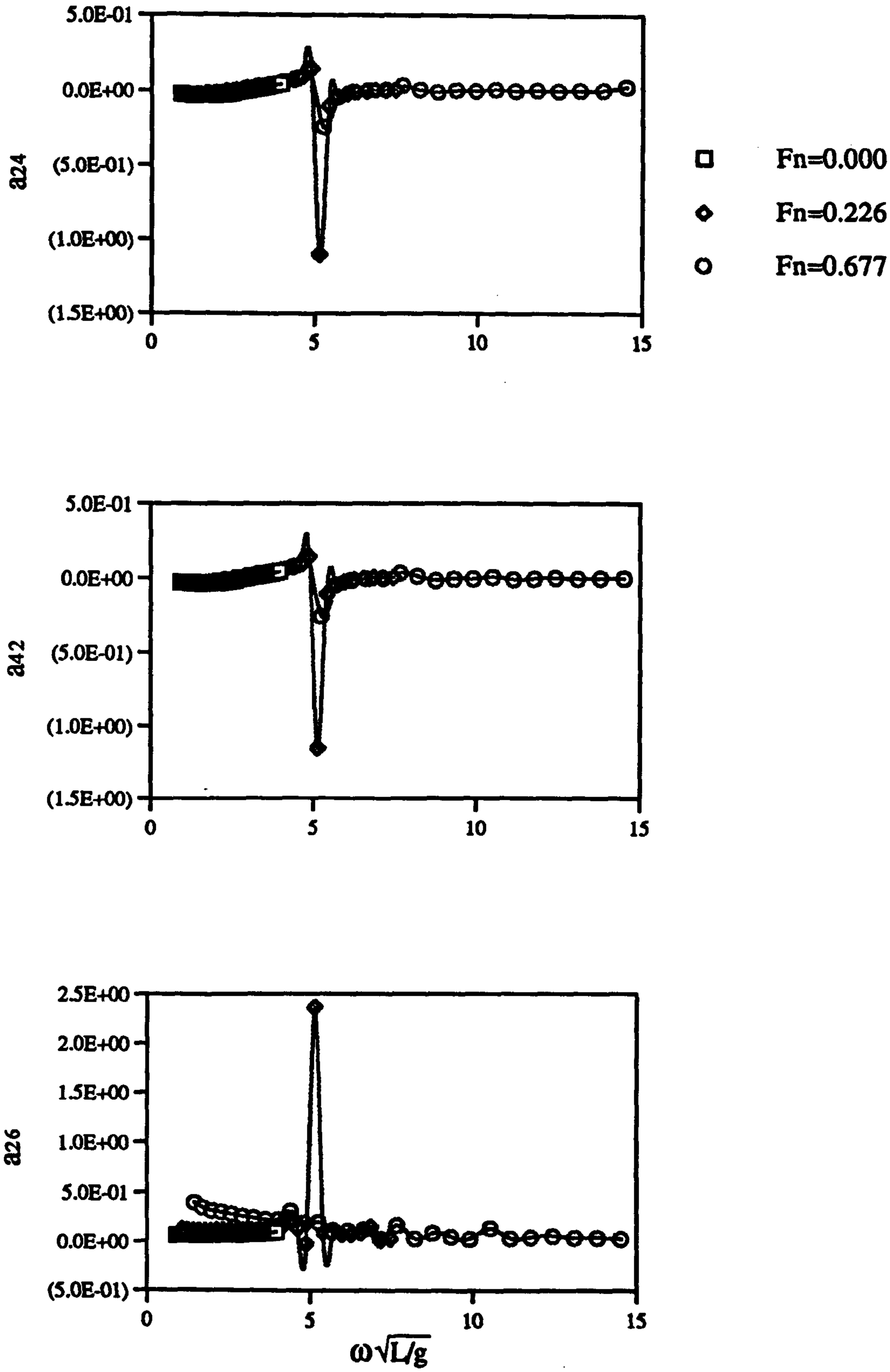

Figure 3.18 : Non-dimensional Coupled Added Mass Coefficients of the V-1 Catamaran at various Froude Numbers(Sway-Roll-Yaw)

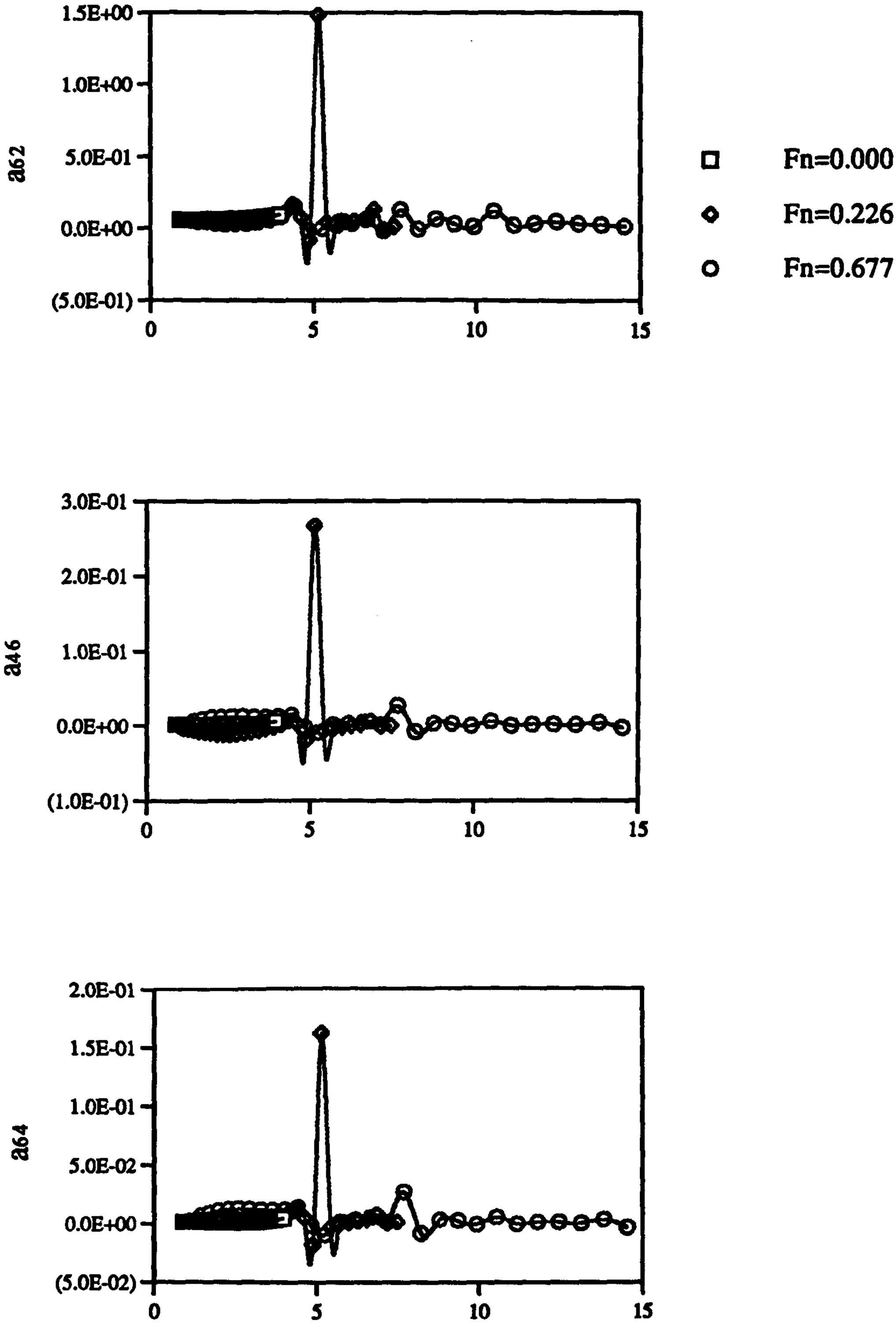

Figure 3.19 : Non-dimensional Coupled Added Mass Coefficients of the V-1 Catamaran at various Froude Numbers(Sway-Roll-Yaw)

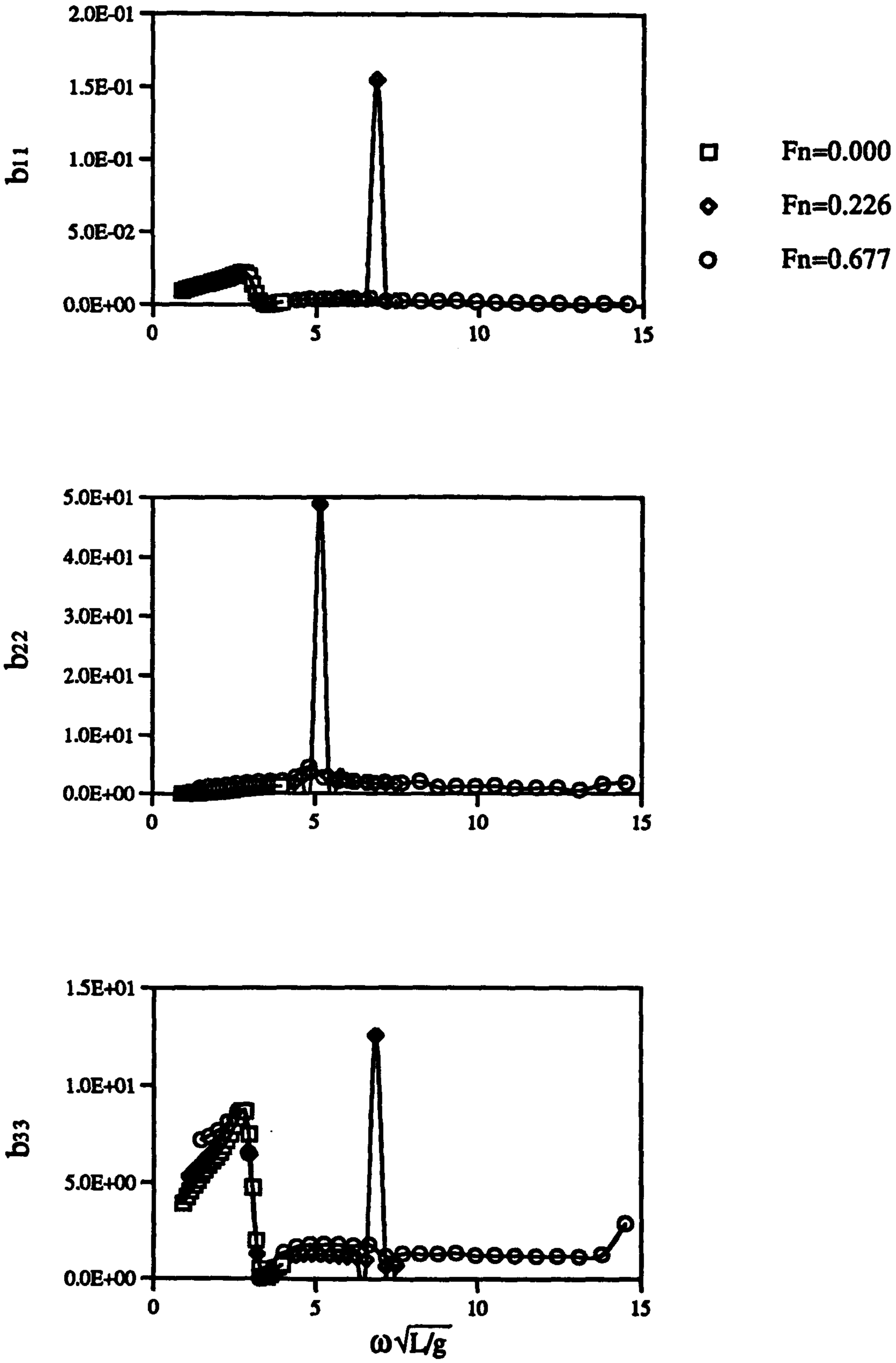

Figure 3.20 : Non-dimensional Damping Coefficients of the V-1 Catamaran at various Froude Numbers(Surge-Sway-Heave)

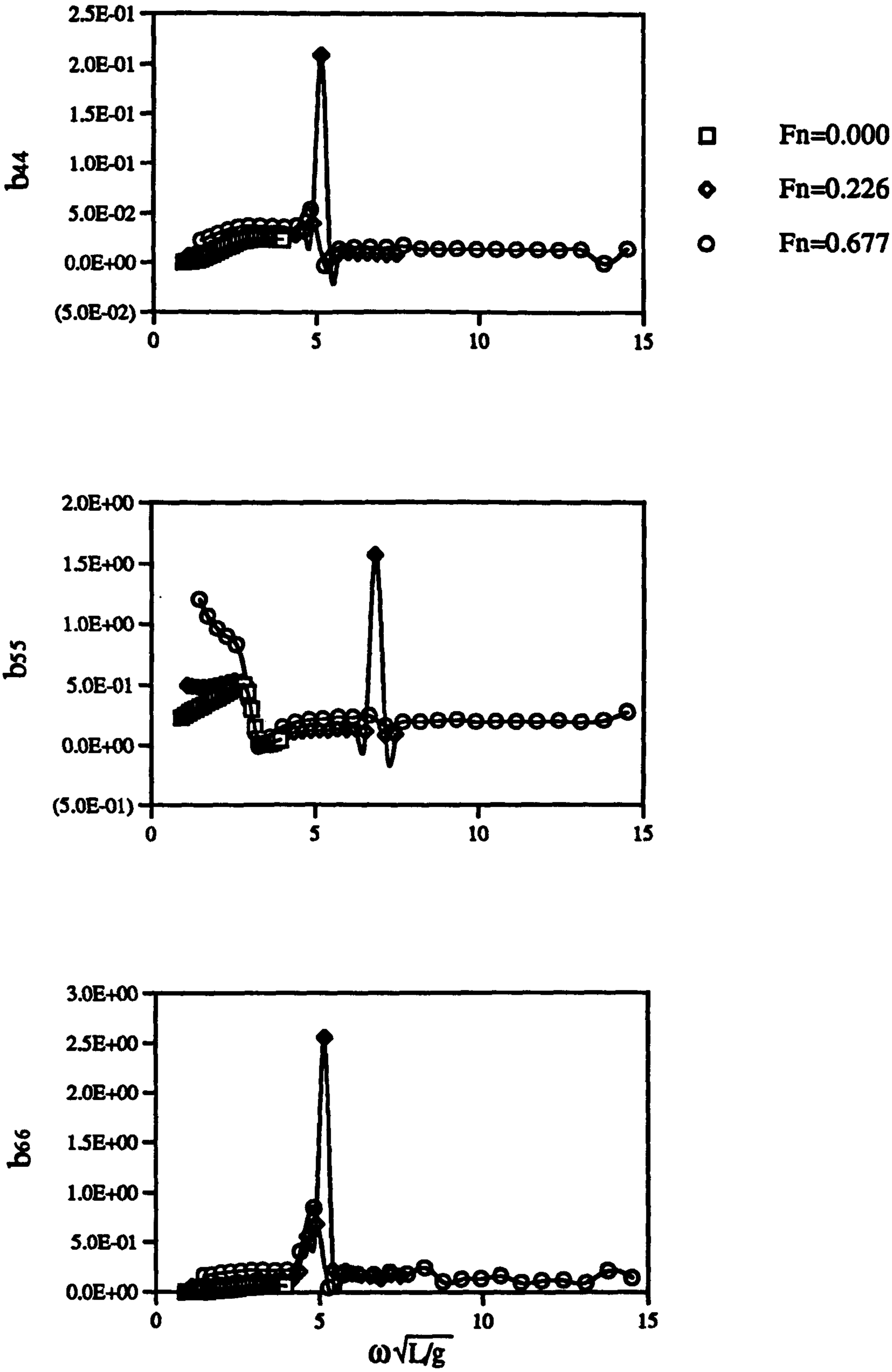

Figure 3.21 : Non-dimensional Damping Coefficients of the V-1 Catamaran at various Froude Numbers(Roll-Pitch-Yaw)

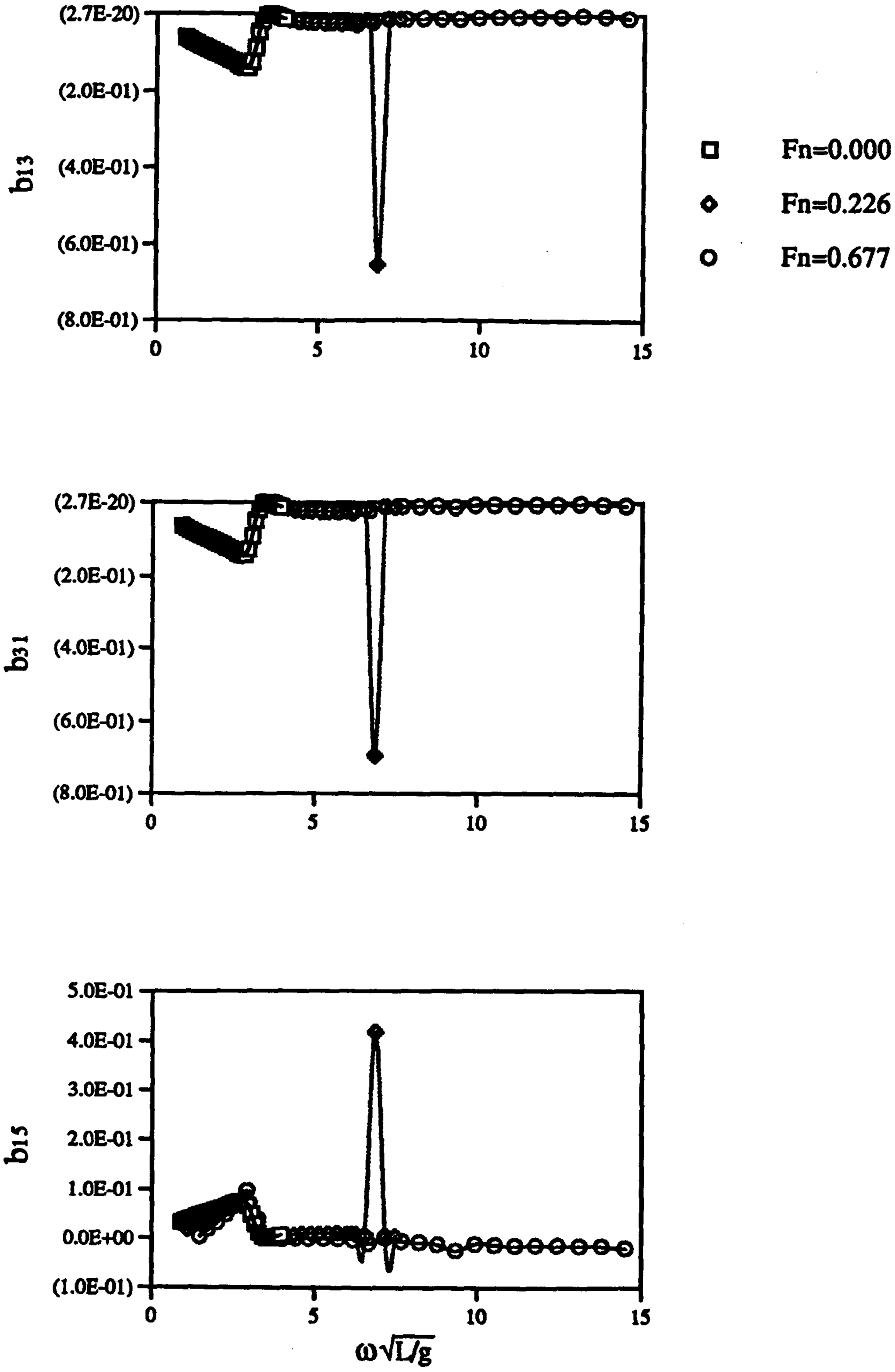

Figure 3.22 : Non-dimensional Coupled Damping Coefficients of the V-1 Catamaran at various Froude Numbers(Surge-Heave-Pitch)

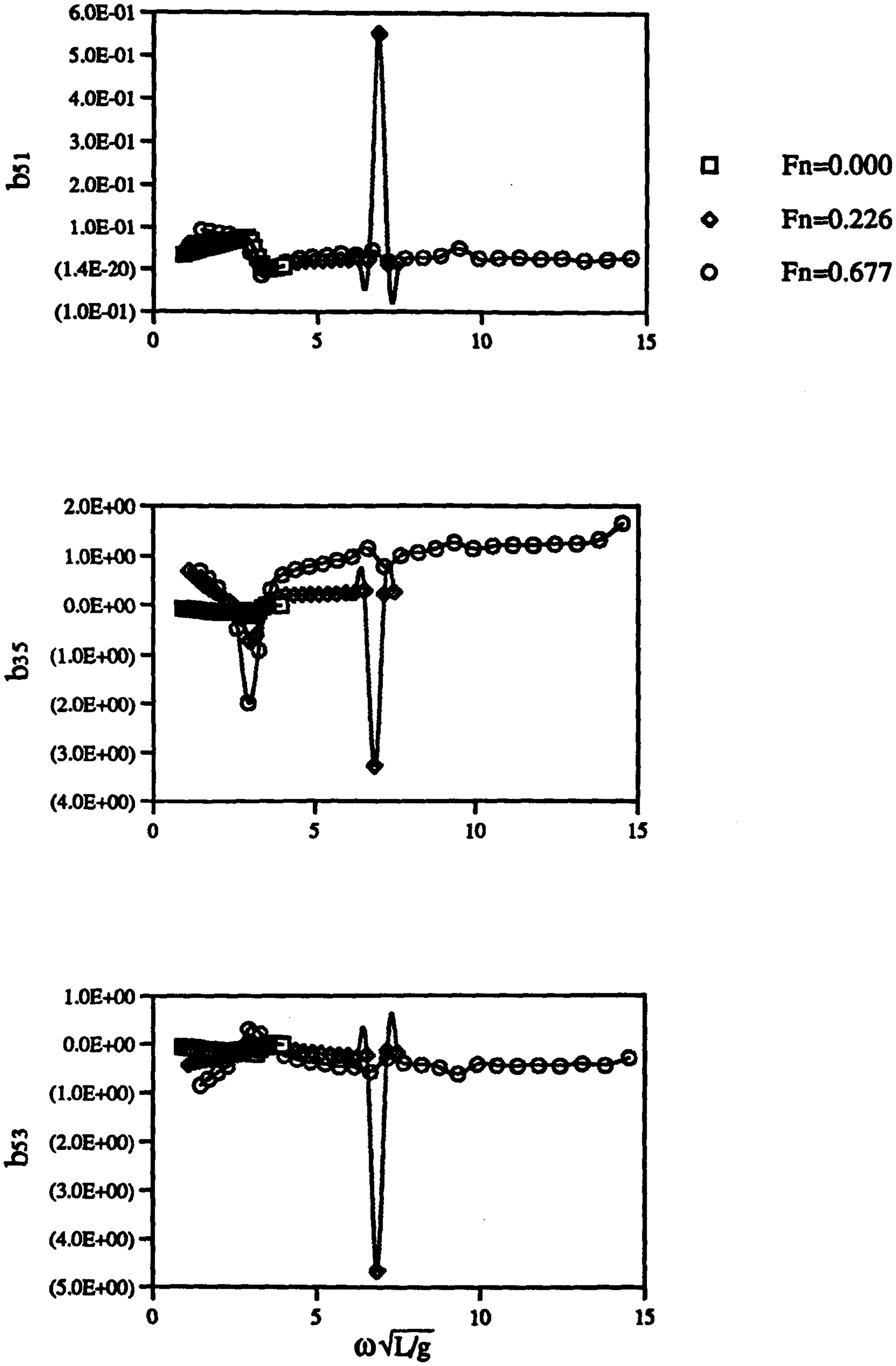

Figure 3.23 : Non-dimensional Coupled Damping Coefficients of the V-1 Catamaran at various Froude Numbers(Surge-Heave-Pitch)

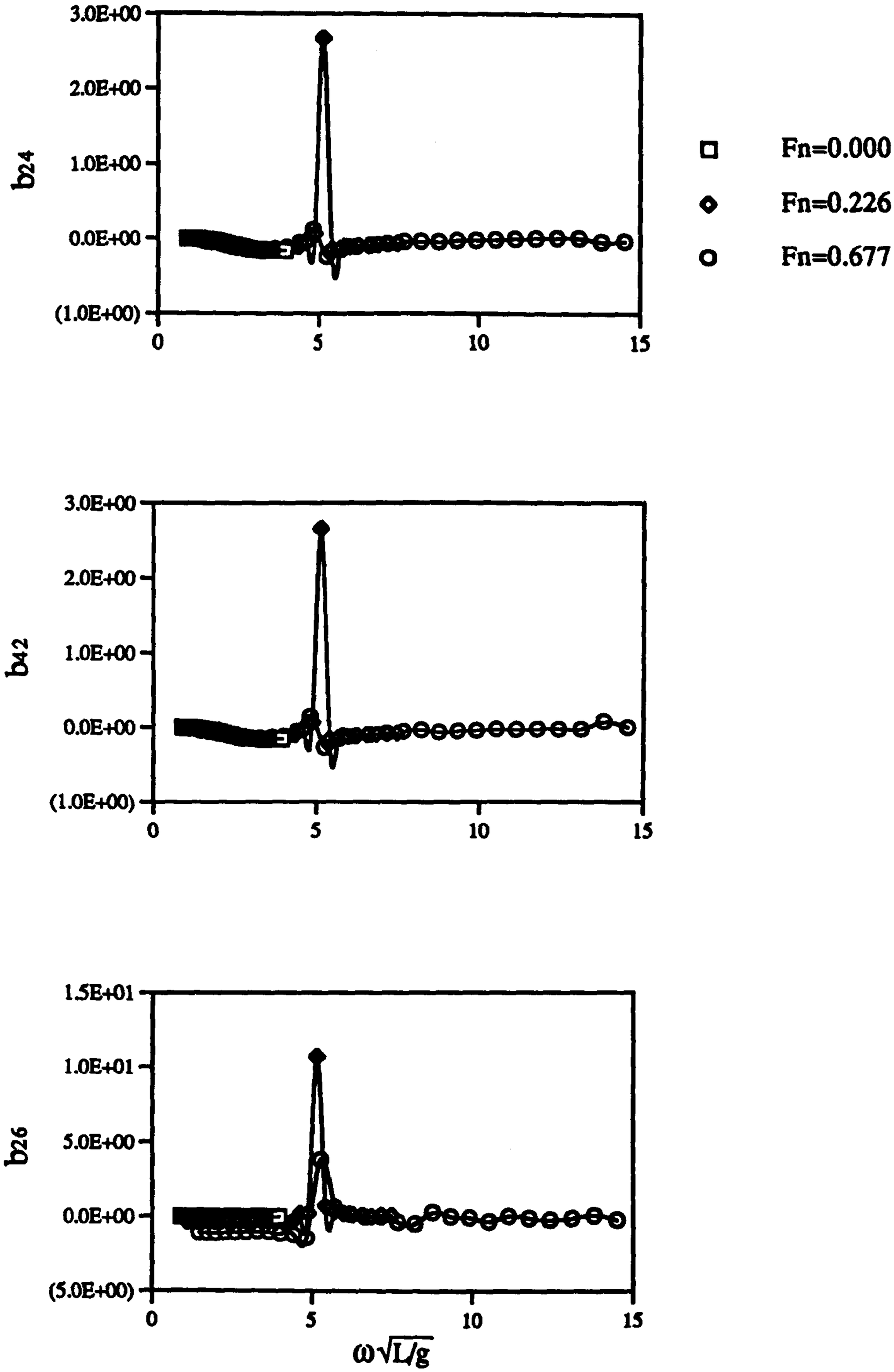

Figure 3.24 : Non-dimensional Coupled Damping Coefficients of the V-1 Catamaran at various Froude Numbers(Sway-Roll-Yaw)

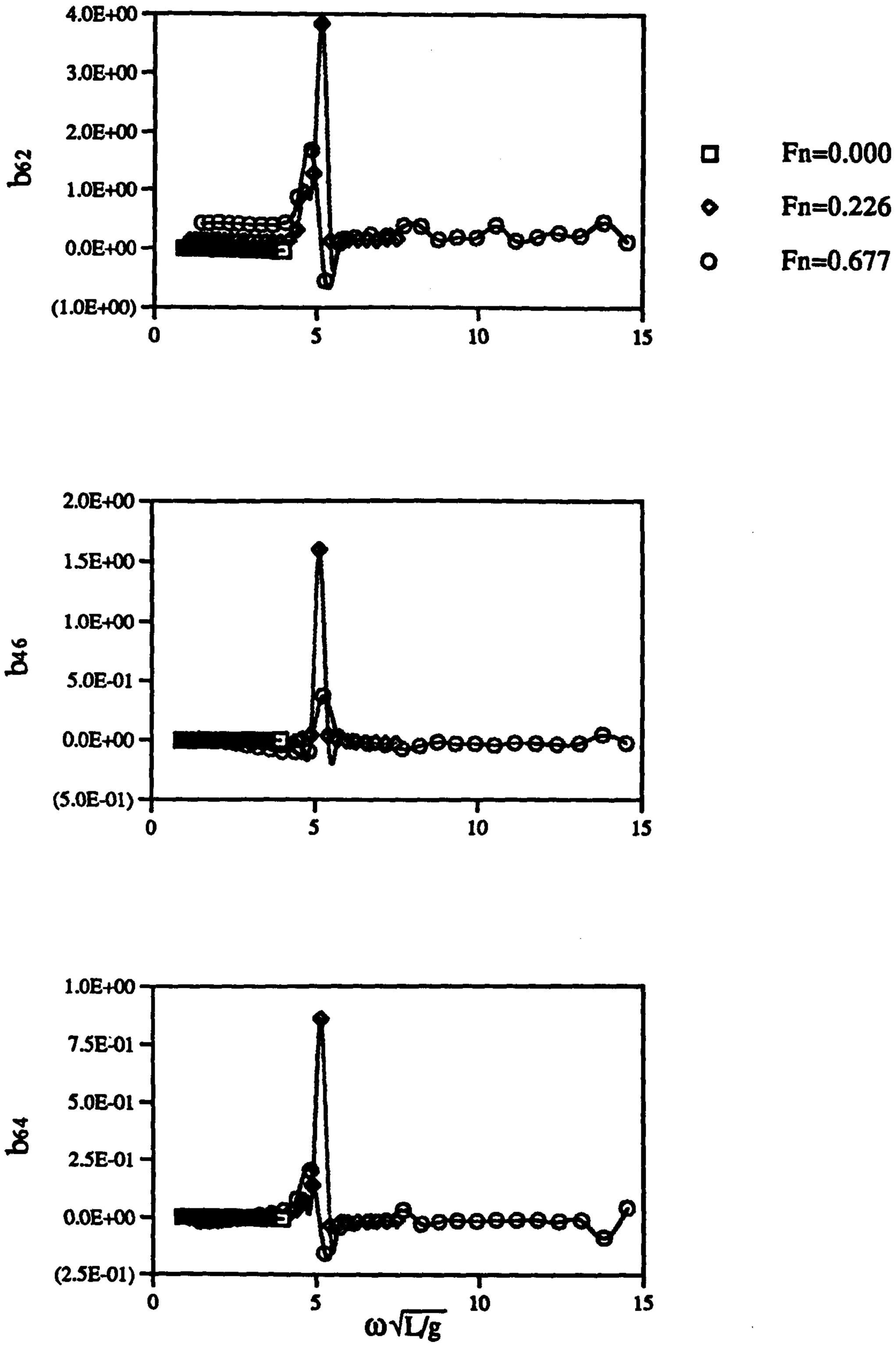

Figure 3.25 : Non-dimensional Coupled Damping Coefficients of the V-1 Catamaran at various Froude Numbers(Sway-Roll-Yaw)

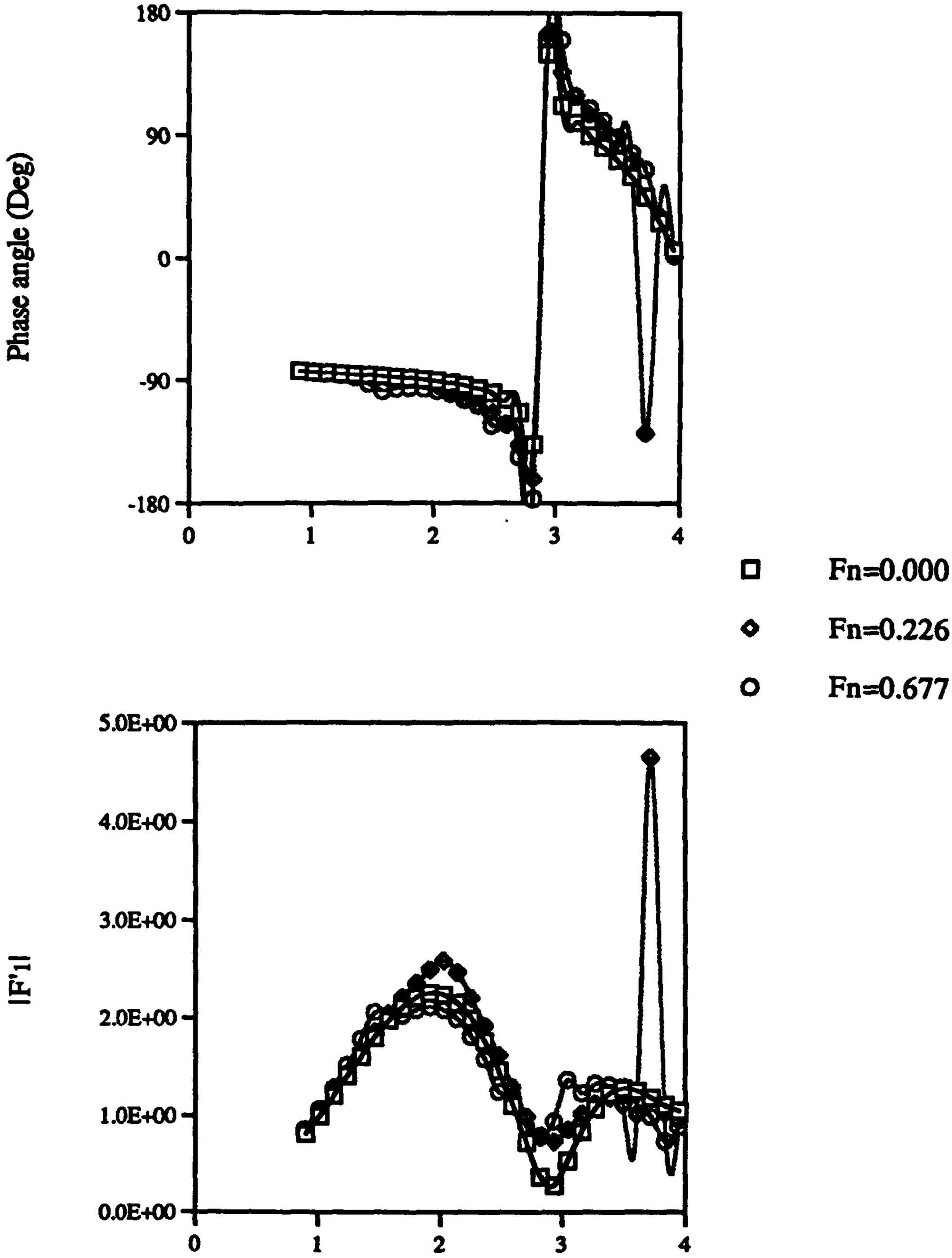

Figure 3.26 :Wave Exciting Force (surge) in 180 deg. heading for the V-1 Catamaran at various Froude Numbers

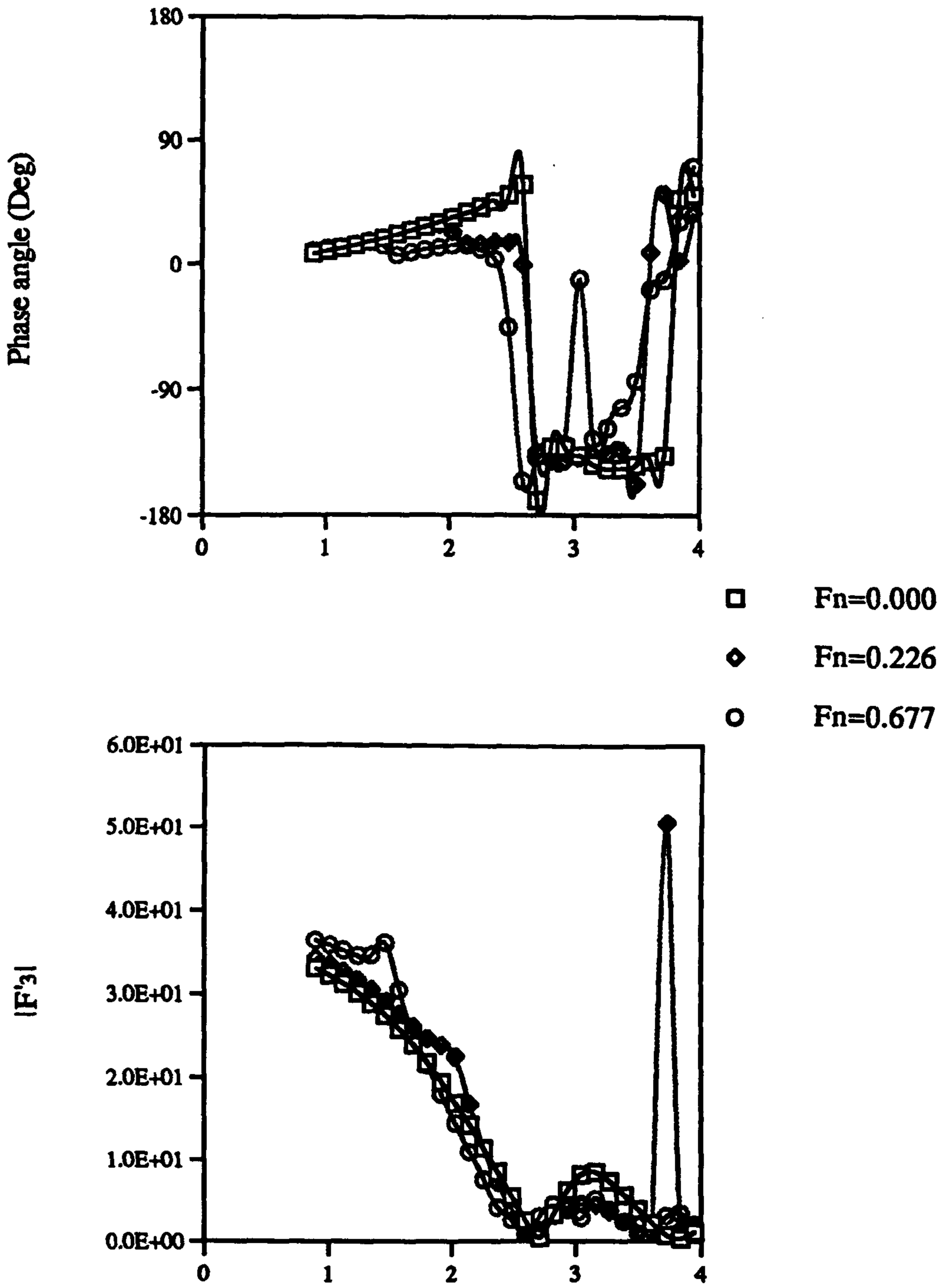

Figure 3.27 : Wave Exciting Force (heave) in 180 deg. heading for the V-1 Catamaran at various Froude Numbers

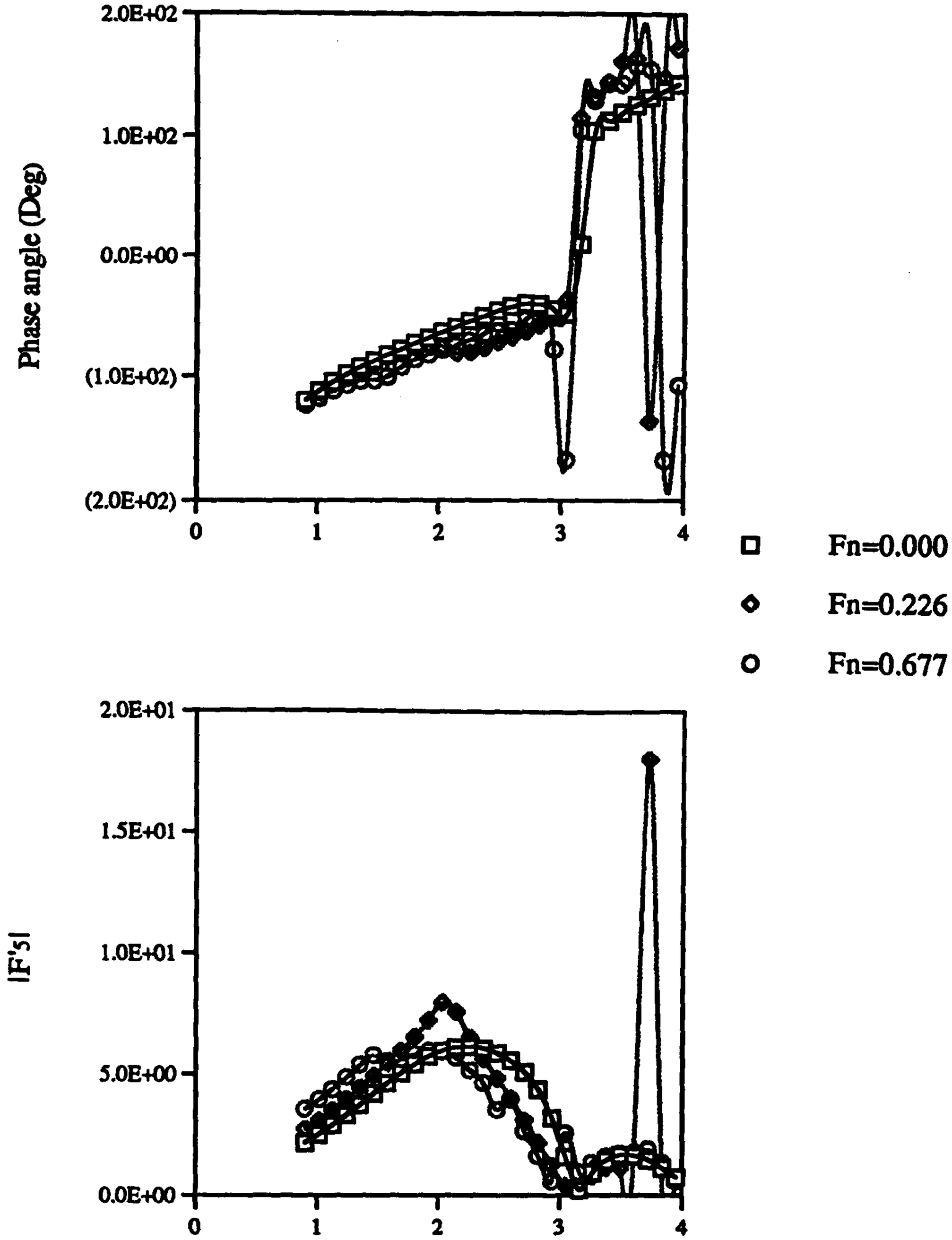

Figure 3.28 : Wave Exciting Moment (pitch) in 180 deg. heading for the V-1 Catamaran at various Froude Numbers

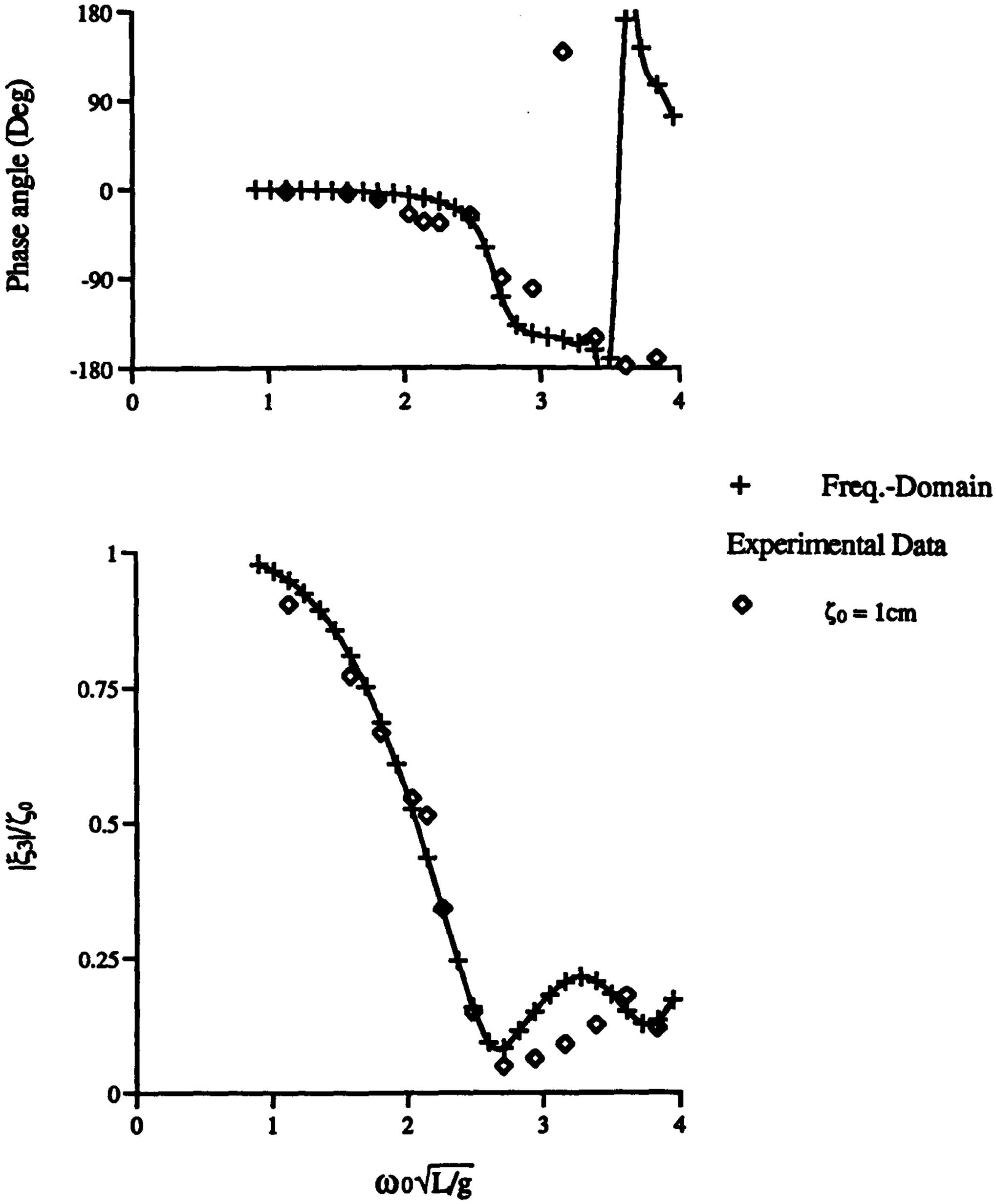

Figure 3.29 : Linear Heave Motion Response of the V-1 Catamaran at Fn=0.0

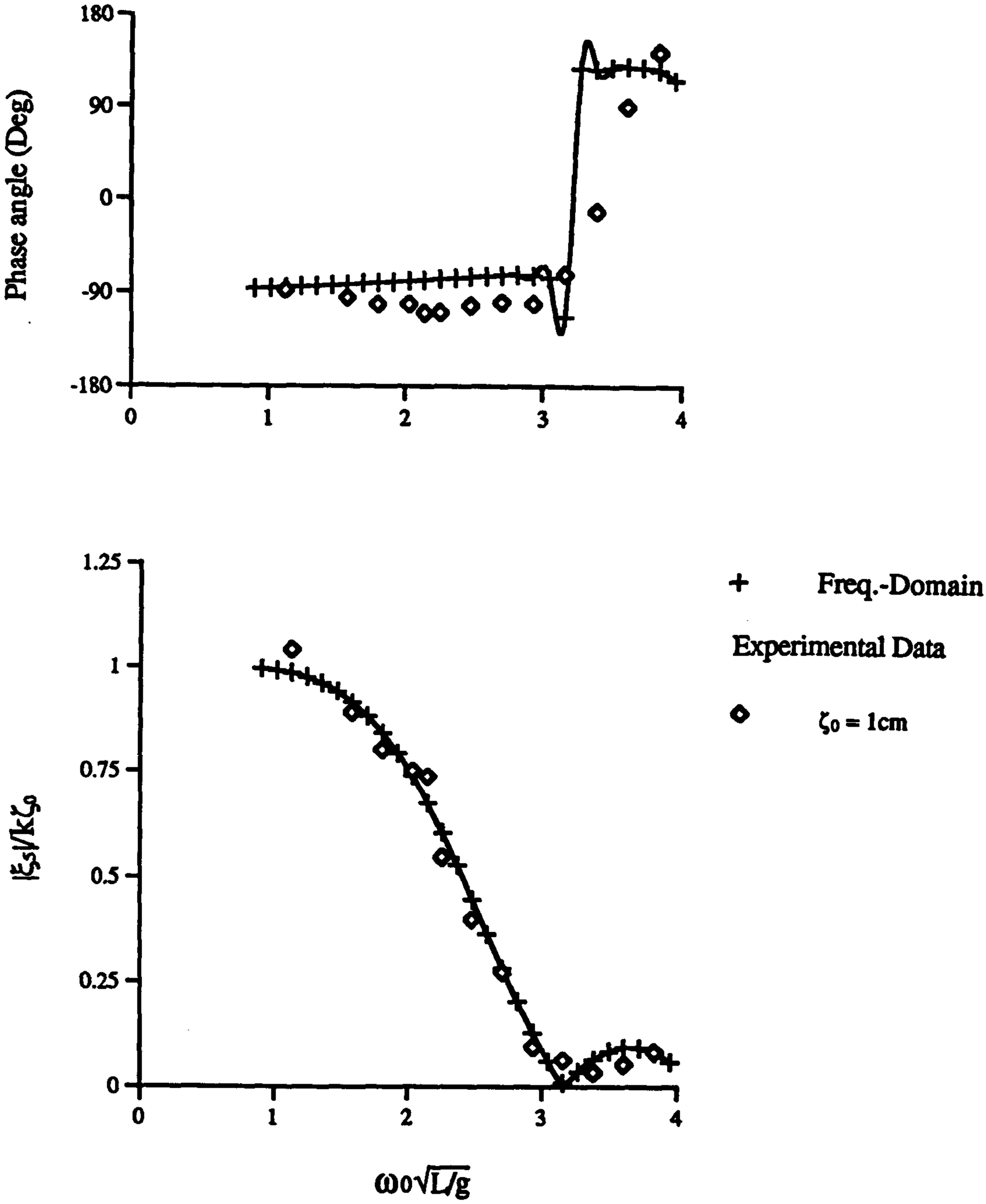

Figure 3.30 : Linear Pitch Motion Response of the V-1 Catamaran at F_n=0.0

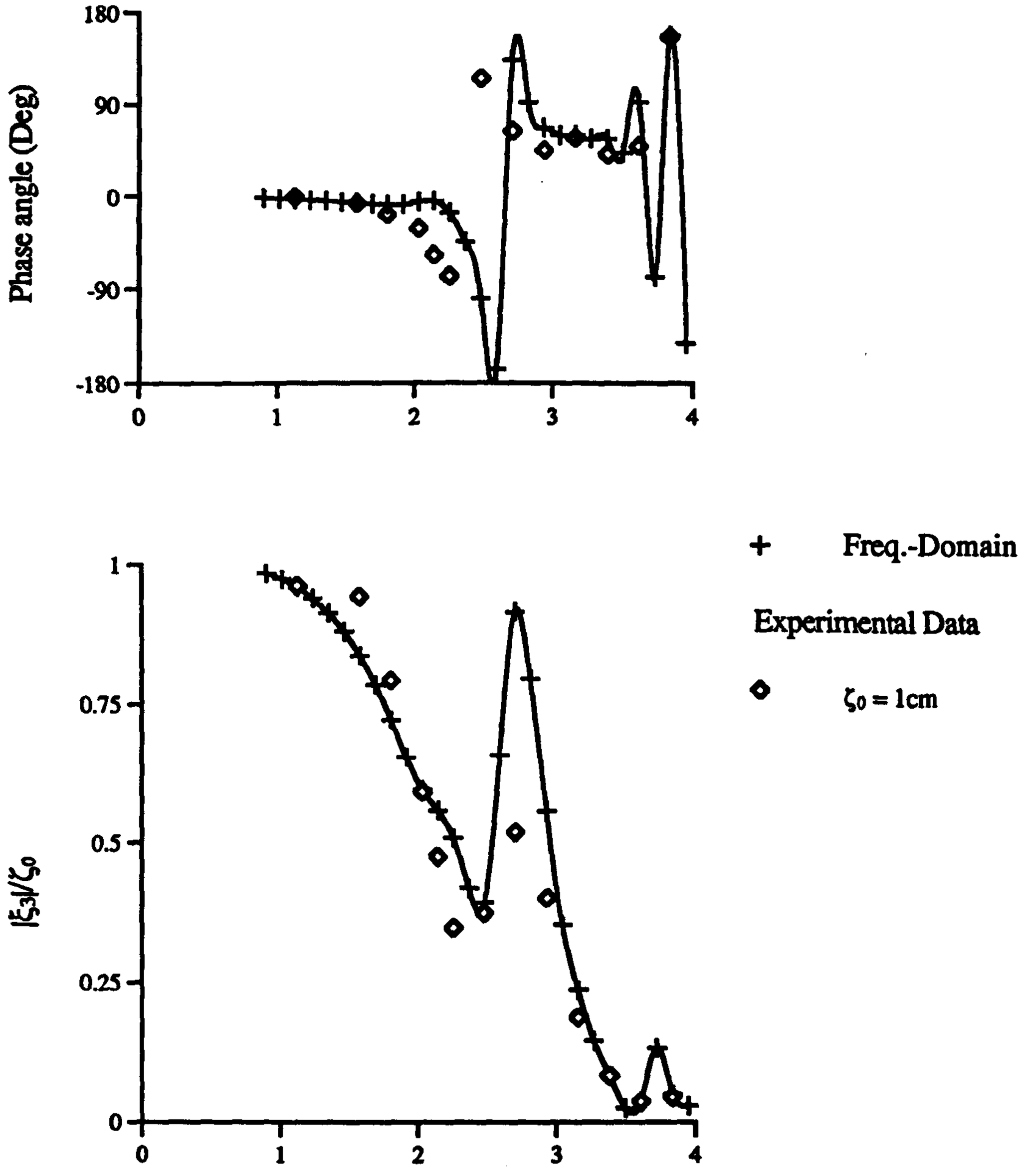

Figure 3.31 : Linear Heave Motion Response of the V-1 Catamaran at F_n=0.226

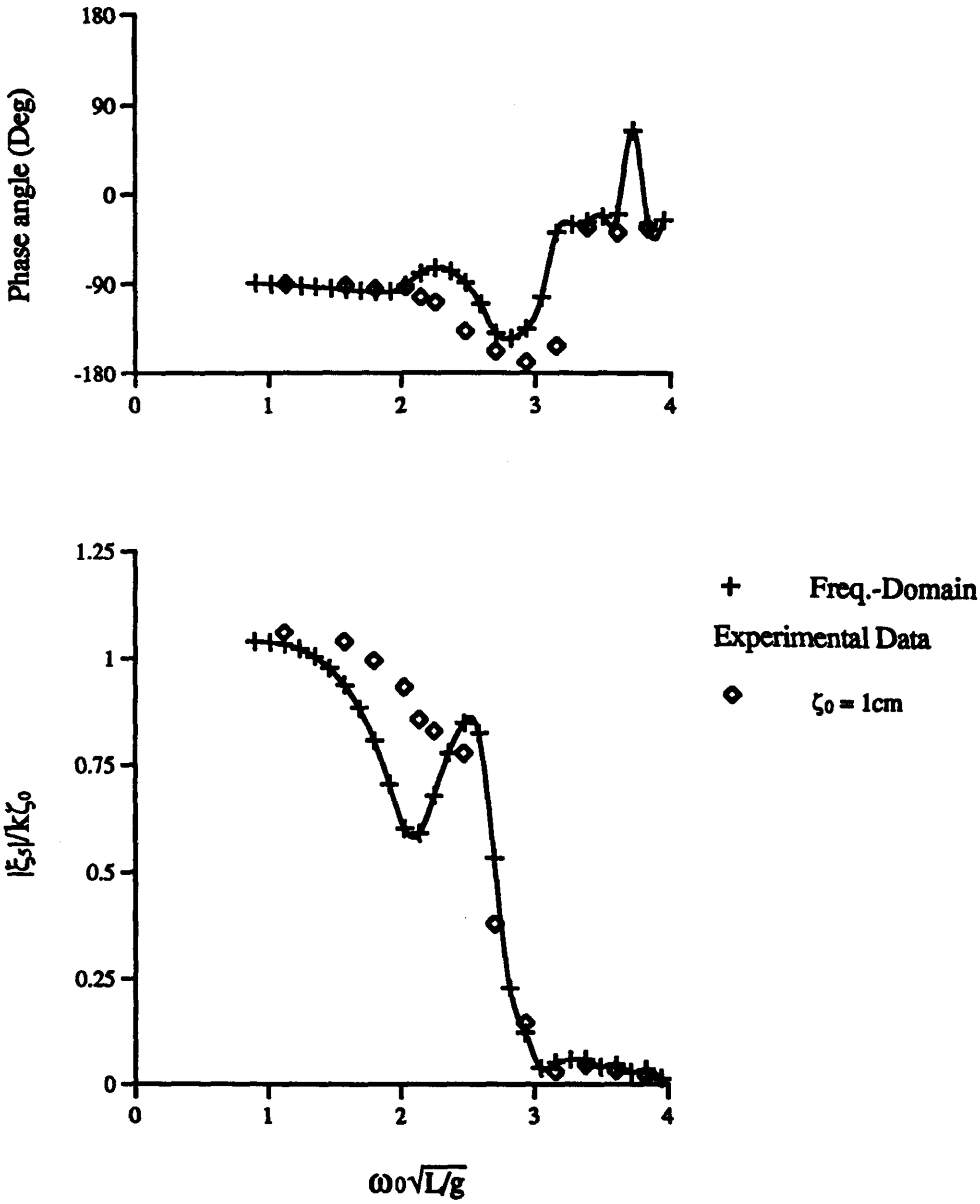

Figure 3.32 : Linear Pitch Motion Response of the V-1 Catamaran at Fn=0.226

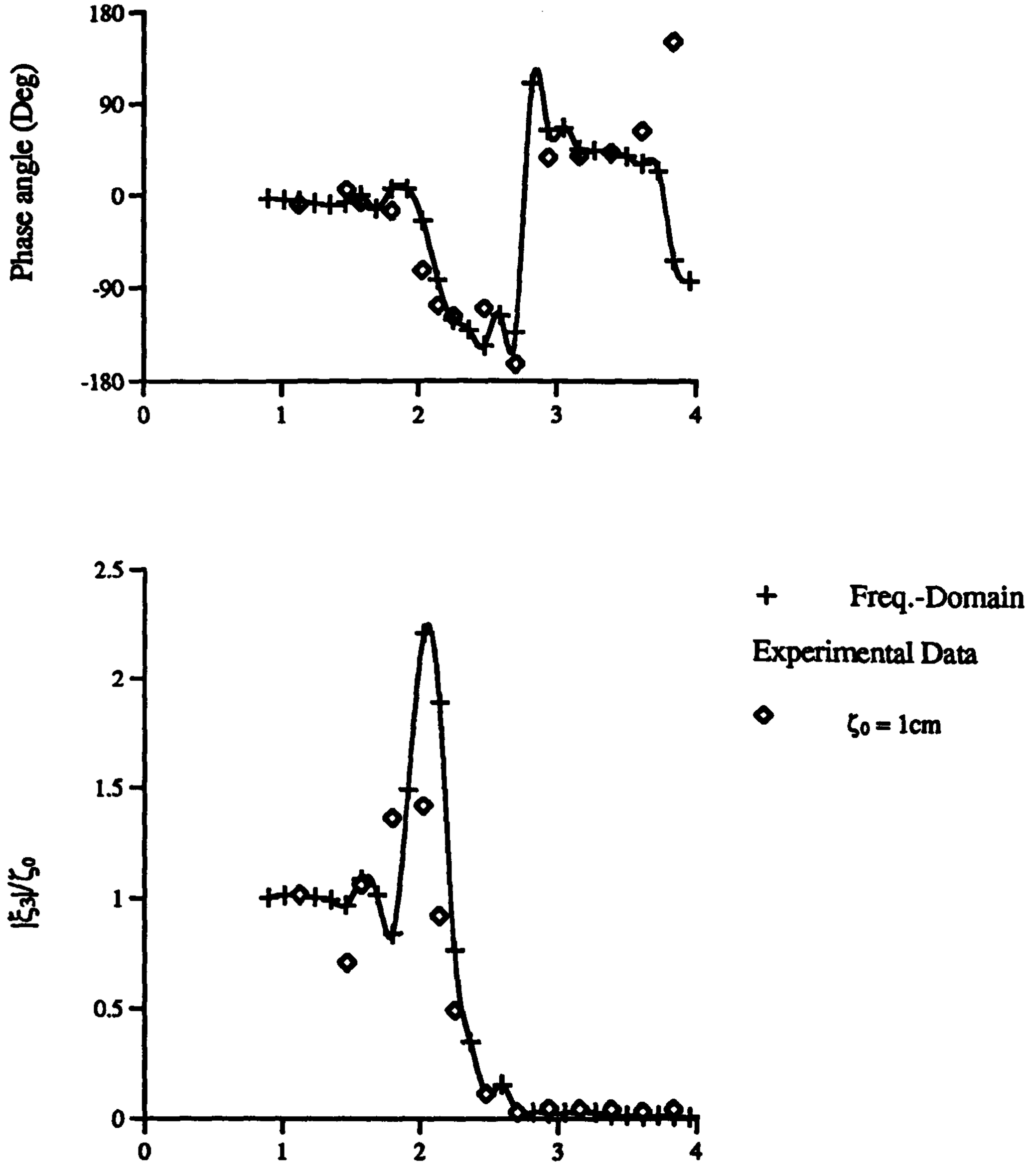

Figure 3.33 : Linear Heave Motion Response of the V-1 Catamaran at F_n=0.677

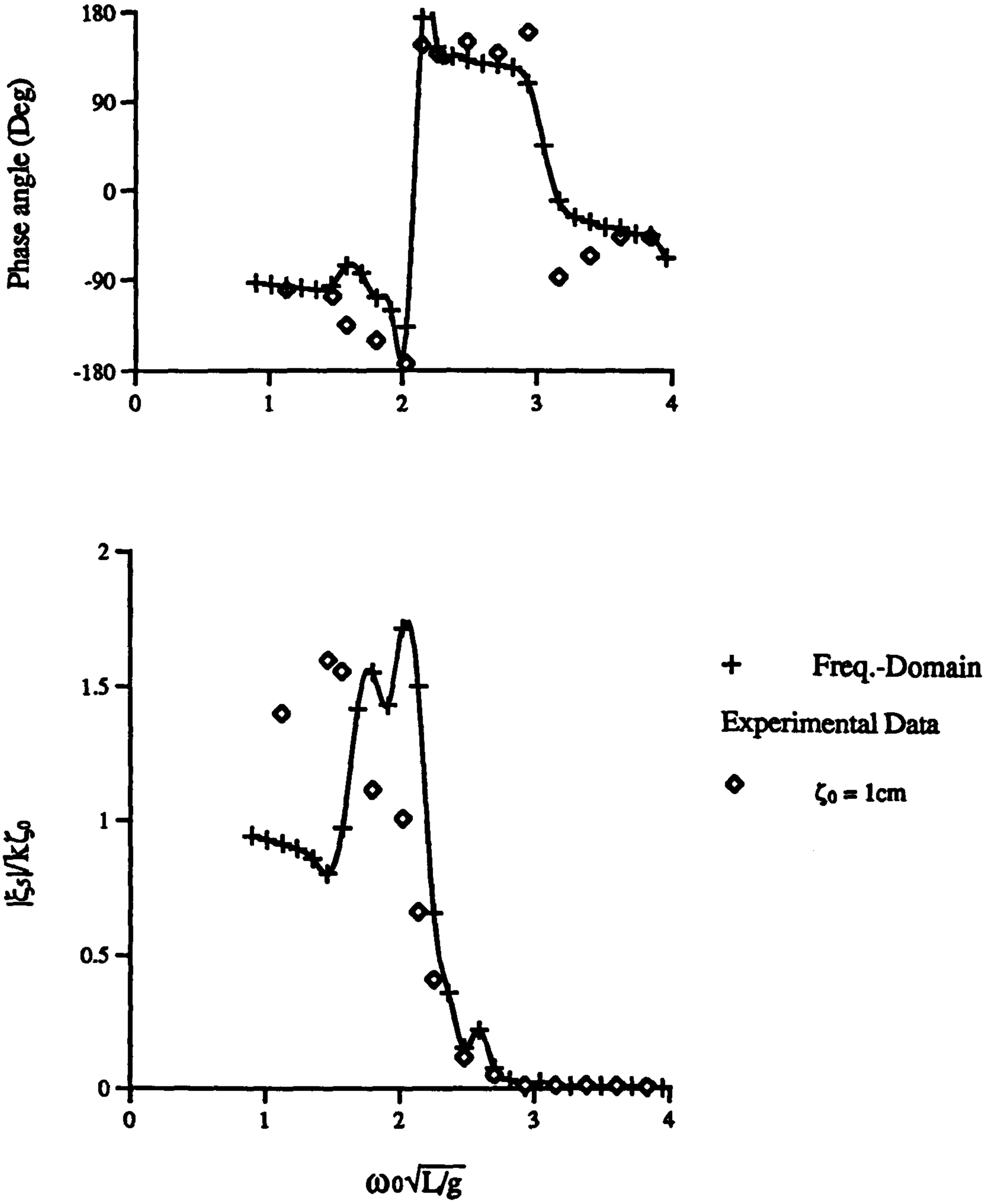

Figure 3.34 : Linear Pitch Motion Response of the V-1 Catamaran at F_n=0.677

CHAPTER 4
LARGE AMPLITUDE MOTIONS OF A CATAMARAN IN WAVES - A PRACTICAL METHOD

4.1 Introduction

The seakeeping performance of a catamaran design is assessed either using experimental measurements or theoretical techniques based on linear frequency domain methods. Although a number of experimental and theoretical investigations of catamaran motions has been conducted in the past, there is a lack of understanding of the nonlinearity of large amplitude motions. A linear behaviour is assumed in most of these investigations. The frequency domain method is restricted to the prediction of small amplitude motions since the free surface condition is assumed to be linearised, and the ship displacements are assumed to be small relative to the ship dimensions. Some of the ship response values, e.g. relative bow motions and the occurrence of green water on the deck, cannot be forecasted by using the linearised approaches. The nonlinear motion of catamaran stated as a mathematical problem with exact initial-boundary conditions is an insurmountable task to solve. A nonlinear time domain simulation technique is an appropriate tool for investigating the large amplitude ship motions.

In recent years, there are several studies about the nonlinear motion problems. The nonlinear strip approach in which the instantaneous water line is considered instead of the mean water line is a kind of quasi-nonlinear method to solve the large amplitude motion problem. The nonlinear equations of motion are solved in the time domain. Zarnick(1978) used a numerical time simulation technique to study the motion responses of planing boat in waves. The sectional hydrodynamic force is assumed to be composed of momentum change and cross flow drag. The results obtained generally agree with Fridsma's(1969) experimental data. Assuming that the transients have died out in each time step, several authors applied the time domain approach by using the hydrodynamic coefficients generated from the frequency domain method to investigate the nonlinear motion and load problem for the mono-hull(Borresen & Tellsgrad, 1980; Elsimillawy & Miller, 1986; Fujino and Yoon, 1986; Chiu and Fujino, 1991; Fang et al., 1993). So far, there are few investigations about the seakeeping problems of twin-hull ships by using the time domain technique. Arthur (1988) applied a time domain simulation technique to predict the motions of a SWATH ship. From his numerical results, Arthur (1988) found that the nonlinear hydrostatic forces are the most significant component in accurately predicting the motions of SWATH ships.

Recently, Fang and Her (1995) also used a similar technique to investigate the nonlinear motions of a SWATH ship in large longitudinal waves. The viscous effects are taken into account with a cross-flow approach. Unfortunately, there is a very limited amount of SWATH seakeeping measurement data at low forward speed and high frequency region to validate the numerical results. The limited comparisons between the predictions and measurements carried in the study show a good agreement.

In this Chapter , a practical method is advocated for predicting the nonlinear ship responses in waves by extending the strip method as described in Chapter 3. The nonlinearity of hydrodynamic forces included in the method comes from the time-variation of ship's submerged portion. The sectional hydrodynamic forces are calculated from a pre-generated database for the time-varying submerged portion at each time step, and then integrated in the longitudinal direction of ship's hull to obtain the total hydrodynamic forces and moments acting on the ship. The coupled equations, heave and pitch, are solved in the time domain. Calculations have been compared with those obtained from the linear theory. Some parametric studies have been also carried out to investigate the nonlinearity of large amplitude motion of the V-1 catamaran in head sea conditions.

4.2 Equations of motion

In order to solve the steady-harmonic motion problem in the time domain, we assume that the catamaran is free to perform heave and pitch rigid body oscillations in the head sea condition and that it maintains its initial course at a constant forward speed. The steady-translating coordinate system o-xyz is used to describe the motions of the catamaran travelling in waves. The x-axis is pointing upstream parallel to the longitudinal plane of the body and the z-axis is pointing vertically upward through the centre of gravity of the body with the origin in the plane of the mean free surface. In this study, the nonlinear incoming waves are not considered and the pitch motions are of the order of the wave slope, which is small. Then, the coupled equations of motion for heave and pitch modes can be written:

$$\begin{bmatrix} M+A_{33}(t) & A_{35}(t) \\ A_{53}(t) & I_{55}+A_{55}(t) \end{bmatrix}\begin{bmatrix} \ddot{\xi}_3(t) \\ \ddot{\xi}_5(t) \end{bmatrix}+\begin{bmatrix} B_{33}(t) & B_{35}(t) \\ B_{53}(t) & B_{55}(t) \end{bmatrix}\begin{bmatrix} \dot{\xi}_3(t) \\ \dot{\xi}_5(t) \end{bmatrix}+\begin{bmatrix} C_{33}(t) & C_{35}(t) \\ C_{53}(t) & C_{55}(t) \end{bmatrix}\begin{bmatrix} \xi_3(t) \\ \xi_5(t) \end{bmatrix}$$

$$= \mathrm{Re}\begin{bmatrix} \overline{F}_3^w(t)\zeta_0 e^{-i\omega t} \\ \overline{F}_5^w(t)\zeta_0 e^{-i\omega t} \end{bmatrix} \qquad (4.1)$$

where $\ddot{\xi}$ and $\dot{\xi}$ are acceleration and velocity respectively; M is the mass; I_{55} is the moment of inertia about the origin in the pitch mode; A_{jk} is the added mass; B_{jk} is the damping; and C_{jk} is the restoring coefficient. $\overline{F}_j^w$ is the complex amplitude of wave exciting force; ζ_0 is the incident wave amplitude.

Equations (4.1) imply that the motions of the catamaran should be a kind of steady-state oscillations. Therefore, all the transients will die out. The solution of large amplitude motions of the catamaran in regular waves can be represented by the time-varying linear system. Based on these assumptions, the sectional hydrodynamic forces are obtained from the linear frequency domain method.

The model is divided into a number of sections and each sectional contour is represented by a set of offset including the deck description. The sectional hydrodynamic coefficients and wave exciting forces including the related velocity potentials are computed for several different draughts at a given frequency using the linear frequency domain method. In each time step, the hydrodynamic coefficients, wave exciting forces and hydrostatic forces are determined at the instantaneous sectional draughts. Details of this procedure will be described in the following sections.

The incident wave, ζ, progressing in head sea condition, $\beta = 180^0$, is written in the translating coordinate o-xyz :

$$\zeta(x,t) = \zeta_0 e^{-i(kx+\omega t)} \qquad (4.2)$$

where ζ_0 is the wave amplitude.

The instantaneous draught for each hull section can be determined by the relative vertical motion between the vertical motion of the at-rest waterline and the incident wave surface. Hence, the instantaneous draught ,$d(x,t)$, is given by

$$d(x,t) = d(x,0) + \zeta(x,t) - (\xi_3(t) - x\xi_5(t)) \tag{4.3}$$

where $d(x,0)$ indicates the at-rest draught.

The hydrodynamic coefficients, wave exciting forces and hydrostatic forces corresponding to the sectional instantaneous draughts are calculated by using the linear interpolation method from the pre-generated database and body offset of the V-1 catamaran at each time step. This nonlinear coupled heave and pitch motion equations are solved in the time domain by using the adaptive stepsize Runge-Kutta method(Press, W.H. et al., 1992).

4.2.1 The nonlinear hydrodynamic coefficients

In the radiation, the radiated waves are generated from the oscillatory motions of a body in calm water. The hydrodynamic forces are obtained by integrating the hydrodynamic pressures in terms of the related velocity potential ϕ_k and its derivatives over the at-rest wetted body surface. These reactive forces can be expressed in terms of the added mass and damping coefficients which are functions of the forward speed, the body geometry and the frequency of motion.

Based on the linear frequency domain theory described in Chapter 3, the added mass and damping coefficients are defined as :

$$A_{jk} = -\frac{\rho}{\omega^2}\mathrm{Re}\iint_{\bar{S}_B} n_j(i\omega + U\frac{\partial}{\partial x})\phi_k ds \tag{4.4}$$

$$B_{jk} = -\frac{\rho}{\omega}\mathrm{Im}\iint_{\bar{S}_B} n_j(i\omega + U\frac{\partial}{\partial x})\phi_k ds \tag{4.5}$$

After some manipulations, the following formulas for the added mass and damping coefficients in the heave-pitch motion at each time step can be derived :

$$A_{33}(t) = \int_L \bar{a}_{33}(x,t)dx + \frac{U}{\omega^2}\bar{b}_{33}(x,t)\Big|_L \tag{4.6}$$

$$B_{33}(t) = \int_L \bar{b}_{33}(x,t)dx - U\bar{a}_{33}(x,t)\Big|_L \tag{4.7}$$

$$A_{53}(t) = -\int_L x\bar{a}_{33}(x,t)dx + \frac{U}{\omega^2}B^0_{33}(t) - \frac{U}{\omega^2}x\bar{b}_{33}(x,t)\Big|_L \tag{4.8}$$

$$B_{53}(t) = -\int_L x\bar{b}_{33}(x,t)dx - U\,A^0_{33}(t) + Ux\bar{a}_{33}(x,t)\Big|_L \tag{4.9}$$

$$A_{35}(t) = A^0_{53}(t) - \frac{U}{\omega^2}B^0_{33}(t) + \frac{U^2}{\omega^2}\bar{a}_{33}(x,t)\Big|_L - \frac{U}{\omega^2}x\bar{b}_{33}(x,t)\Big|_L \tag{4.10}$$

$$B_{35}(t) = B^0_{53}(t) + UA^0_{33}(t) + Ux\bar{a}_{33}(x,t)\Big|_L + \frac{U^2}{\omega^2}\bar{b}_{33}(x,t)\Big|_L \tag{4.11}$$

$$A_{55}(t) = \int_L x^2\bar{a}_{33}(x,t)dx + \frac{U^2}{\omega^2}A^0_{33}(t) - \frac{U^2}{\omega^2}x\bar{a}_{33}(x,t)\Big|_L + \frac{U}{\omega^2}x^2\bar{b}_{33}(x,t)\Big|_L \tag{4.12}$$

$$B_{55}(t) = \int_L x^2\bar{b}_{33}(x,t)dx + \frac{U^2}{\omega^2}B^0_{33}(t) - Ux^2\bar{a}_{33}(x,t)\Big|_L - \frac{U^2}{\omega^2}x\bar{b}_{33}(x,t)\Big|_L \tag{4.13}$$

where the superscript "0" indicates the term at zero speed. $\Big|_L$ indicates $\Big|_{-l_1}^{l_2}$. l_1 and l_2 are the distances of stern and bow sections from the longitudinal centre of gravity, respectively. The sectional hydrodynamic coefficients in the integral, such as $\bar{a}_{33}(x,t)$ and $\bar{b}_{33}(x,t)$, denote the sectional coefficients for the heave motion. The forward speed effects on the hydrodynamic coefficients are included in equations (4.6) to (4.13) at each time step.

In order to solve the large amplitude motion problem, the solution will be obtained by numerical integration in the time domain. This will cause some difficulties to calculate the nonlinear hydrodynamic forces obtained from the related time-varying velocity potential. In this study, however, a section may have large displacements from the at-rest position, then the added mass and damping coefficients will depend on the instantaneous draught $d(x,t)$ with a given frequency of motion :

$$\bar{a}_{33}(x,t) \cong \bar{a}_{33}(d(x,t),\omega) \tag{4.14}$$

$$\bar{b}_{33}(x,t) \cong \bar{b}_{33}(d(x,t),\omega) \tag{4.15}$$

This is an approximation which is questionable in the high frequency range where the hydrodynamic forces will dominate. For a completely submerged section the added mass and damping coefficients will be kept constant and equal to the values at the time of submergence.

4.2.2 The nonlinear wave exciting forces

In the linear theory, the hydrodynamic exciting forces are due to the incident and scattered waves and are proportional to the wave amplitude. It is assumed that the body is restrained from any oscillatory motion and is subjected to the actions of incident waves in the diffraction problem. The hydrodynamic exciting forces are a function of the wave frequency, wave heading, forward speed and the body geometry. Based on the assumption of sinusoidal incident wave case, the hydrodynamic exciting forces, F_j^W, per unit wave amplitude can be expressed in the form as defined in Chapter 3:

$$F_j^W = -\rho \iint_{\bar{S}_B} n_j (i\omega + U\frac{\partial}{\partial x})(\phi_0 + \phi_7) ds e^{-i\omega t} \qquad (4.16)$$
$$= \bar{F}_j^W \cdot e^{-i\omega t} = (\bar{F}_j^k + \bar{F}_j^D) e^{-i\omega t}$$

where $\bar{F}_j^k$ and $\bar{F}_j^D$ are the complex amplitude of the Froude-Krylov force and the diffraction force respectively.

The nonlinear wave exciting forces are composed of the Froude-Krylov forces and diffraction forces as mentioned in the linear theory. Therefore, the Forude-Krylov forces and moments for the heave and pitch motions at each time step are:

$$\bar{F}_3^k(t) = \int_L f_{K3}(x,t) dx \qquad (4.17)$$

$$\bar{F}_5^k(t) = -\int_L x \cdot f_{K3}(x,t) dx \qquad (4.18)$$

where

$$f_{K3}(x,t) = e^{-ikx} \rho g \int_{S_B} e^{kz} dy \qquad (4.19)$$

and, the nonlinear diffraction forces and moments for the heave and pitch motions are:

$$\bar{F}_3^D(t) = \int_L e^{-ikx} dx \int_{S_B} i\rho\omega\phi_7(x,y,z,k;t) dl + \frac{U}{i\omega} e^{-ikx} \int_{S_B} i\rho\omega\phi_7(x,y,z,k;t) dl \Big|_L \qquad (4.20)$$

$$\overline{F}_5^D(t) = -\int_L xe^{-ikx}dx\int_{s_s} i\rho\omega\phi_7(x,y,z,k;t)dl$$
$$+\frac{U}{i\omega}\int_L e^{-ikx}dx\int_{s_s} i\rho\omega\phi_7(x,y,z,k;t)dl - \frac{Ux}{i\omega}e^{-ikx}\int_{s_s} i\rho\omega\phi_7(x,y,z,k;t)dl\Big|_L \quad (4.21)$$

The procedure to calculate the wave exciting forces in the time domain is similar to the one used in the calculations of the hydrodynamic coefficients. The sectional nonlinear wave exciting forces are a function of the instantaneous draught, $d(x,t)$, and frequency of motion. Once the sectional instantaneous draughts are determined, the corresponding sectional wave exciting forces will be retrieved from the pre-generated database by using the linear interpolation method.

4.2.3 The nonlinear hydrostatic coefficients

It is necessary to determine the ship position in waves to calculate the restoring forces and moments at any instant of time. Based on the linear theory, the nonlinear hydrostatic coefficients in each time step can be expressed as :

$$C_{33}(t) = 2\rho g\int_L B_w(x,t)dx \quad (4.22)$$

$$C_{55}(t) = 2\rho g\int_L x^2 B_w(x,t)dx + \rho g\nabla(t)(z_b(t) - z_G(t)) \quad (4.23)$$

$$C_{35}(t) = C_{53}(t) = -2\rho g\int_L xB_w(x,t)dx \quad (4.24)$$

where $B_w(x,t)$ is the beam of each demi-hull at instantaneous draught; $\nabla(t)$ is the volume of displacement; $z_b(t)$ and $z_G(t)$ are the vertical coordinates of the centre of buoyancy and centre of gravity of the hull, respectively.

According to the instantaneous draught, the immersed portion of cross section can be decided by a set of offset points including the deck description. The linear interpolation method is used to calculate the beam of each demi-hull, $B_w(x,t)$, related to the sectional instantaneous draught. Moreover, the cross-sectional area and the centre of buoyancy are calculated by using the cubic spline technique and are integrated along the length of ship to obtain the volume of displacement at each time step.

4.3 Time-domain solutions of the V-1 catamaran

The coupled equations of motion for heave and pitch modes are solved by using the numerical integration technique in the time domain. For this purpose, a computer program has been developed by using the adaptive stepsize Runge-Kutta method.

Equations (4.1) are a kind of second-order differential equations. For advancing the numerical simulation in time domain, these coupled equations are reduced to four first-order differential equations as follows:

$$\begin{bmatrix} \frac{d\xi_3(t)}{dt} \\ \frac{d\xi_5(t)}{dt} \end{bmatrix} = \begin{bmatrix} \dot{\xi}_3(t) \\ \dot{\xi}_5(t) \end{bmatrix} \tag{4.25}$$

$$\begin{bmatrix} \frac{d\dot{\xi}_3(t)}{dt} \\ \frac{d\dot{\xi}_5(t)}{dt} \end{bmatrix} = \begin{bmatrix} M + A_{33}(t) & A_{35}(t) \\ A_{53}(t) & I_{55} + A_{55}(t) \end{bmatrix}^{-1} \begin{bmatrix} F_3(t) \\ F_5(t) \end{bmatrix} \tag{4.26}$$

where

$$\begin{bmatrix} F_3(t) \\ F_5(t) \end{bmatrix} = \mathrm{Re}\begin{bmatrix} \bar{F}_3^w(t)\zeta_0 e^{-i\omega t} \\ \bar{F}_5^w(t)\zeta_0 e^{-i\omega t} \end{bmatrix} - \begin{bmatrix} B_{33}(t) & B_{35}(t) \\ B_{53}(t) & B_{55}(t) \end{bmatrix} \begin{bmatrix} \dot{\xi}_3(t) \\ \dot{\xi}_5(t) \end{bmatrix} - \begin{bmatrix} C_{33}(t) & C_{35}(t) \\ C_{53}(t) & C_{55}(t) \end{bmatrix} \begin{bmatrix} \xi_3(t) \\ \xi_5(t) \end{bmatrix} \tag{4.27}$$

Equations (4.25) and (4.26) represent an initial value problem which can be solved by setting initial values of the time-dependent variables $\left[\xi_3(0), \xi_5(0), \dot{\xi}_3(0), \dot{\xi}_5(0)\right]$ and then the solutions for the heave and pitch motions including the displacement and velocity at each time step can be obtained. Details of how to set the initial values will be discussed in the next section.

In order to save computational time, the time dependent hydrodynamic coefficients and wave excitation forces are obtained from a hydrodynamic database by applying the linear interpolation method at a given wave frequency. The hydrodynamic database of the V-1 catamaran is generated by using the linear frequency domain technique. These coefficients are a function of the wave frequency, section position, forward speed, sectional draught and body geometry.

In this study, the V-1 catamaran is divided into 15 sections and the at-rest waterline is 6.72 cm as mentioned in Chapter 3. Figures 4.1 to 4.18 show some examples which sectional hydrodynamic coefficients and wave exciting forces are related to a set of given draughts which include the still waterline and chine-line points in each section at a certain wave frequency and forward speed. Due to the large variation of these coefficients in the shallow draught region, the linear interpolation method is selected to calculate the time-varying hydrodynamic coefficients and wave exciting forces which are used to simulate the motion responses of the catamaran travelling in regular waves from equations (4.1).

4.3.1 Initial value problem

Equations (4.25) and (4.26) are formulated as steady-state sinusoidal equations. It is assumed that all "transient effects" have died out and a periodic solution exists. To solve these equations in the time domain, the proper initial values which describe the position and velocity of the system have to be specified. However, the numerical solutions will diverge if the damping of the coupled system is low to cope with the initial conditions. We observe that the characteristics of divergence depend on the numerical method employed, the wave encounter frequency, the incident wave amplitudes and the damping of system.

In order to reduce the effects of transient, a ramp function, $R(t)$, is applied to gradually increase the amplitude of incident wave :

$$R(t) = \frac{1}{2}(1-\cos(\frac{\pi}{NT_e}t)), \qquad t \le NT_e \tag{4.28}$$

The time dependency of $R(t)$ will increase from zero at t=0, to unity at $t = NT_e$, where T_e is the encounter period of wave.

An alternative method for solving the problem of divergence is to assume the initial values of the differential equations from the results of the linear theory in the frequency domain. When the amplitudes of incident wave are small, computations have confirmed that the solutions of this method will be more quickly approximated to the steady-state oscillations than the ramp function model as shown in figure 4.19. In the cases of motion simulation of a catamaran at high speeds or large amplitude wave, the

numerical solutions are unsteady. Both methods are used to initialise the nonlinear motion problem in the regular waves.

4.3.2 Small amplitude motion simulations

In order to validate the time domain technique in the linear region, a wave amplitude of $\zeta_0 = 0.1cm$ is chosen. This eliminates the nonlinear effects. The results obtained from the time domain technique have been compared with those obtained from the frequency domain method for the V-1 catamaran travelling in the head sea condition.

Parts of the time histories for the linear motions of the V-1 catamaran in heave and pitch modes are shown in figure 4.20 to 4.27. These results are calculated over a range of wave frequencies with three different forward speeds (Fn=0.00, 0.226, 0.677). Only a limited number of time history examples for the V-1 catamaran are presented in here. As can be seen from figures 4.20 to 4.27, the motion amplitudes and phase angles obtained from linear and nonlinear simulations have a perfect match.

Figures 4.28 to 4.33 are the non-dimensional heave and pitch motion predictions obtained from the frequency domain and time domain analyses of the V-1 catamaran in head sea condition. The results show an excellent agreement between these two techniques. Although the small incident wave amplitude is chosen, there are some minor nonlinearities observed around the resonance frequencies when the forward speed increases as shown in figures 4.30 to 4.33. The motion response values obtained from the time domain technique are slightly lower than those obtained from the frequency domain predictions around the resonance frequencies. Based on this validation, it can be concluded that the time domain technique can be used to predict the motion responses of V-1 catamaran in the longitudinal waves.

4.3.3 Large amplitude motion simulations

The time domain simulations have been carried out with three incident wave amplitudes (1cm, 3cm, 4.5cm) and three forward speeds (Fn=0.00, 0.226, 0.677) to evaluate the nonlinear motions of the V-1 catamaran in the head sea condition. In this study, the functional dependence of wave amplitudes can be traced from the large amplitude motion simulations obtained from the time domain technique.

Some of the time histories for the non-dimensional heave and pitch motions of the V-1 catamaran with various incident wave amplitudes are presented in figures 4.34 to 4.38. In figure 4.34, the non-dimensional heave motion responses increase as large wave amplitudes increase at zero forward speed and wave frequency ω_0=4.75 rad/sec. It is interesting to note that the amplitudes of negative peaks observed from the time domain simulations are almost the same when the incident wave amplitudes increase. However, the pitch motion responses are quite linear and the phase shifts are not very significant when the wave amplitudes increase.

Although the results obtained from the linear theory are used for initial values, there are some numerical instabilities observed in the beginning of heave motion response simulations when the incident wave amplitudes are larger than 3.0cm as shown in figure 4.35. These numerical instabilities will increase with the forward speeds and wave amplitudes. In order to eliminate these effects, the ramp function introduced in 4.3.1 is incorporated with the linear theory results to initialise the equations of motion. In figure 4.35, both heave and pitch motion responses show some nonlinear behaviour which is a function of incident wave amplitude. The positive peak amplitude of non-dimensional heave and pitch motion decreases while the incident wave amplitude increases. Some phase angle shifts are also observed from these time histories.

The distorted negative peaks are observed in the time histories of heave motions of the V-1 catamaran at large wave amplitude, $\zeta_0 = 4.5cm$, as shown in figure 4.36. From figure 4.37, the nonlinear effects are more appreciable for the heave and pitch motions at large incident wave amplitudes when the Froude number is equal to 0.226. For the heave motion, the non-dimensional amplitudes decrease when incident wave amplitudes increase. But the pitch motion results show the opposite trend when the wave amplitudes increase up to 3cm and 4.5cm. Moreover, the phase angle shifts are more significant on both heave and pitch motions with larger incident wave amplitudes.

At the high forward speed case, Fn=0.677, $\omega_0 = 6.25rad/\sec$, figure 4.38 shows that the mean values of the non-dimensional heave and pitch motions obtained in the time domain will shift toward negative axis when the incident wave amplitudes increase.

Based on these time history investigations, the positive and negative amplitudes are of different magnitudes in the large amplitude motions of the V-1 catamaran. In the

linear theory, magnitudes of positive and negative amplitudes are identical. This asymmetric phenomena observed in the time domain simulations will be an important effect when we calculate the relative motions to solve the impact problem of a catamaran travelling in waves.

Comparisons between results obtained from the linear theory in the frequency domain and from nonlinear calculations in the time domain with three different incident wave amplitudes are presented in figures 4.39 to 4.44. The non-dimensional heave and pitch motions are plotted against the non-dimensional wave frequencies at three different forward speeds.

For the zero speed case, the numerical results show that the non-dimensional heave and pitch motions increase slightly when the incident wave amplitudes increase at the non-dimensional wave frequencies, $\omega_0\sqrt{L/g}$, between 1.58 and 2.822. At the resonance point, the non-dimensional motion responses decrease slightly when the wave amplitudes increase.

At Froude number Fn=0.226, figures 4.41 and 4.42 show that the nonlinear effects are more significant at the resonance region for the large amplitude motions of V-1 catamaran. Generally the non-dimensional heave motion responses decrease while the wave amplitudes increase except at $\omega_0\sqrt{L/g}$=2.257. However, the pitch motion results show the opposite trend. The non-dimensional pitch motion responses increase when the wave amplitudes increase at Fn=0.226. It may be noticed from figures 4.41 and 4.42 that there are some phase shifts observed in the phase angle calculations. From the related time history observations shown in figure 4.37, it can be seen that not only the motion responses but also phase angles show a nonlinear behaviour during the large amplitude motion simulations of the V-1 catamaran in regular waves.

Figures 4.43 and 4.44 are the non-dimensional motion response values and phase angles in heave and pitch modes of the V-1 catamaran at Fn=0.677. Both heave and pitch motions show the same nonlinear phenomena that the non-dimensional motion responses notably decrease while the incident wave amplitudes increase except at $\omega_0\sqrt{L/g}$=1.69.

From the numerical simulations of the large amplitude motions of the V-1 catamaran travelling in head sea, it can be concluded that the nonlinear effects are more significant when the forward speeds and wave amplitudes increase around the resonance frequencies.

4.4 Parametric studies

To investigate the components of nonlinearity due to large amplitude motions of the V-1 catamaran in waves, some parametric studies have been performed by comparing results obtained from different numerical models which are based on : linear frequency domain method; nonlinear hydrodynamic coefficient model; nonlinear wave exciting force model; linear hydrostatic force model; nonlinear hydrostatic force model and nonlinear time domain method. Details of these numerical models are defined in table 4.1.

In this study, we select six test conditions which include varied forward speeds, wave frequencies and wave amplitudes. Detail results for the parametric studies on the heave and pitch motions of V-1 catamaran are presented in tables 4.2 to 4.7. Related time histories are also shown in figures 4.45 to 4.68.

Table 4.2 shows that nonlinear effects in large heave motions are due to hydrodynamic coefficients, wave exciting forces and hydrostatic forces. It is difficult to classify the dominating effect in this test condition. There are no significant nonlinear effects observed in the time histories for the pitch motions. However, the phase angle predictions obtained from the nonlinear hydrostatic force model are similar to those obtained from the time domain method. At zero speed and high incident wave frequency case, $\omega_0 = 8.5 rad/\sec$, the nonlinear wave exciting forces play an important role in the prediction of the nonlinear motions of the V-1 catamaran in head sea condition as shown in figure 4.50.

Figures 4.53 to 4.56 show some interesting time domain traces for the heave and pitch motions of the V-1 catamaran at Fn=0.226, $\omega_0 = 4.0 rad/\sec$, $\zeta_0 = 4.5 cm$. Both heave and pitch response curves are asymmetrical. Furthermore, the twin-peak shapes are observed at the negative peaks of the heave displacements. These phenomena are due to the nonlinear hydrostatic forces as shown in figure 4.56. The total nonlinearities are contributed by all nonlinear components in this test condition. In table 4.5, the heave motion results obtained from the nonlinear hydrostatic force model are very similar to those obtained from the nonlinear time domain method. However, the nonlinearities of pitch motions come from the nonlinear wave exciting and hydrostatic forces as shown in figures 4.58 and 4.60.

At the high forward speed, Fn=0.677, tables 4.6 and 4.7 show that the nonlinear hydrostatic forces provide a significant contribution to the nonlinear response values.

The nonlinear hydrodynamic coefficients and wave exciting forces still have some minor effects on the nonlinearity.

In the linear theory, the results of motion equations are dominated by the hydrostatic restoring and Froude-Krylov forces in the low frequency region and by hydrodynamic coefficients in the high frequency region. However, this behaviour is not always observed in these numerical investigations. This may be due to the configuration of V-1 catamaran. The demi-hull of V-1 catamaran is a kind of V-type section which may give rise to large nonlinear hydrostatic forces when large motion responses occur. It is also interesting to notice that most of the hydrodynamic coefficients of the V-1 catamaran become constant while the sectional draught increases as shown in figures 4.1 to 4.18.

4.5 Conclusions

The problem of large amplitude motions of the V-1 catamaran in head sea condition has been formulated in the time domain by extending the linear frequency domain method. A hydrodynamic coefficient database has been pre-generated using the two-dimensional potential theory. The coupled equations of motion have been solved in the time domain by using the Runge-Kutta method with the proper initial values.

The time domain technique has been validated by comparing the results obtained from the linear theory with those obtained from the nonlinear theory with a small incident wave amplitude. Then, a series of systematical analyses for the V-1 catamaran motions with three wave amplitudes have been carried out by using the nonlinear time domain method. A nonlinear behaviour of the V-1 catamaran has been observed from the time domain large amplitude motion simulations. In general, the nonlinear effects are more significant around the resonance frequencies when the forward speed and wave amplitude increase. Moreover, the positive and negative amplitudes are of different magnitudes in the time histories when the large amplitude motions of V-1 catamaran occur. Parametric studies have been carried out to investigate the effects of nonlinear terms. Based on these studies, it has been found that the effects caused by the nonlinear hydrodynamic coefficients, wave exciting forces and hydrostatic forces are difficult to separate in different test conditions. In the case of the V-1 catamaran configuration, the hydrodynamic coefficients and wave exciting forces play an important role in the prediction of nonlinear motions at the low forward speed. In the

high forward speed region, the hydrostatic forces give rise to a significant contribution to the nonlinear response values.

However, this time domain technique is a kind of practical tool to predict the large amplitude motions of catamarans in regular waves. Strictly, the classical definition of frequency dependent added mass and damping coefficients is no longer valid in the nonlinear large amplitude motion problem. The added mass and damping forces are then replaced by the nonlinear hydrodynamic forces obtained from the nonlinear initial-boundary value problem for the time-varying velocity potential. Some fundamental researches have been carried out by the author for solving the initial-boundary value problem. Details will be discussed in Chapter 6.

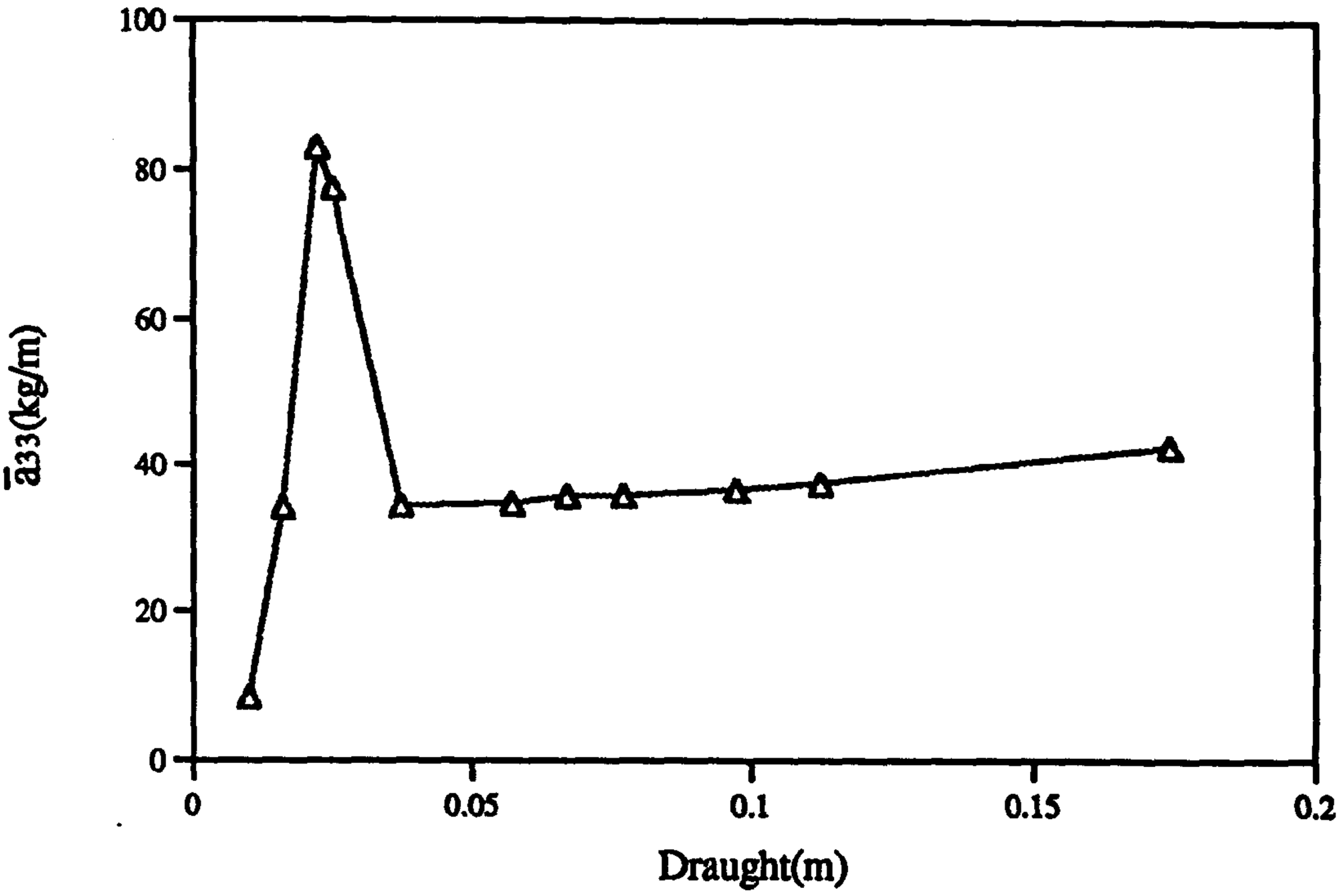

Figure 4.1 : The Added Mass for the V-1 Catamaran with Different Draught at Section No. 8.(Fn=0.00,ω_0=3.25 rad/sec)

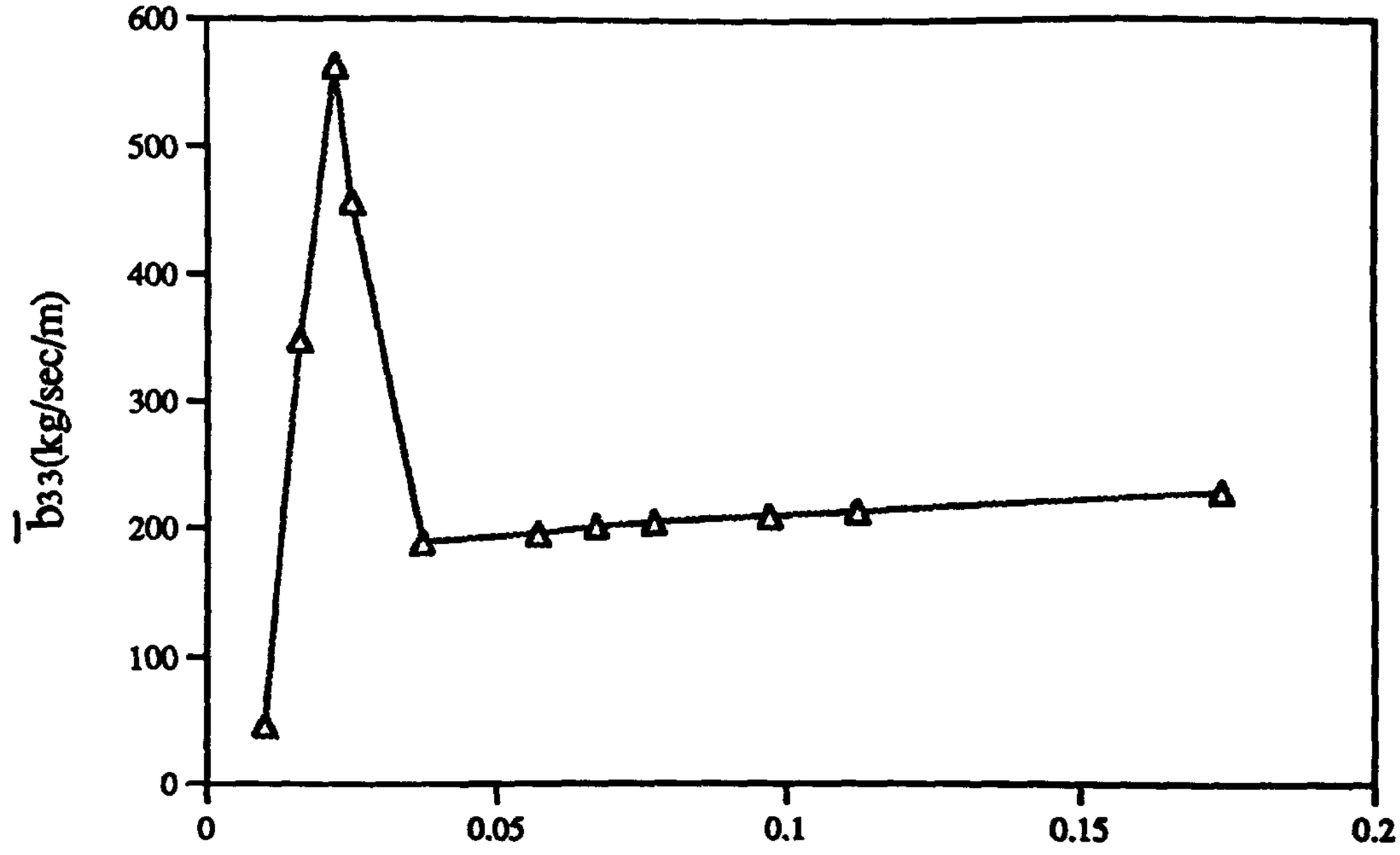

Figure 4.2 : The Damping for the V-1 Catamaran with Different Draught at Section No. 8.(Fn=0.00,ω_0=3.25 rad/sec)

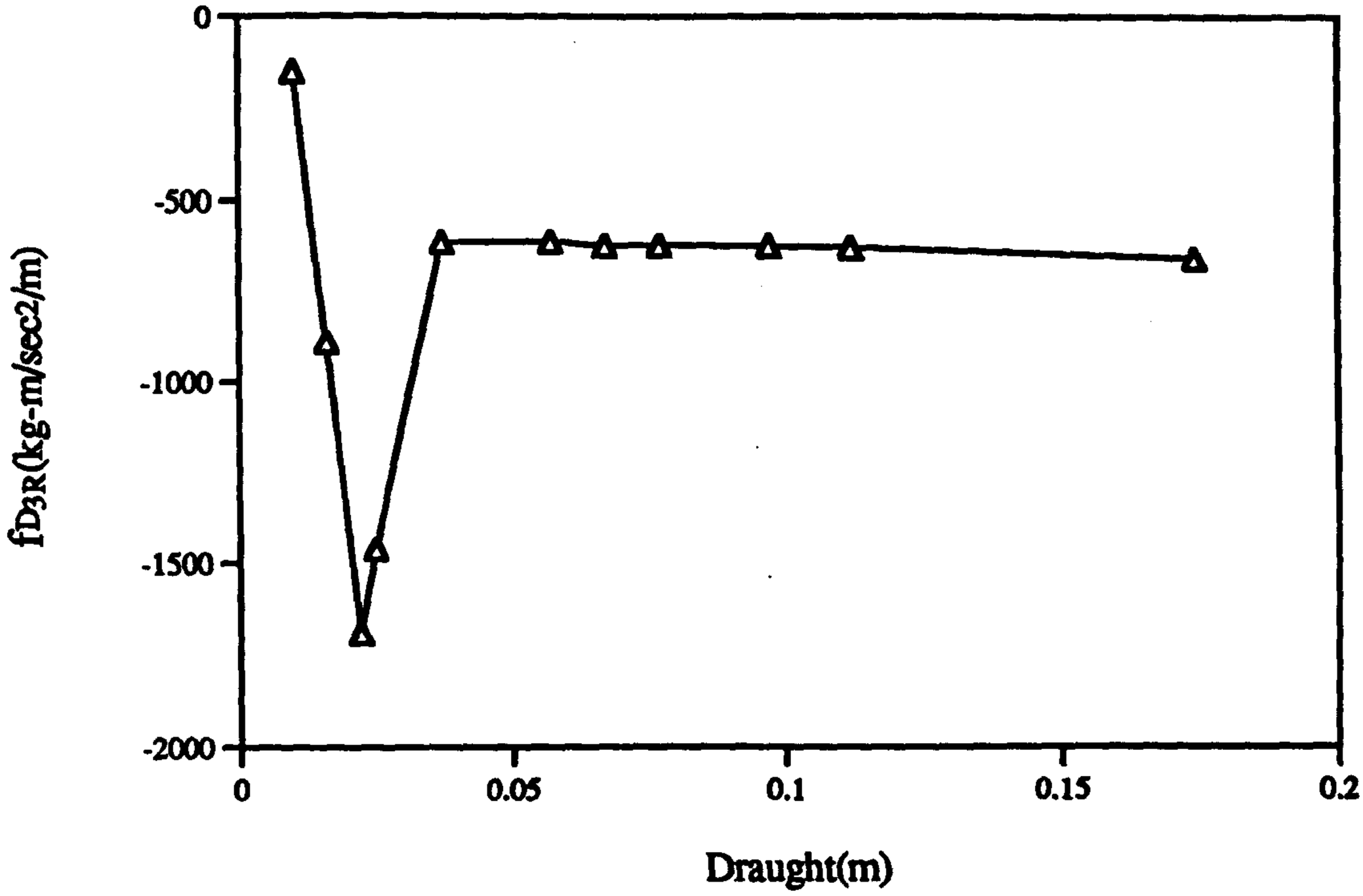

Figure 4.3 : The Real Part of Diffraction Exciting Force for the V-1 Catamaran with Different Draught at Section No. 8. (Fn=0.00,ω_0=3.25 rad/sec)

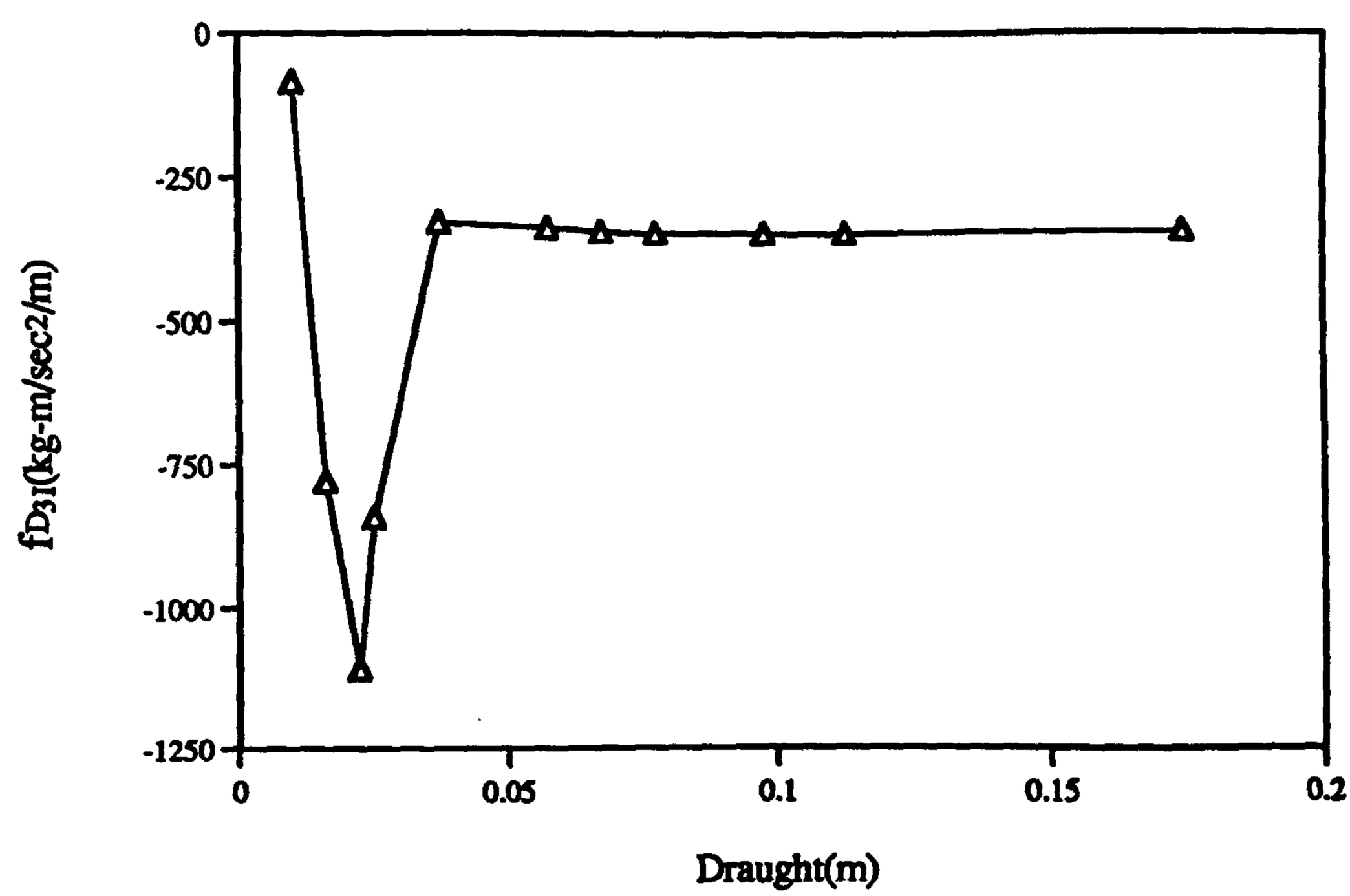

Figure 4.4 : The Imaginary Part of Diffraction Exciting Force for the V-1 Catamaran with Different Draught at Section No. 8. (Fn=0.00,ω_0=3.25 rad/sec)

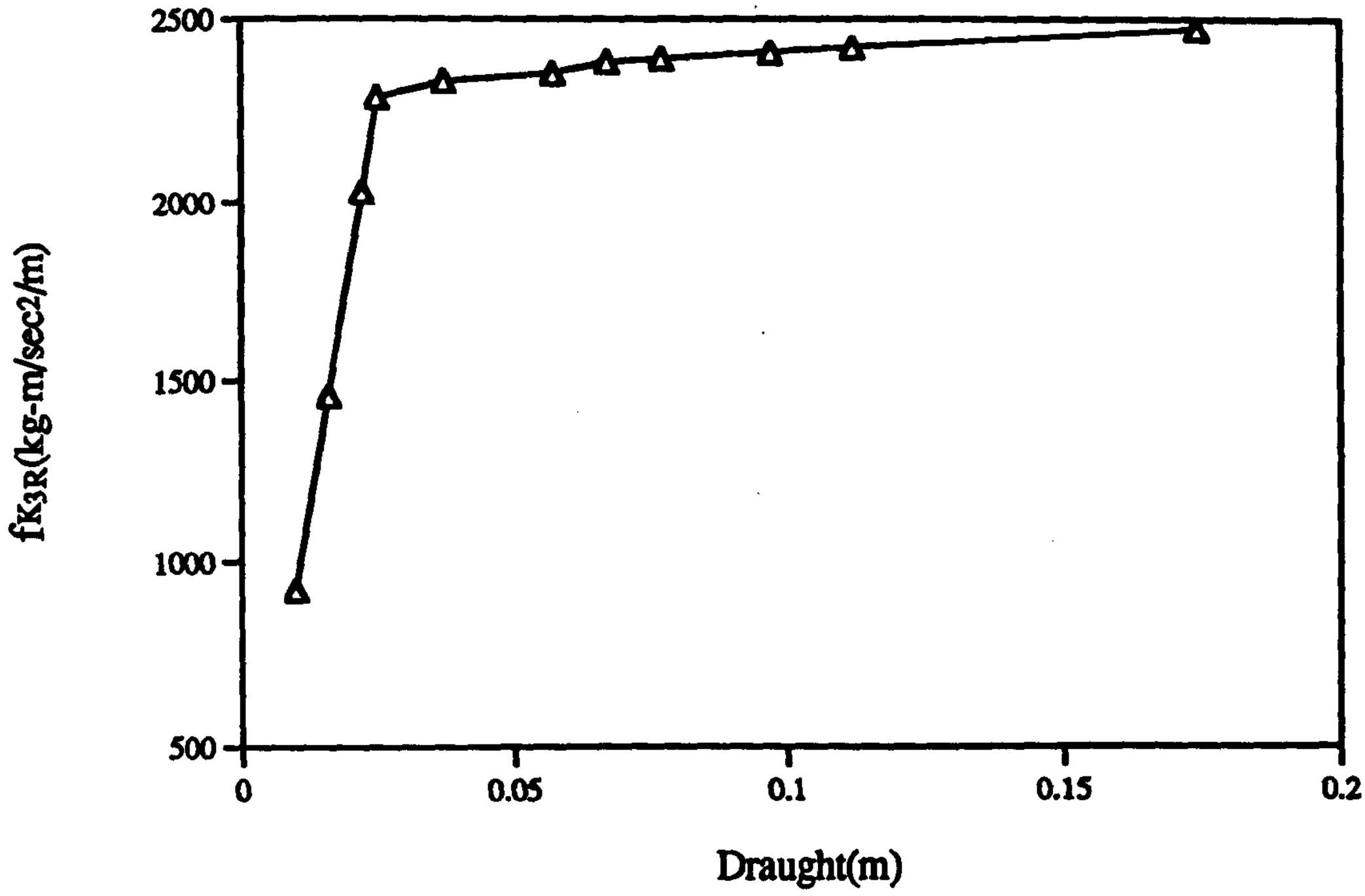

Figure 4.5 : The Real Part of Froude-Krylov Force for the V-1 Catamaran with Different Draught at Section No. 8. (Fn=0.00,ω_0=3.25 rad/sec)

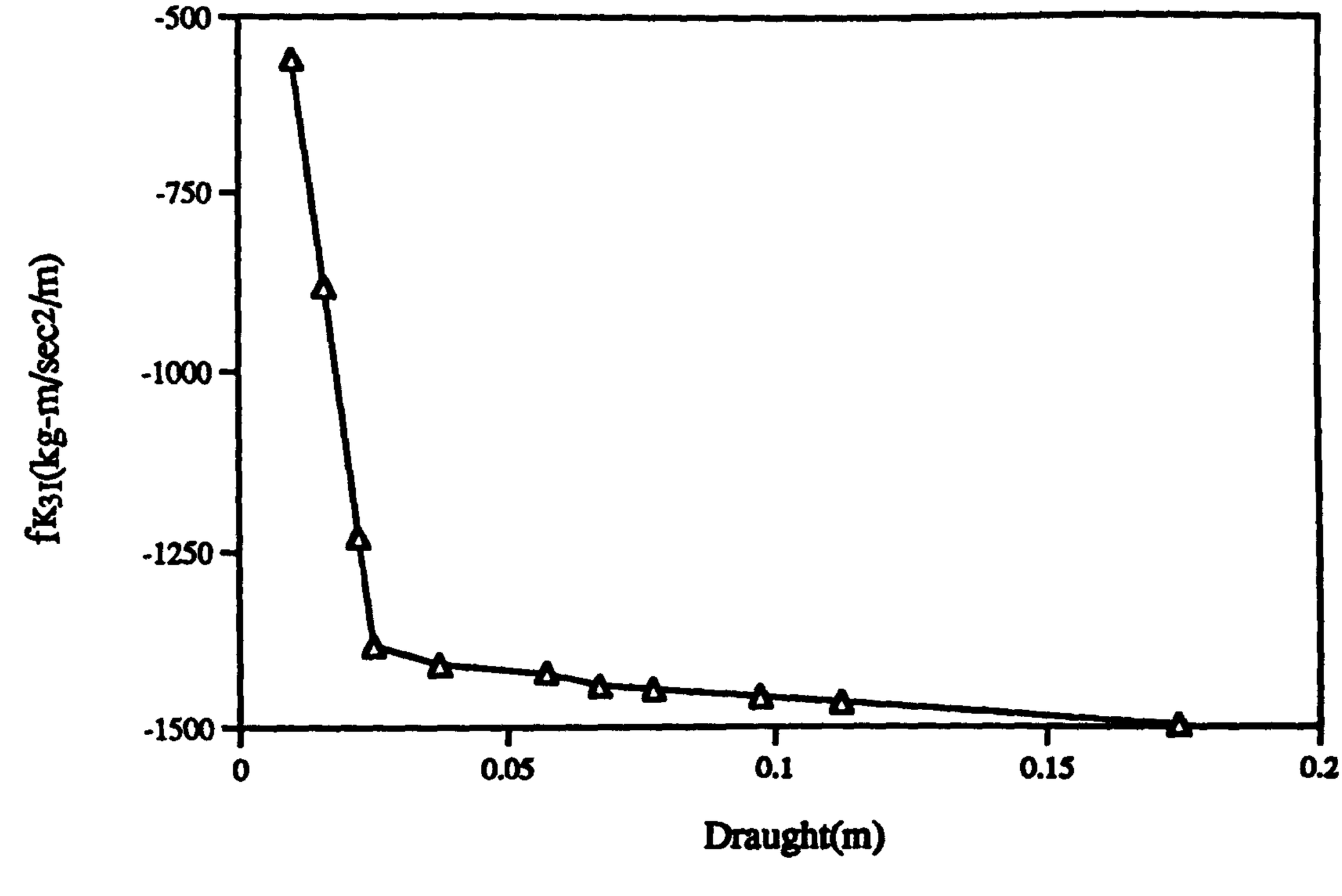

Figure 4.6 : The Imaginary Part of Froude-Krylov Force for the V-1 Catamaran with Different Draught at Section No. 8. (Fn=0.00,ω_0=3.25 rad/sec)

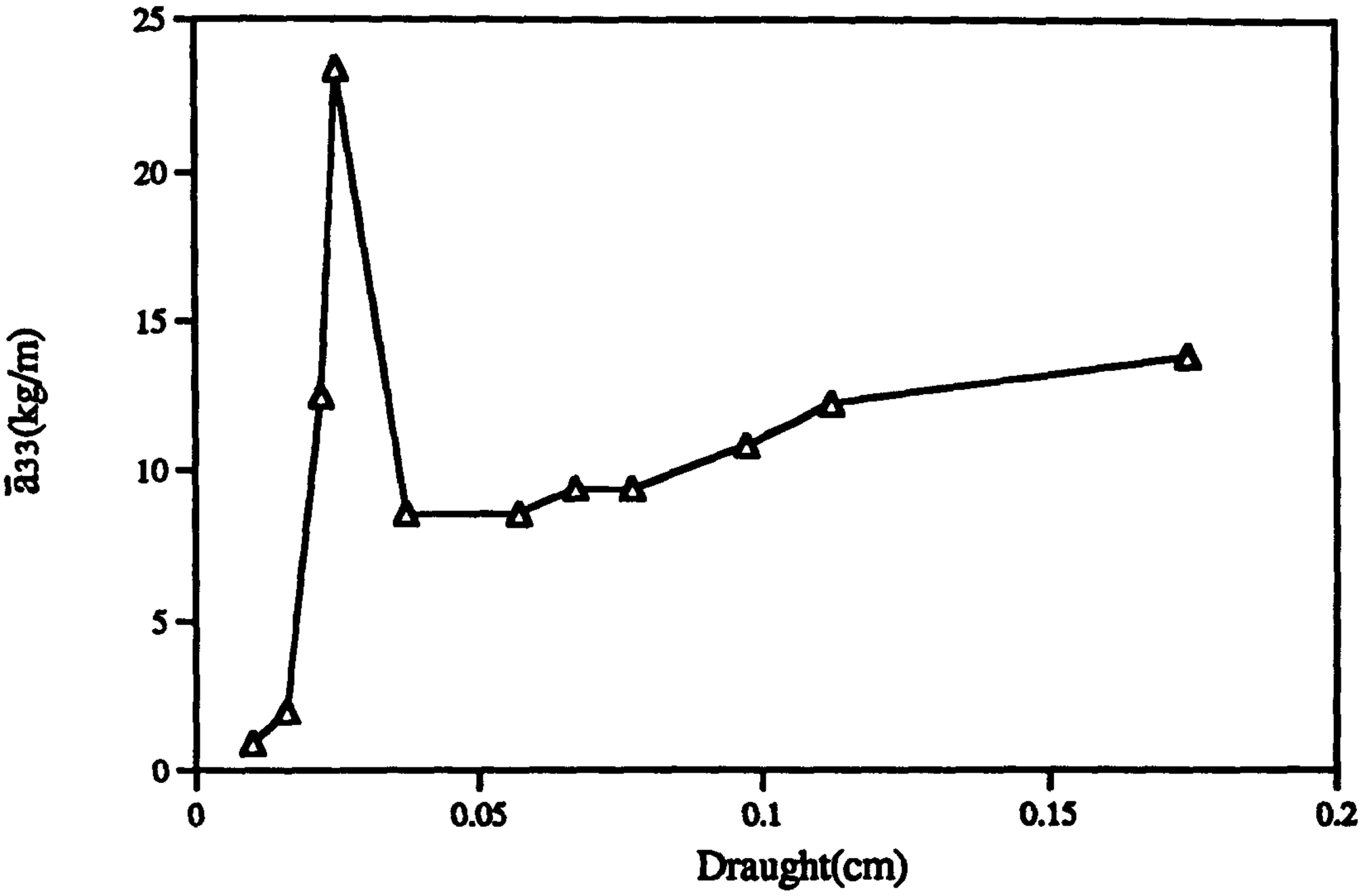

Figure 4.7 : The Added Mass for the V-1 Catamaran with Different Draught at Section No. 8.(Fn=0.00,ω_0=5.5 rad/sec)

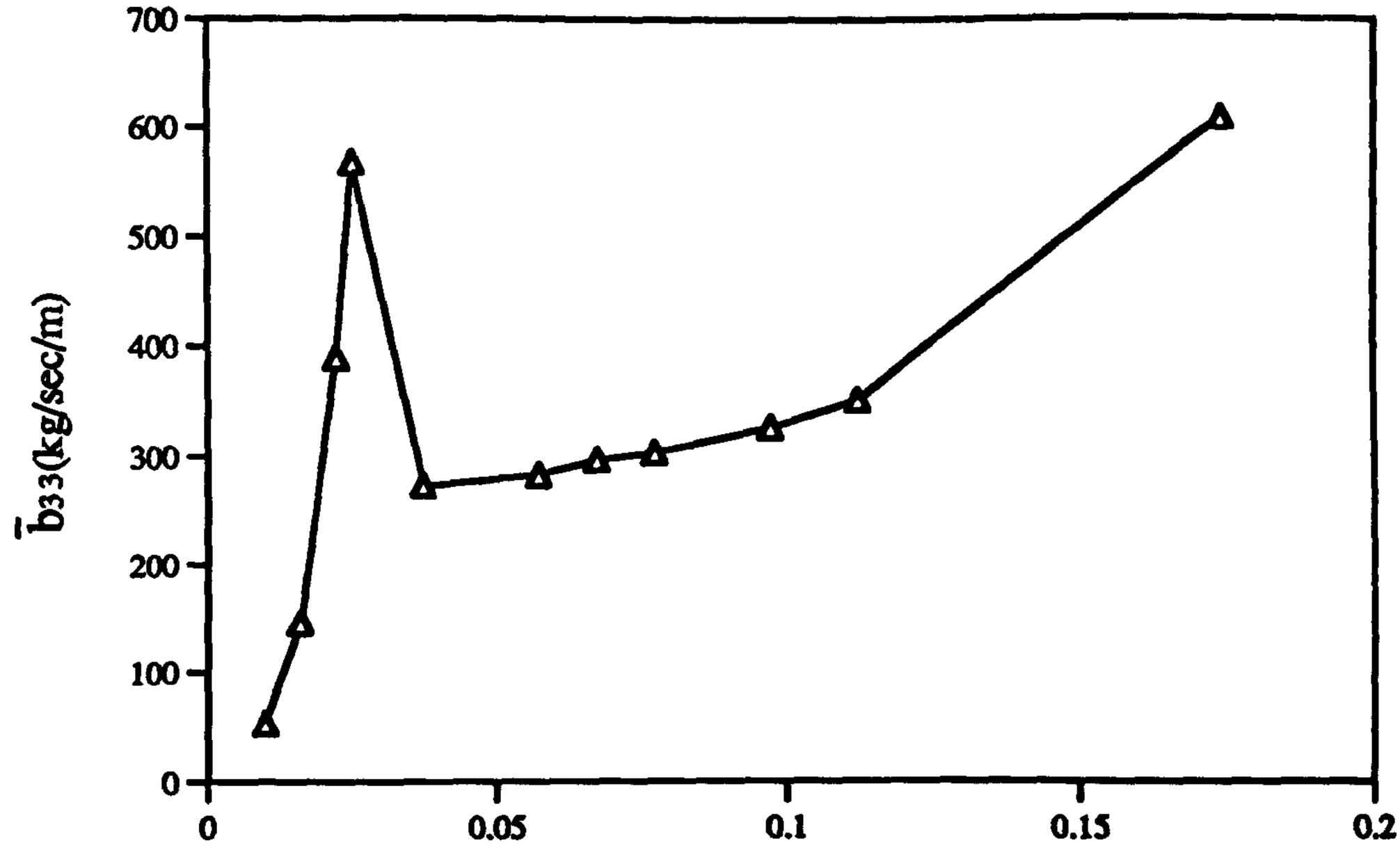

Figure 4.8 : The Damping for the V-1 Catamaran with Different Draught at Section No. 8.(Fn=0.00,ω_0=5.5 rad/sec)

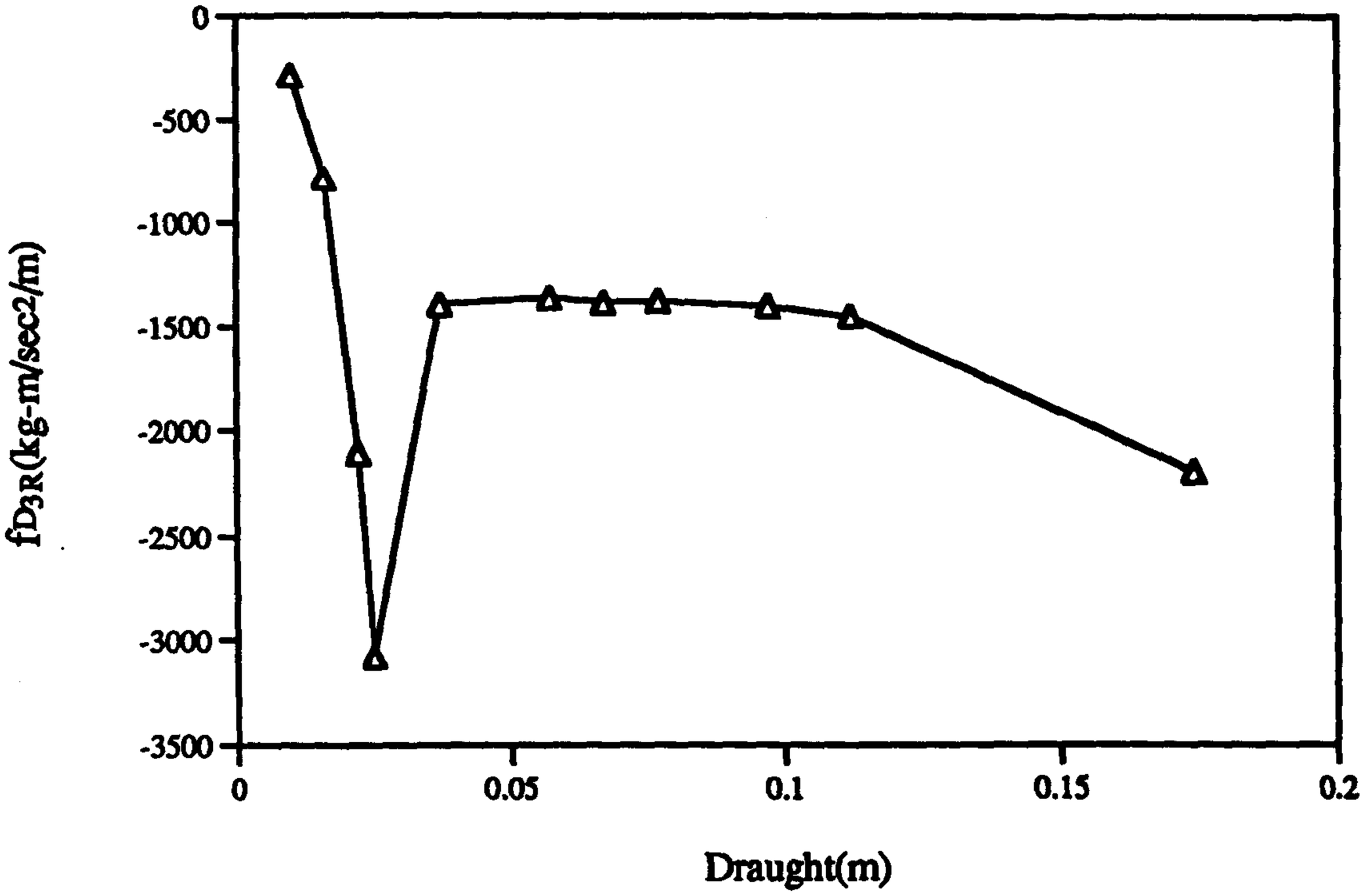

Figure 4.9 : The Real Part of Diffraction Exciting Force for the V-1 Catamaran with Different Draught at Section No. 8. (Fn=0.00,ω_0=5.5 rad/sec)

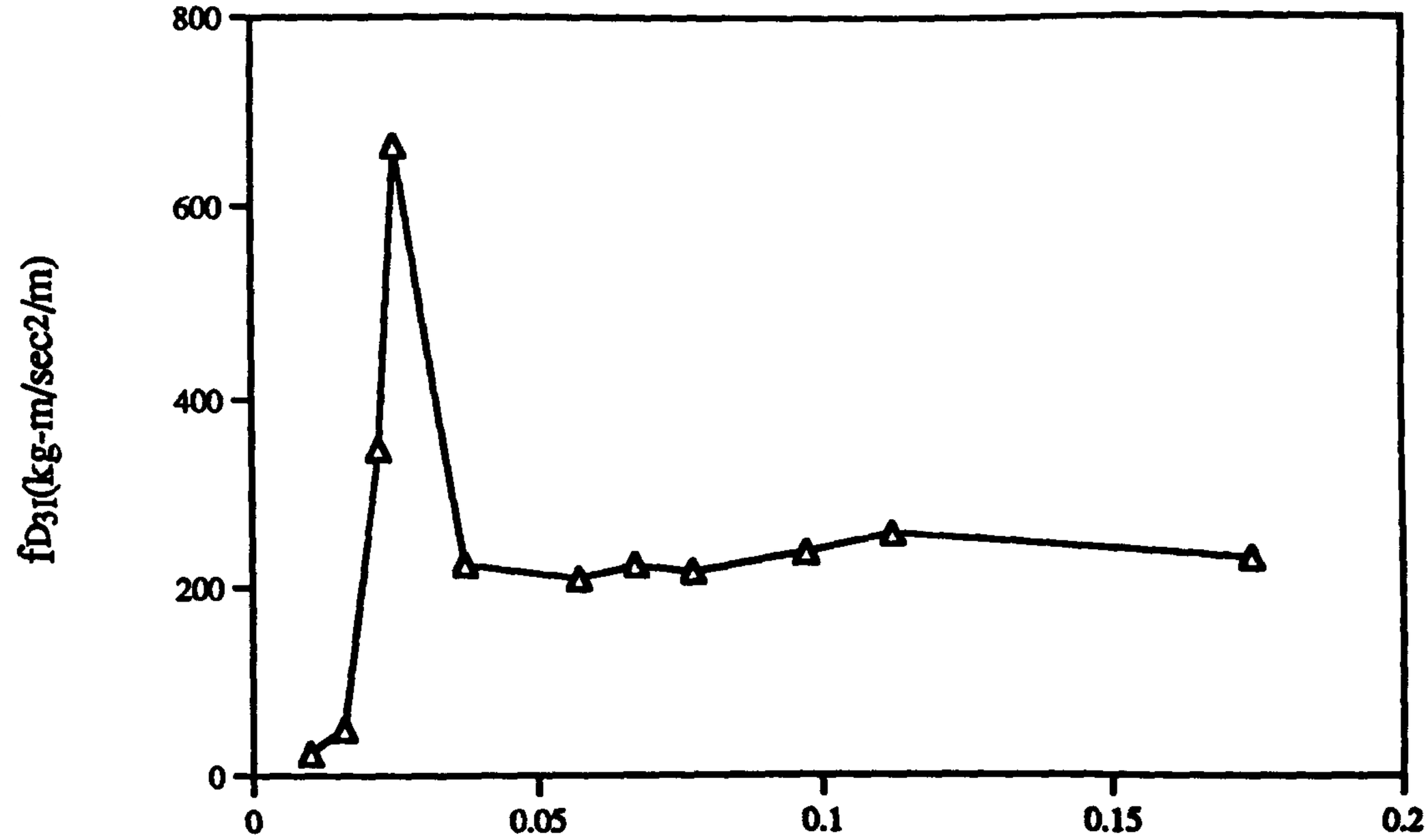

Figure 4.10 : The Imaginary Part of Diffraction Exciting Force for the V-1 Catamaran with Different Draught at Section No. 8. (Fn=0.00,ω_0=5.5 rad/sec)

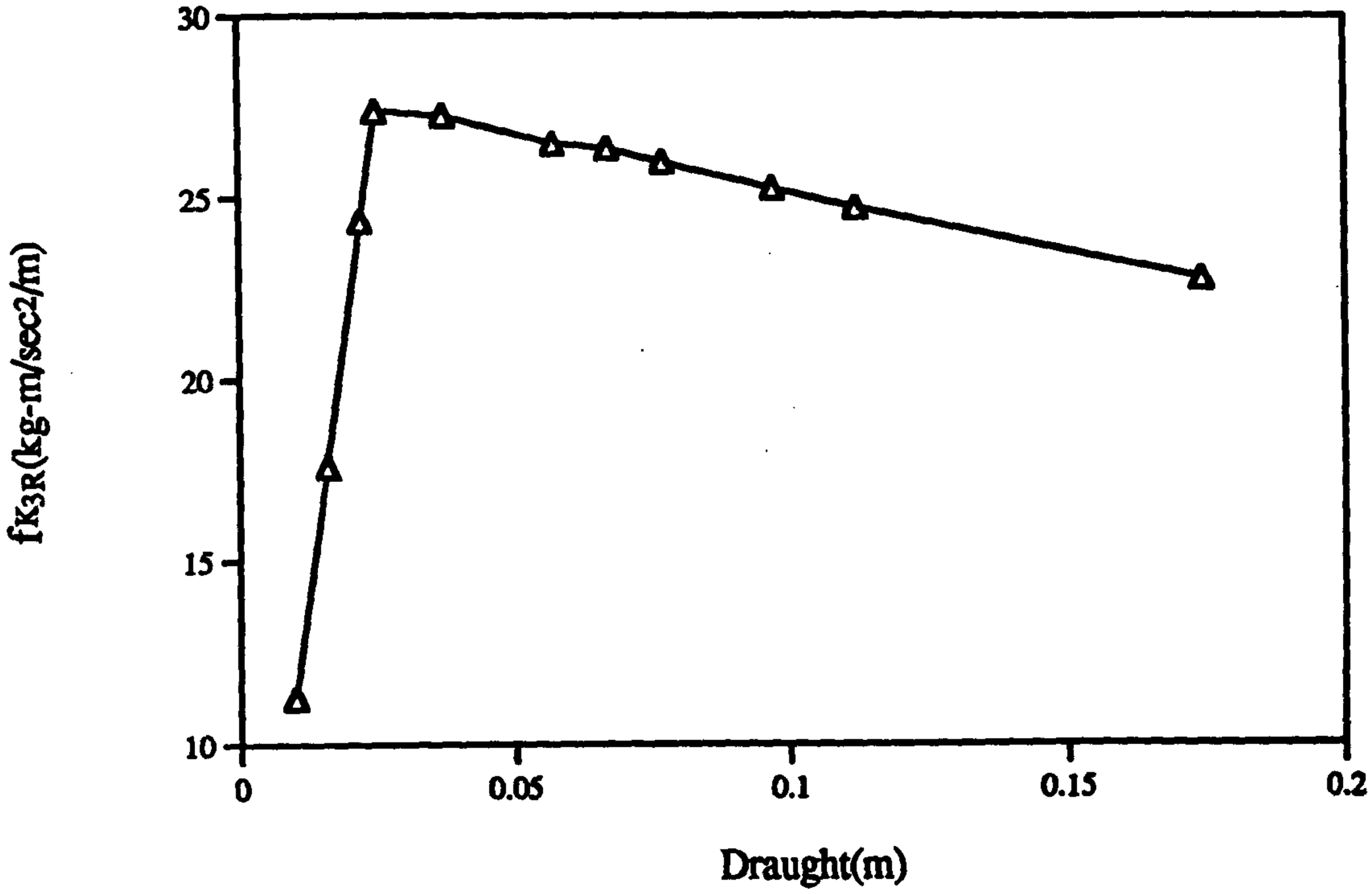

Figure 4.11 : The Real Part of Froude-Krylov Force for the V-1 Catamaran with Different Draught at Section No. 8. (Fn=0.00,ω_0=5.5 rad/sec)

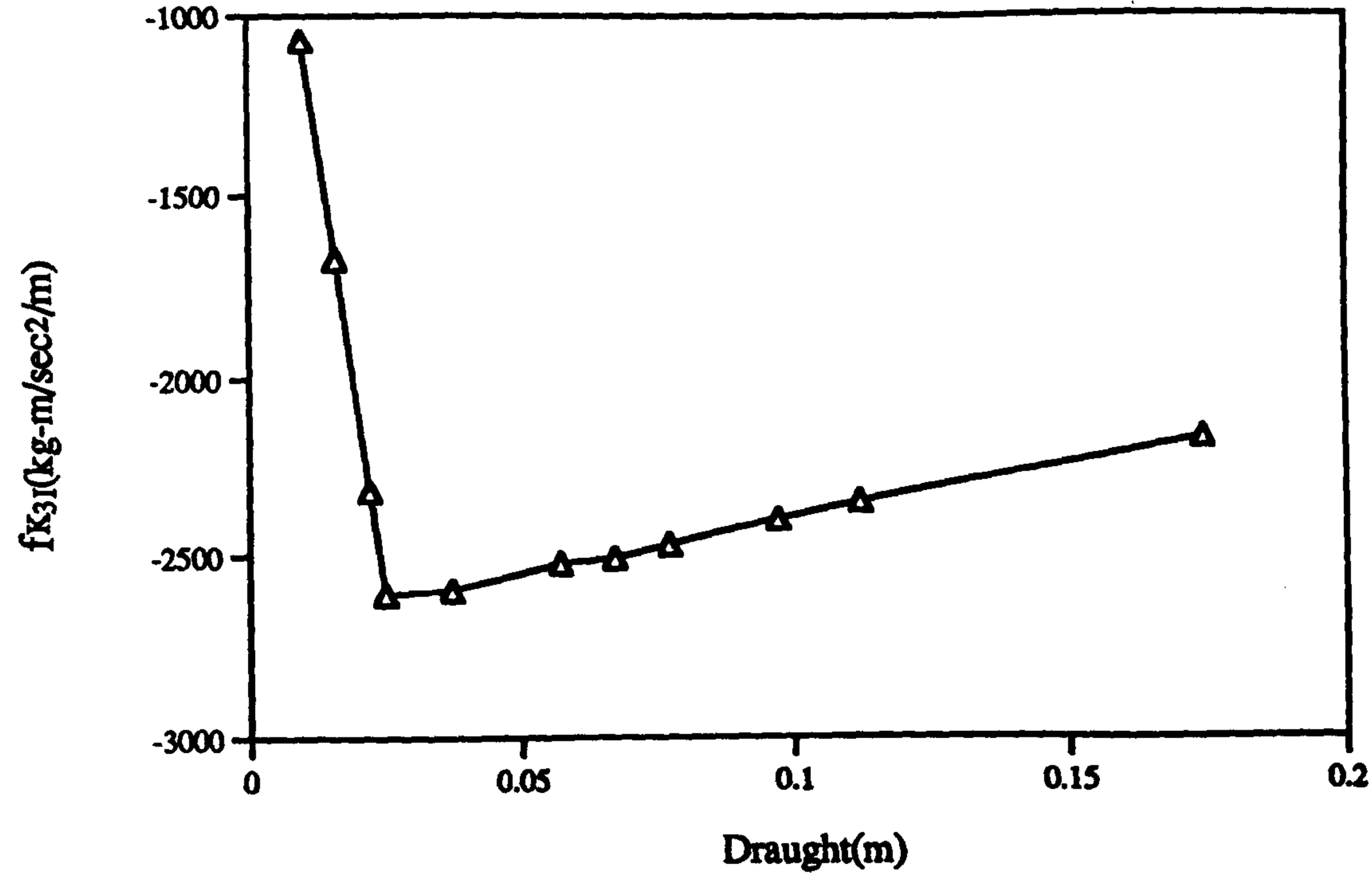

Figure 4.12 : The Imaginary Part of Froude-Krylov Force for the V-1 Catamaran with Different Draught at Section No. 8. (Fn=0.00,ω_0=5.5 rad/sec)

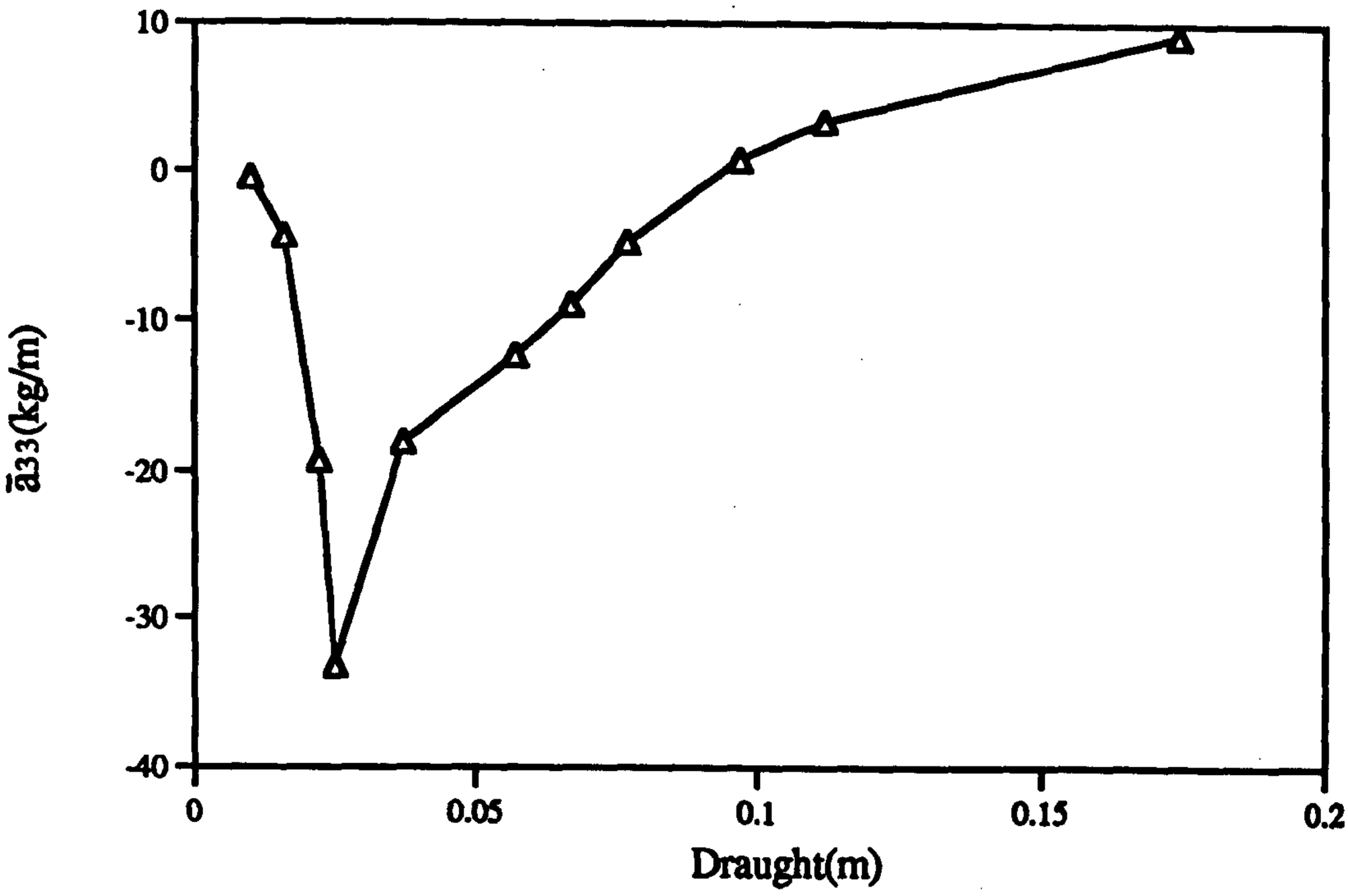

Figure 4.13 : The Added Mass for the V-1 Catamaran with Different Draught at Section No. 8.(Fn=0.00,ω_0=7.5 rad/sec)

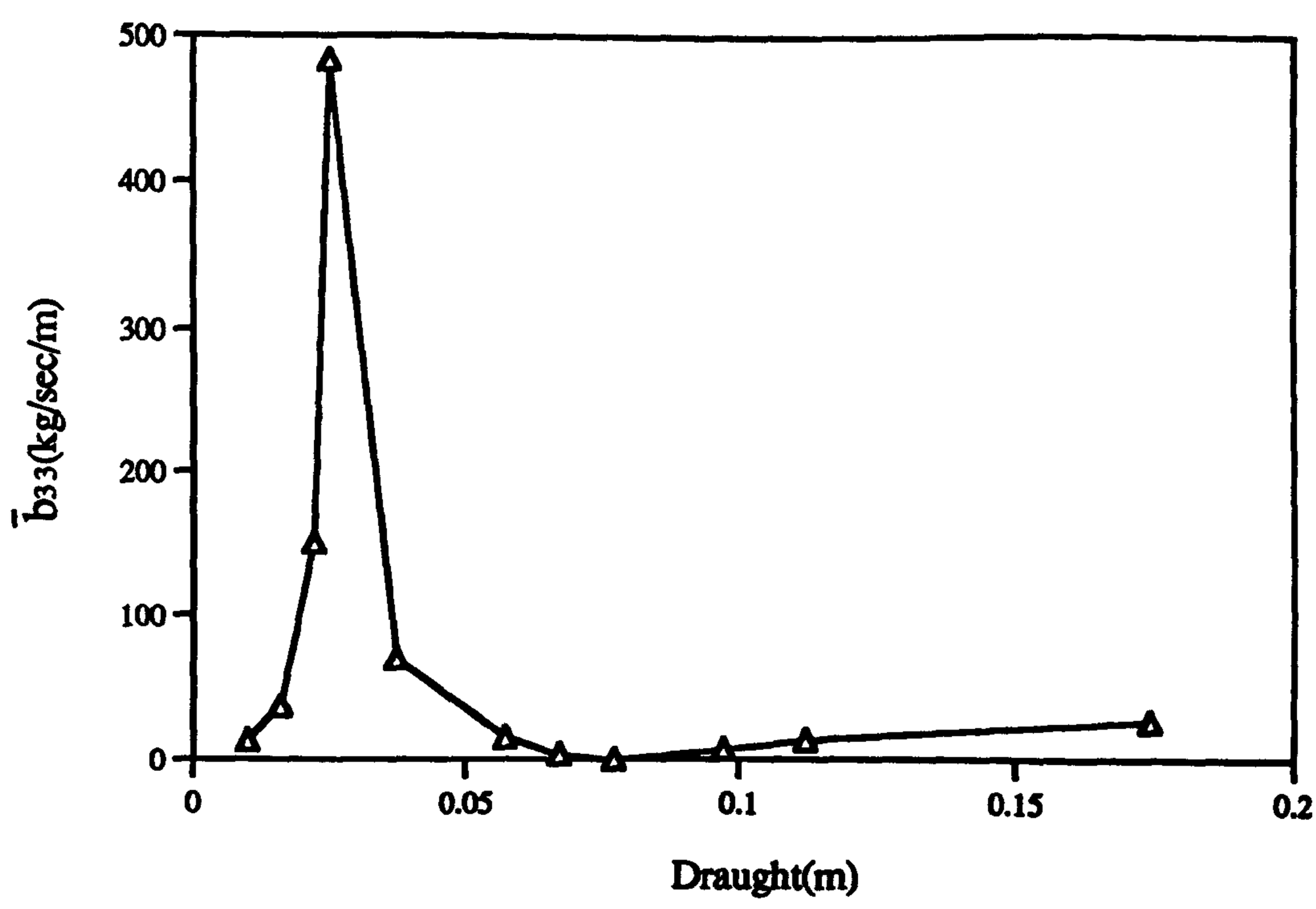

Figure 4.14 : The Damping for the V-1 Catamaran with Different Draught at Section No. 8.(Fn=0.00,ω_0=7.5 rad/sec)

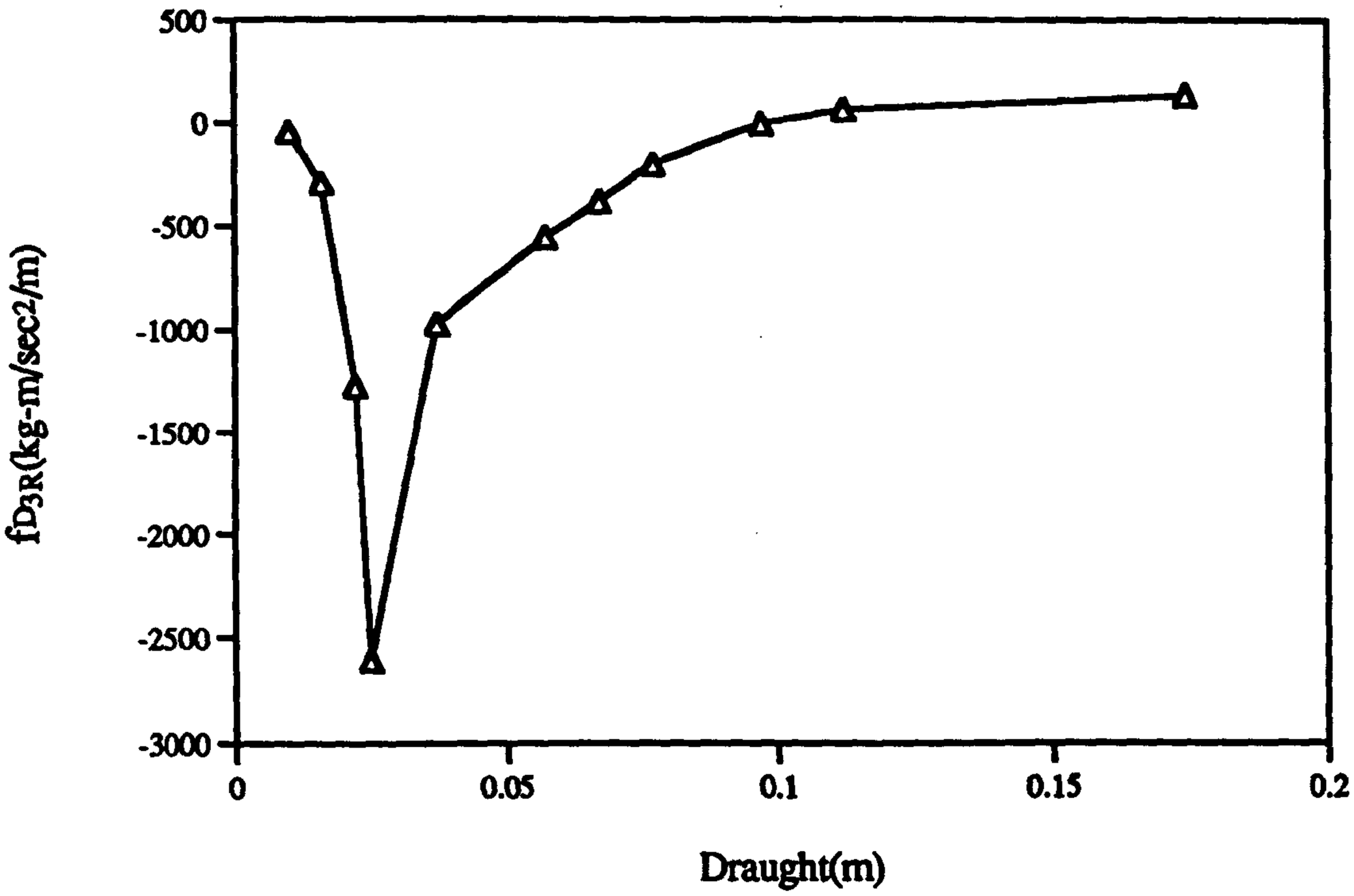

Figure 4.15 : The Real Part of Diffraction Exciting Force for the V-1 Catamaran with Different Draught at Section No. 8. (Fn=0.00,ω_0=7.5 rad/sec)

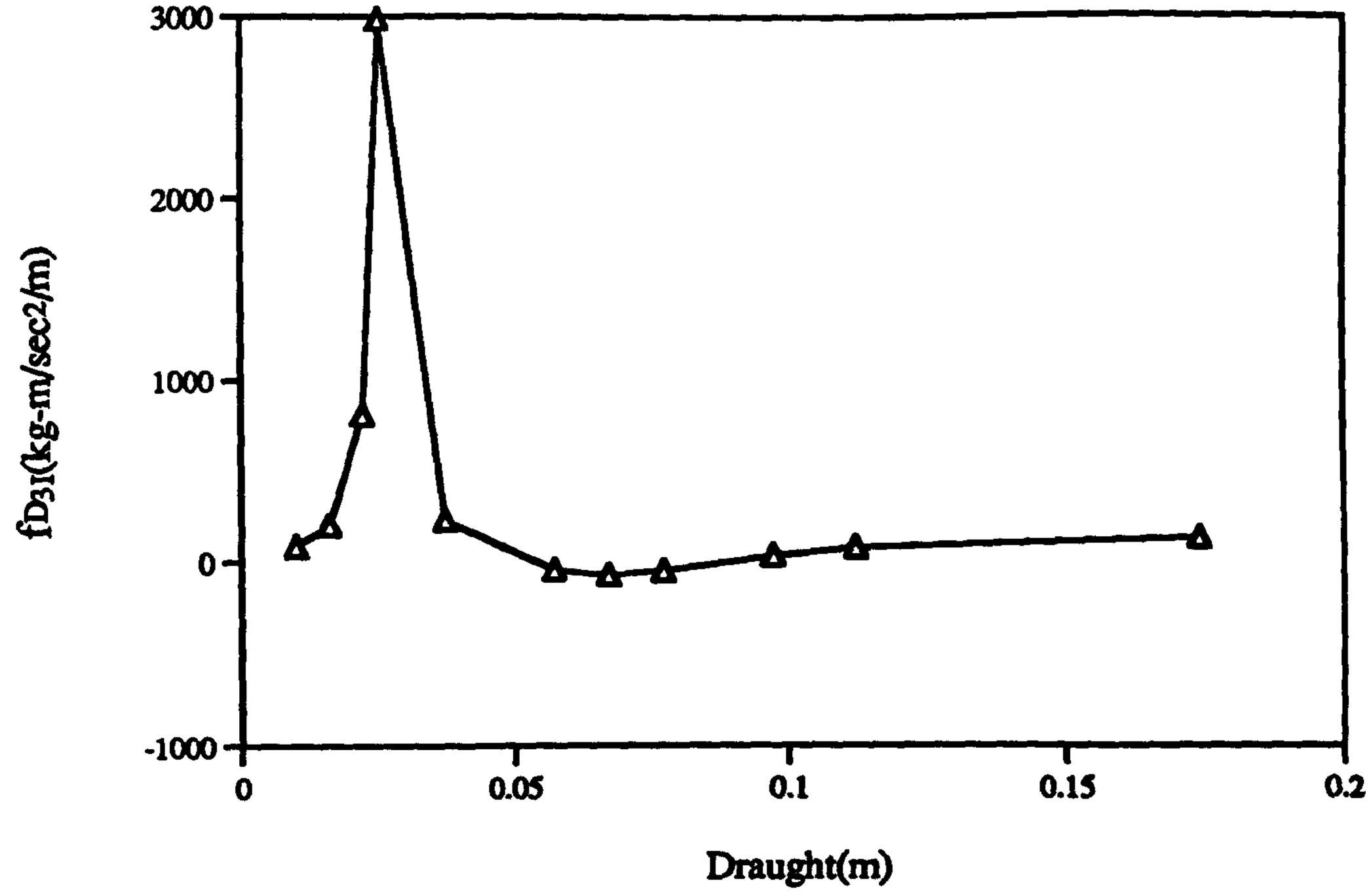

Figure 4.16 : The Imaginary Part of Diffraction Exciting Force for the V-1 Catamaran with Different Draught at Section No. 8. (Fn=0.00,ω_0=7.5 rad/sec)

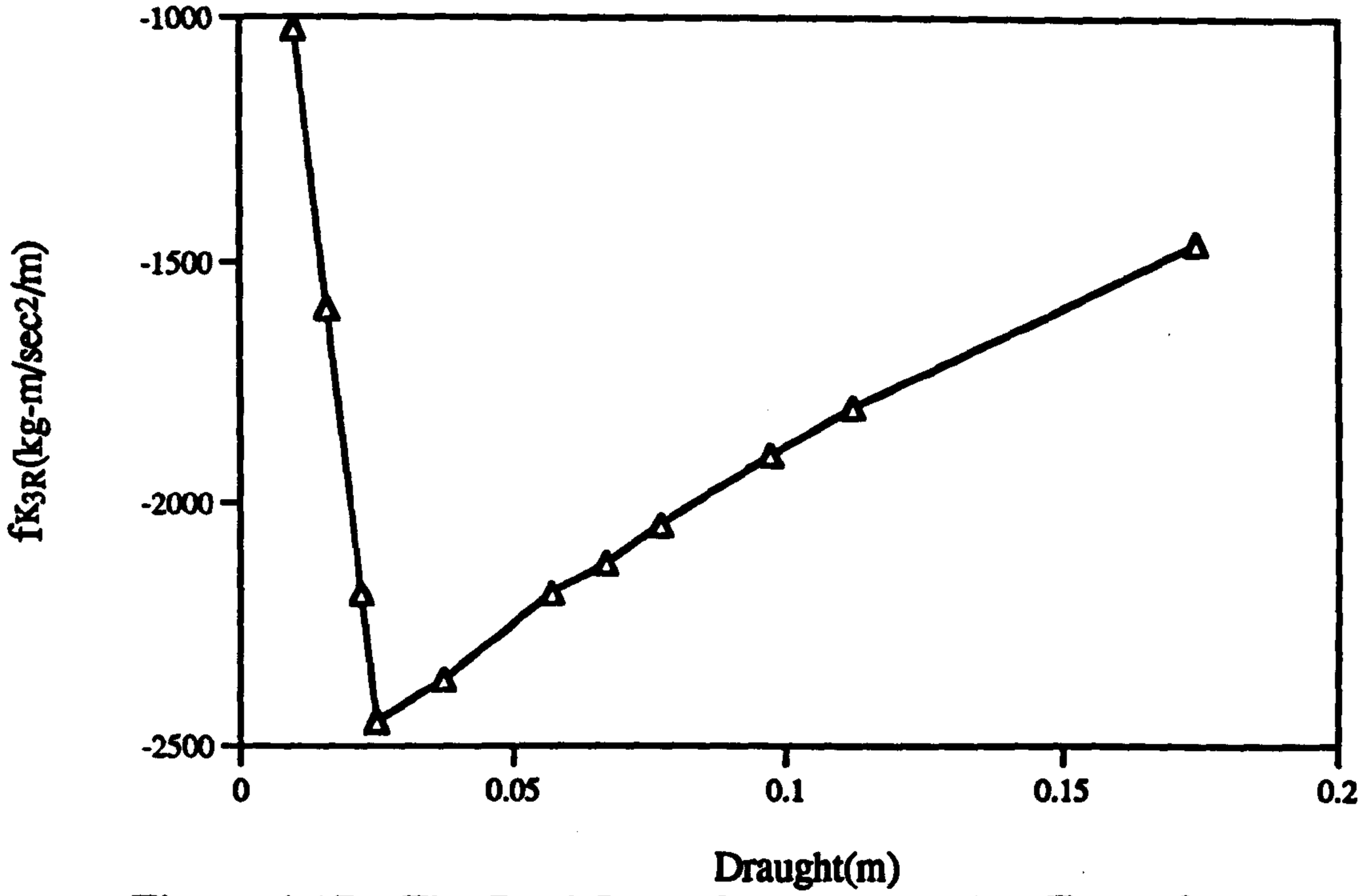

Figure 4.17 : The Real Part of Froude-Krylov Force for the V-1 Catamaran with Different Draught at Section No. 8. (Fn=0.00,ω_0=7.5 rad/sec)

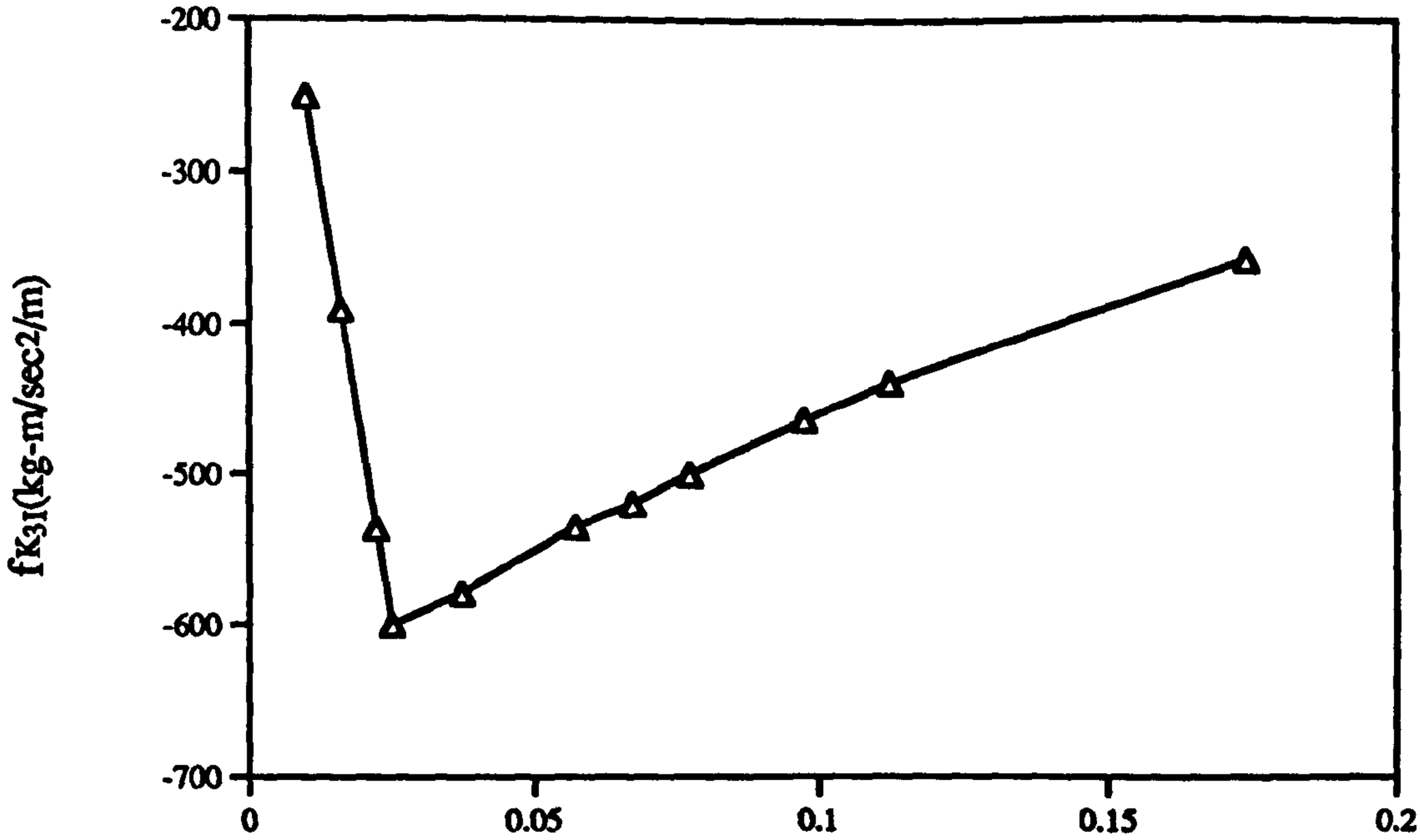

Figure 4.18 : The Imaginary Part of Froude-Krylov Force for the V-1 Catamaran with Different Draught at Section No. 8. (Fn=0.00,ω_0=7.5 rad/sec)

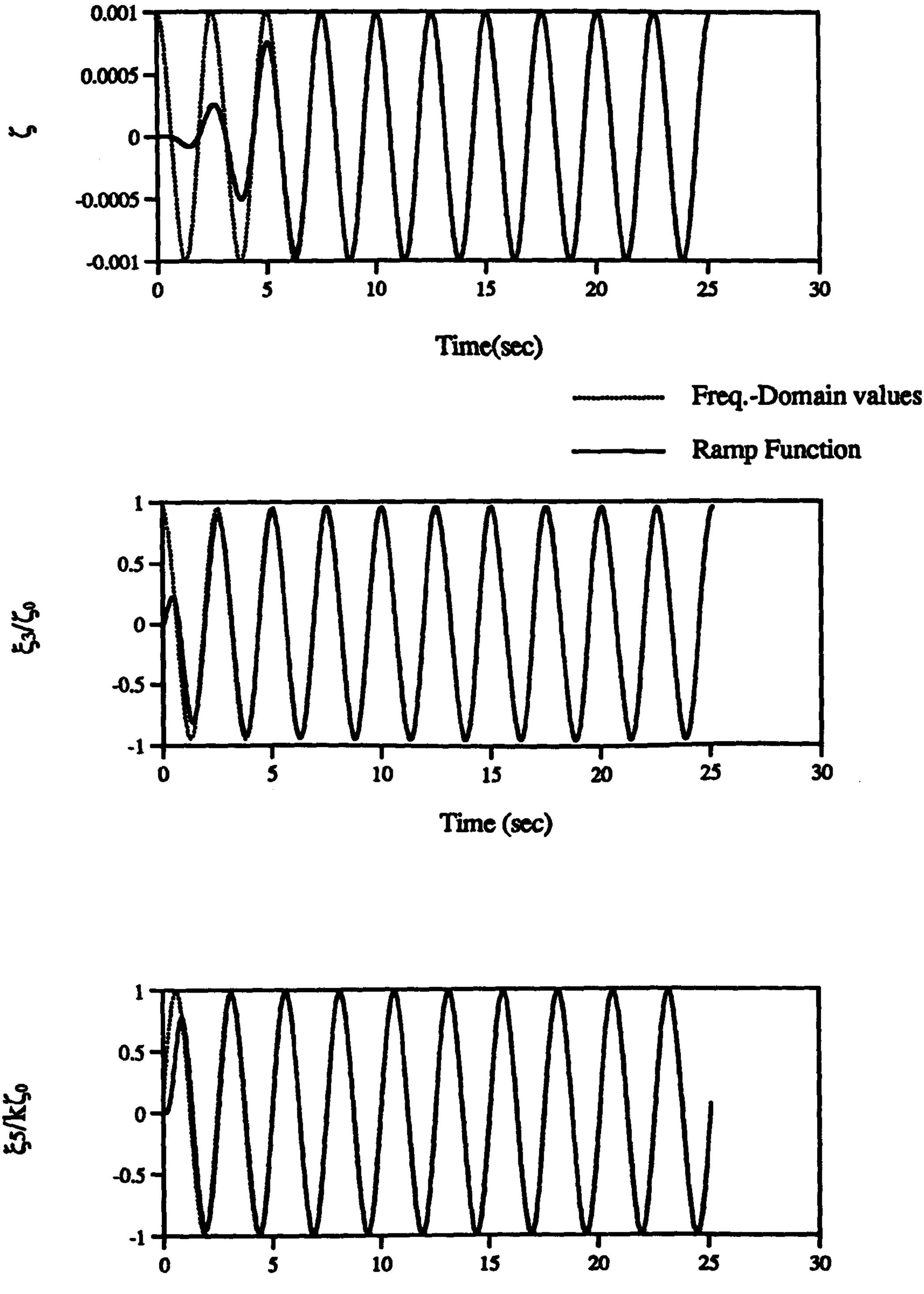

Figure 4.19 : Initial Value Problem for the Time Domain Simulation (Fn=0.00, ω_o=2.5 rad/sec)

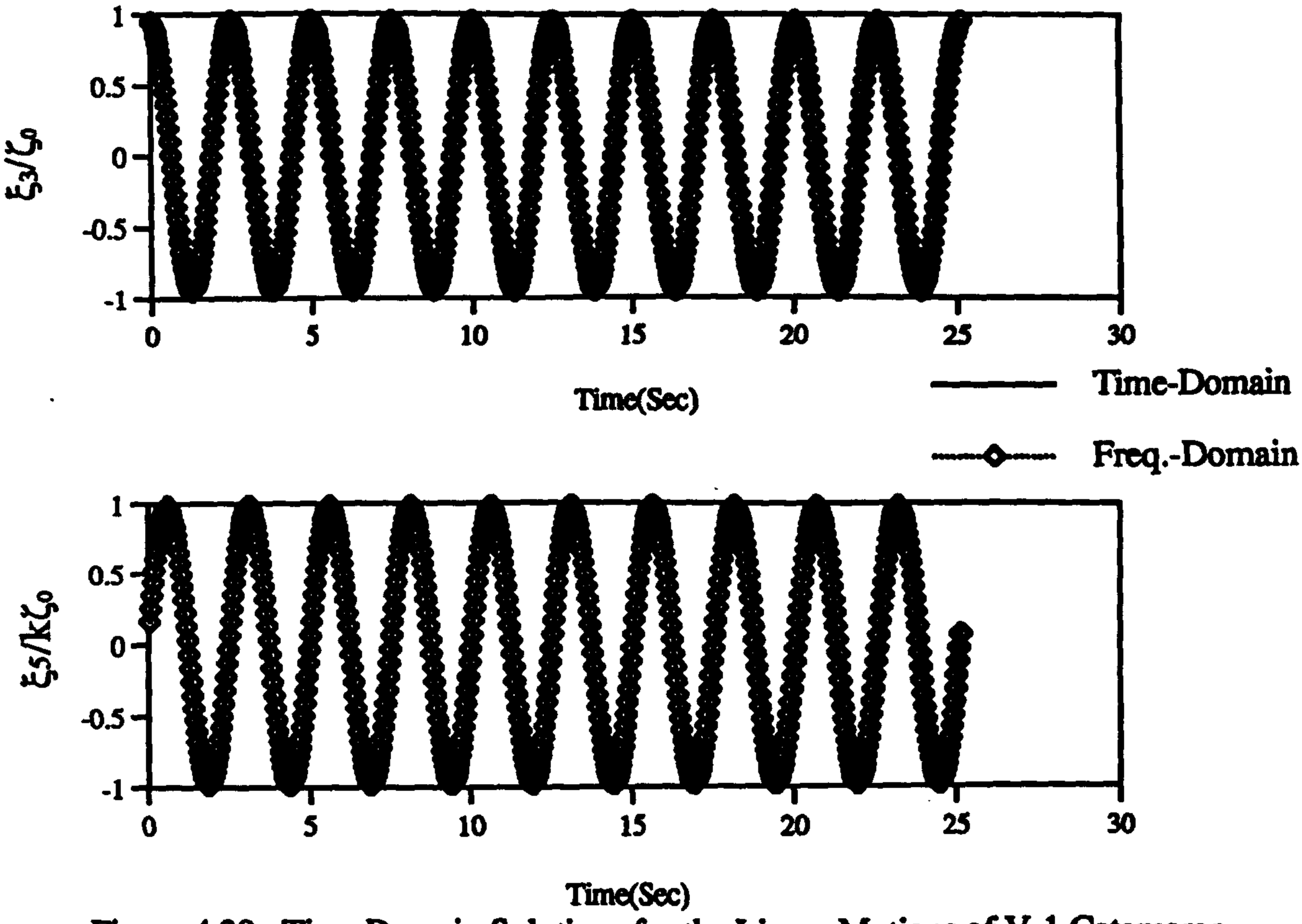

Figure 4.20 : Time Domain Solutions for the Linear Motions of V-1 Catamaran (Fn=0.00,ζ_0=0.1cm,ω_0=2.5 rad/sec)

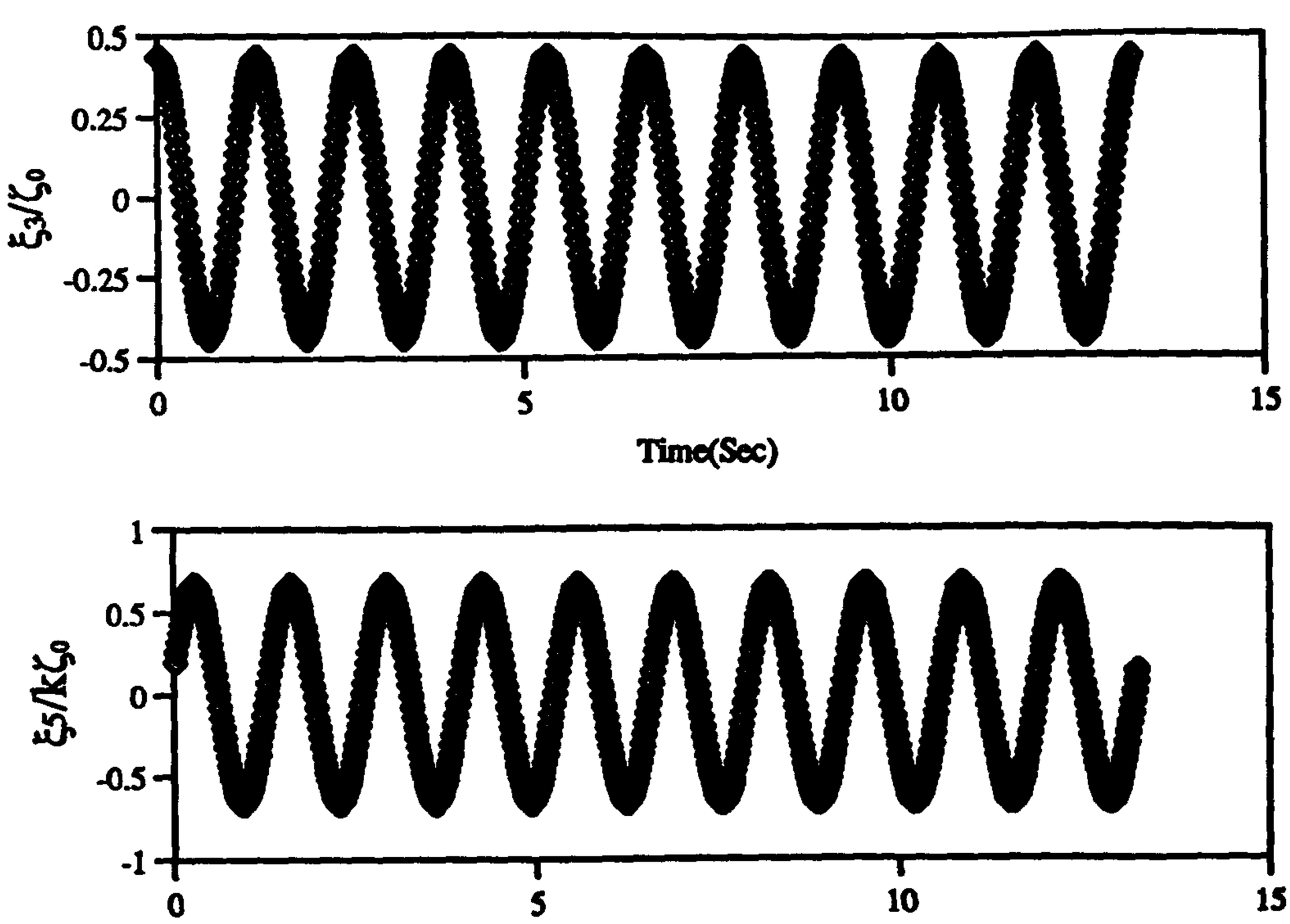

Figure 4.21 : Time Domain Solutions for the Linear Motions of V-1 Catamaran (Fn=0.00,ζ_0=0.1cm,ω_0=4.75 rad/sec)

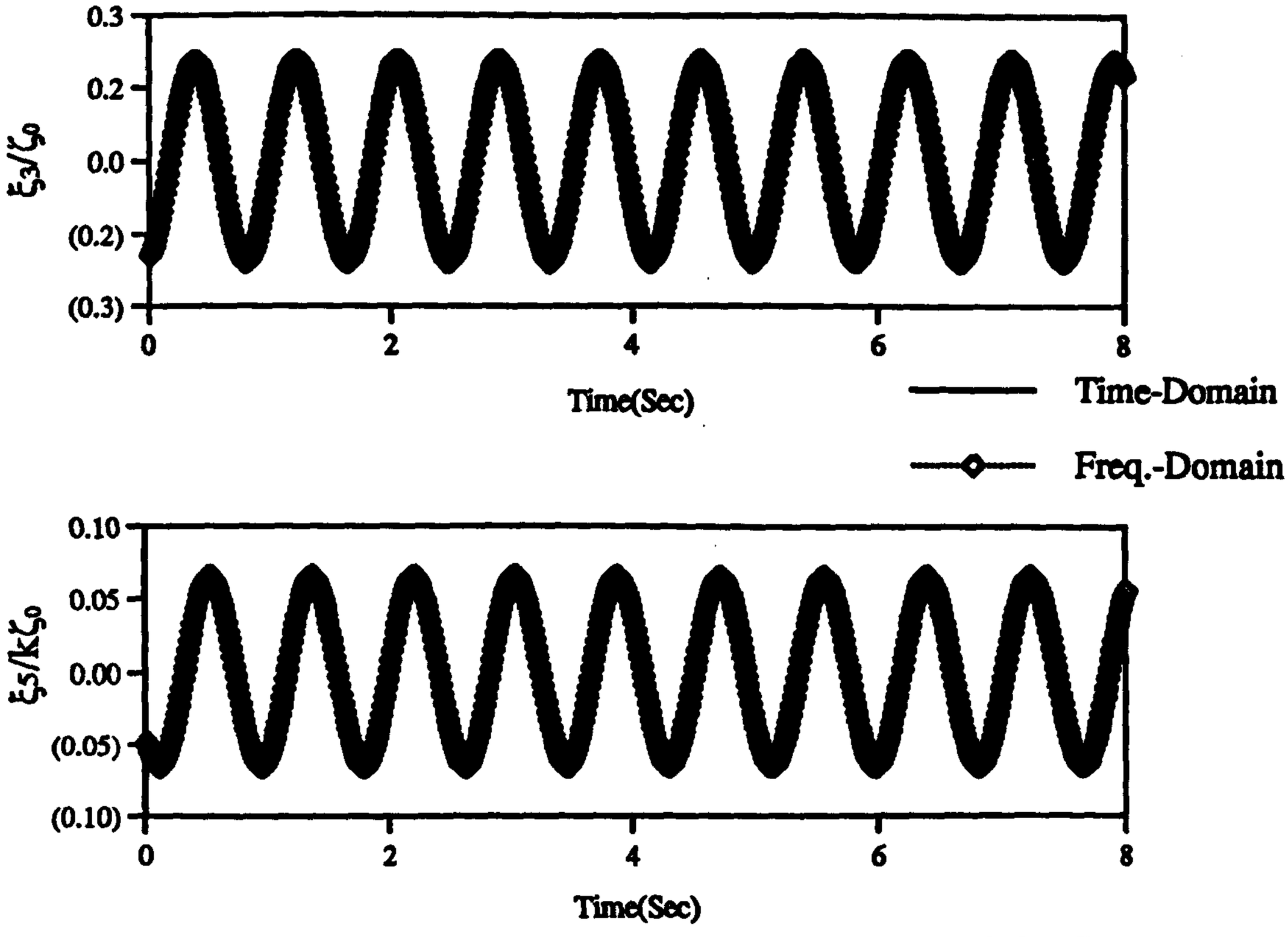

Figure 4.22 : Time Domain Solutions for the Linear Motions of V-1 Catamaran (Fn=0.00,ζ_0=0.1cm,ω_0=7.5 rad/sec)

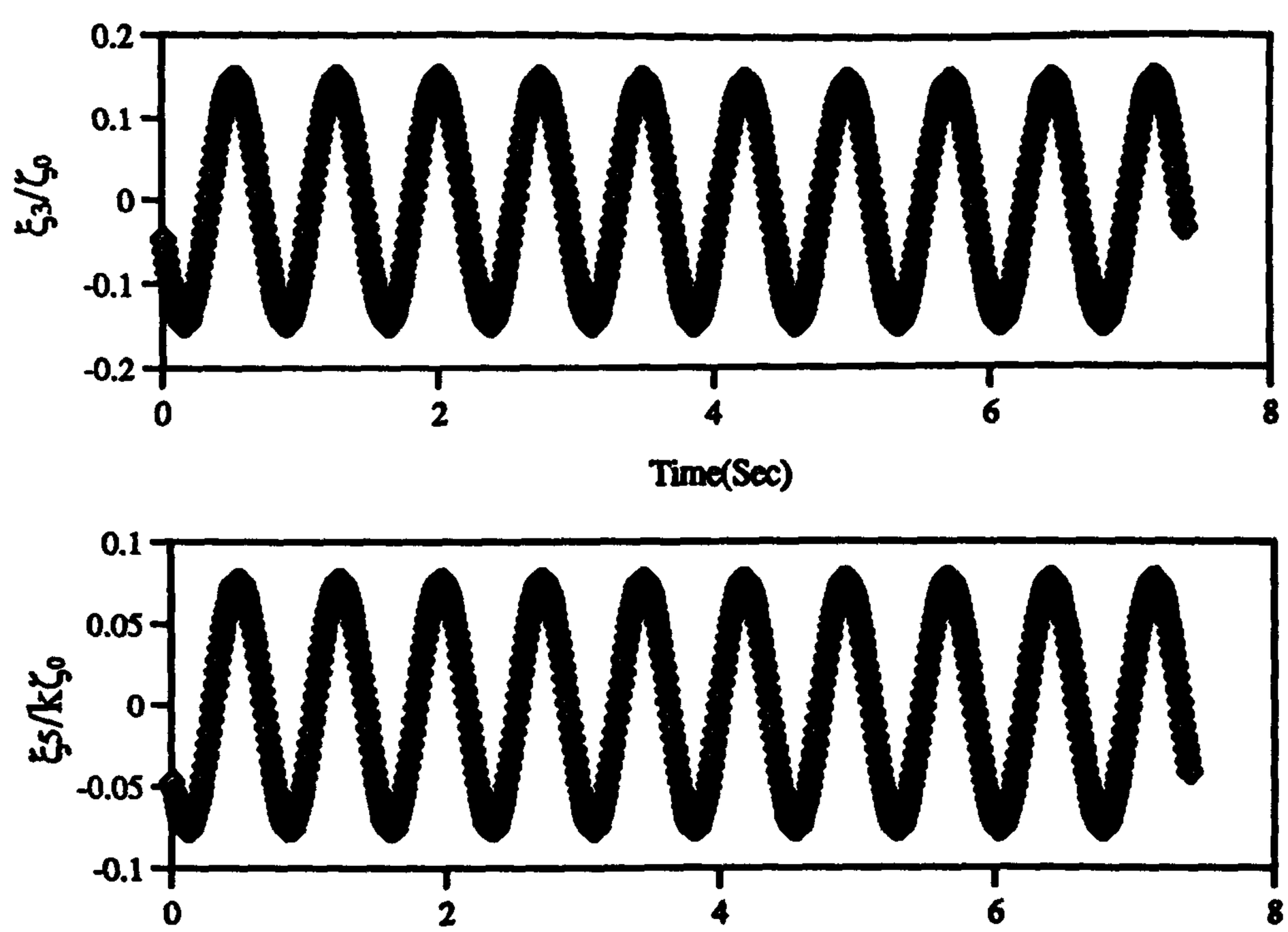

Figure 4.23 : Time Domain Solutions for the Linear Motions of V-1 Catamaran (Fn=0.00,ζ_0=0.1cm,ω_0=8.5 rad/sec)

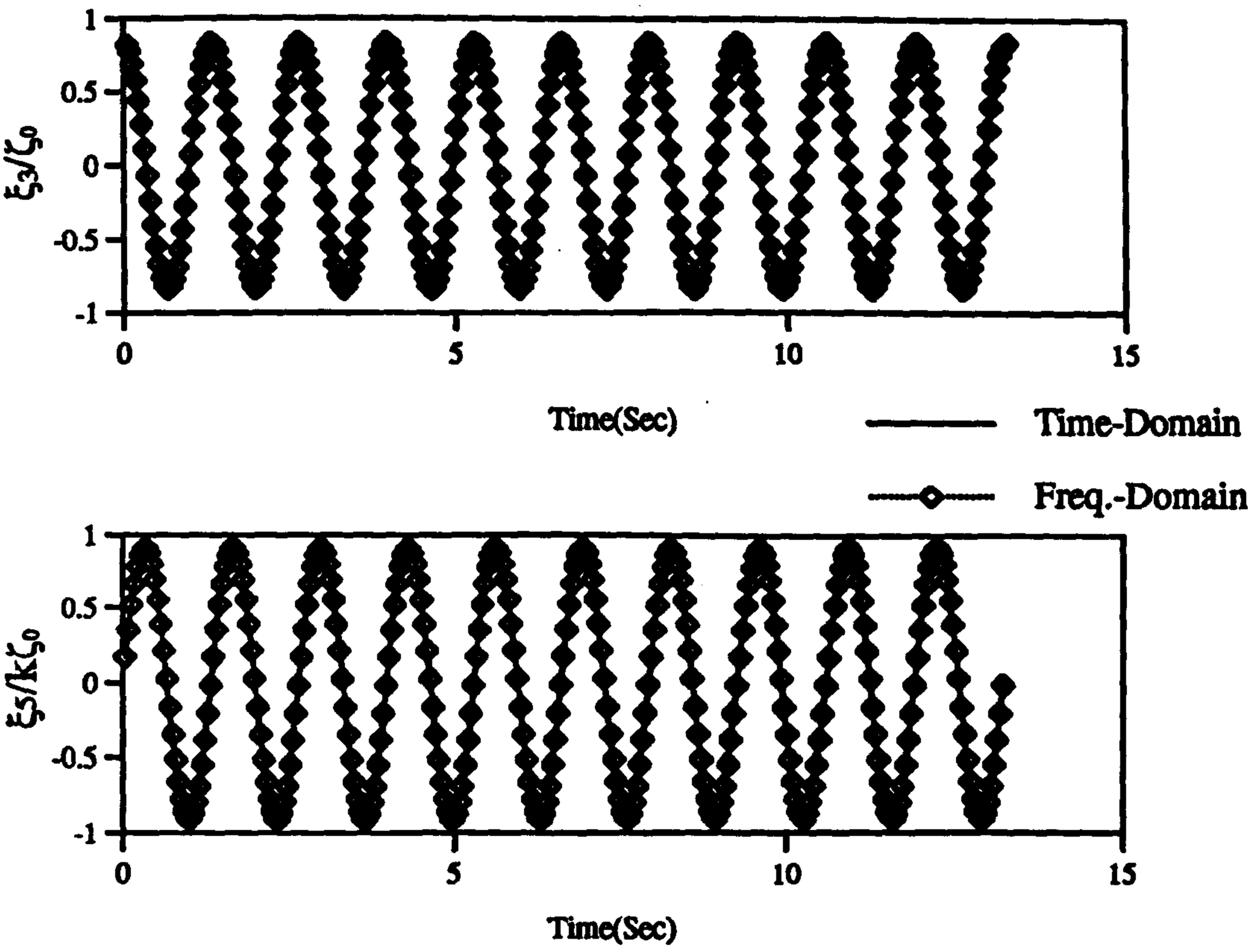

Figure 4.24 : Time Domain Solutions for the Linear Motions of V-1 Catamaran (Fn=0.226,ζ_0=0.1cm,ω_0=3.5 rad/sec)

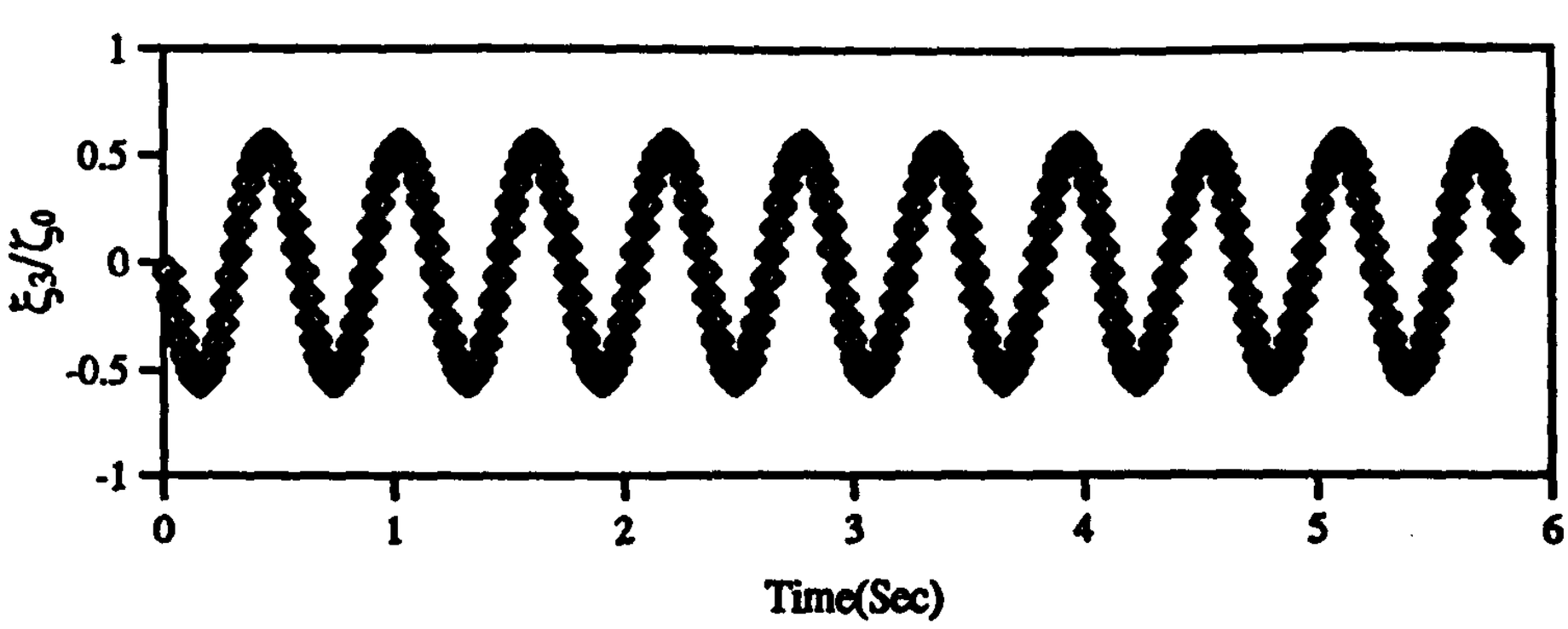

Figure 4.25 : Time Domain Solutions for the Linear Motions of V-1 Catamaran (Fn=0.226,ζ_0=0.1cm,ω_0=6.5 rad/sec)

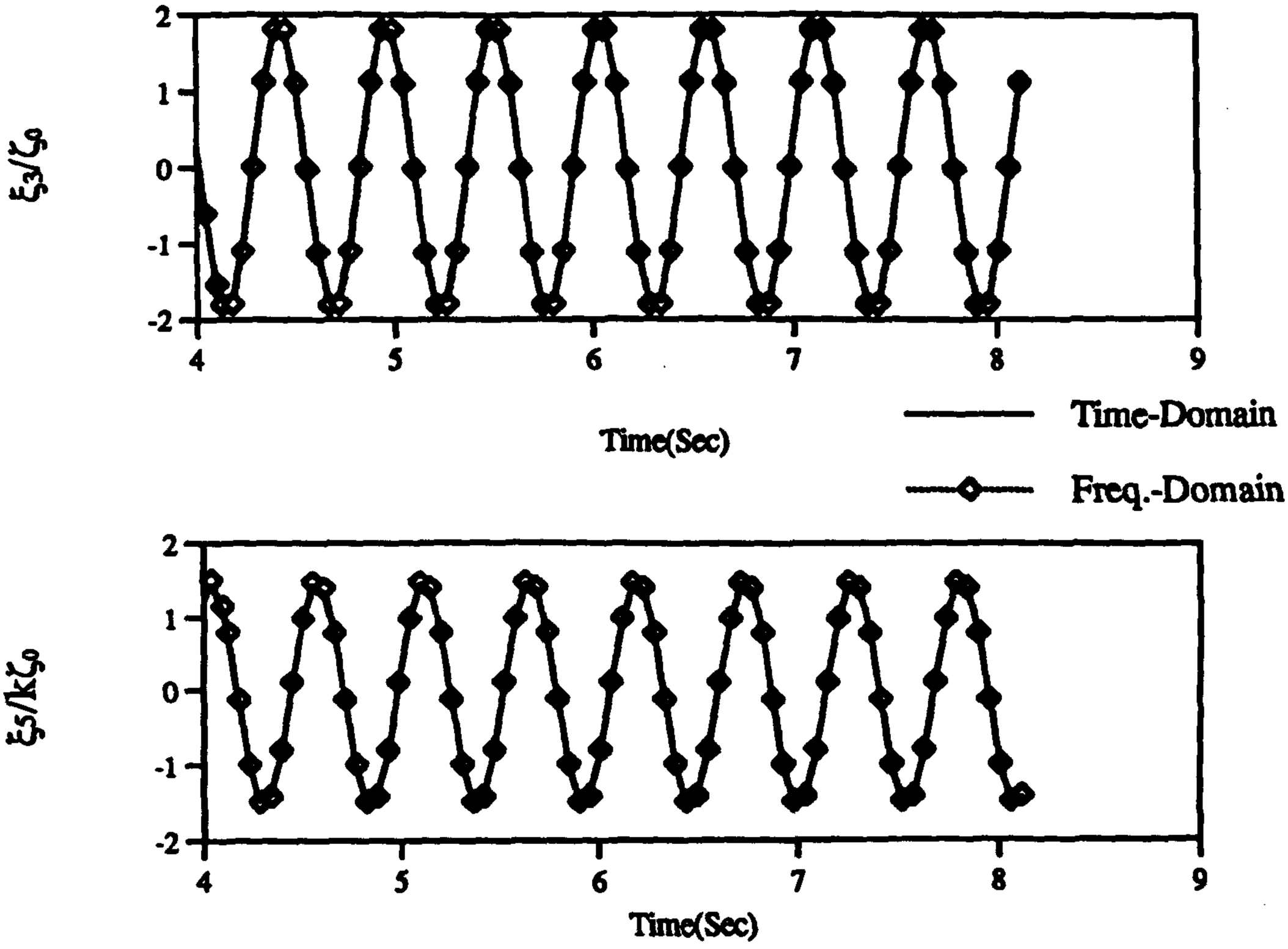

Figure 4.26 : Time Domain Solutions for the Linear Motions of V-1 Catamaran ($Fn=0.677, \zeta_0=0.1cm, \omega_0=4.75$ rad/sec)

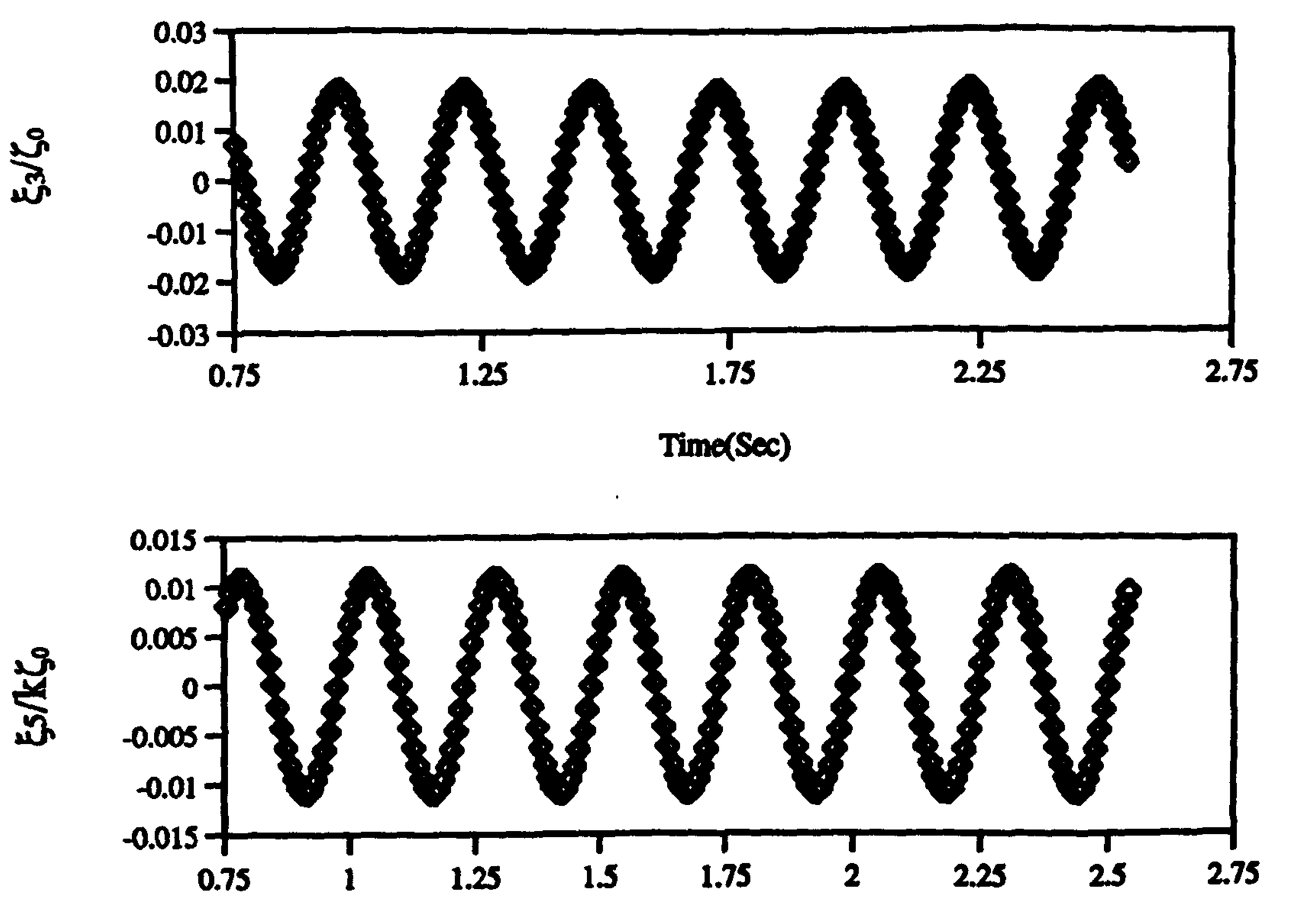

Figure 4.27 : Time Domain Solutions for the Linear Motions of V-1 Catamaran ($Fn=0.677, \zeta_0=0.1cm, \omega_0=7.5$ rad/sec)

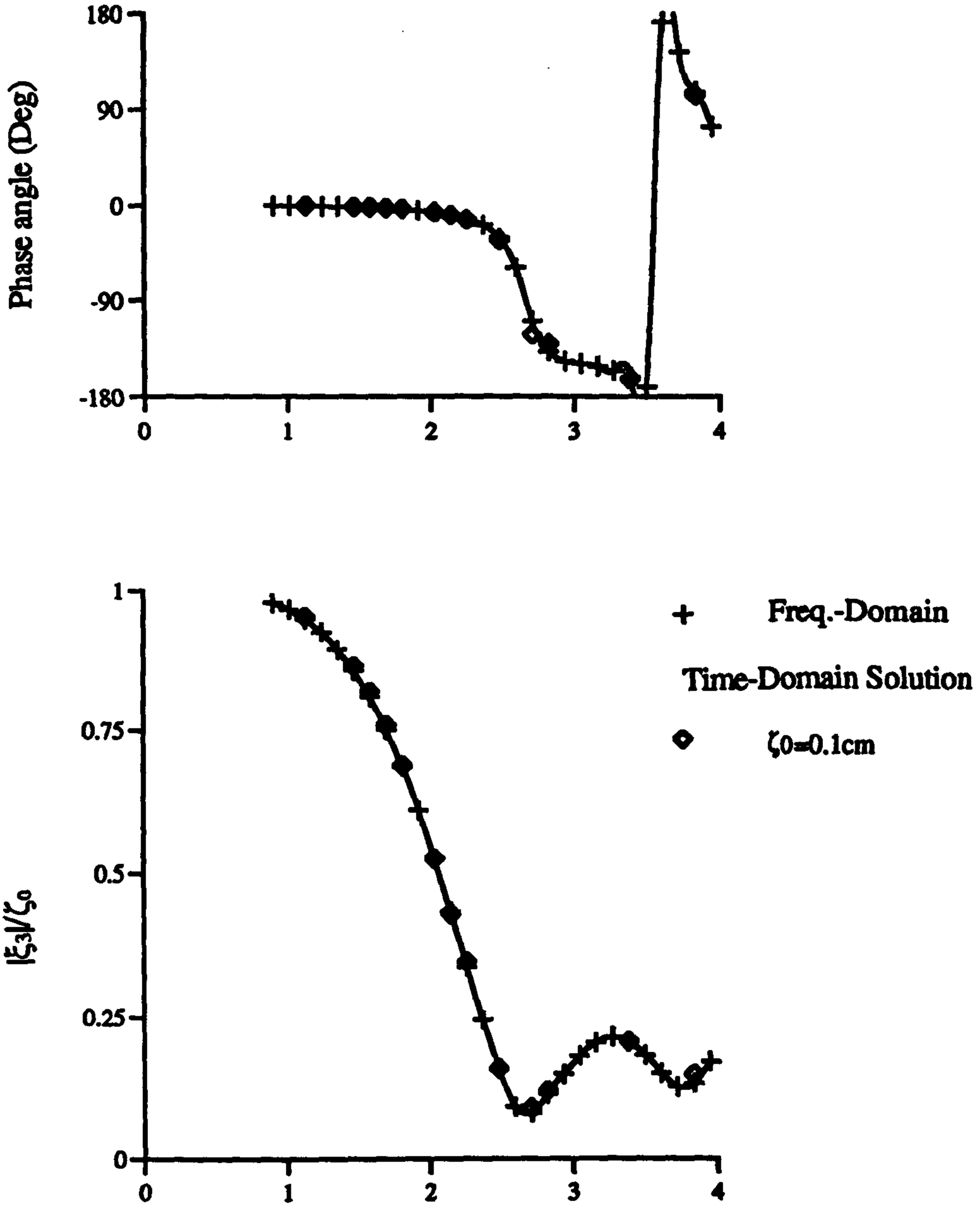

Figure 4.28 : Linear Heave Motion Response of the V-1 Catamaran at F_n=0.0 (ζ_o =0.1cm)

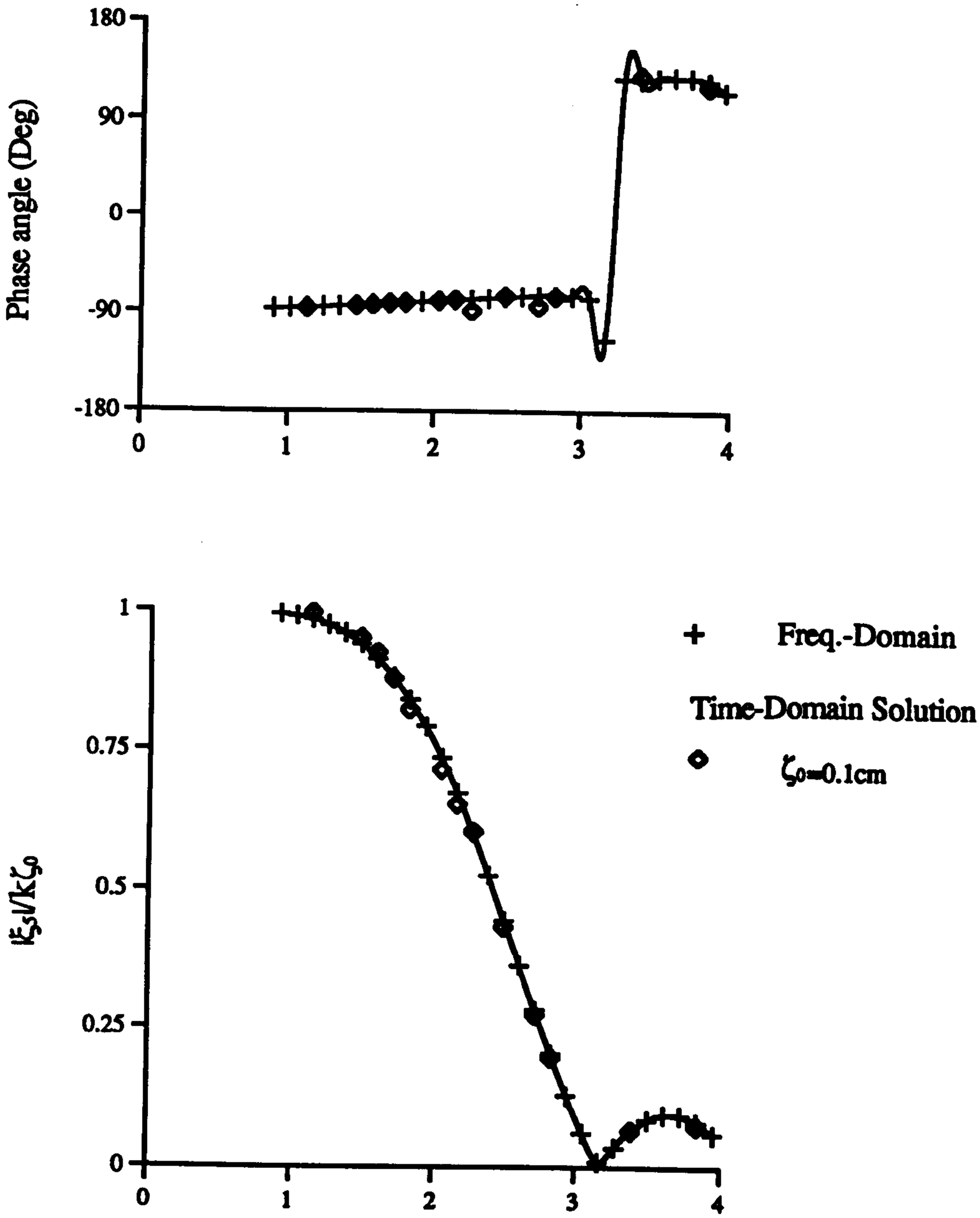

Figure 4.29 : Linear Pitch Motion Response of the V-1 Catamaran at F_n=0.0 (ζ_0 =0.1cm)

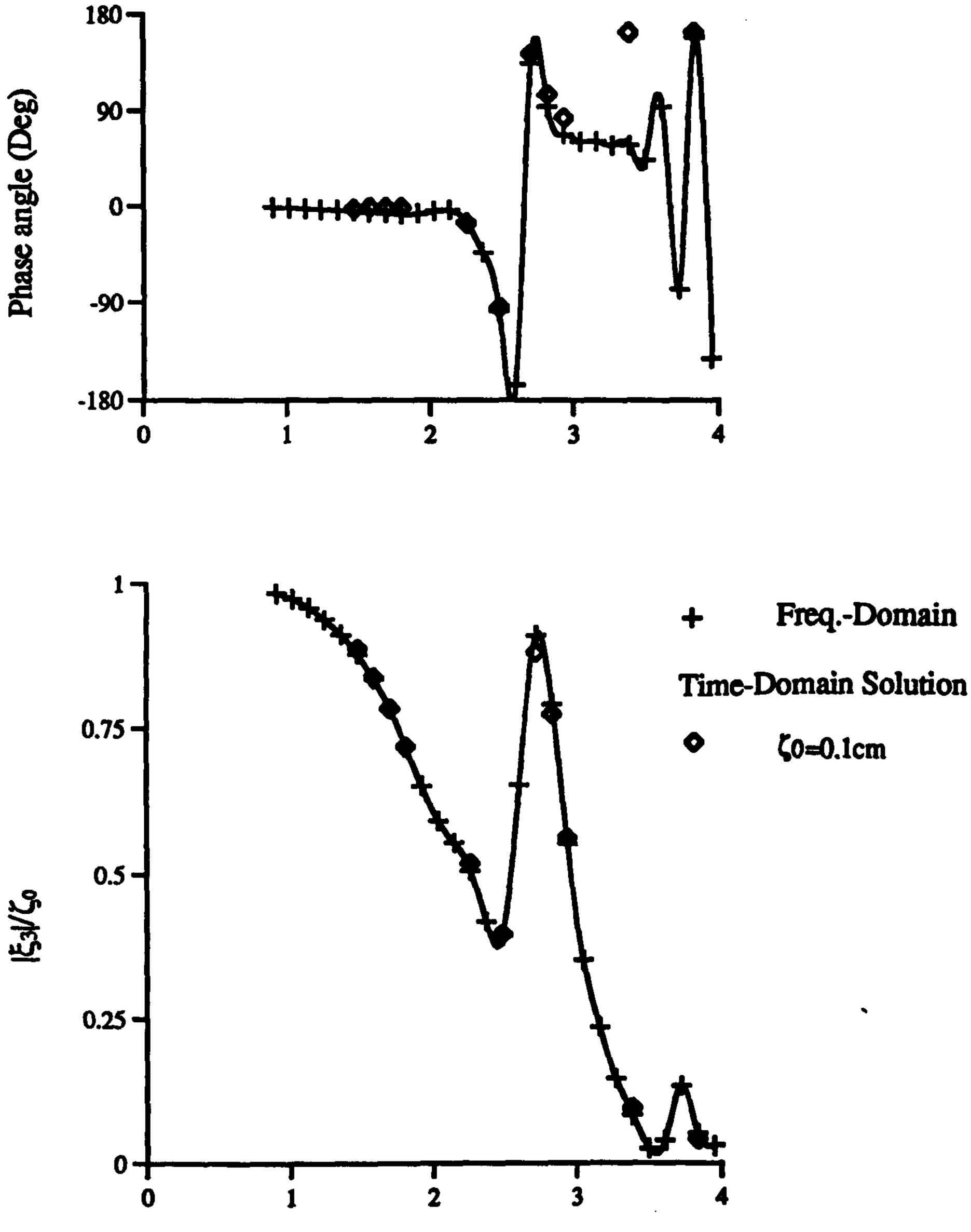

Figure 4.30 : Linear Heave Motion Response of the V-1 Catamaran at F_n=0.226 (ζ_0 =0.1cm)

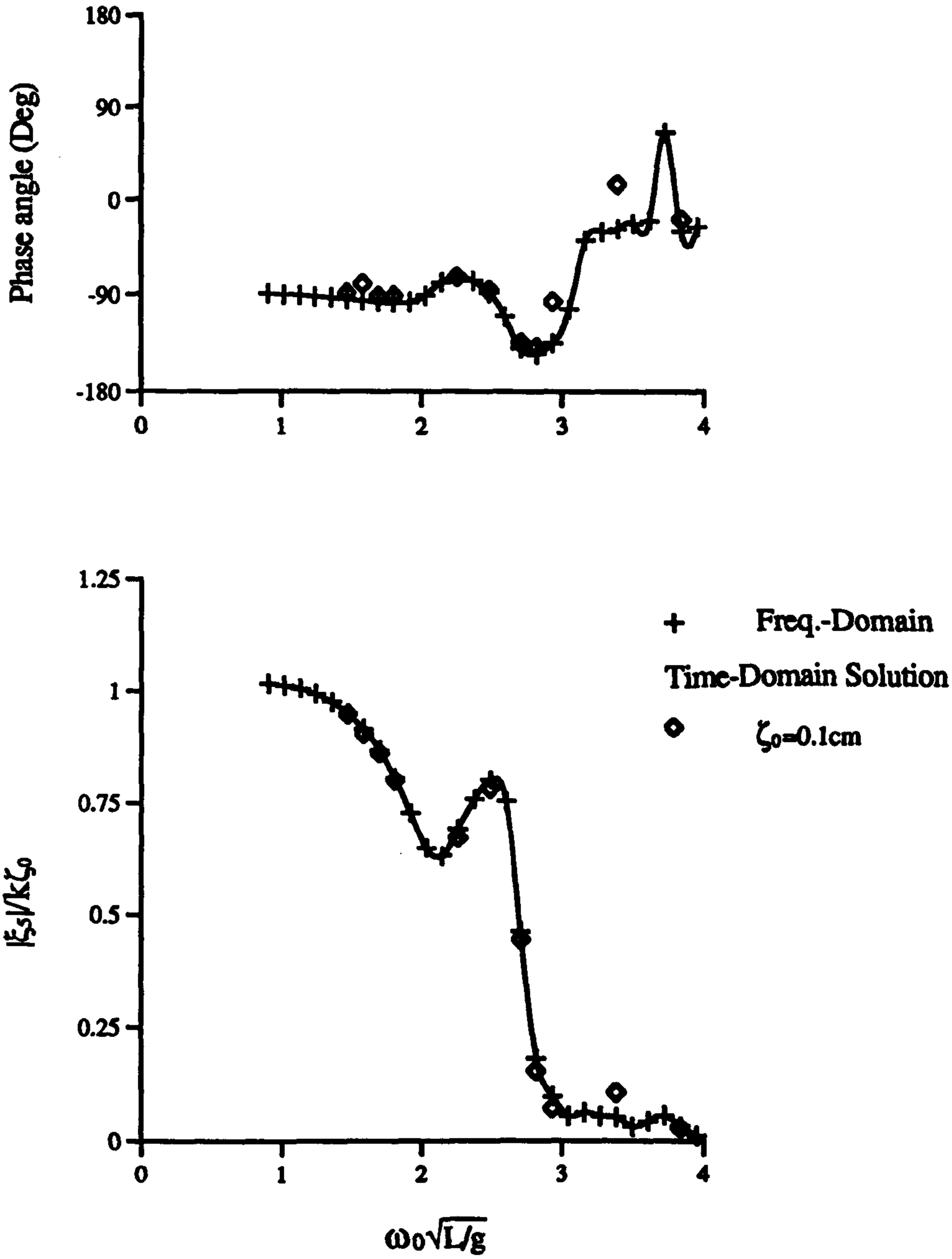

Figure 4.31 : Linear Pitch Motion Response of the V-1 Catamaran at F_n=0.226 (ζ_0 =0.1cm)

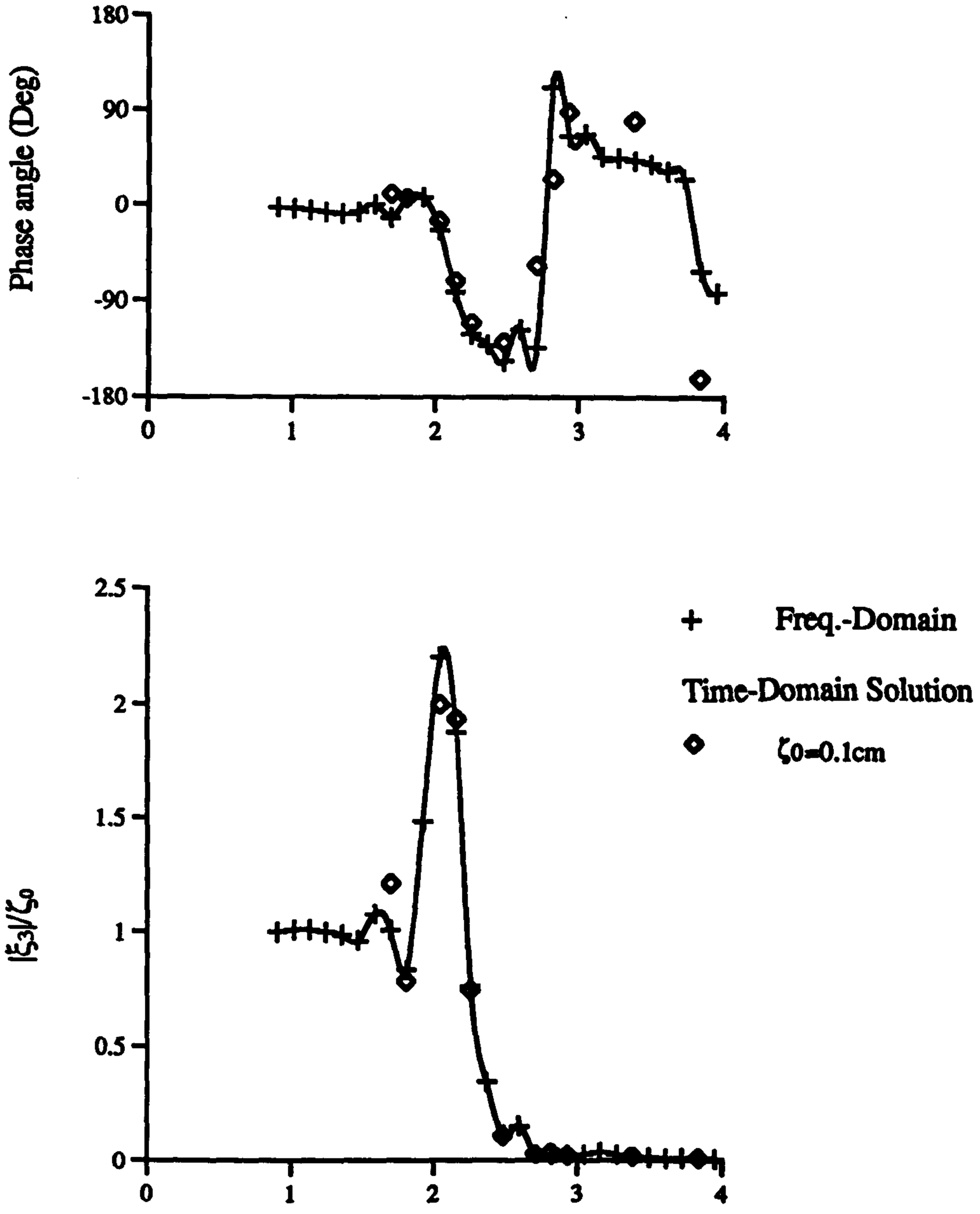

Figure 4.32 : Linear Heave Motion Response of the V-1 Catamaran at F_n=0.677 (ζ_0 =0.1cm)

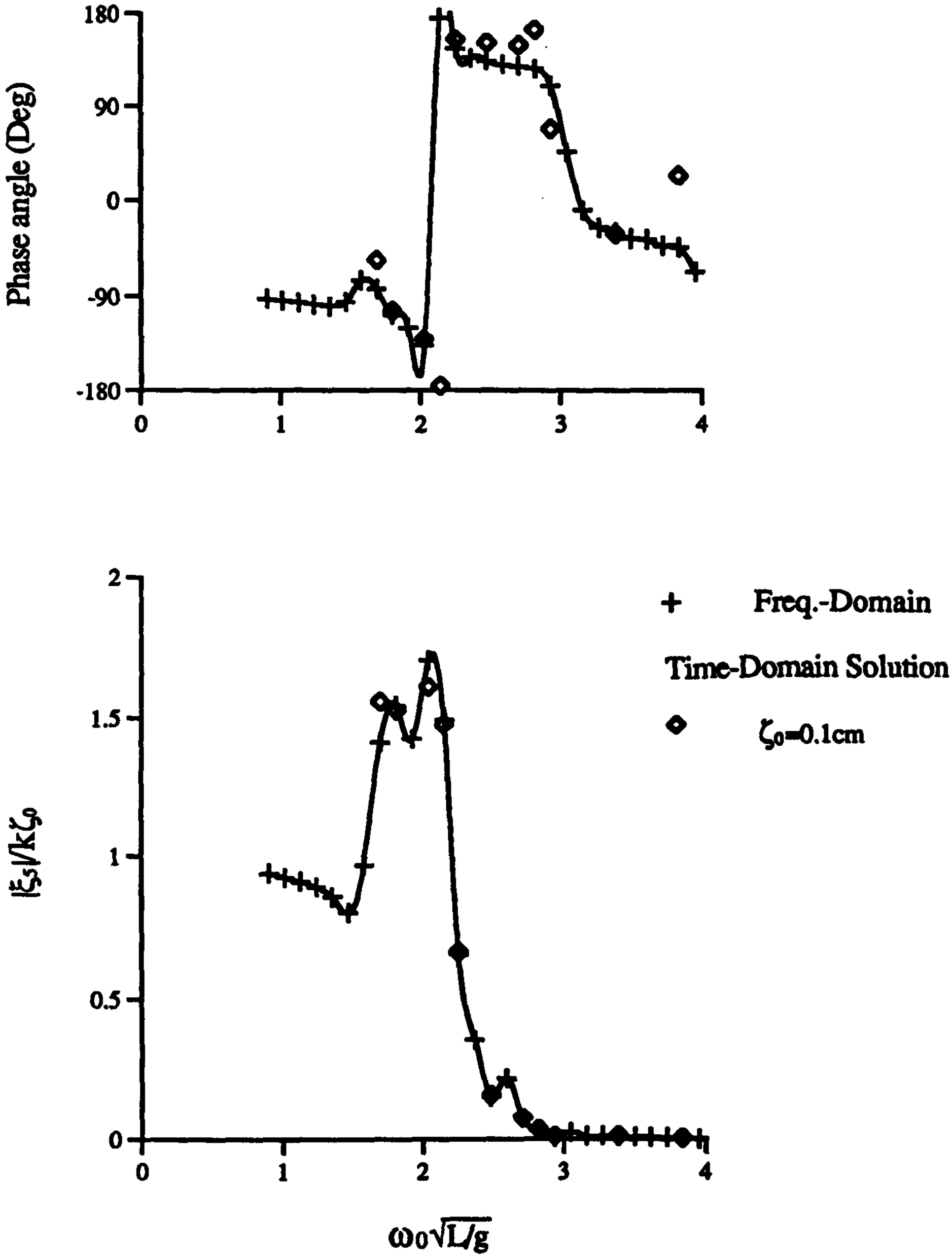

Figure 4.33 : Linear Pitch Motion Response of the V-1 Catamaran at F_n=0.677 (ζ_0 =0.1cm)

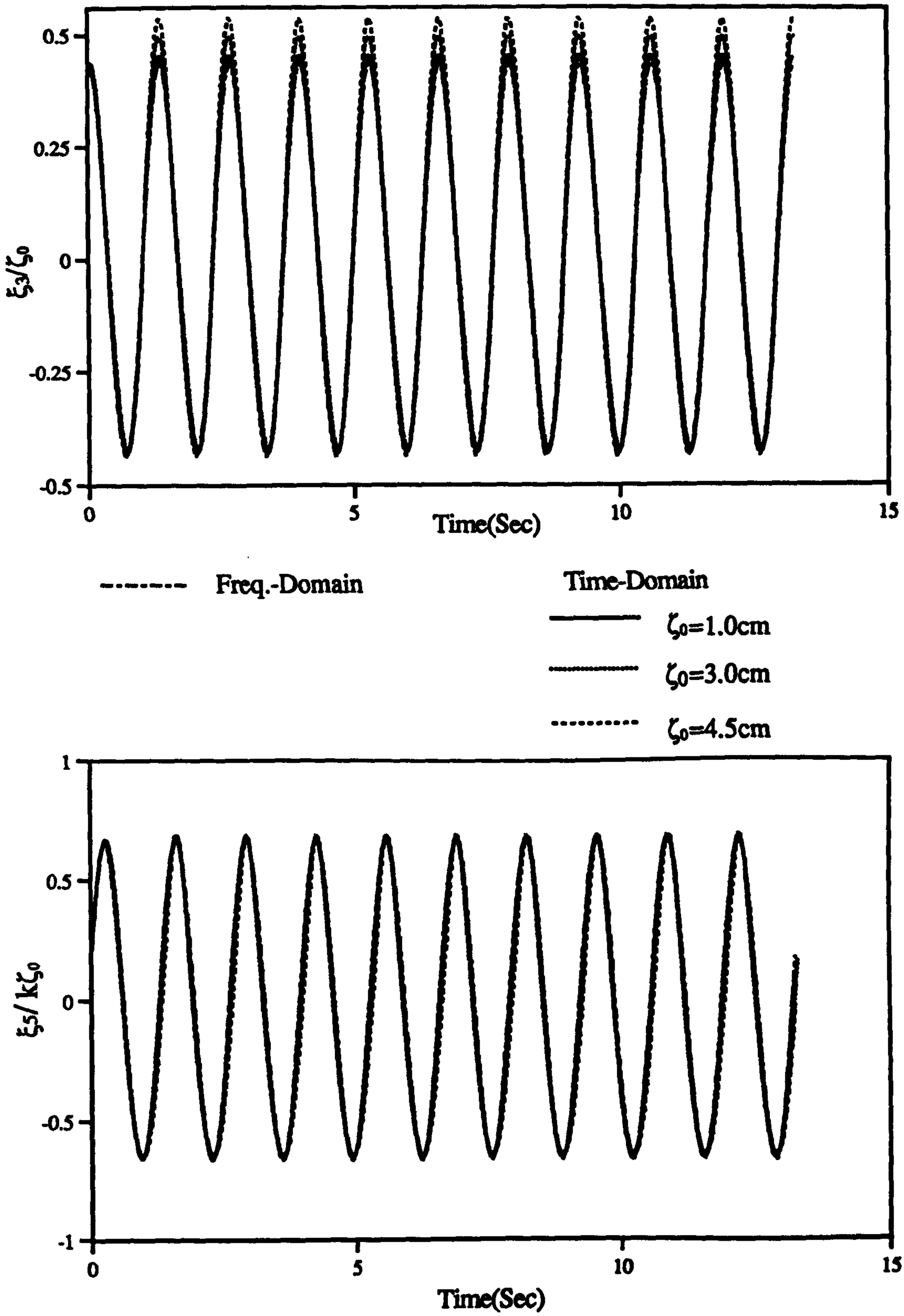

Figure 4.34 : Time Domain Solutions for the Heave and Pitch Motions of V-1 Catamaran with Various Incident Wave Amplitudes.
(Fn=0.00,ω_0=4.75 rad/sec)

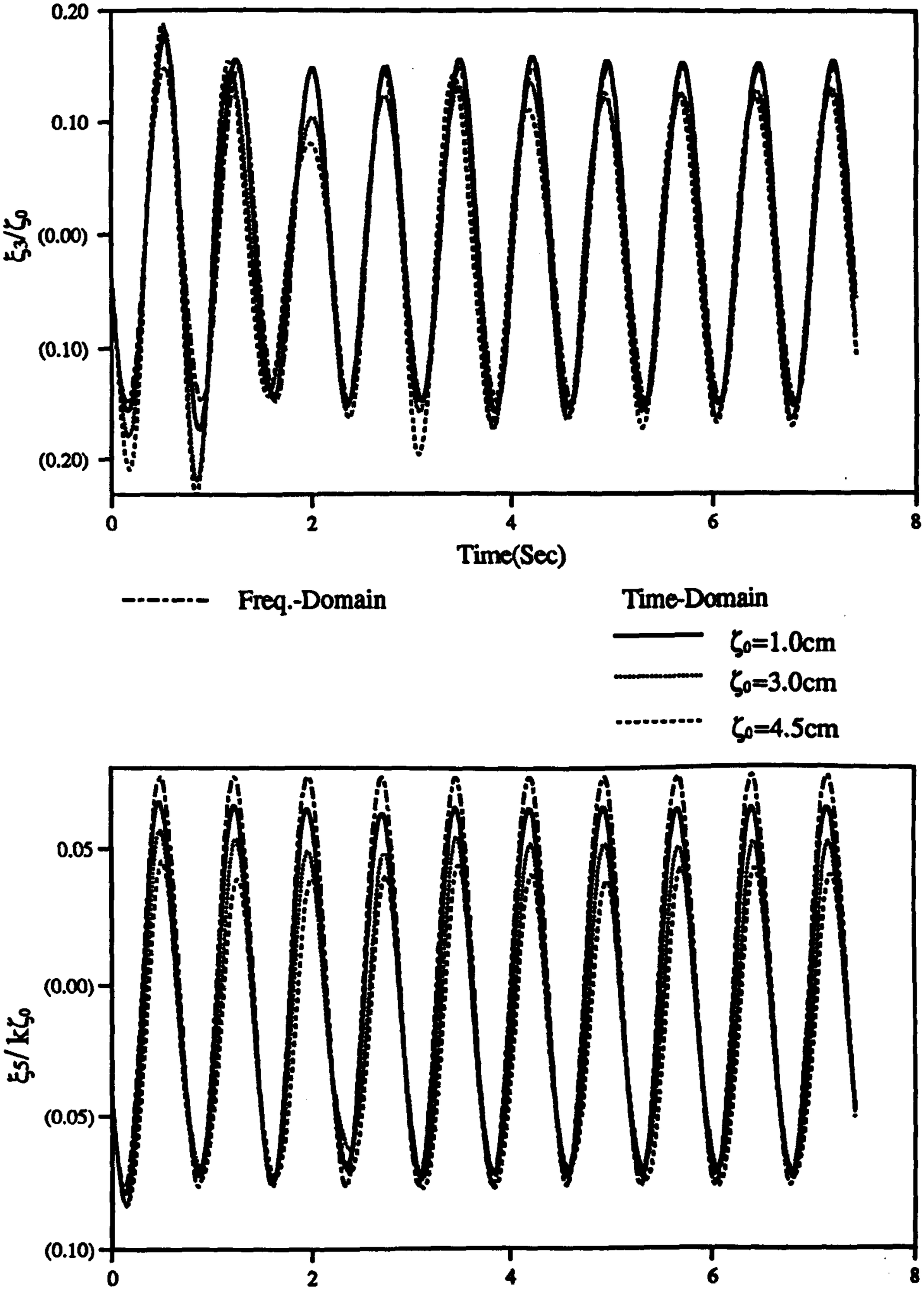

Figure 4.35 : Time Domain Solutions for the Heave and Pitch Motions of V-1 Catamaran with Various Incident Wave Amplitudes.
(Fn=0.00,ω_0=8.5 rad/sec)

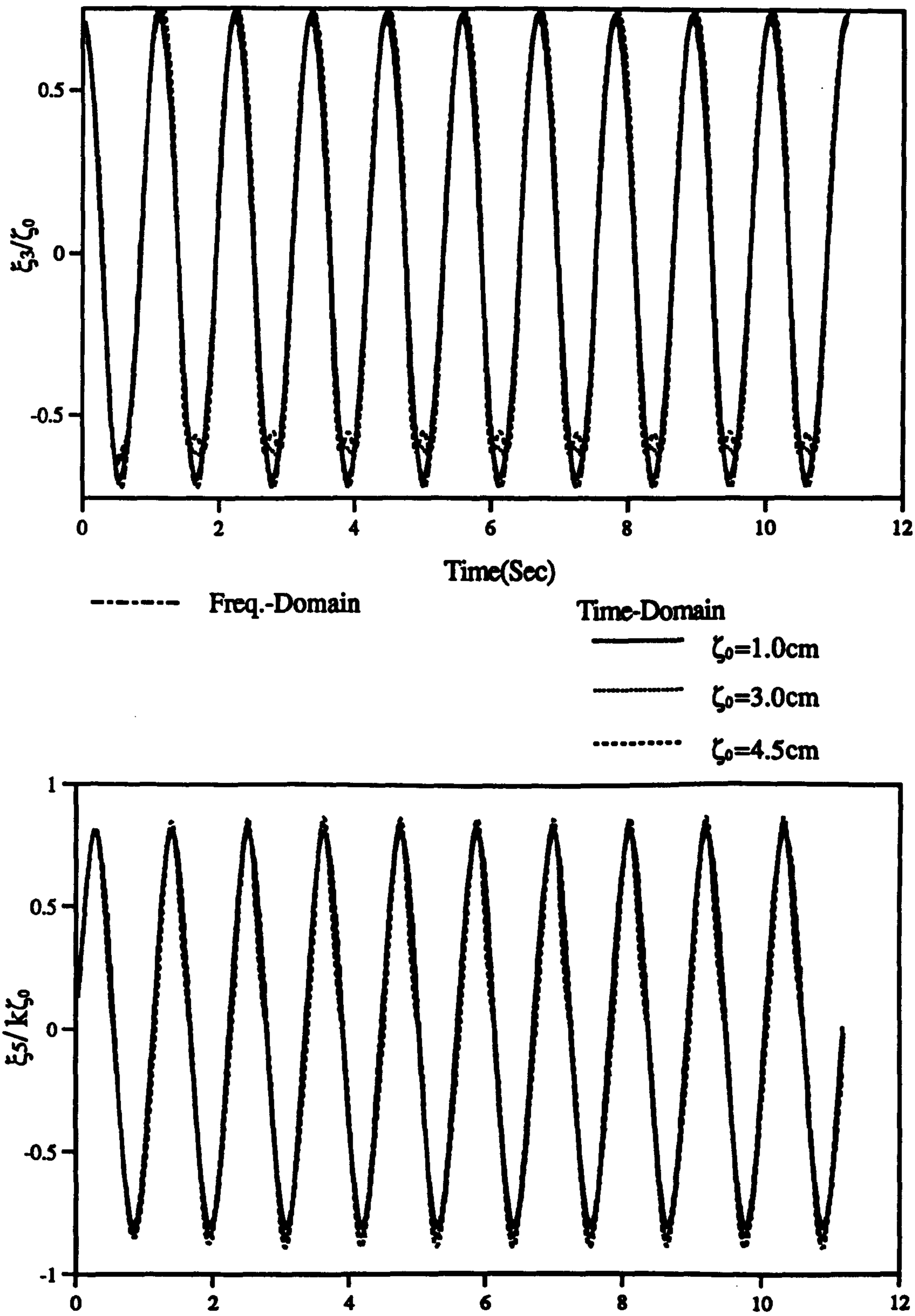

Figure 4.36 : Time Domain Solutions for the Heave and Pitch Motions of V-1 Catamaran with Various Incident Wave Amplitudes.
(Fn=0.226,ω_0=4.0 rad/sec)

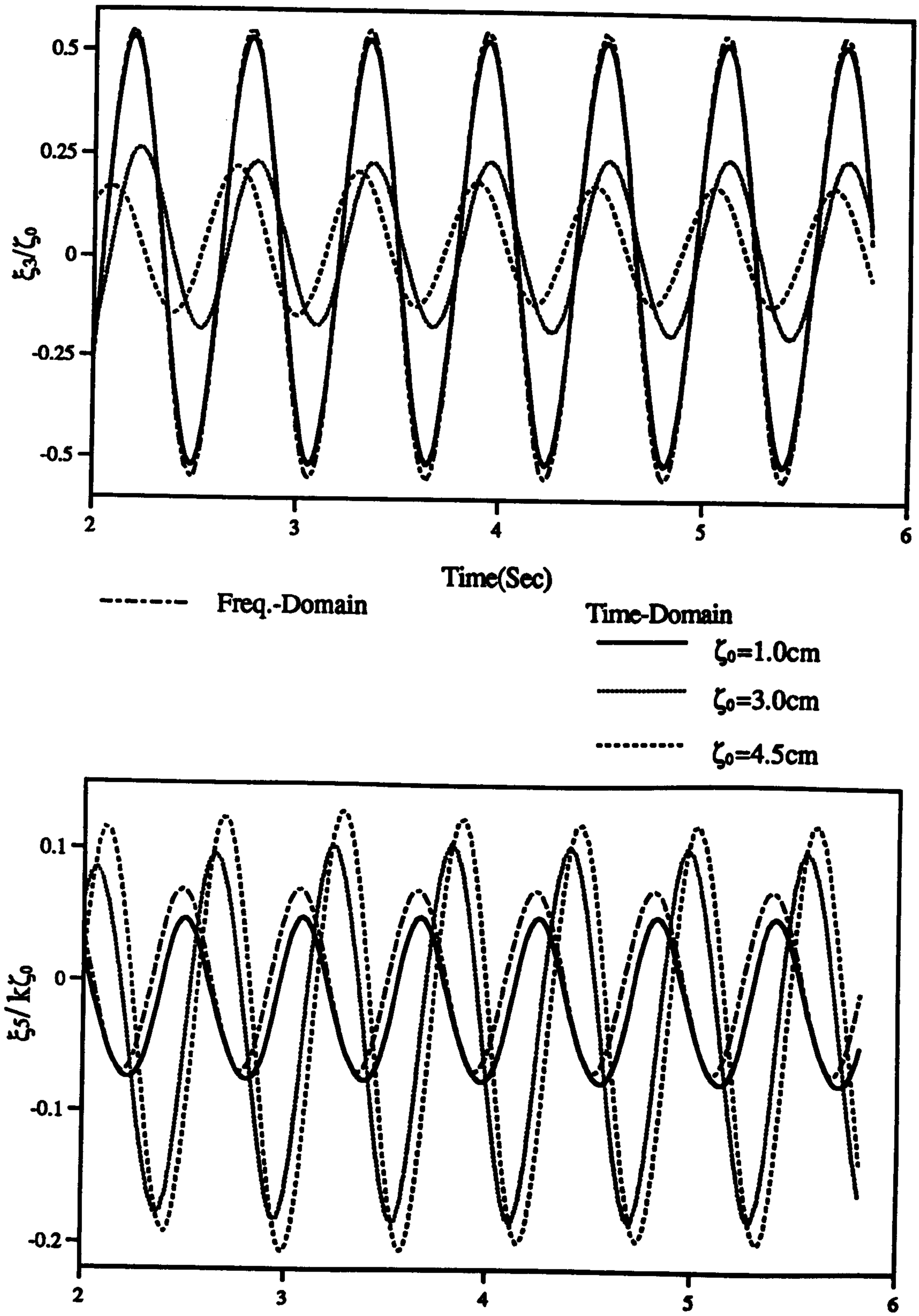

Figure 4.37 : Time Domain Solutions for the Heave and Pitch Motions of V-1 Catamaran with Various Incident Wave Amplitudes.
(Fn=0.226,ω_0=6.5 rad/sec)

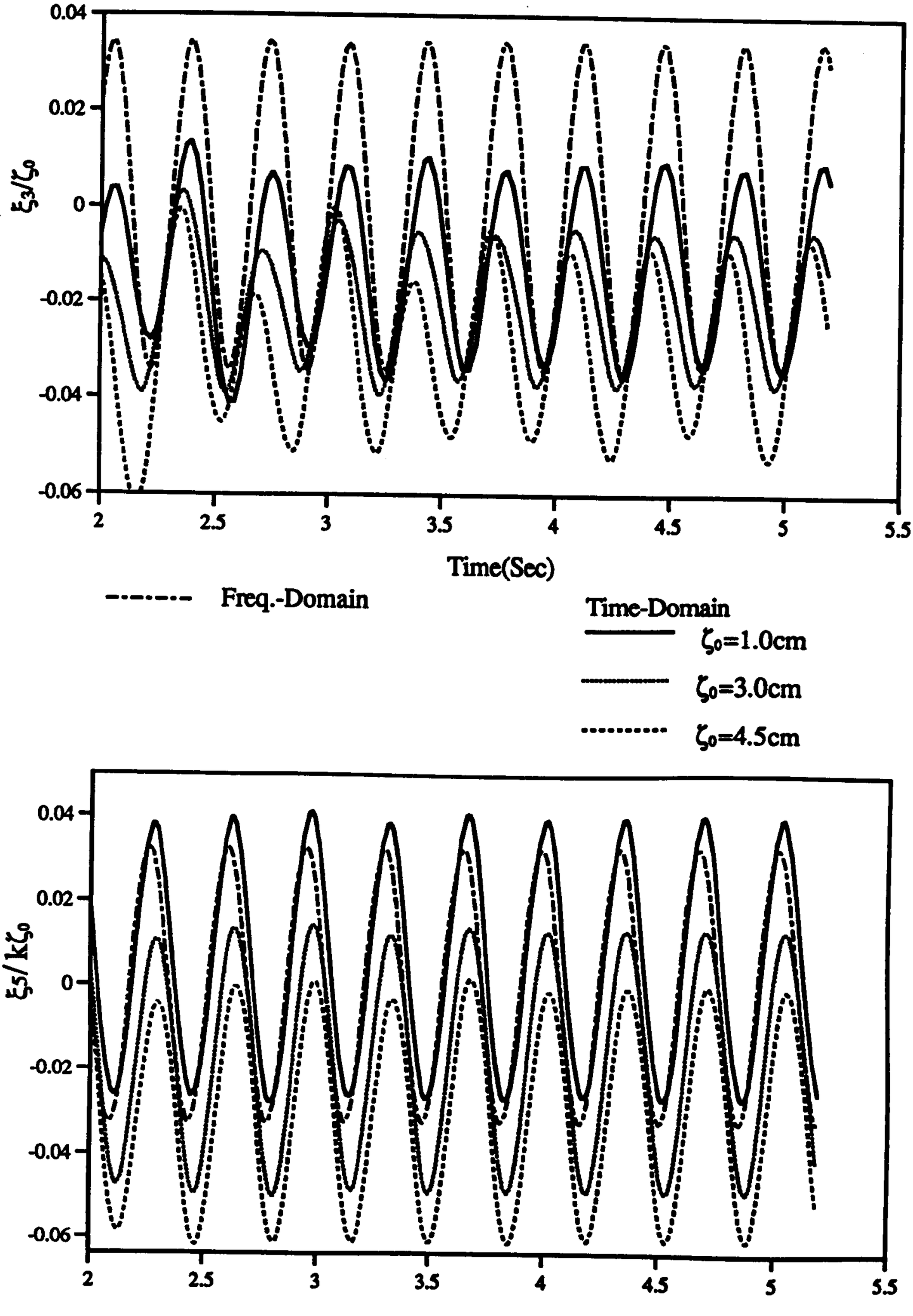

Figure 4.38 : Time Domain Solutions for the Heave and Pitch Motions of V-1 Catamaran with Various Incident Wave Amplitudes.
(Fn=0.677,ω_0=6.25 rad/sec)

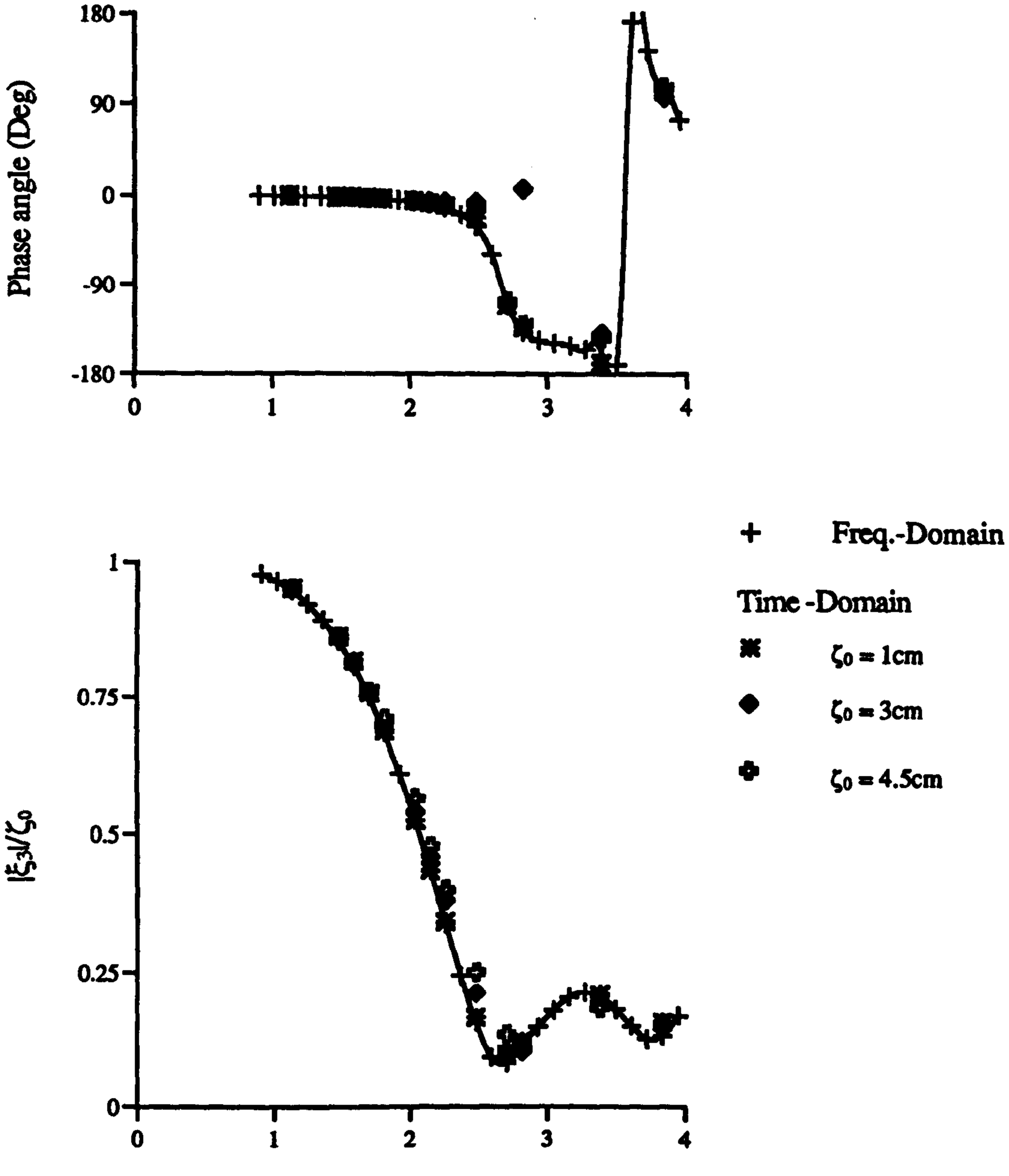

Figure 4.39 : Heave Motion Response of the V-1 Catamaran at Fn=0.0 (ζ_0=1cm, 3cm, 4.5cm)

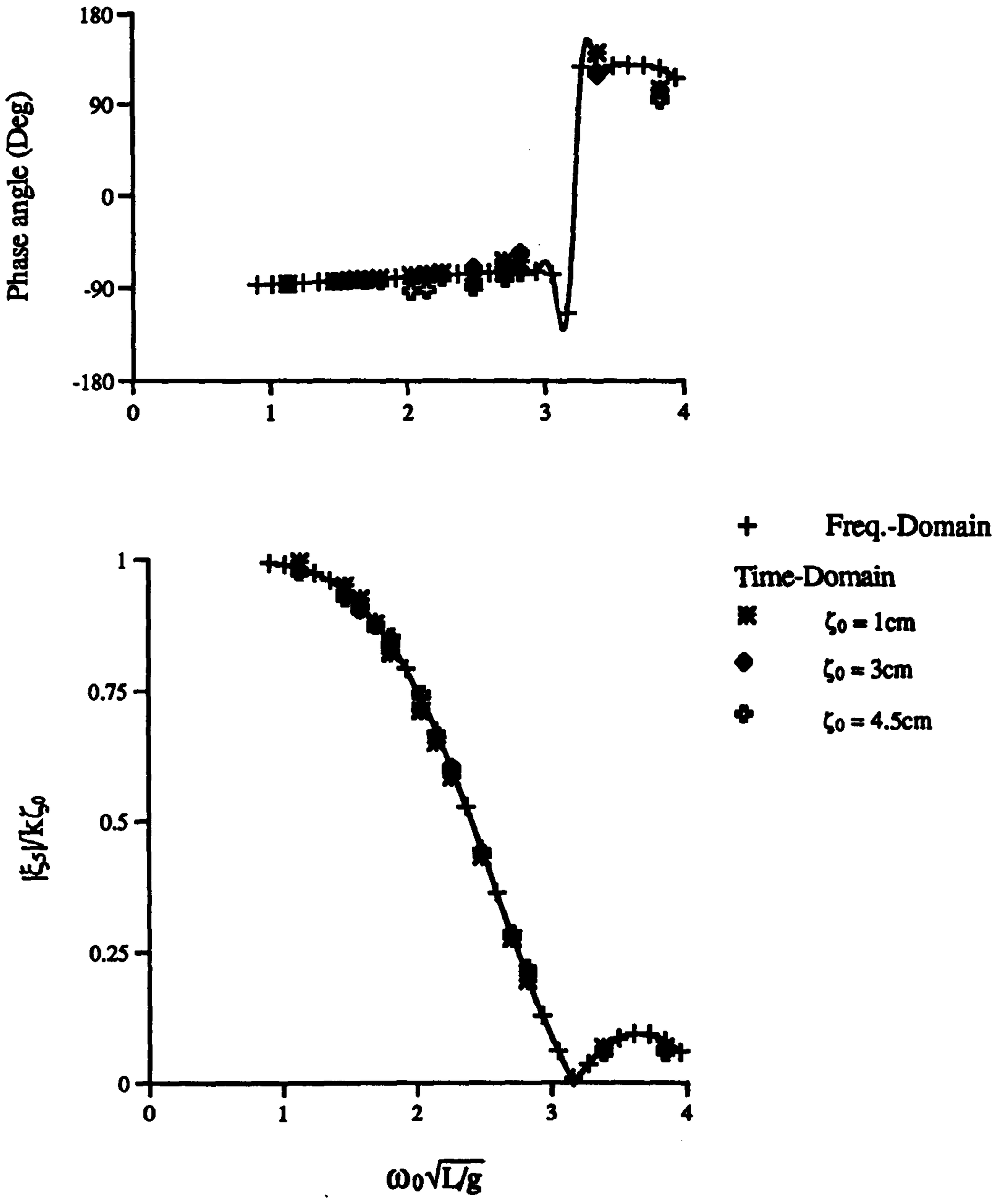

Figure 4.40 : Pitch Motion Response of the V-1 Catamaran at F_n=0.0 (ζ_0=1cm, 3cm, 4.5cm)

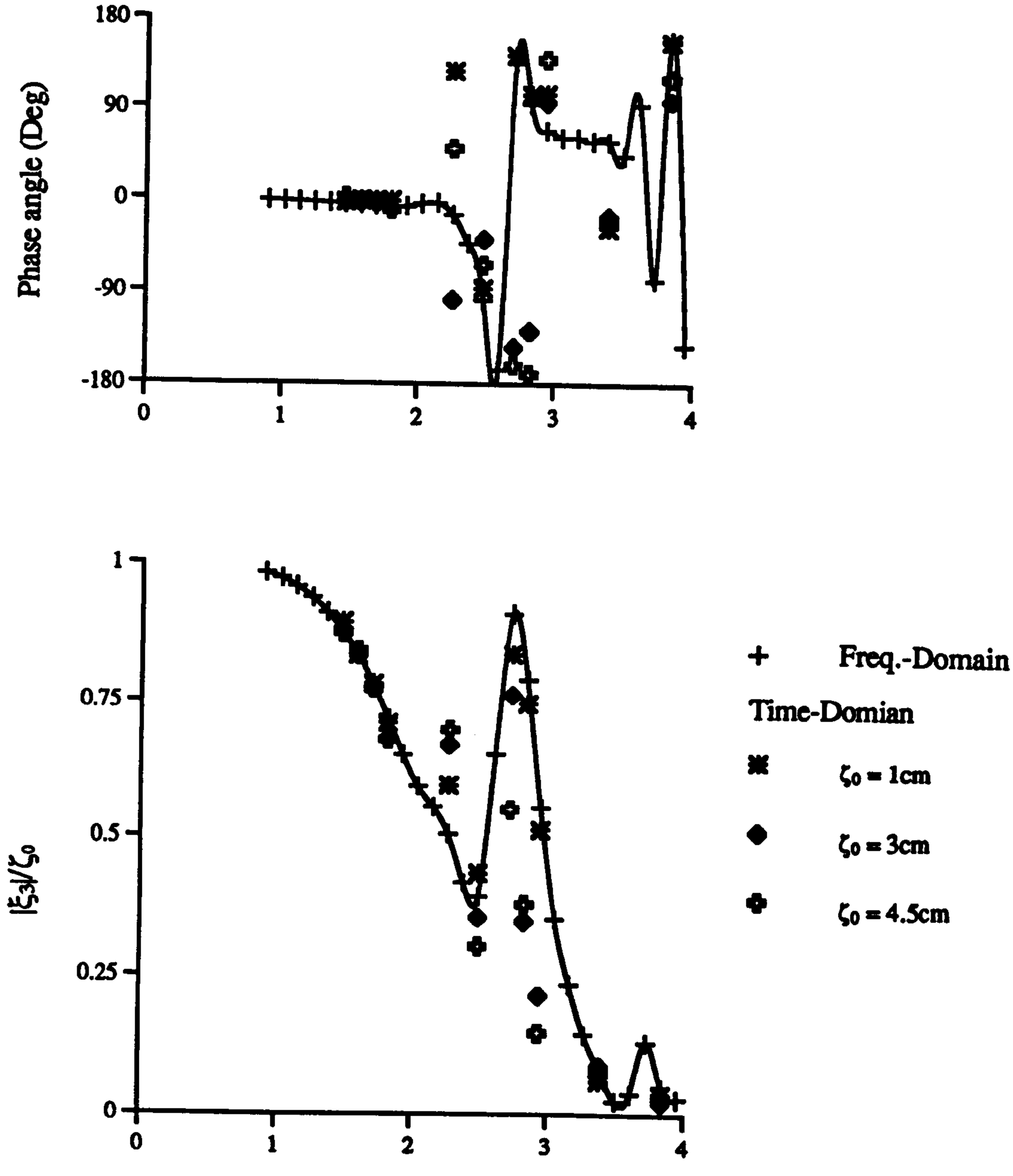

Figure 4.41 : Heave Motion Response of the V-1 Catamaran at F_n=0.226 (ζ_0=1cm, 3cm, 4.5cm)

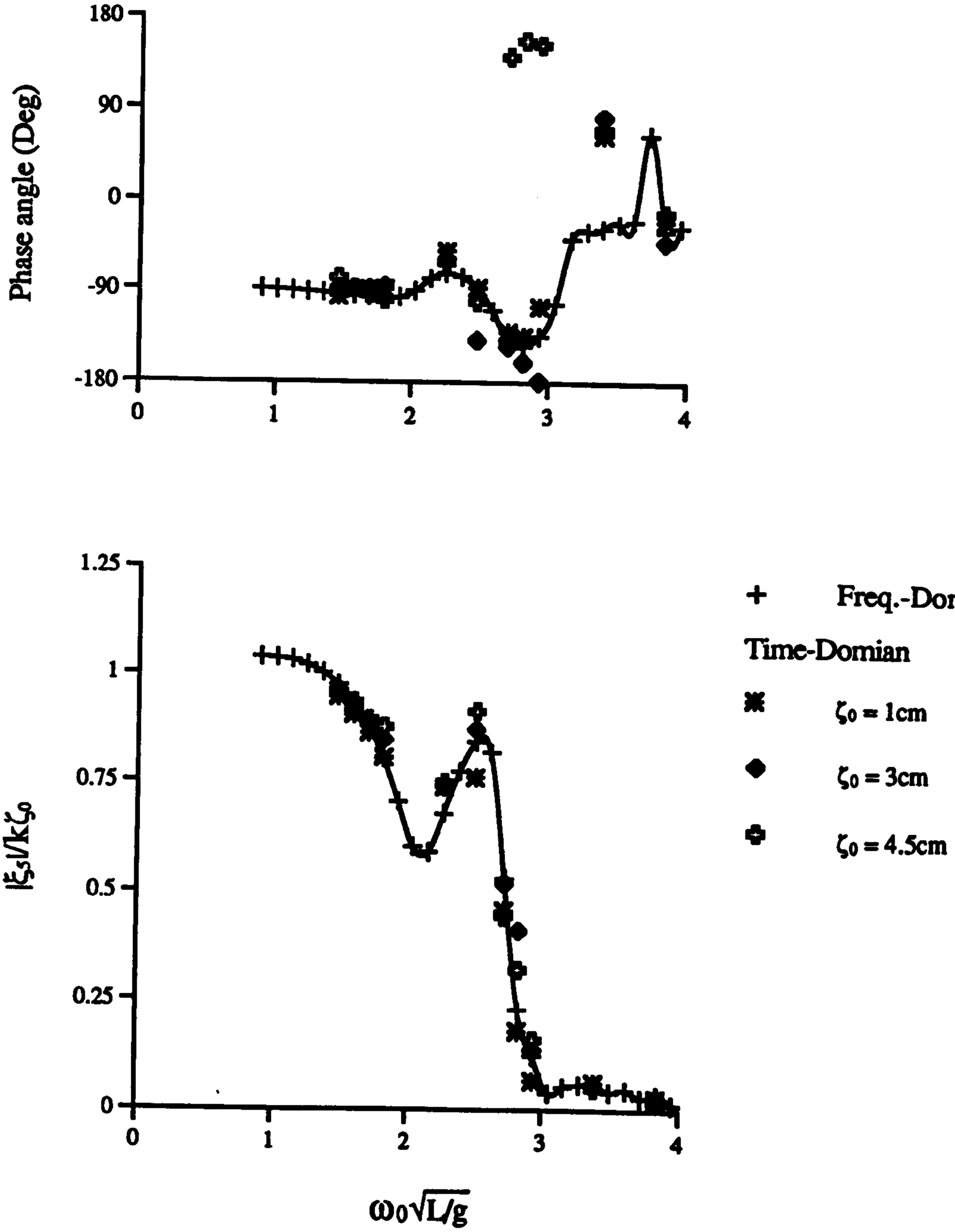

Figure 4.42 : Pitch Motion Response of the V-1 Catamaran at Fn=0.226 (ζ_0=1cm, 3cm, 4.5cm)

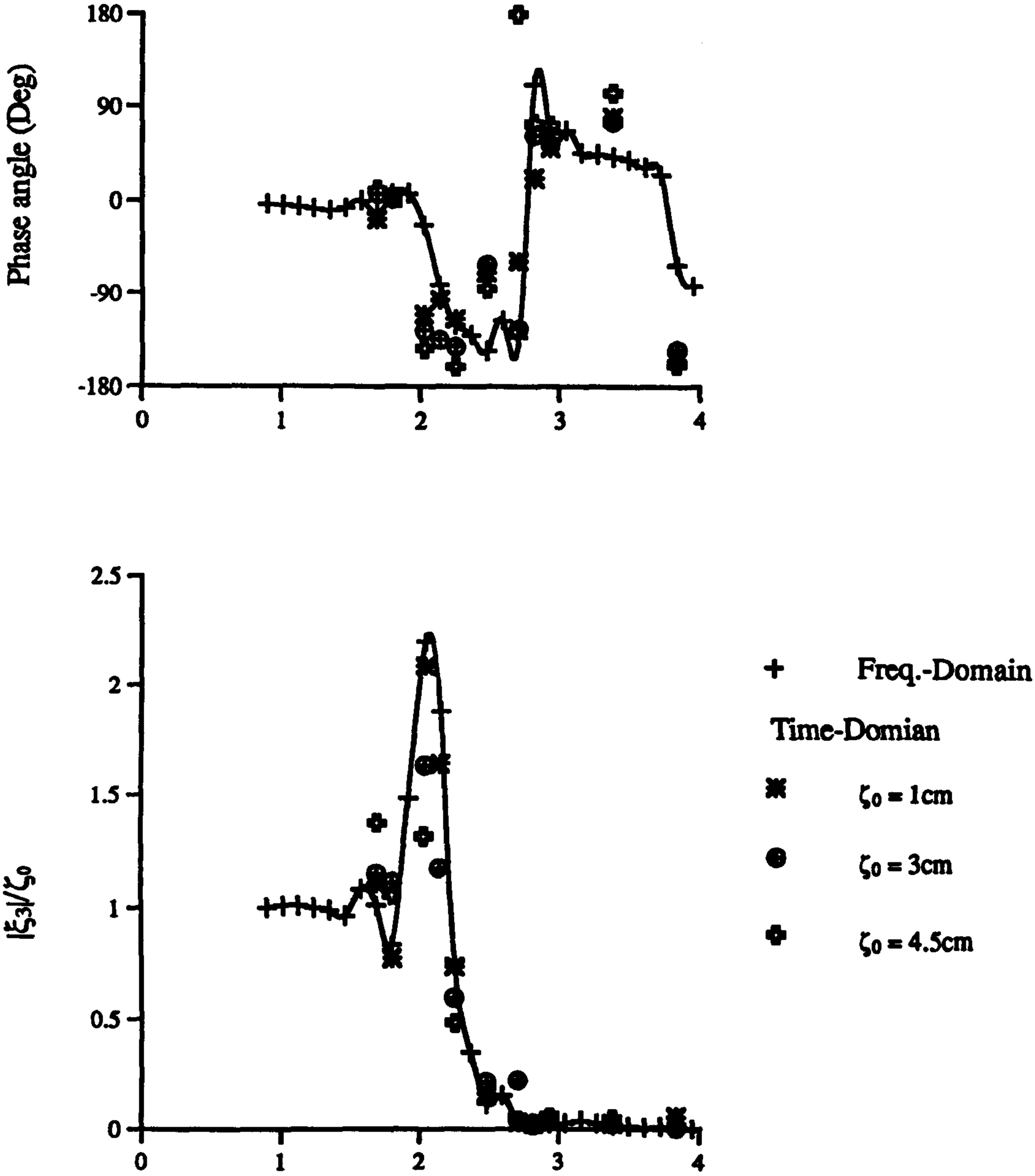

Figure 4.43 : Heave Motion Response of the V-1 Catamaran at F_n=0.677 (ζ_0=1cm, 3cm, 4.5cm)

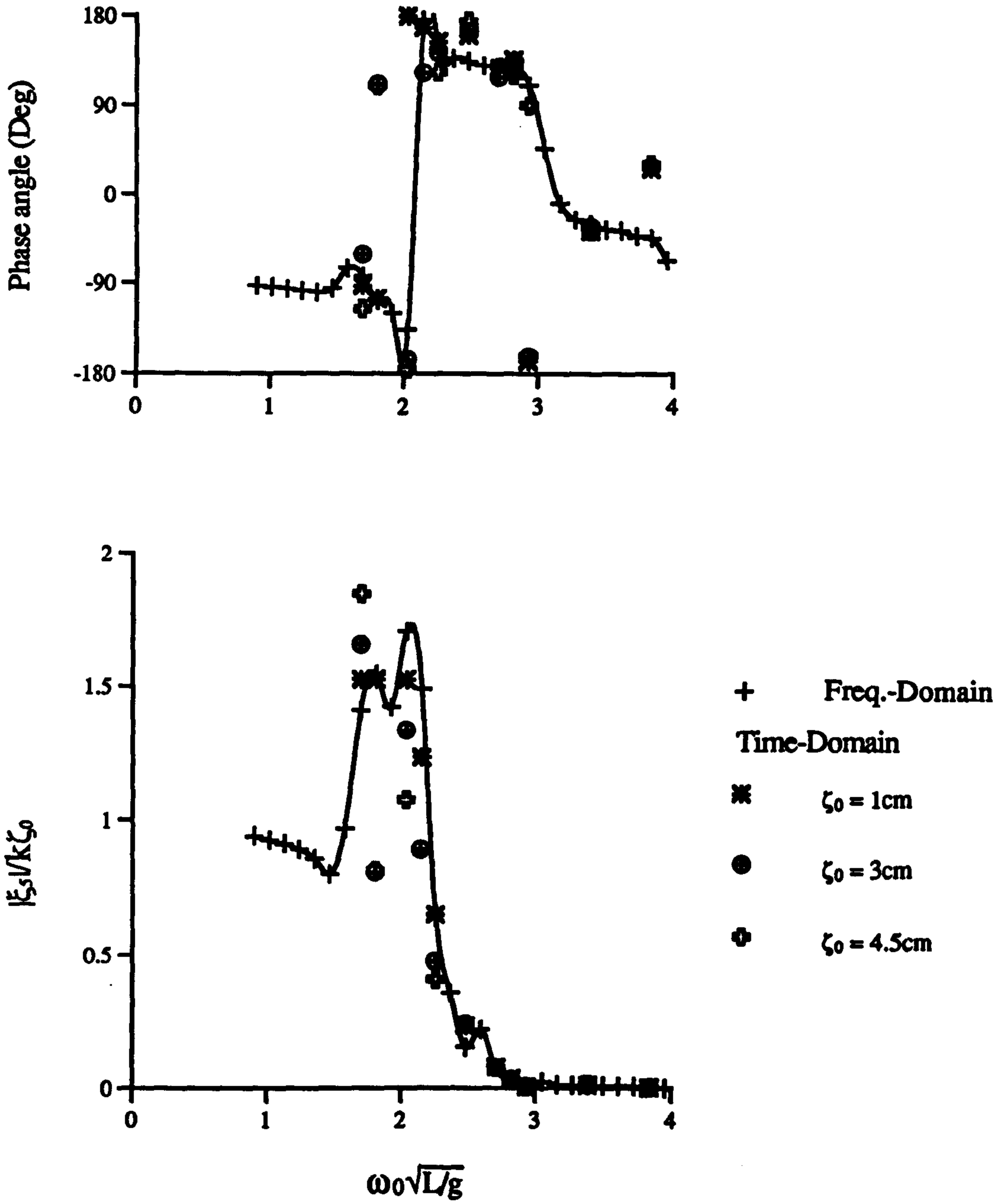

Figure 4.44 : Pitch Motion Response of the V-1 Catamaran at F_n=0.677 (ζ_0=1cm, 3cm, 4.5cm)

A: Frequency Domain Method
B: Nonlinear Hydrodynamic Coefficients
C: Nonlinear Wave Exciting Forces
L: Linear Component Model

D: Linear Hydrostatic Forces
E: Nonlinear Hydrostatic Forces
F: Nonlinear Time Domain Method
N/L: Nonlinear Component Model

	A	B	C	D	E	F
A_{jk}	L	N/L	L	N/L	L	N/L
B_{jk}	L	N/L	L	N/L	L	N/L
C_{jk}	L	L	L	L	N/L	N/L
$\bar{F}_j^w$	L	L	N/L	N/L	L	N/L

Table 4.1 : Definition of Parametric Studies on the Nonlinear Motions for Different Numerical Models.

	A	B	C	D	E	F
$\lvert\xi_3\rvert/\zeta_0$	0.1599	0.1685	0.1793	0.1681	0.1801	0.2114
θ_3(deg.)	-33.26	-52.27	-25.4	-24.39	-5.971	-6.748
$\lvert\xi_5\rvert/k\zeta_0$	0.4380	0.4323	0.4244	0.4302	0.4438	0.4394
θ_5(deg.)	-74.74	-74.89	-86.49	-80.2	-72.86	-70.37
Figures	4.45-48	4.45	4.46	4.47	4.48	4.45-48

Table 4.2 : Parametric Studies on the Nonlinear Motions of the V-1 Catamaran Model.(Fn=0.00, ω_0=5.5 rad/sec, ζ_0=3.0cm)

	A	B	C	D	E	F
$\lvert\xi_3\rvert/\zeta_0$	0.1484	0.1488	0.1587	0.1605	0.1560	0.1522
θ_3(deg.)	103.1	104.7	91.32	93.15	85.75	114.6
$\lvert\xi_5\rvert/k\zeta_0$	0.07673	0.0772	0.05761	0.05914	0.07663	0.06309
θ_5(deg.)	122.5	122	103	103.2	108	111.1
Figures	4.49-52	4.49	4.50	4.51	4.52	4.49-52

Table 4.3 : Parametric Studies on the Nonlinear Motions of the V-1 Catamaran Model.(Fn=0.00, ω_0=8.5 rad/sec, ζ_0=3.0cm)

	A	B	C	D	E	F
$\lvert\xi_3\rvert/\zeta_0$	0.7187	0.7502	0.8434	0.7014	0.7441	0.6801
θ_3(deg.)	-1.734	6.195	-3.631	5.37	-5.9	-6.0
$\lvert\xi_5\rvert/k\zeta_0$	0.800	0.7798	0.7361	0.8276	0.9307	0.8793
θ_5(deg.)	-91.84	-96.57	-94.97	-99.66	-94.21	-95.26
Figures	4.53-56	4.53	4.54	4.55	4.56	4.53-56

Table 4.4 : Parametric Studies on the Nonlinear Motions of the V-1 Catamaran Model.(Fn=0.226, ω_0=4.0 rad/sec, ζ_0=4.5cm)

	A	B	C	D	E	F
$\lvert\xi_3\rvert/\zeta_0$	0.8913	0.9133	0.8979	0.9162	0.8665	0.8615
θ_3(deg.)	143.3	131.1	144.2	143.9	141	143.2
$\lvert\xi_5\rvert/k\zeta_0$	0.45	0.4442	0.4448	0.4329	0.4369	0.4568
θ_5(deg.)	-134.8	-136.1	-133.5	-134.9	-131.5	-130.4
Figures	4.57-60	4.57	4.58	4.59	4.60	4.57-60

Table 4.5 : Parametric Studies on the Nonlinear Motions of the V-1 Catamaran Model.(Fn=0.226, ω_0=6.0 rad/sec, ζ_0=1.0cm)

	A	B	C	D	E	F
$\lvert\xi_3\rvert/\zeta_0$	1.891	1.871	1.800	1.858	1.614	1.657
θ_3(deg.)	-71.53	-73.35	-72.76	-73.79	-110.9	-97.54
$\lvert\xi_5\rvert/k\zeta_0$	1.5234	1.523	1.485	1.483	1.233	1.263
θ_5(deg.)	-175.5	-174.9	-176.5	-163.8	165.1	167.6
Figures	4.61-64	4.61	4.62	4.63	4.64	4.61-64

Table 4.6 : Parametric Studies on the Nonlinear Motions of the V-1 Catamaran Model.(Fn=0.677, ω_0=4.75 rad/sec, ζ_0=1.0cm)

	A	B	C	D	E	F
$\lvert\xi_3\rvert/\zeta_0$	0.7757	0.7611	0.6776	0.6986	0.5886	0.605
θ_3(deg.)	-112.4	-122.0	-118.9	-126.1	-149.8	-151.6
$\lvert\xi_5\rvert/k\zeta_0$	0.6761	0.6503	0.6067	0.6174	0.4877	0.4839
θ_5(deg.)	153.4	155.2	164.1	154.3	142.2	141.5
Figures	4.65-68	4.65	4.66	4.67	4.68	4.65-68

Table 4.7 : Parametric Studies on the Nonlinear Motions of the V-1 Catamaran Model.(Fn=0.677, ω_0=5.0 rad/sec, ζ_0=3.0cm)

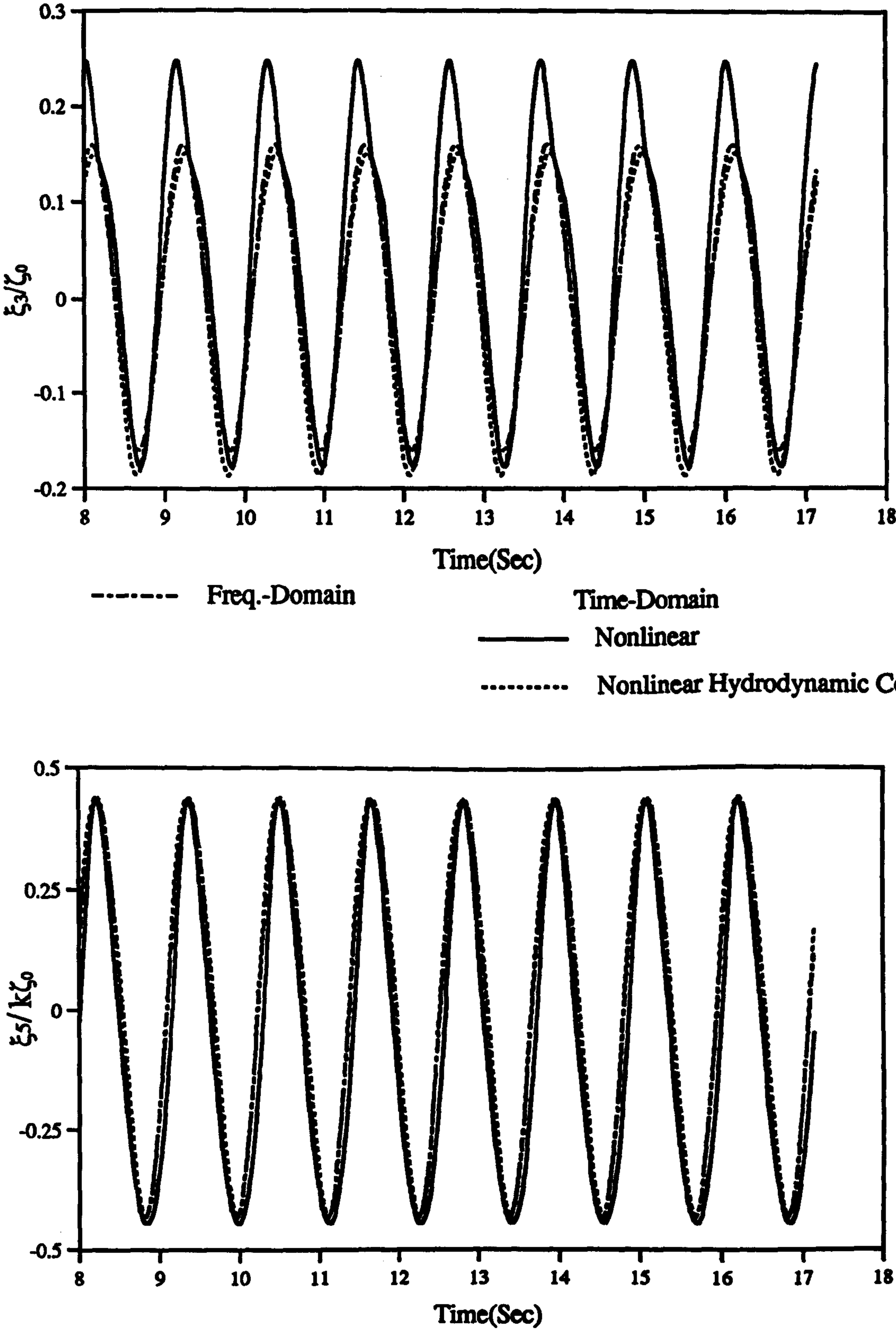

Figure 4.45 : Time Domain Solutions for the Heave and Pitch Motions of V-1 Catamaran with the Nonlinear Hydrodynamic Coefficients (Fn=0.00,ω_0=5.5 rad/sec,ζ_0=3.0cm)

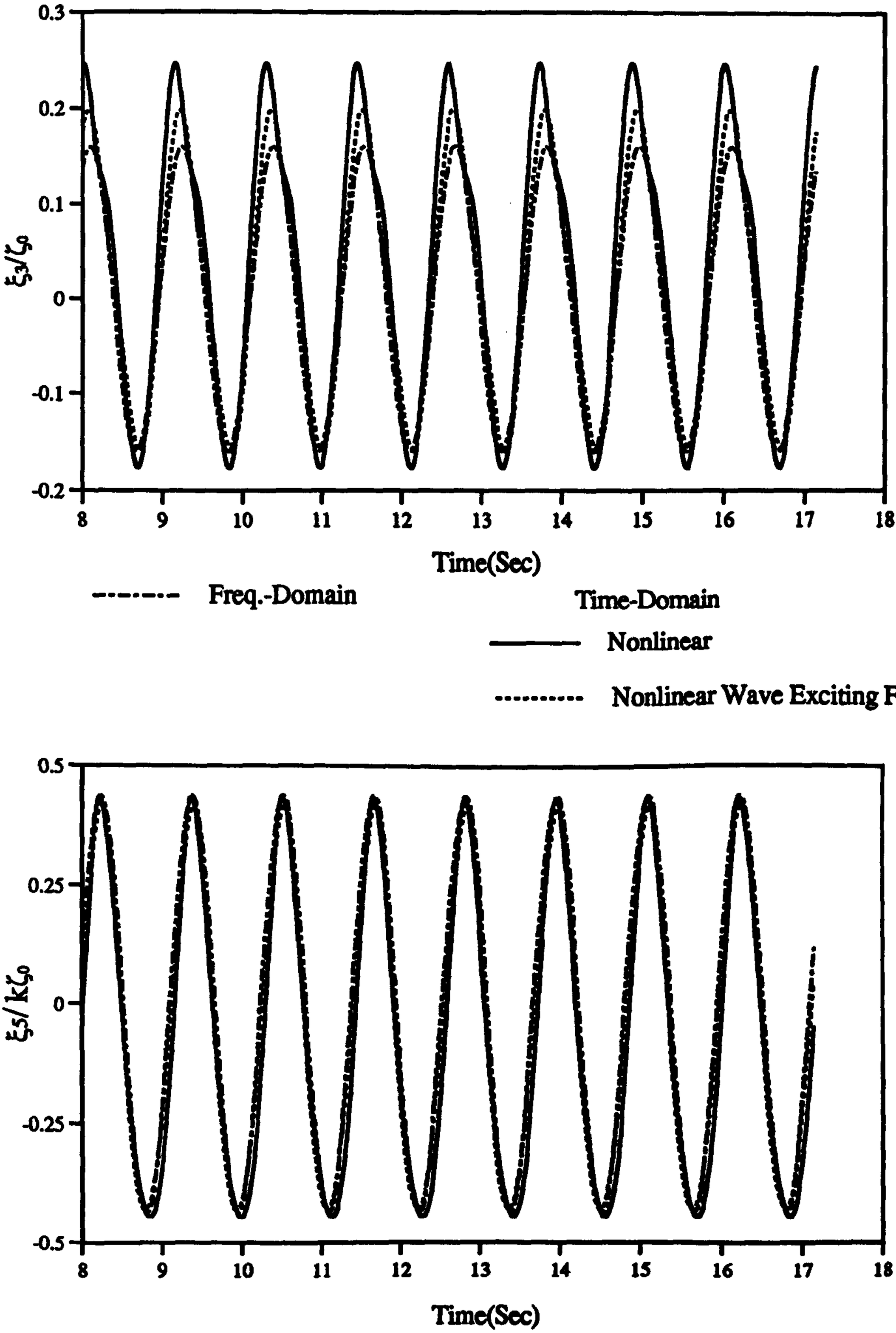

Figure 4.46 : Time Domain Solutions for the Heave and Pitch Motions of V-1 Catamaran with the Nonlinear Wave Exciting Forces (Fn=0.00,ω_0=5.5 rad/sec,ζ_0=3.0cm)

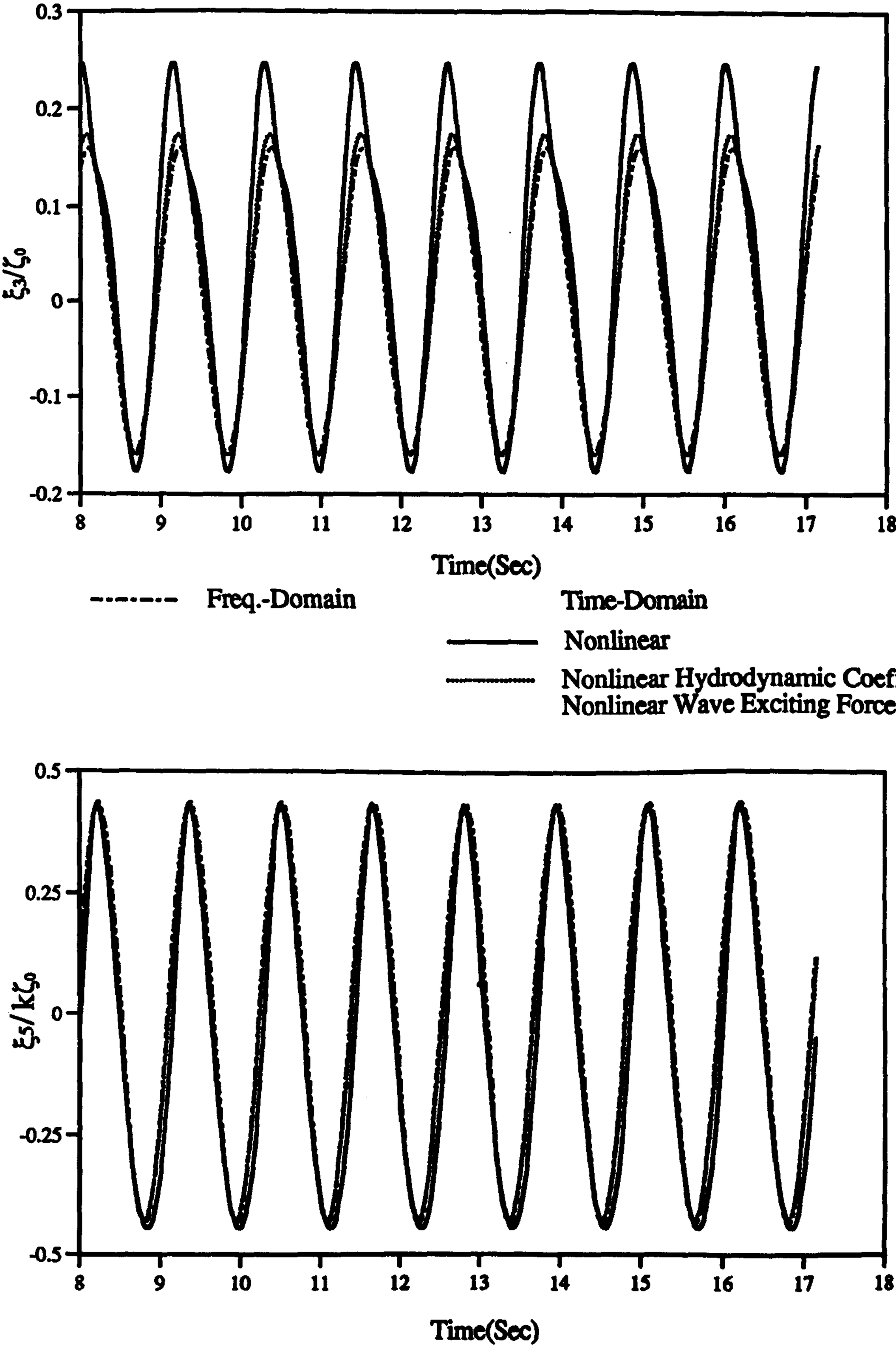

Figure 4.47: Time Domain Solutions for the Heave and Pitch Motions of V-1 Catamaran with the Linear Hydrostatic Forces
(Fn=0.00,ω_0=5.5 rad/sec,ζ_0=3.0cm)

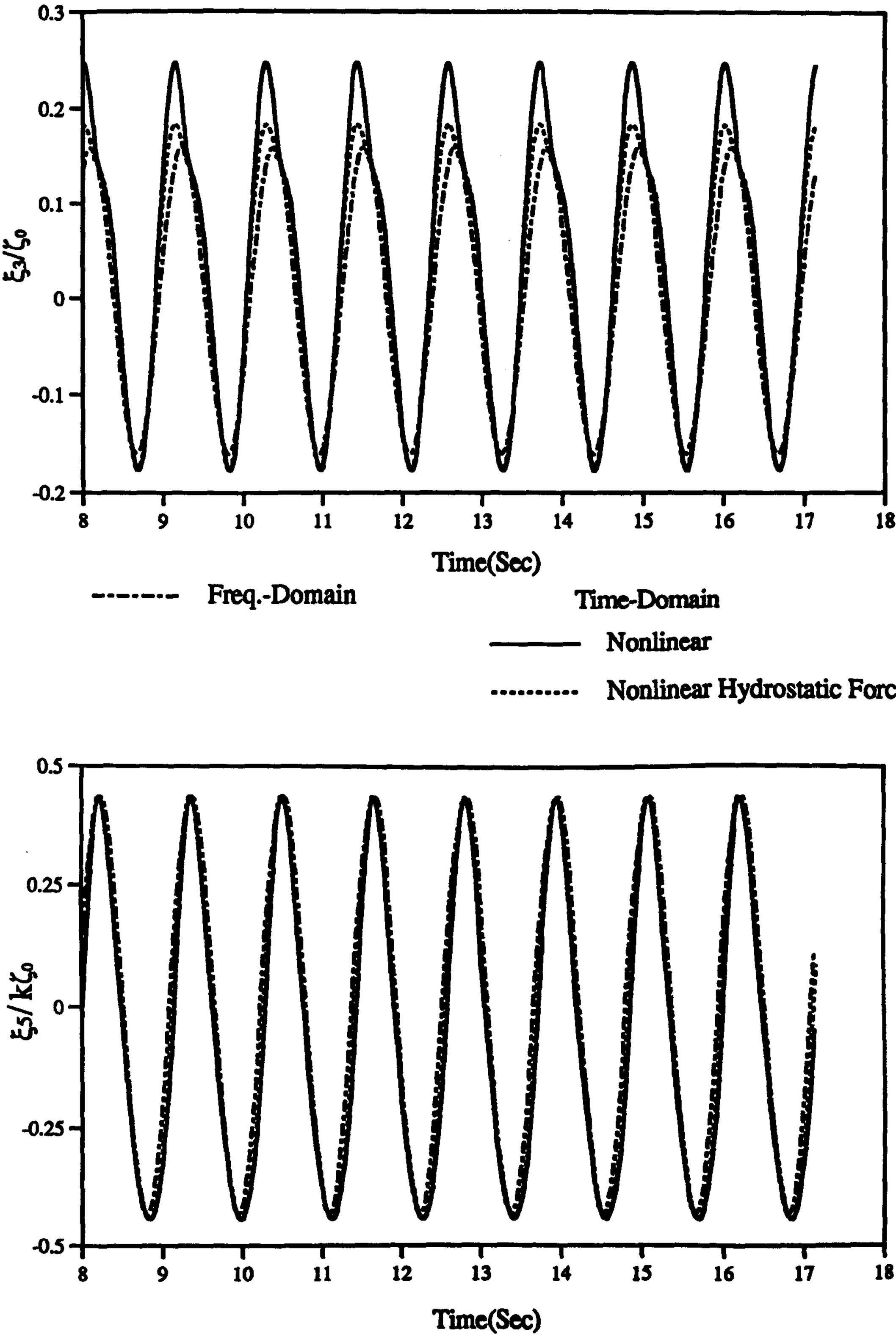

Figure 4.48 : Time Domain Solutions for the Heave and Pitch Motions of V-1 Catamaran with the Nonlinear Hydrostatic Forces
(Fn=0.00,ω_0=5.5 rad/sec,ζ_0=3.0cm)

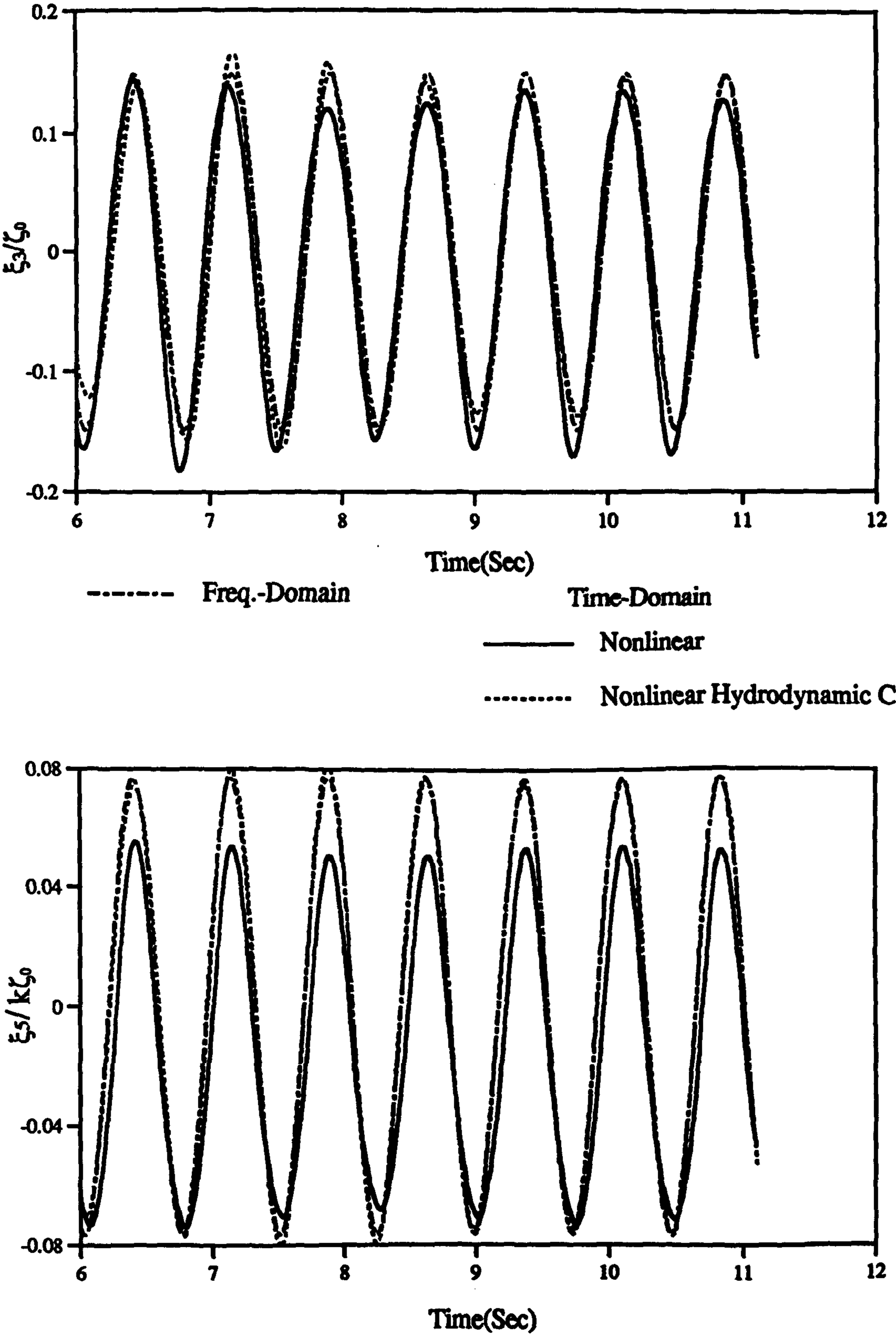

Figure 4.49 : Time Domain Solutions for the Heave and Pitch Motions of V-1 Catamaran with the Nonlinear Hydrodynamic Coefficients
(Fn=0.00,ω_0=8.5 rad/sec,ζ_0=3.0cm)

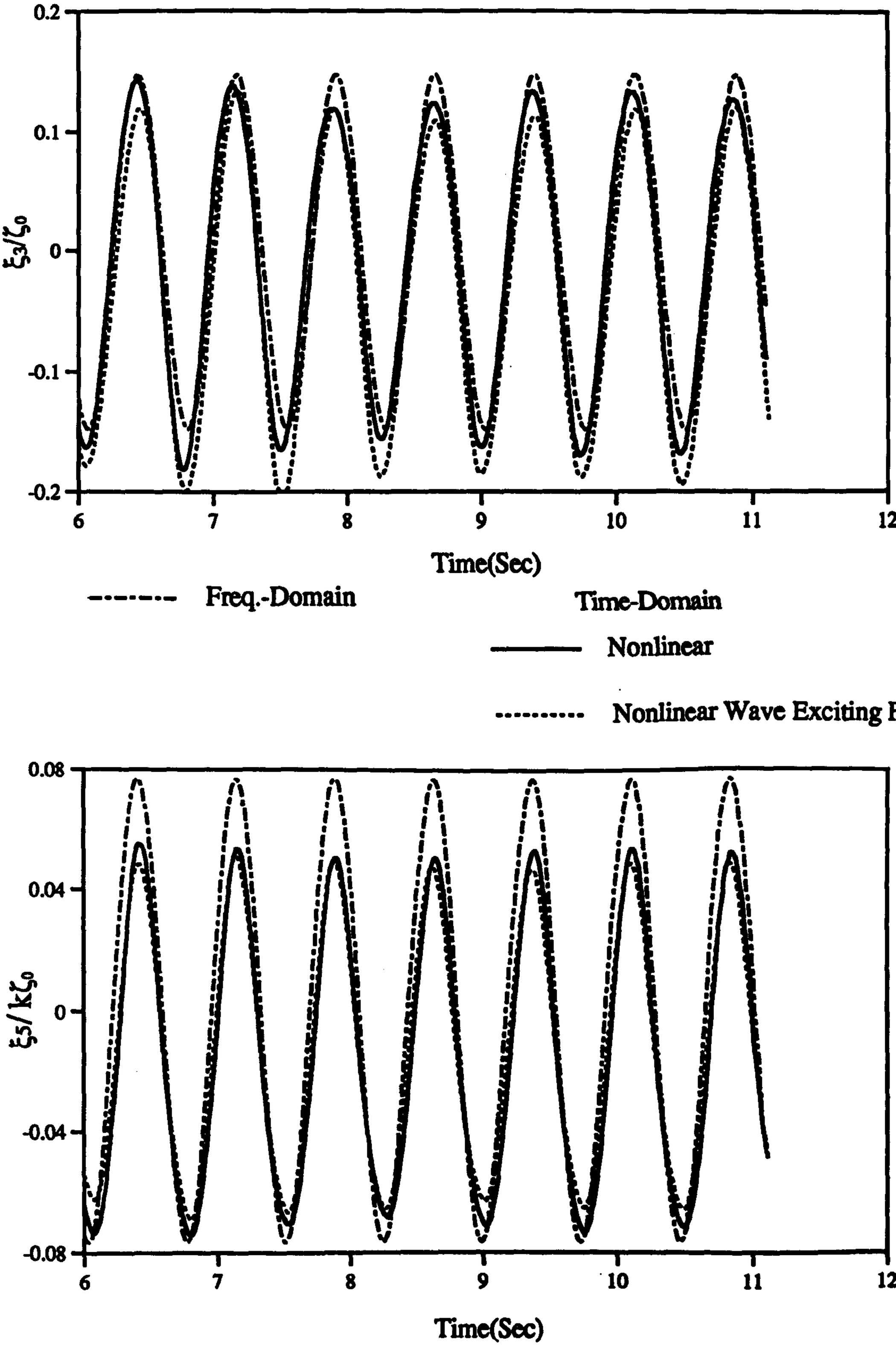

Figure 4.50 : Time Domain Solutions for the Heave and Pitch Motions of V-1 Catamaran with the Nonlinear Wave Exciting Forces
(Fn=0.00,ω_0=8.5 rad/sec,ζ_0=3.0cm)

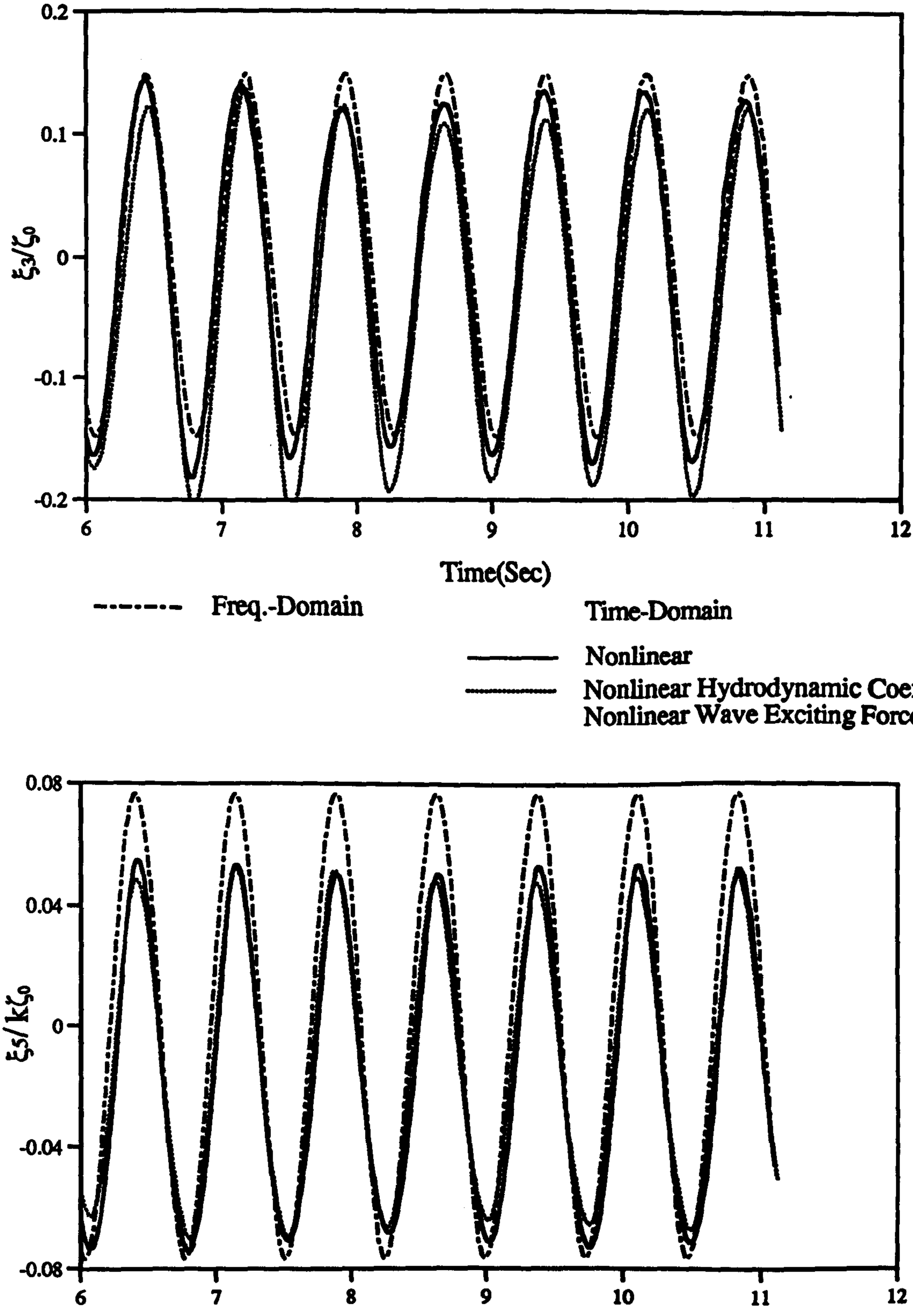

Figure 4.51 : Time Domain Solutions for the Heave and Pitch Motions of V-1 Catamaran with the Linear Hydrostatic Forces
($Fn=0.00, \omega_0=8.5$ rad/sec, $\zeta_0=3.0$cm)

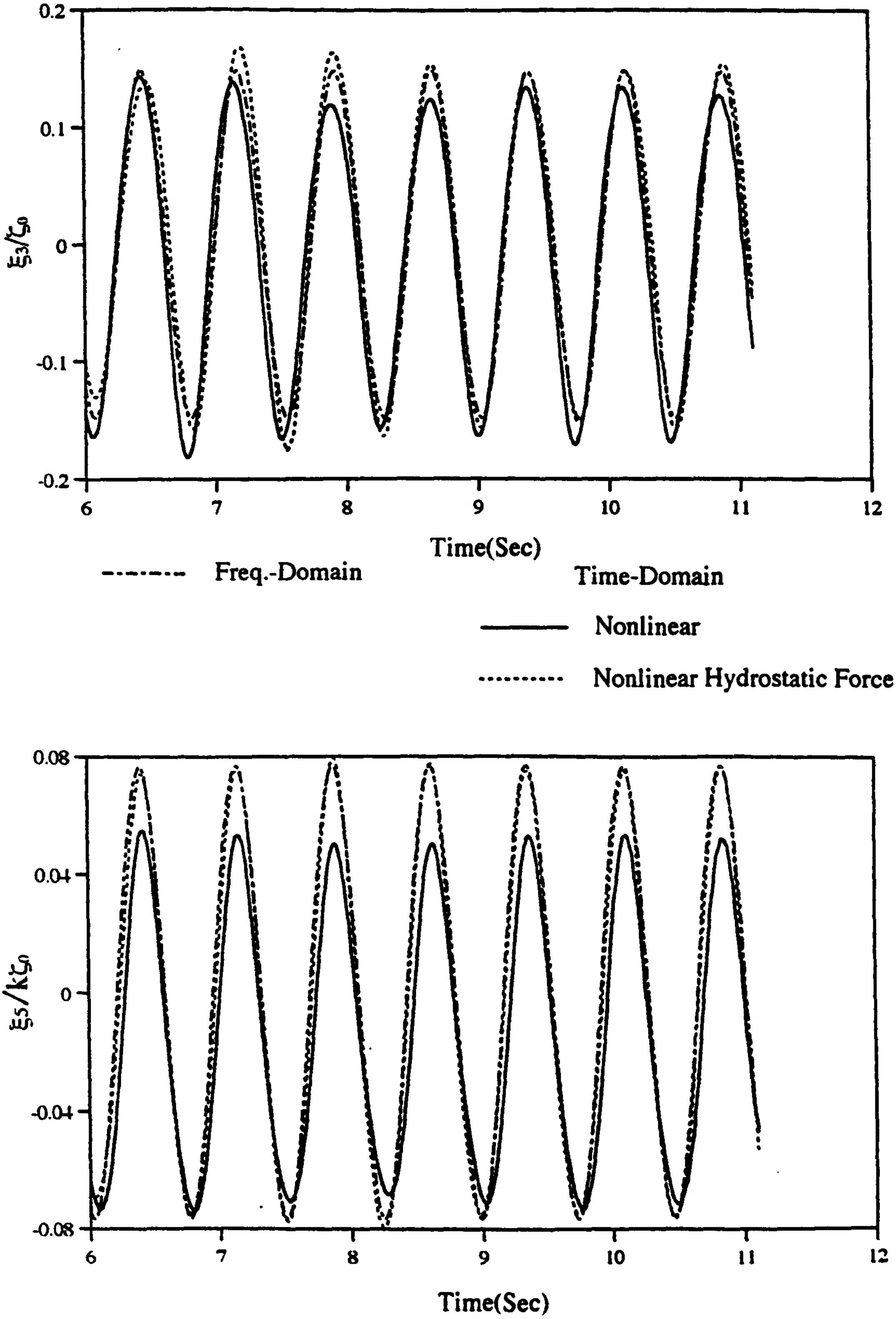

Figure 4.52 : Time Domain Solutions for the Heave and Pitch Motions of V-1 Catamaran with the Nonlinear Hydrostatic Forces
(Fn=0.00, ω_0=8.5 rad/sec, ζ_0=3.0cm)

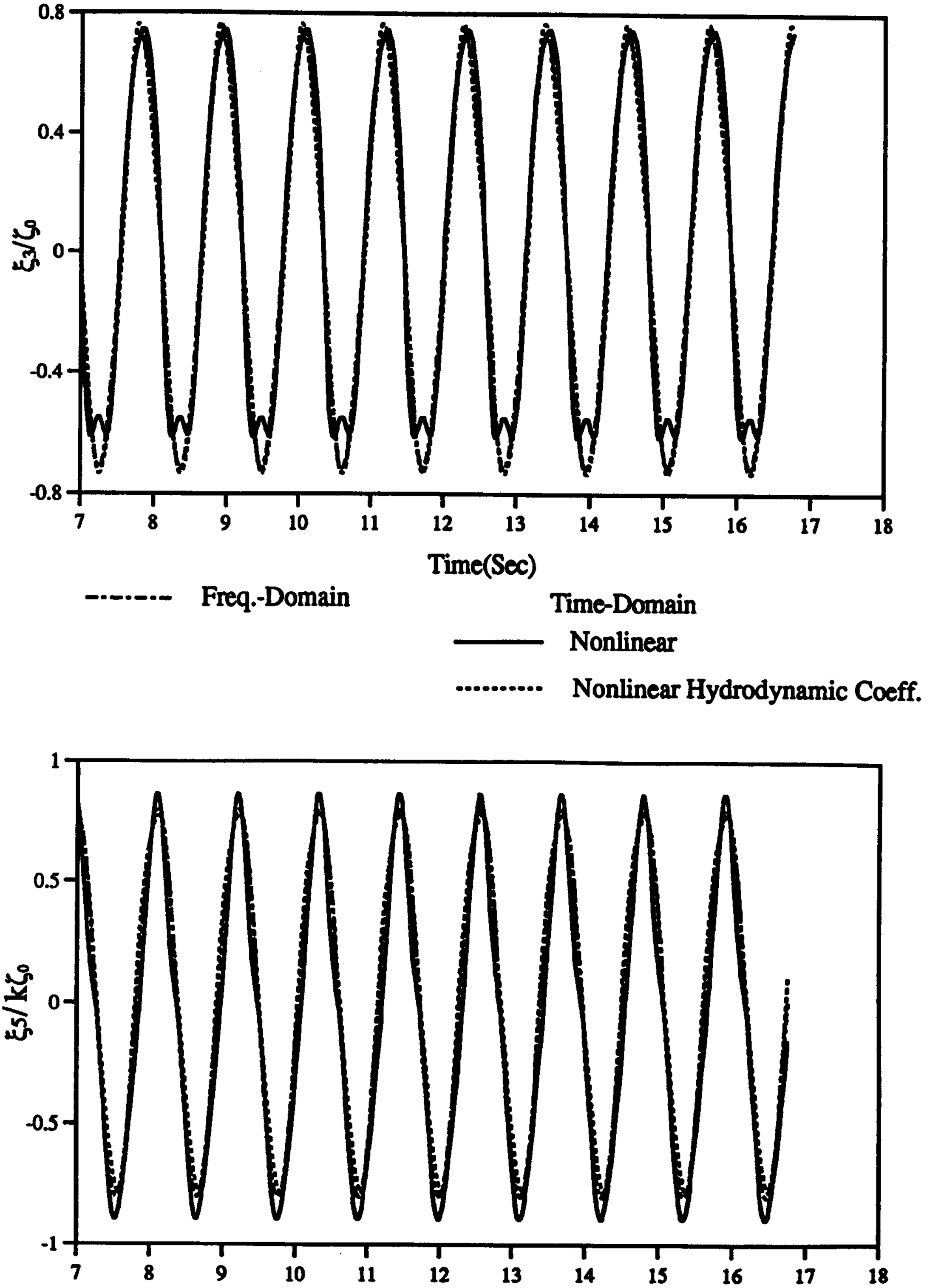

Figure 4.53 : Time Domain Solutions for the Heave and Pitch Motions of V-1 Catamaran with the Nonlinear Hydrodynamic Coefficients (Fn=0.226,ω_0=4.0 rad/sec,ζ_0=4.5cm)

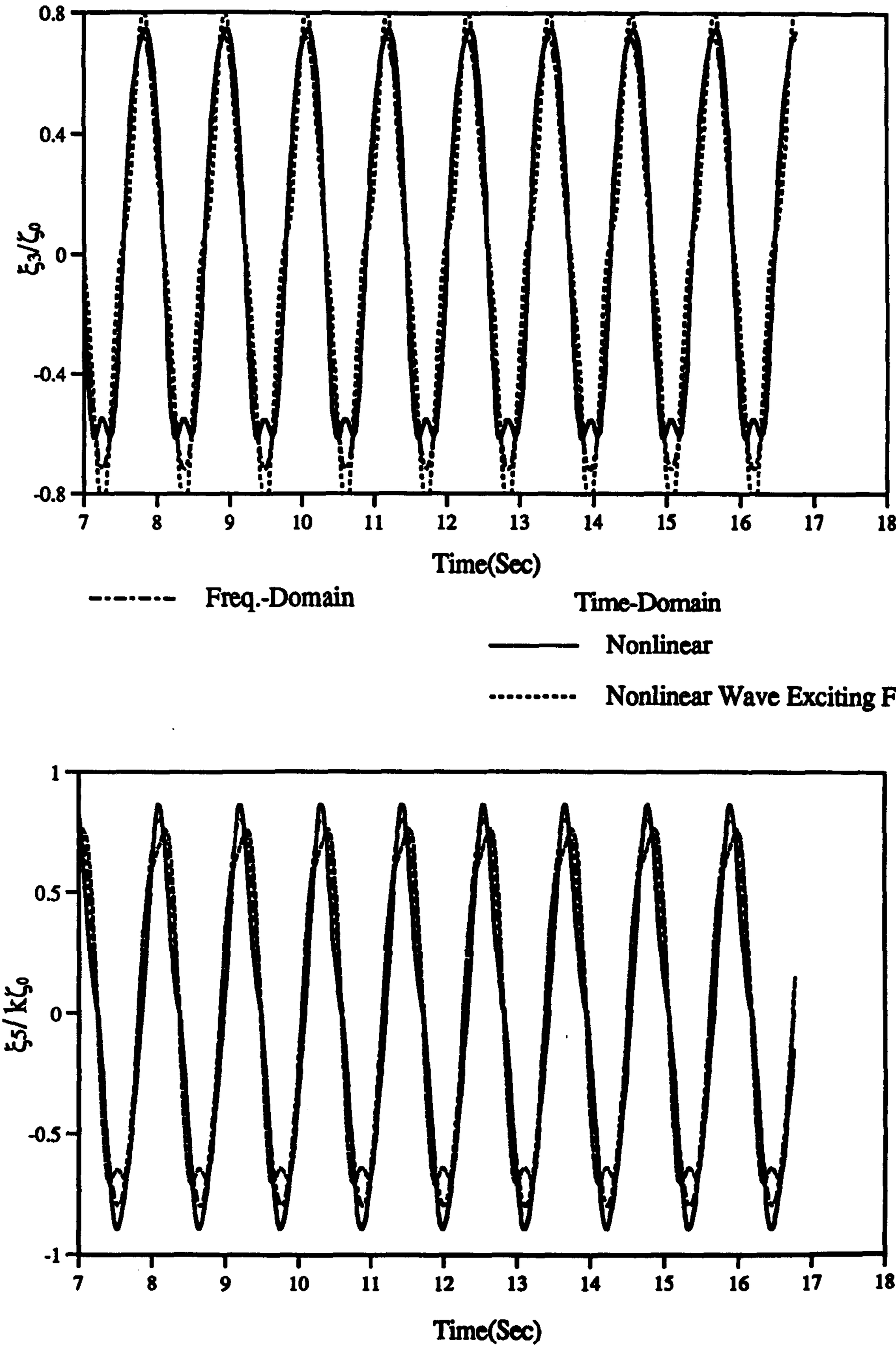

Figure 4.54: Time Domain Solutions for the Heave and Pitch Motions of V-1 Catamaran with the Nonlinear Wave Exciting Forces
(Fn=0.226,ω_0=4.0 rad/sec,ζ_0=4.5cm)

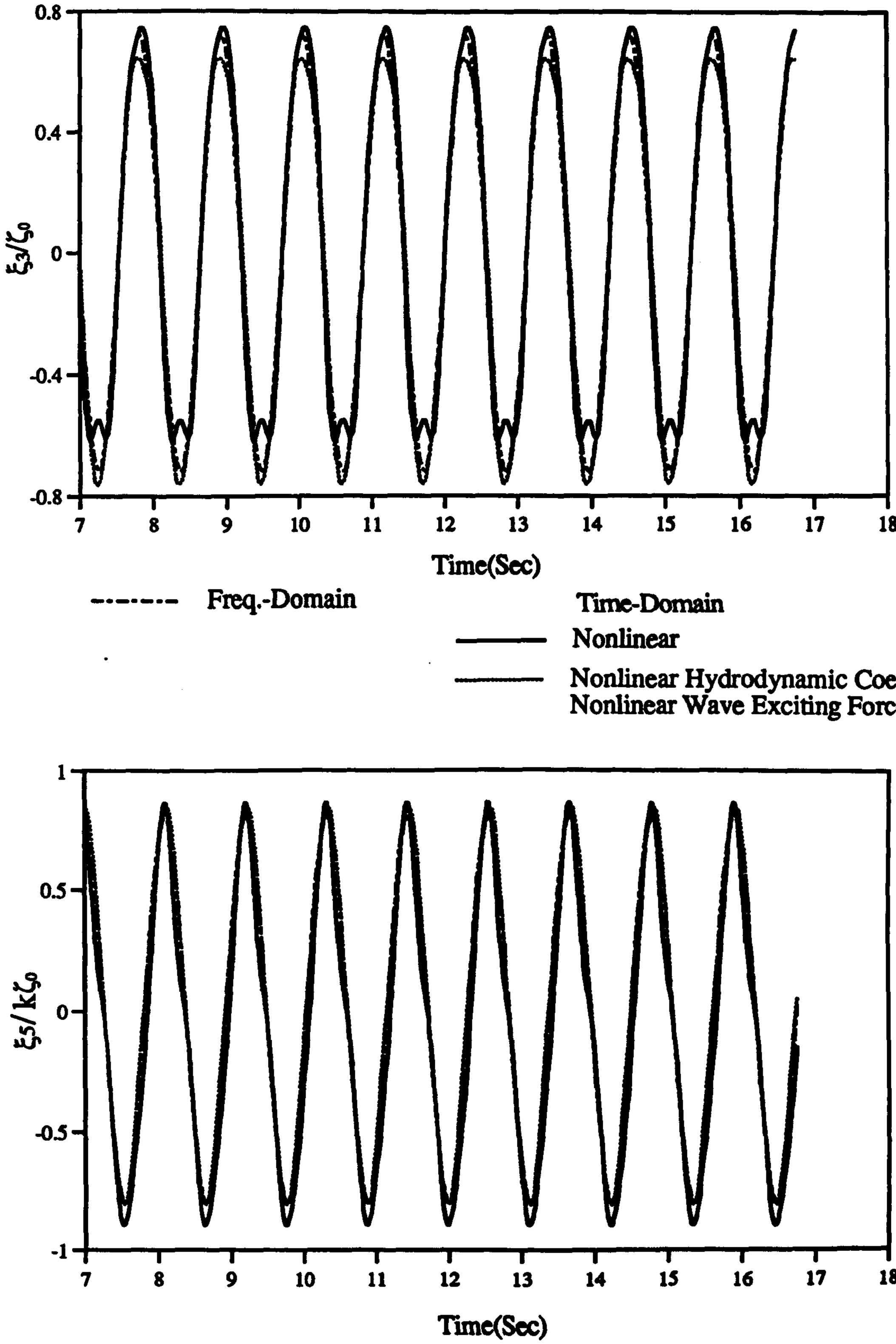

Figure 4.55 : Time Domain Solutions for the Heave and Pitch Motions of V-1 Catamaran with the Linear Hydrostatic Forces
(Fn=0.226,ω_0=4.0 rad/sec,ζ_0=4.5cm)

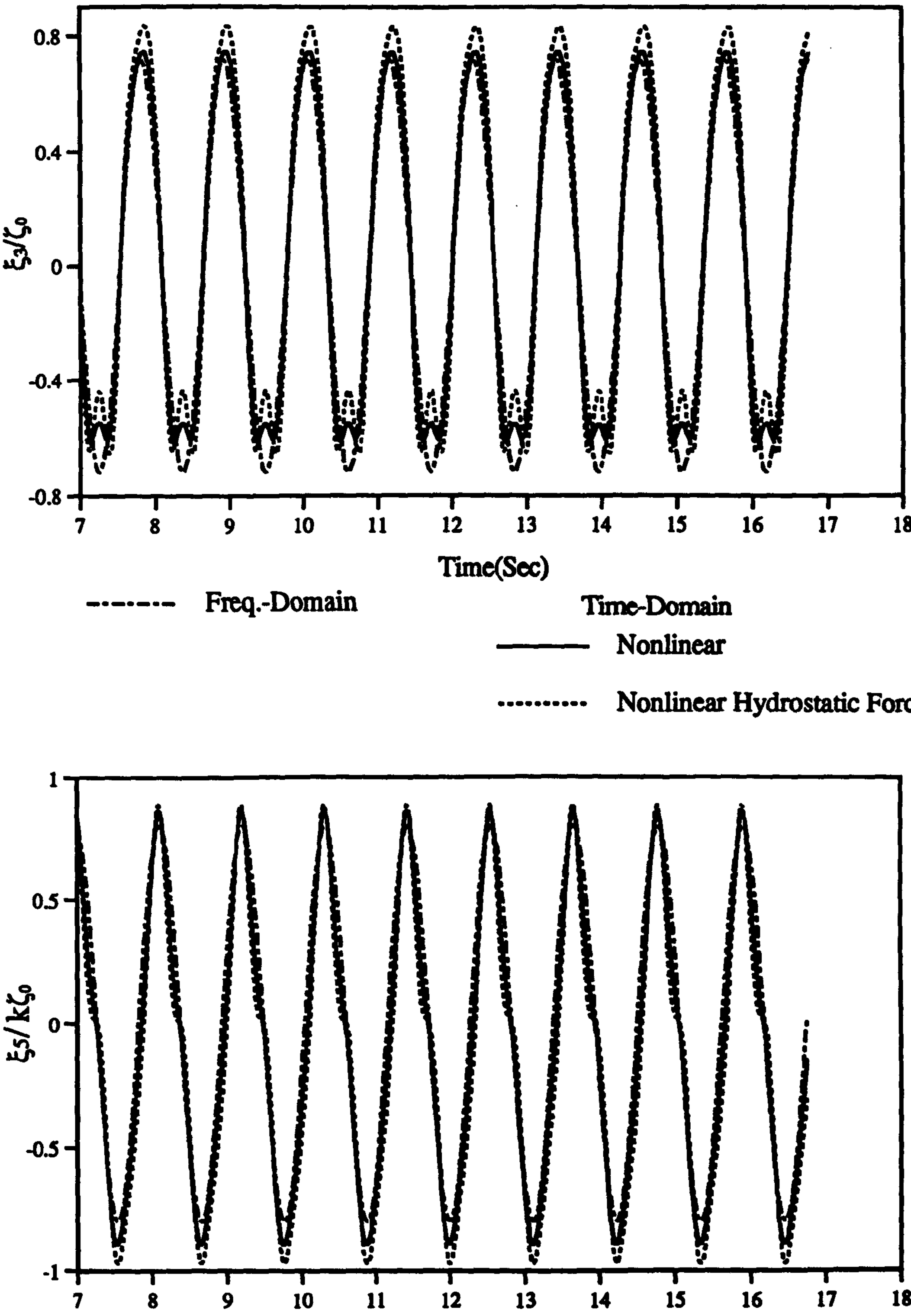

Figure 4.56 : Time Domain Solutions for the Heave and Pitch Motions of V-1 Catamaran with the Nonlinear Hydrostatic Forces
(Fn=0.226,ω_0=4.0 rad/sec,ζ_0=4.5cm)

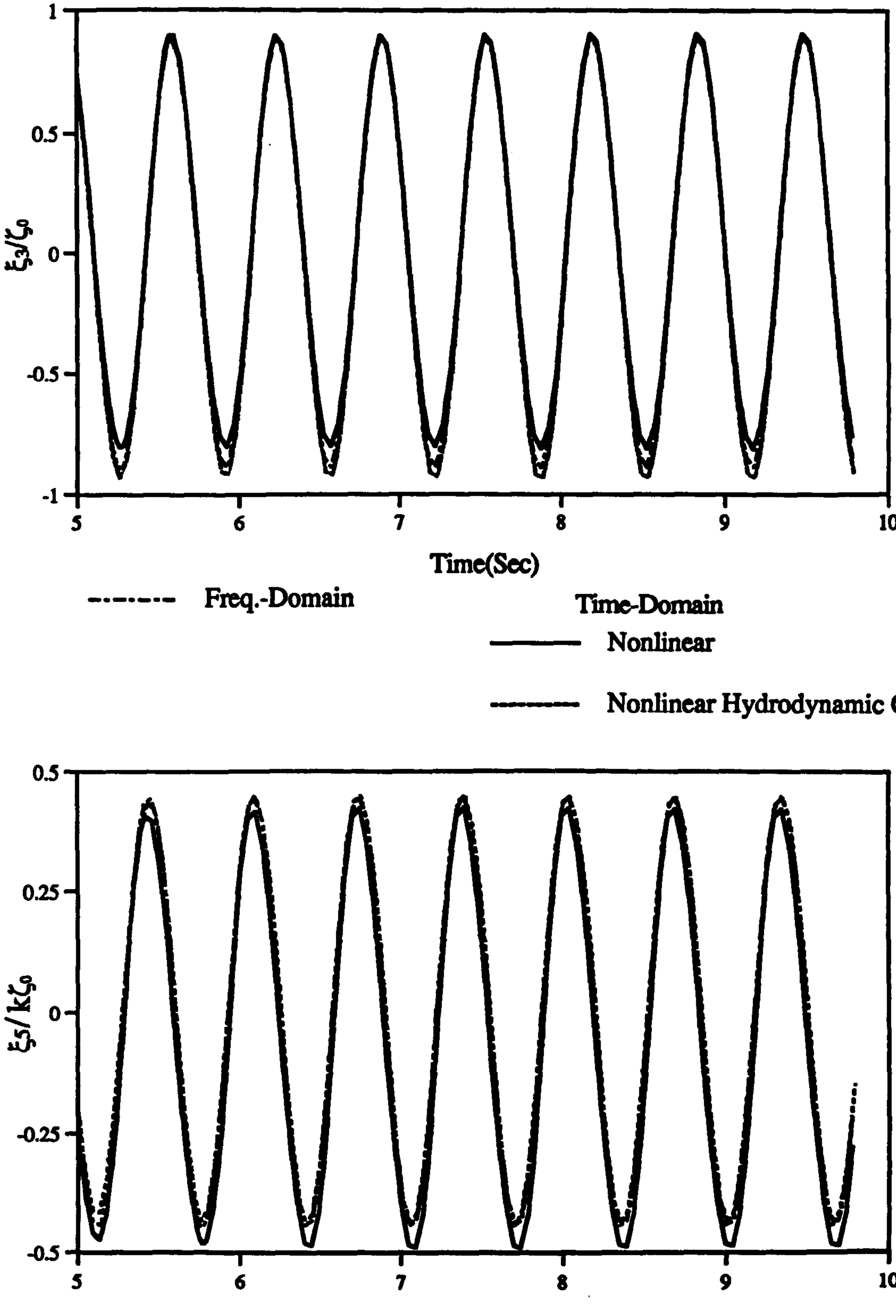

Figure 4.57 : Time Domain Solutions for the Heave and Pitch Motions of V-1 Catamaran with the Nonlinear Hydrodynamic Coefficients ($Fn=0.226, \omega_0=6.0$ rad/sec, $\zeta_0=1.0$cm)

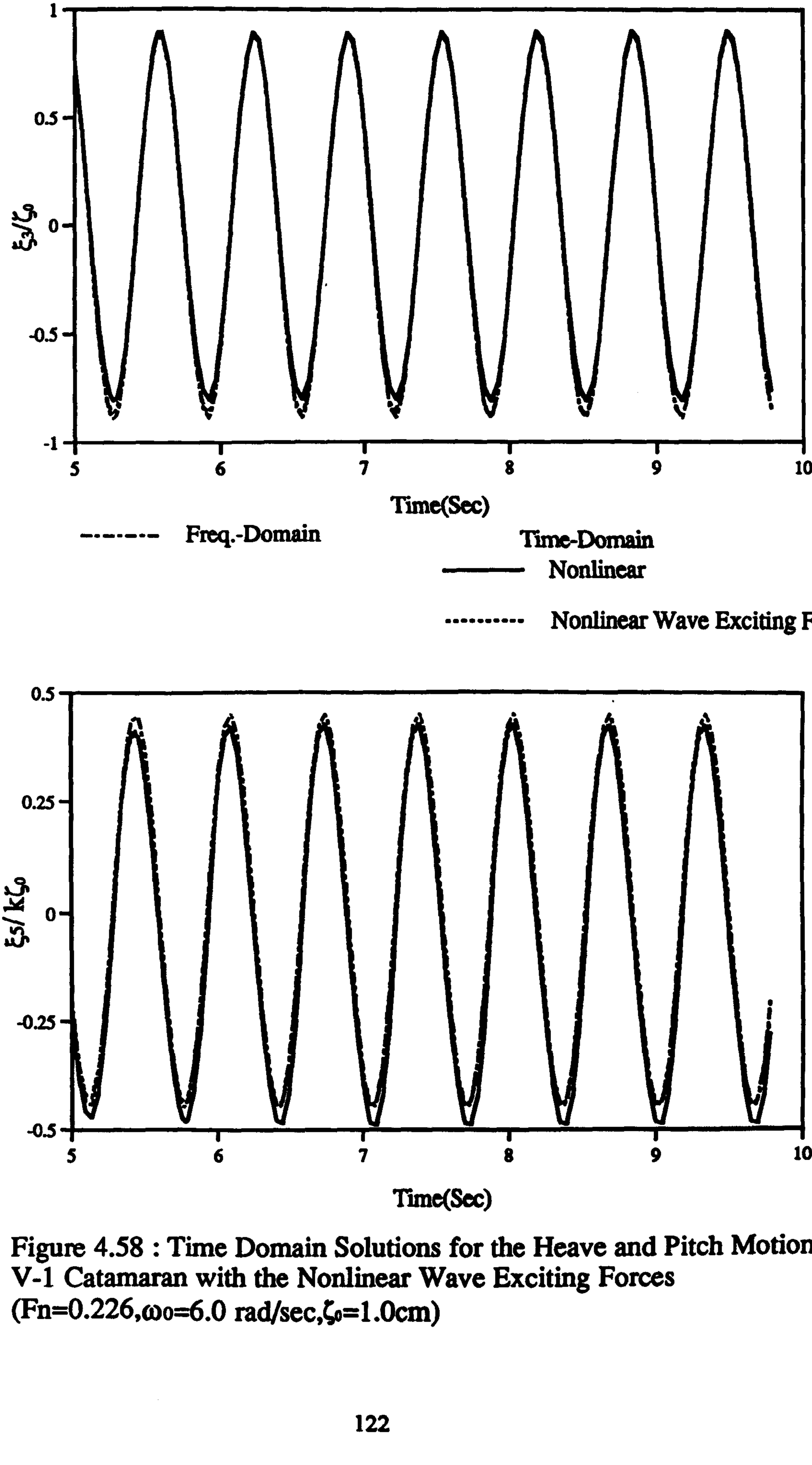

Figure 4.58 : Time Domain Solutions for the Heave and Pitch Motions of V-1 Catamaran with the Nonlinear Wave Exciting Forces ($Fn=0.226, \omega_0=6.0$ rad/sec, $\zeta_0=1.0$cm)

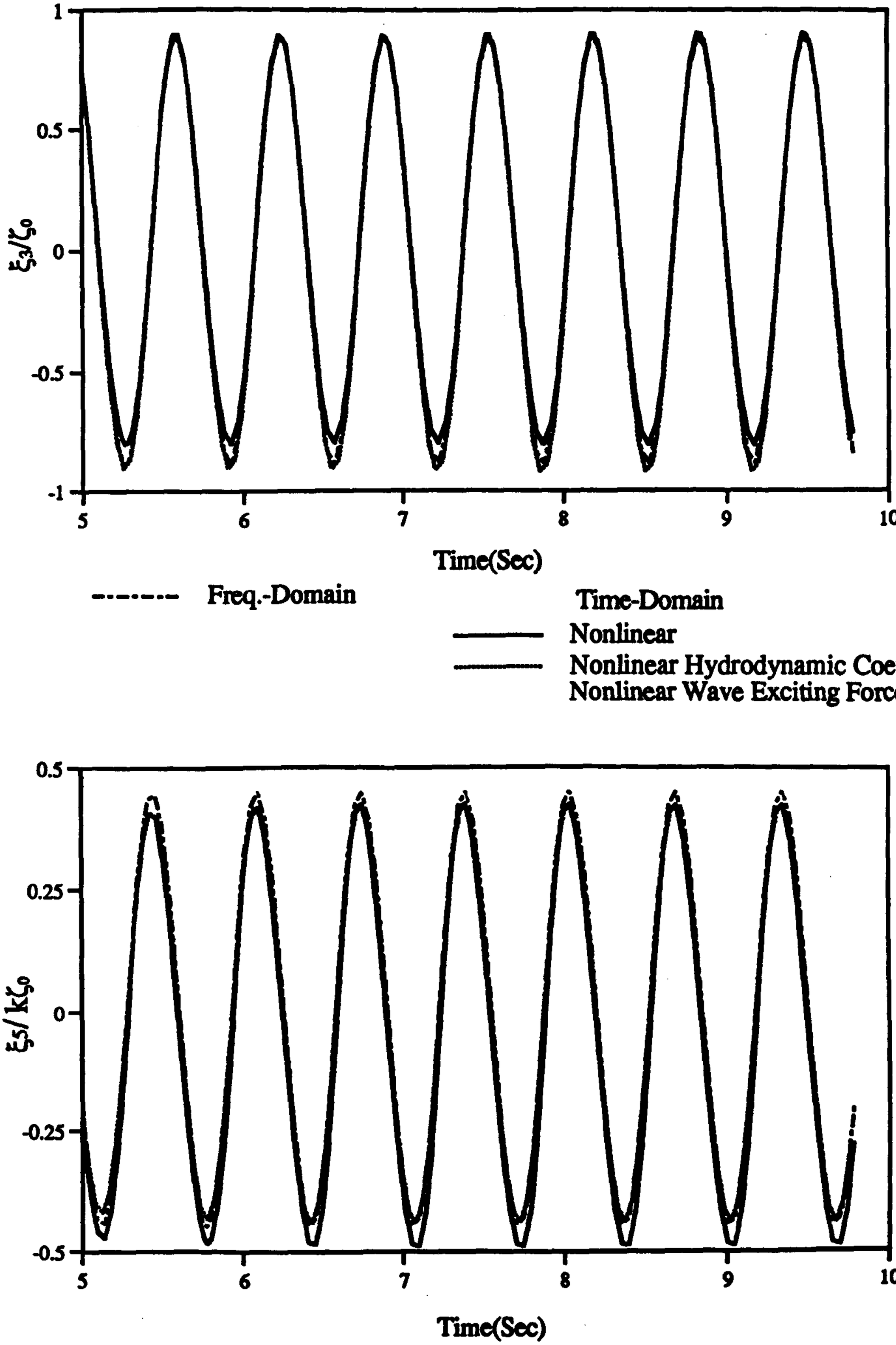

Figure 4.59 : Time Domain Solutions for the Heave and Pitch Motions of V-1 Catamaran with the Linear Hydrostatic Forces
(Fn=0.226,ω_0=6.0 rad/sec,ζ_0=1.0cm)

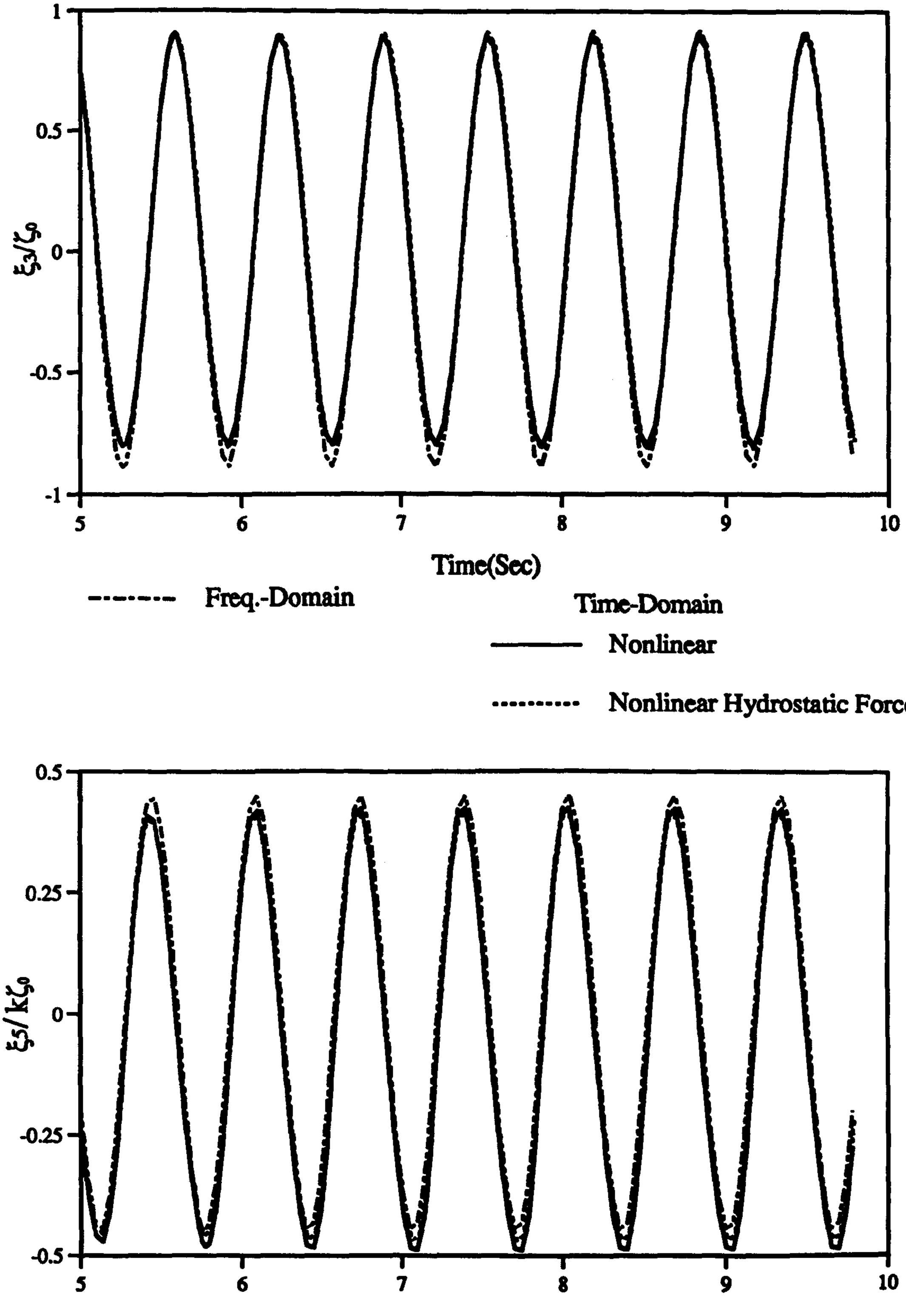

Figure 4.60 : Time Domain Solutions for the Heave and Pitch Motions of V-1 Catamaran with the Nonlinear Hydrostatic Forces
(Fn=0.226,ω_0=6.0 rad/sec,ζ_0=1.0cm)

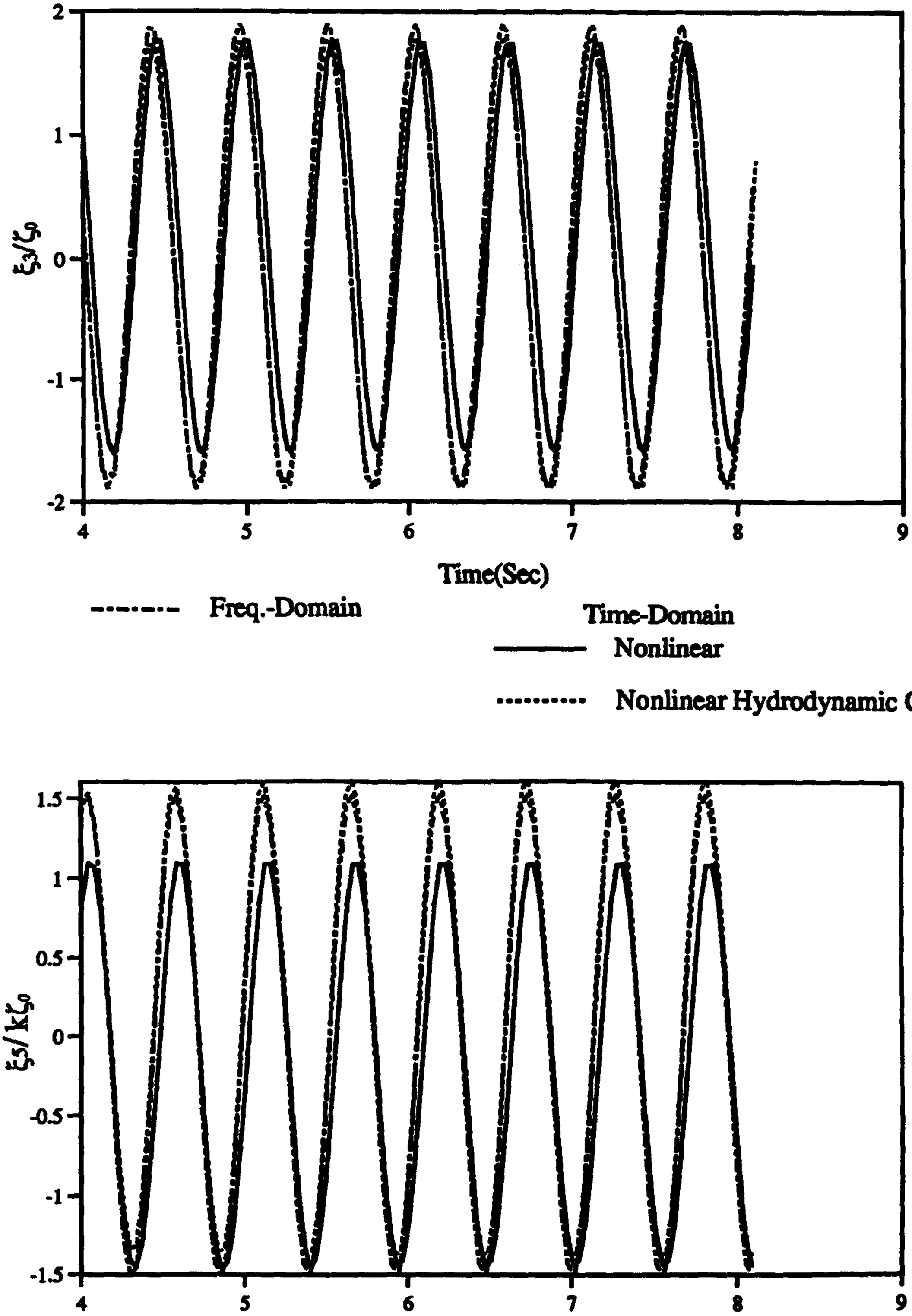

Figure 4.61 : Time Domain Solutions for the Heave and Pitch Motions of V-1 Catamaran with the Nonlinear Hydrodynamic Coefficients (Fn=0.677, ω_0=4.75 rad/sec, ζ_0=1.0cm)

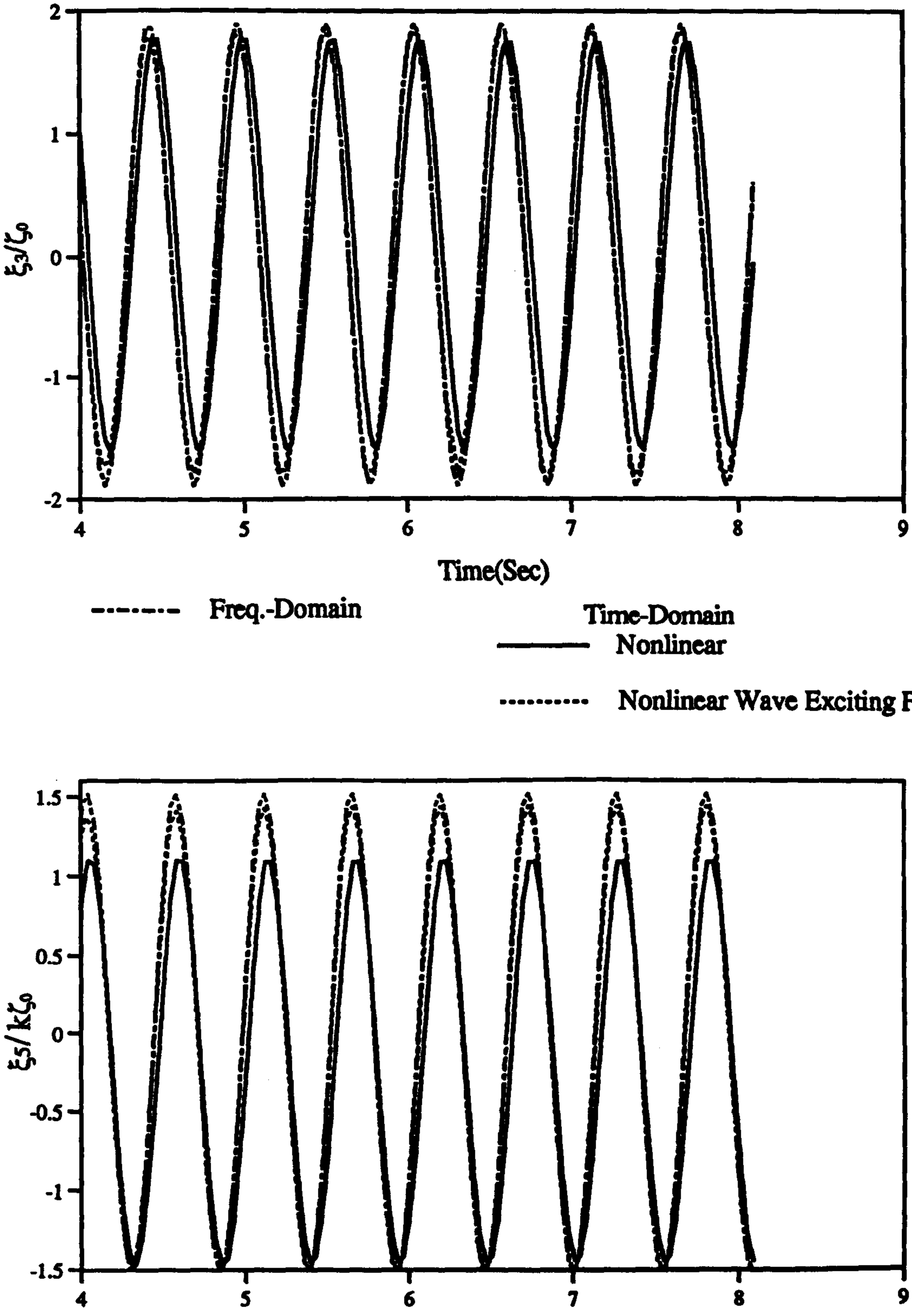

Figure 4.62 : Time Domain Solutions for the Heave and Pitch Motions of V-1 Catamaran with the Nonlinear Wave Exciting Forces
(Fn=0.677, ω_0=4.75 rad/sec, ζ_0=1.0cm)

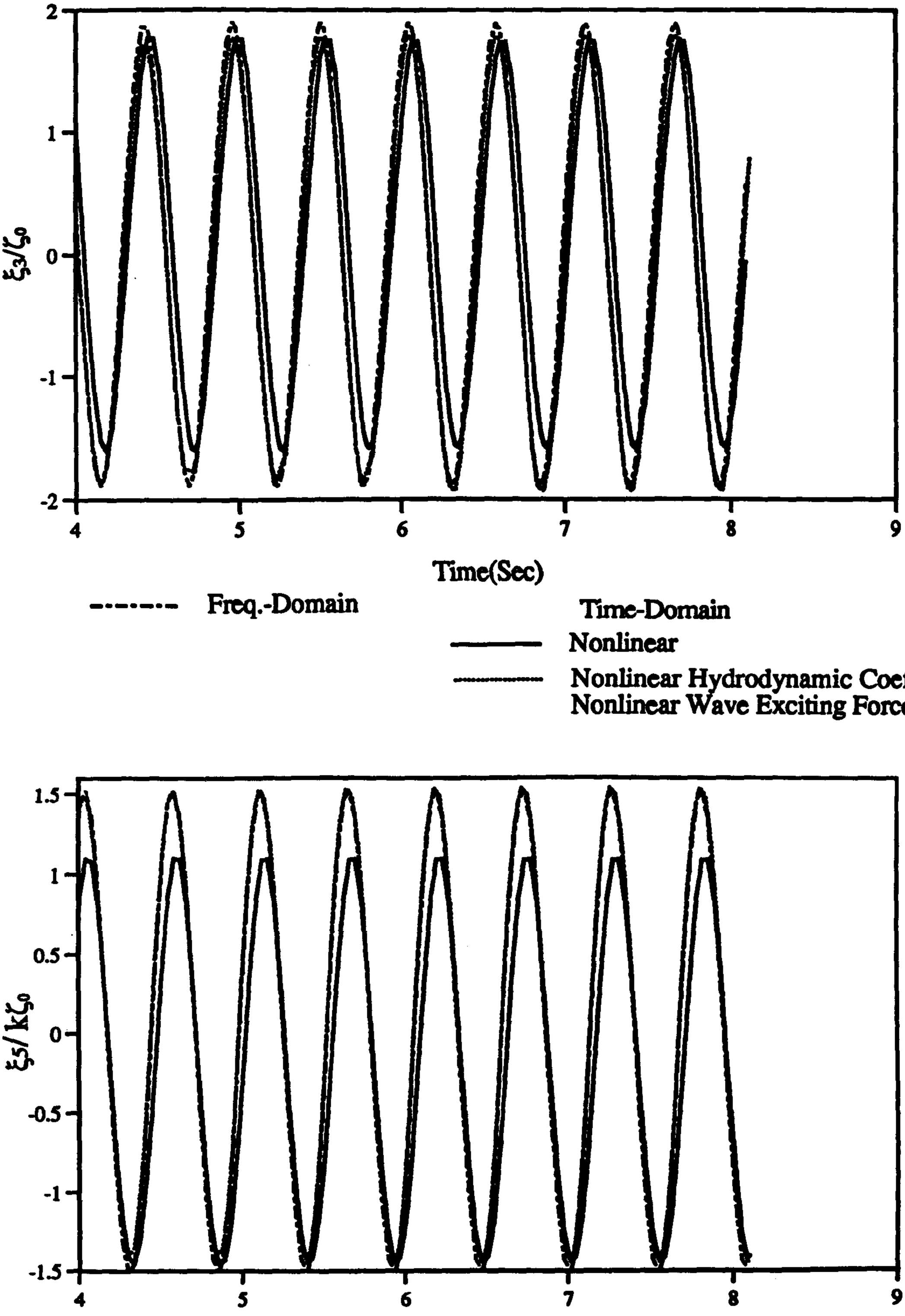

Figure 4.63 : Time Domain Solutions for the Heave and Pitch Motions of V-1 Catamaran with the Linear Hydrostatic Forces
(Fn=0.677,ω_0=4.75 rad/sec,ζ_0=1.0cm)

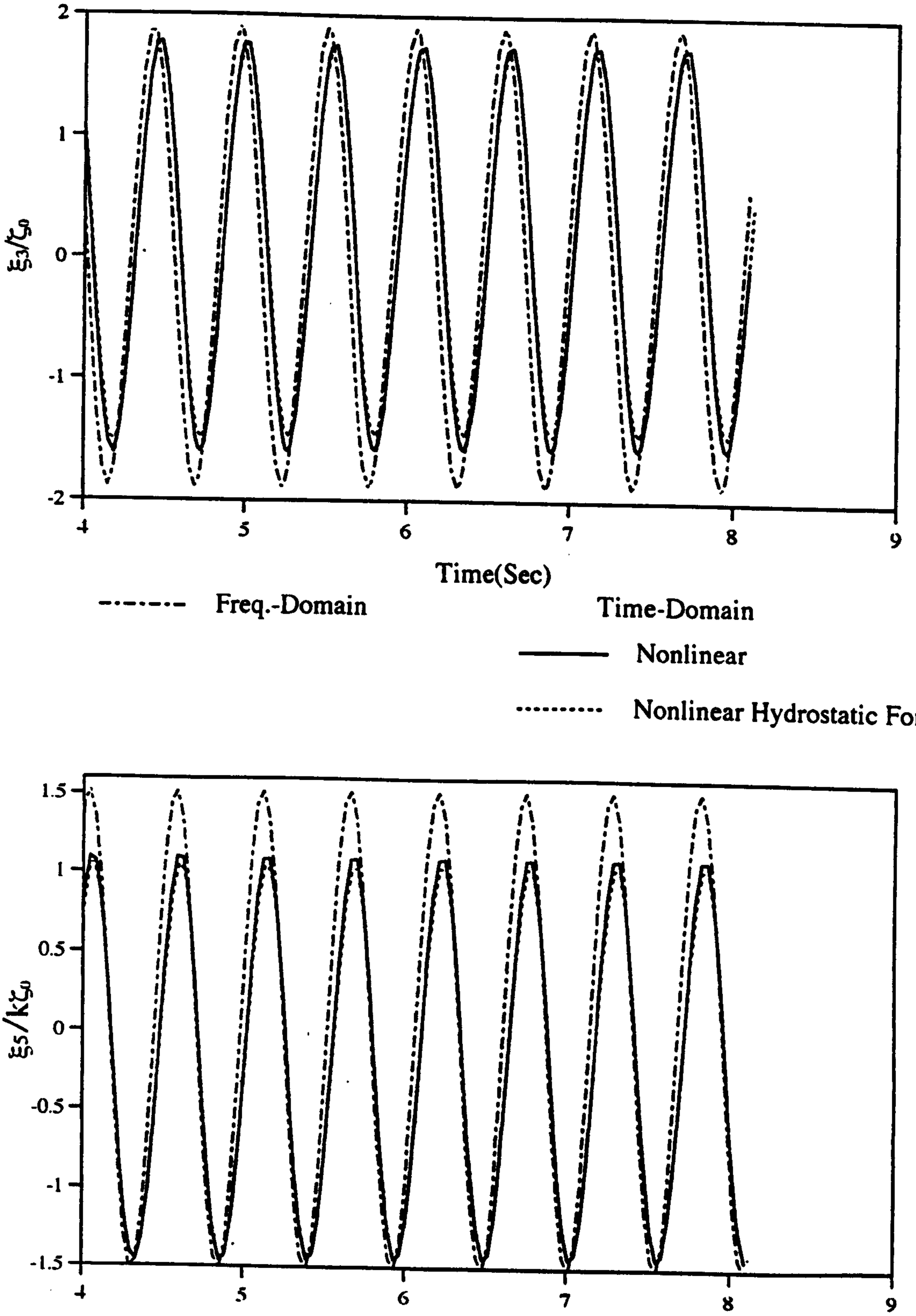

Figure 4.64 : Time Domain Solutions for the Heave and Pitch Motions of V-1 Catamaran with the Nonlinear Hydrostatic Forces
(Fn=0.677, ω_0=4.75 rad/sec, ζ_0=1.0cm)

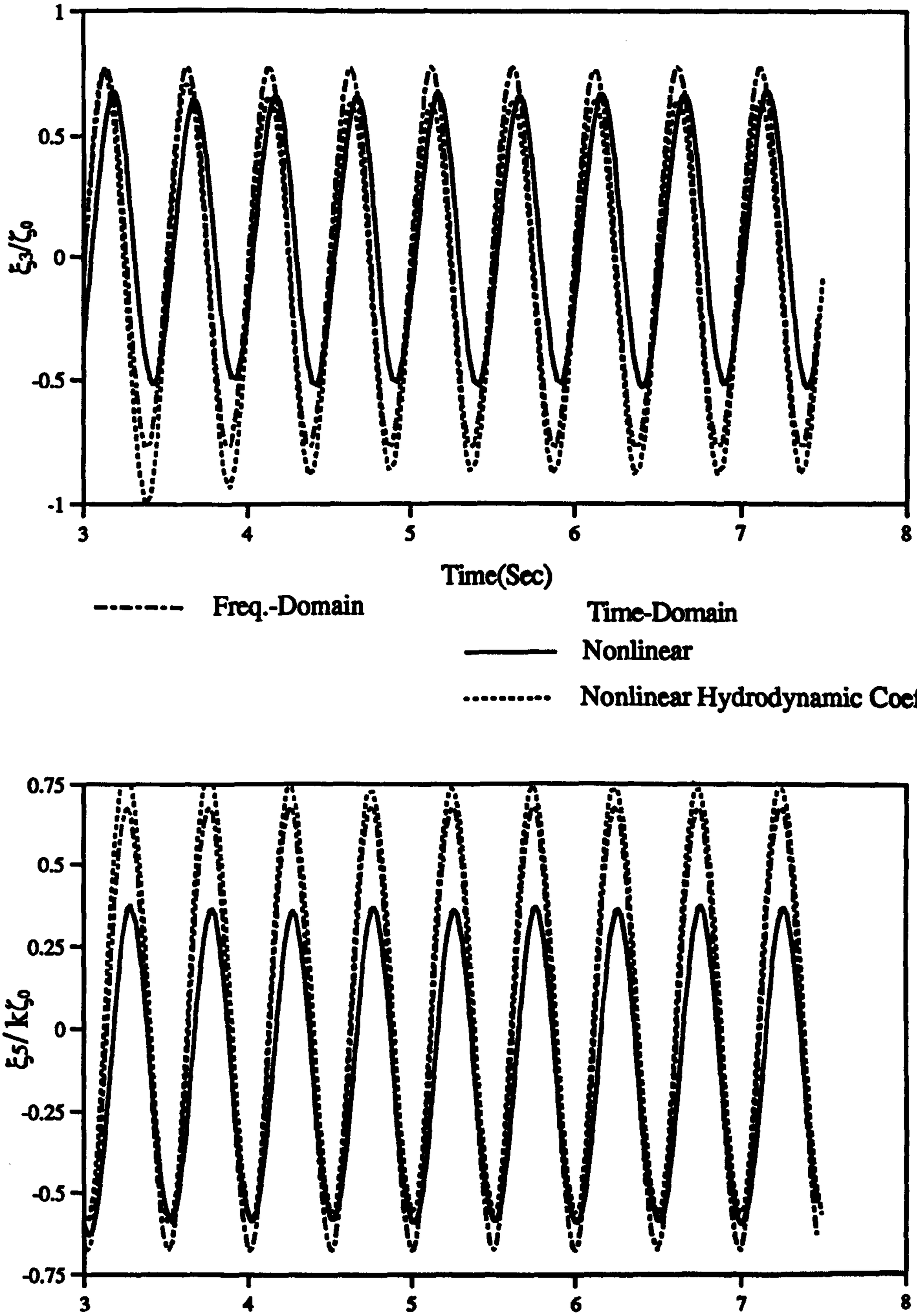

Figure 4.65 : Time Domain Solutions for the Heave and Pitch Motions of V-1 Catamaran with the Nonlinear Hydrodynamic Coefficients
(Fn=0.677, ω_0=5.0 rad/sec, ζ_0=3.0cm)

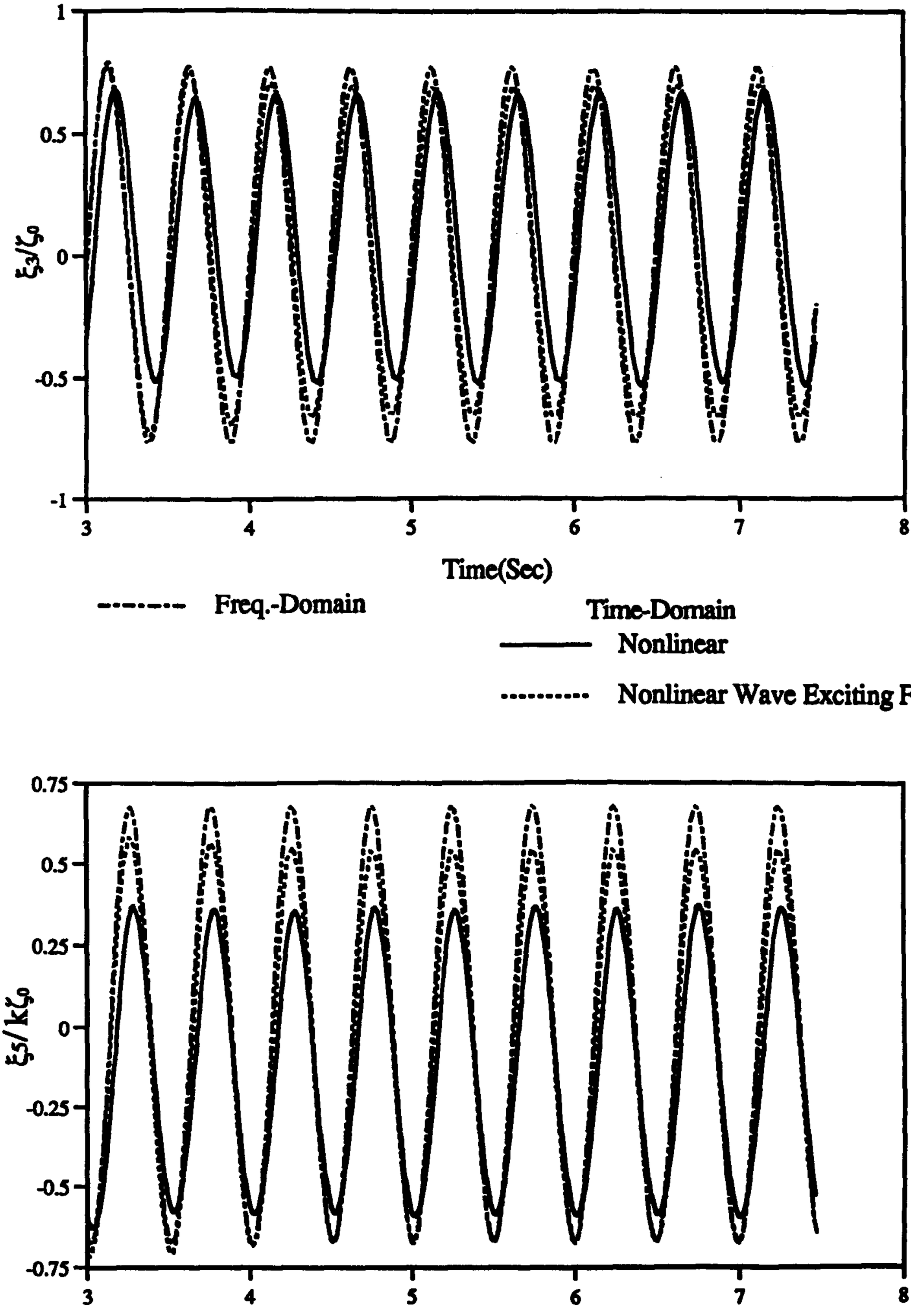

Figure 4.66 : Time Domain Solutions for the Heave and Pitch Motions of V-1 Catamaran with the Nonlinear Wave Exciting Forces ($Fn=0.677, \omega_0=5.0$ rad/sec, $\zeta_0=3.0$cm)

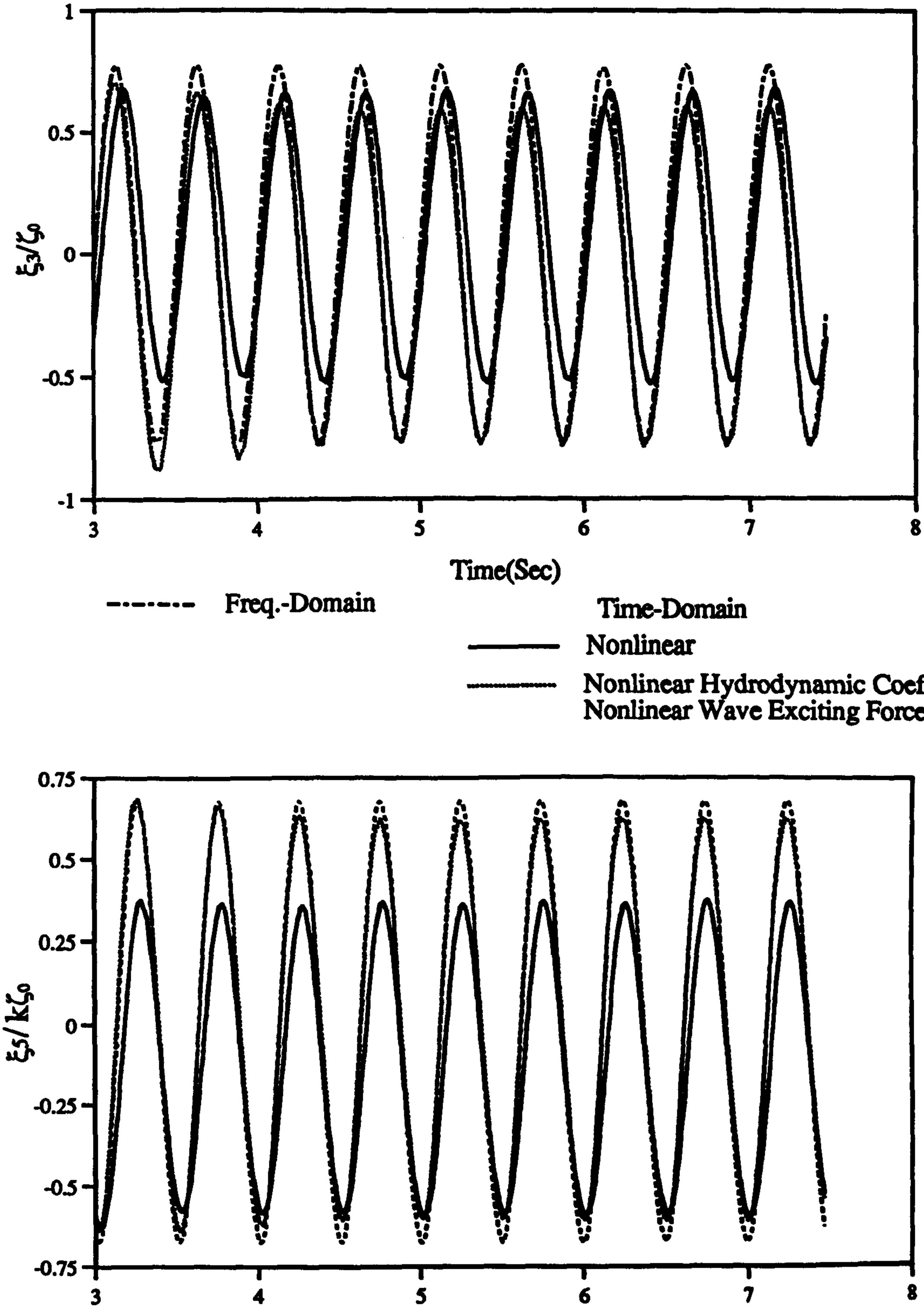

Figure 4.67 : Time Domain Solutions for the Heave and Pitch Motions of V-1 Catamaran with the Linear Hydrostatic Forces
(Fn=0.677,ω_0=5.0 rad/sec,ζ_0=3.0cm)

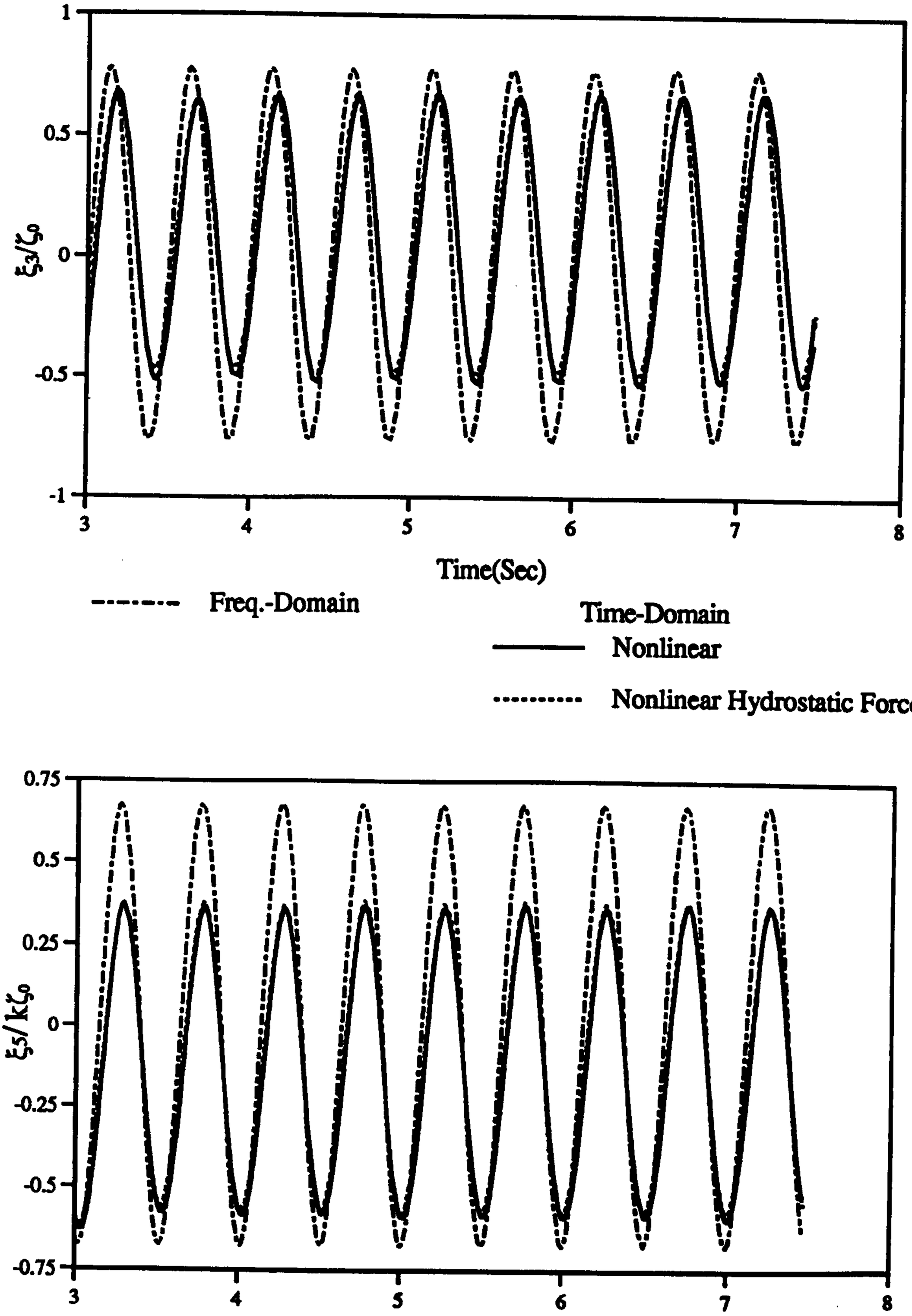

Figure 4.68 : Time Domain Solutions for the Heave and Pitch Motions of V-1 Catamaran with the Nonlinear Hydrostatic Forces
(Fn=0.677, ω_0=5.0 rad/sec, ζ_0=3.0cm)

CHAPTER 5
EXPERIMENTAL INVESTIGATION OF LARGE AMPLITUDE MOTIONS OF A CATAMARAN IN WAVES

5.1 Introduction

Model tests provide an attractive alternative to study the nonlinear problem of large amplitude motions beside the theoretical predictions. The physical phenomena of large amplitude motions of catamarans travelling in waves can be investigated in detail through experimental observations. At the present time, most published experimental data for the motions of catamarans are limited to a linear behaviour. In order to investigate the large amplitude motions of catamarans travelling in waves, a series of experiments with a catamaran model was carried out in the Towing Tank of the Hydrodynamics Laboratory at the University of Glasgow.

The V-1 catamaran model developed from the V.I.L. catamaran (Incecik et al., 1991) was selected for the test model. Tests were carried out at three different model speeds of 0m/s, 1m/s, 3m/s, three different wave amplitudes of 1cm, 3cm, 4.5cm and 14 different wave frequencies in order to evaluate the nonlinear motions of the V-1 catamaran in regular waves. A post-towing measurement system was designed and tested for the high-speed ships to carry out the motion tests in waves.

The calm water tests were carried out with the V-1 catamaran in order to measure the total resistance, C.G. rise and trim change over a speed range up to Fn=1.129. Results are compared with previous work (Incecik et al., 1991). Comparisons between the experimental measurements and those results obtained from linear frequency domain and nonlinear time domain techniques have been made to investigate the large amplitude motions of the V-1 catamaran in regular waves. A set of consecutive photographs of the test model is presented to develop physical understanding of the nonlinear impact behaviour of the V-1 catamaran travelling in head sea condition.

5.2 Model configuration and test conditions

5.2.1 Description of the model

The V-1 catamaran model is a hard-chine type planing craft. Lines of the model is presented in figure 3.12. The draught of test model with hull separation/beam = 1.429 is set at 0.0672m and the measured initial trim angle is 0.02deg., trim by bow, in the

still water condition. Details about the model configuration of the V-1 catamaran can be found in table 3.3. The catamaran model was constructed with glass-reinforced plastic fibres. A pair of aluminium bars were used to provide a rigid coupling between the hulls. The turbulence stimulation was provided by studs of 3 mm diameter and 3 mm height at a spacing of 25mm. These studs were situated from 1.9 to 2.0 m forward of stern. No other underwater appendages were attached to the V-1 model during the tests.

5.2.2 Test Condition

There were three stages during these experiments. Firstly, in order to compare the measurements with previous work (Incecik et al., 1991) and to validate the new measurement system, a set of calm water tests was carried out. Then, the small amplitude incident wave tests, $\zeta_0 = 1cm$, were designed to validate the theoretical predictions obtained from the linear frequency domain method. Finally, two sets of larger amplitude incident wave tests, $\zeta_0 = 3cm, 4.5cm$, were carried out to investigate the nonlinear effects during large amplitude motions of the V-1 catamaran in regular waves with three different forward speeds (Fn=0.00, 0.226, 0.677).

1. Calm water tests:

The total resistance, running trim and sinkage of the catamaran model were measured over a speed range up to F_n=1.129. Tests with 10 different forward speeds from 0.0 to 4.875 m/s were carried out during these tests.

2. Regular wave tests:

During the motion response measurements in the head sea condition, the model was tested to investigate the nonlinear effects of large amplitude motions at three different model speeds (0m/s, 1m/s, 3m/s), three different wave amplitudes (1cm, 3cm, 4.5cm) and 14 different wave frequencies (2.0 rad/sec to 8.5 rad/sec).

5.3 Facilities and tests

5.3.1 General

All the experiments were carried out in the Towing Tank of the Hydrodynamics Laboratory at the University of Glasgow which has the following principal particulars:

Length :77m
Breadth :4.6m
Water depth :2.7m

The Hydrodynamics Laboratory is equipped with an electronically controlled towing carriage. The maximum carriage speed is 6.4 m/s. The wave frequency is ranging from 0.4 up to 1.4 Hz and wave amplitudes from 0.6 to 11 cm could be generated by a plunger-type wavemaker placed at the top end of the tank. Waves are generated at one end of the tank by a wavemaker and absorbed by a beach at the other. Figure 5.1 shows the general arrangement of the Towing Tank.

5.3.2 Measurement devices

A measurement system was designed and tested to investigate the nonlinear effects during large amplitude motions of a catamaran in the head sea condition. The model was towed by an vertical post which allowed freedom in pitch and heave motion with restraints in roll and yaw motions as shown in figure 5.2. The towing point was positioned at the centre of gravity of the model which was free to pitch around a hinge pin at its centre of gravity. The pitch pivot was mounted at the end of a vertical rod frame which slid in linear bearings allowing the model free to heave. Additional yaw restraints were provided by two vertical rods mounted in the stern and bow of the model and passing between two pairs of horizontal rollers mounted longitudinally on the carriage. No surge motion is allowed in this facility. This measurement system was designed to carry out tests not only with twin-hull models but also with mono-hull by rearranging the towing post frame.

Compared with the former towing system in the Towing Tank, the present technique offers a number of improvements as detailed in the following:

1. The post towing type system is more suitable than wire type towing system for carrying out motion response experiments in waves. The oscillatory motions of a test model will result an oscillatory towing force when the wire type towing system is used. Moreover, the towing wheel of a wire type towing system may hit the bottom of the model (mono-hull) or disturb the inner flow between two demi-hulls (catamaran) when the large amplitude motions occur.

2. The present measurement system does not induce any parasitic inertia effects on the model since the yaw restraint rods are fixed on the model and considered to be a part of ballast weights of the model. However, the pitch motion may be effected by any frictions due to the yaw restraint devices. The towing point is positioned on the centre of gravity of model to prevent the extra moments due to the shift of towing forces.

3. Since the motion response of a high speed craft is sensitive to the weight distribution values, the material and dimension of the towing system were carefully selected. It allowed more freedom to adjust the mass distribution so that the designed centre of gravity and radius of gyration of model were achieved precisely.

The total resistance was measured by a designed force gauge transducer installed at the middle of the towing post frame as shown in figure 5.2. A pair of small light-emitting diodes (LED, **selspot system**) positioned on the deck of the model was used to measure the heave and pitch oscillations of the model. The selspot system is designed to measure the coordinates of multiple points at the same time. A versatile optoelectronic camera detects the position of the diodes for registration and analysis of static as well as dynamic processes in real time. When the infrared light from the LED is focused on the detector surface , a photocurrent, divided among the four electrodes, will occur. The current can be used to obtain two signals linearly related to the vertical and horizontal coordinates of the LED without any contact with the model.

Four resistance type wave probes were used to measure the wave heights in this study. The resistance type wave probe measured the resistances of the water between two wires as a function of the depth of immersion. One resistance type wave probe was situated on the carriage and was parallel to the bow line (122.5cm forward of C.G.). The phase difference between the wave excitation and the model motion responses were measured by this wave probe. There are some disadvantages in using the resistance type wave probe in the forward speed tests. The surface-piercing probe will be deformed significantly due to the current load acting on it as the carriage travels at high forward speeds. This effect may cause some measurement errors in calculating the incident wave amplitudes and phase shifts. In order to accurately measure the incident wave amplitude, three resistance type wave probes were located at B/2, B/3 and B/4 from the tank side wall where B is the tank width and approximately 5.5m in front of the wavemaker.

The setup of data-acquisition system used in this experiment is shown in figure 5.3. All the analog signals passed through multi-channel amplifiers and filters before

entering into AMUX-64 system which is an analog-to-digital converter. Then, the digital signals were recorded by a Macintosh-IIci microcomputer in real time and displayed graphically to ensure that the acquisition and measuring system worked properly during the tests.

5.3.3 Calibration of the measurement devices

In order to identify the linearity of measurement devices and get the calibration coefficients which can relate an output voltage to a physical quantity, a series of calibrations were made before carrying out the experiment.

1.The calibration of force transducer:

A semiconductor gauge type load cell was designed to measure the resistance of the catamaran model. The calibration of force transducer was carried out by applying weights of 0 to 10 kg with 2 kg steps from two different force locations to investigate the existence of moment. All the data were recorded and analysed in the microcomputer. The results showed that the effects of moment existed but the force transducer still kept linearity as the horizontal forces were measured in the forward speed direction; the accuracy of the measurement was within $\pm 0.012kg$.

2.The calibration of selspot system:

In order to measure the linearity of the selspot system, one LED was mounted on a vertical rod. The distance between the LED and the camera was 80cm. The calibration process was carried out by lifting the LED gradually at 2 cm intervals up to 10 cm and the new positions of LED were recorded in the computer at each time step. The calibration results showed a good linear relationship for the selspot system; the accuracy of the measurement was within $\pm 0.01cm$.

3.The calibration of accelerometer:

A gravity type accelerometer was used to measure the vertical bow acceleration at FP (Forward Perpendicular). The calibration of the accelerometer was carried out before it was mounted on the transverse beam of model. The accelerometer was rotated 90 degrees and the position of the pen corresponding to 9.81 m/sec^2 was marked on the chart-recorder.

4.The calibration of wave probes:

The calibration process was carried out by lifting the wave probes at 5 cm steps up to 15 cm and at each time step the new positions of the pens were marked on the chart-recorder and recorded in the computer. The calibration results showed a linear relationship for the wave probes; the accuracy of the measurement was within $\pm 0.02cm$.

5.3.4 Flowchart of the experiments

The experimental process was carried out by the following flowchart as shown in figure 5.4. Details are described as follows:

1. A model built for previous investigation was used to carry out experiments reported here. Four spray rails fitted on the previous V.I.L. model were dismantled and the towing foundations at LCG position were fitted on the bottom of each demi-hull with wooden material. The plastic covers were used on each deck of demi-hull for waterproofing during the experiments.

2. The longitudinal ballast distributions were adjusted to satisfy the longitudinal centre of gravity.

3. The transverse ballast distribution were adjusted to keep the zero heel angle.

4. The height of ballast weights were adjusted to satisfy the vertical centre of gravity.

5. The force transducer, selspot system, accelerometer and wave probes were calibrated to identify the linearity of transducers and to obtain calibration coefficients to relate an output voltage to a physical quantity being measured.

6. The radius of gyration of model in pitch and yaw motions were measured by Bifilar suspension method (Lloyd, 1989).

7. Equipment and model setup at the towing carriage are shown in figure 5.2. Some calibrations on site were also carried out to validate the setup of the transducers before starting the experiments.

8. The initial trim angle and draught of model were measured with the trim gauges.

9. Calm water tests: (refer to 5.2.2 test condition)

Having set the datum to zero in the data-acquisition, the catamaran model was towed by the towing carriage with a constant forward speed. Speed and force records were taken by the data-acquisition system when the required steady speed was reached.

10. Regular wave tests: (refer to 5.2.2 test condition)

Firstly, the initial values were measured by the data-acquisition system to set the datum to zero. Then, the wavemaker controlled by the Dell-200 microcomputer system was started to generate the regular incident waves. The catamaran model was towed by the towing carriage with a constant forward speed into the regular waves. When the model behaviour in waves reached the most steady and consistent pattern, the data-acquisition system was started. Figure 5.5 shows a set of sample records of the incident wave and motion response traces from the calm water condition to fully periodical motions.

11.The measurement devices were re-calibrated at the end of each test series.

5.3.5 Data analysis

The experimental data acquired by the Macintosh-IIci microcomputer were transferred into the VAX3100 workstation computer by means of the file server. The data analysis program, PHASE_ANGLE.FOR, was developed for the analysis of the data on the VAX workstation computer.

The total resistance, running trim and sinkage of the model were obtained by analysing the experimental data in real time. These results are shown in figures 5.6 to 5.8. The motion transfer functions, encounter wave frequencies and phase angles were calculated by using the zero-crossing technique in the time domain. The selspot system gives signals which are proportional to the absolute motions at the attachment points and these can be considered to give estimates of the heave and pitch amplitudes as follows:

$$\text{Heave}=\frac{s_1+s_2}{2} \tag{5.1}$$

$$\text{Pitch}=\tan^{-1}\frac{s_2-s_1}{2x} \tag{5.2}$$

where s_1 and s_2 are the absolute motions measured forward and aft and $2x$ is the longitudinal separation of the two measurement locations.

The wave is defined by the vertical displacement of the water surface at the C.G. section. In this study, the resistance type wave probe was situated at the towing carriage and paralleled with the model at 122.5cm forward of C.G. in order to reduce the perturbations generated by the motions of model. The phase angle shift in the recorded motions is corrected for this difference in the analysis. The wave and the motions in the head sea condition may then be described in the translational coordinate system o-xyz by:

$$\zeta(x,t)=\zeta_0\cos(kx+\omega t) \quad \text{:Wave} \tag{5.3}$$

$$\xi_3(t)=|\xi_3|\cos(\omega t+\varepsilon_3) \quad \text{:Heave} \tag{5.4}$$

$$\xi_5(t)=|\xi_5|\cos(\omega t+\varepsilon_5) \quad \text{:Pitch} \tag{5.5}$$

where ω is the encounter frequency; ζ_0 is the wave amplitude; k is the wave number.

In figures 5.9 to 5.14, the test results are given as non-dimensional amplitude characteristics ($|\xi_3|/\zeta_0$ for heave, $|\xi_5|/k\zeta_0$ for pitch) and phase angles in degree related to non-dimensional wave frequency. The phase angle, ε_i, gives the phase relationship between the motion and the wave. A positive value means that the maximum positive motion occurs before the maximum wave displacement is experienced at C.G.. Negative values imply that the motion lags the wave crest.

5.4 Results and discussion

The calm water tests were carried out with the V-1 catamaran model and the results were compared with previous work (Incecik et al., 1991). For the motion responses of the V-1 catamaran in regular waves, the numerical results obtained from linear frequency domain and nonlinear time domain programs have been compared with the experimental data at different forward speeds and incident wave amplitudes.

5.4.1 Performance in calm water

The total resistance, C.G. rise and trim change of the V-1 catamaran model were measured over a speed range up to Fn=1.129 in still water condition. The results are presented in figures 5.6 to 5.8 and compared with previous experiments (Incecik et al., 1991).

In order to satisfy the required centre of gravity, the draught of V-1 model was set to a slightly different level than the model of V.I.L. catamaran. Four spray rails fitted on the V.I.L. model were also dismantled to simplify the hydrodynamic problem. Compared with the previous work, the calm water resistance curves are similar but the curves of C.G. rise and trim change are slightly different. These differences are believed to be due to the different towing system and towing point used as discussed in section 5.3.2. Moreover, the hydrodynamic lift generated by the spray rails of V.I.L. model would provide a significant effect. They produced a positive contribution to lift of V.I.L. model. Although these spray rails induced an increase in the resistance of the V.I.L. model, the wetted surface of model was reduced due to the hydrodynamic lift. This resulted in similar resistance curves of V-1 and V.I.L. models at different draught conditions. It should be noted that the width of each spray rail was 2.54 cm in the previous work.

5.4.2 Motion response in regular waves

In this study, the catamaran model was tested to investigate the large amplitude motions at three different speeds 0m/s,1m/s and 3m/s corresponding to the Froude numbers of 0.0,0.226 and 0.677. Therefore, the V-1 model was travelling in the so called "high-speed displacement hull" condition. In this study, the numerical methods did not take the effects due to trim and sinkage of the V-1 catamaran model into account to estimate the motion response in regular waves.

Due to the limitations of the measurement system and the freeboard of V-1 model, parts of the experimental program were not carried out in the highest speed of 3m/s with large amplitude wave(3cm and 4.5cm) conditions. In order to further confirm the nonlinear effects due to variable forward speeds, two incident waves of 2cm amplitude were added to the high speed motion tests as shown in figures 5.13 and 5.14.

The heave and pitch motion results of the V-1 catamaran based upon the linear frequency domain method were computed and compared with experimental data. Non-dimensional amplitudes and phase angles are plotted as a function of non-dimensional wave frequencies in figures 5.9 and 5.10 for zero forward speed, figures 5.11 and 5.12 for Fn=0.226, figures 5.13 and 5.14 for Fn=0.677.

In very long waves, both non-dimensional heave and pitch motion responses are equal to 1.0 except the experimental measurements for pitch motion at Fn=0.677. Theoretically it means that the ship follows the wave slope. The maximum heave motion amplitude is equal to the incident wave amplitude and the maximum pitch is equal to the maximum wave-slope. The heave phase angle is equal to 0°. It indicates that the maximum heave occurs in the wave crest. The pitch phase angle is equal to -90°. This indicates that the maximum positive (bow down) pitch motion occurs at one quarter of an encounter period after the wave crest has passed the C.G. of model.

In general, the magnitude of the motion amplitude at the resonant wave frequencies is overestimated by the linear frequency method and increases with the forward speed. For the zero speed case, the theoretical results correlate very well with measurements for heave and pitch motions. At the resonance point, the experimental results show that the motion response slightly decreases when the wave amplitude increases. The nonlinear effects at high speeds can be easily examined from figures 5.11 and 5.12 for Fn=0.226, figures 5.13 and 5.14 for Fn=0.677. It can be confirmed by these test data that the nonlinear effects are more significant when the forward speed and wave amplitude increase. The peak values of heave and pitch motions measured around the resonance are smaller than those obtained from the small amplitude motion predictions.

Time histories from towing tests and numerical simulations with three forward speeds are presented in figures 5.15 to 5.17. ξ_{3m} and ξ_{5m} represent the sinkage and trim values which come from the calm water towing test as shown in figures 5.7 and 5.8.

Comparisons illustrate that generally the heave and pitch response values are better predicted by the nonlinear time domain simulation than by the linear method. For the zero speed case, the phase predictions obtained from the linear and nonlinear methods in heave motion are similar as shown in figure 5.15. Although the time domain technique can provide good predictions for the large amplitude motions of the V-1 catamaran, there still exist some nonlinearities which can not be well predicted by the

technique presented here. Figure 5.15 shows that the heave traces of experimental measurements have nonlinear characteristics when the large incident wave amplitudes $\zeta_0 = 4.5cm$. However, the amplitude and phase angle of the linear and nonlinear pitch motion predictions are in good agreement with the measurements. Figure 5.16 illustrates that the predictions of pitch motion are better than the heave motion predictions at Fn=0.226, $\omega_0 = 6.5rad/\sec$ and $\zeta_0 = 3.0cm$ when the nonlinear method is used. There are some phase shifts observed between theoretical and experimental time history curves of heave displacements. At Froude number Fn=0.677, both linear and nonlinear simulations have overpredicted the amplitudes of heave and pitch motions as shown in figure 5.17. However, the nonlinear time domain technique still provides better predictions compared with the experimental data as shown in the time history curves. In addition, the positive and negative amplitudes are of different magnitudes as observed in the experimental measurements as well as in the nonlinear time domain simulations. These phenomena can not be predicted by the linear frequency domain method.

Figures 5.18 to 5.23 show the experimental and theoretical motion response values of the V-1 catamaran for three different wave amplitudes at zero forward speed. The heave and pitch motion response predictions of the V-1 catamaran are similar as results obtained from the linear and nonlinear simulations. These predictions also correlated well with experimental data in this test condition. Although the nonlinear effects are not appreciable even in the large amplitude motions of the model, the time domain results are closer to the experimental measurements than the linear frequency domain predictions as shown in figures 5.22 and 5.23. At Froude number Fn=0.226, calculations obtained from both linear and nonlinear methods overpredicted the amplitudes of heave motions around the resonance frequencies. However, the results obtained from the nonlinear program show a better agreement with the experimental measurements than the linear predictions, especially in the high frequency region, as shown in figures 5.24 to 5.29. In the pitch motions, experimental measurements are higher than the numerical predictions obtained from the linear and nonlinear techniques when the non-dimensional wave frequencies are lower than $\omega_0\sqrt{L/g} = 2.5$. There are some discrepancies observed in the pitch motion predictions at $\omega_0\sqrt{L/g} = 2.257$. The experimental measurements and nonlinear predictions show an opposite trend when the incident wave amplitude increases. In figures 5.30 to 5.35, due to limitations of the measurement system, there are not enough experimental data at the large incident wave amplitude condition around the resonance frequencies to validate the theoretical investigations. It still can be concluded that the nonlinear time domain technique provides better predictions for the heave and pitch motion responses of V-1 catamaran

than the linear frequency domain method at Froude number Fn=0.677.

Some nonlinear characteristics of the heave and pitch motions of V-1 catamaran with various incident wave amplitudes are presented in figures 5.36 to 5.41. Comparisons between results obtained from the linear method, nonlinear time domain simulations and model tests are presented. At zero speed and wave frequency $\omega_0 = 4.0 rad/\sec$, the heave and pitch motion values show a linear behaviour even at large wave amplitude. In the high frequency case, figure 5.37 shows that the nonlinear method predicts nonlinearities better in pitch motions than in heave motions. For the forward speed cases, the nonlinear predictions generally give a good agreement with experimental data when the amplitude of wave is large. Figure 5.41 shows that the linear theory can predict better motion amplitude values than the nonlinear technique for various wave amplitudes at Fn=0.677, $\omega_0 = 5.5 rad/\sec$. However, the results obtained from the time domain simulation show similar trends to the experimental measurements as far as the nonlinear characteristics of large amplitude displacements are concerned.

In the case of a catamaran, the slamming usually occurs on the underside of the deck between the two hulls. The impact can cause not only structural damage but also damage to the on board instrumentation due to vibrations. A set of consecutive photographs of the V-1 model motion in regular wave test is presented in figures 5.42 to 5.51 to illustrate the physical phenomena of nonlinear motions. Figure 5.42 shows that the V-1 catamaran model is towed by the towing carriage with a constant forward speed (U=3m/s) into the regular waves ($\zeta_0 = 3.0cm, \omega_0 = 4.75 rad/\sec$). The growth of bow impact waves in time can be clearly observed through figures 5.43 to 5.48. The inner impact flow which is located around 70cm forward of C.G. is far severer than the outside impact spray as shown in figures 5.46 to 5.48. Furthermore, the inner impact waves will shift afterward and the interior flow between twin hulls will be significantly raised after the impact as observed in figures 5.49 to 5.51. Figures 5.52 and 5.53 show the nonlinear behaviour of the model in the head sea condition at Fn=0.226, $\zeta_0 = 4.5cm$ and $\omega_0 = 5.0 rad/\sec$. The exit of bow keel of the V-1 catamaran from the water surface can be easily observed from figure 5.52. The inner flow slamming is found at the locations of 70 to 122.5 cm forward of C.G. as shown in figure 5.53. Some forward speed effects on the impact phenomena of the V-1 catamaran can be noticed when figures 5.47 and 5.53 are compared. As the forward speed increases, the shape of outside impact spray will vary from quadrilateral to triangularity and the location of cross-structure slamming will shift afterward.

5.5 Conclusions

An experimental setup has been designed and tested to investigate the nonlinear effects of large amplitude motions of catamarans in waves. The validation of mathematical analyses has been carried out by comparing numerical results obtained from the linear frequency domain method and nonlinear time domain technique with the experimental data of the V-1 catamaran. Some conclusions may be drawn as follows:

1. The new experimental setup is a very suitable system to investigate the motion responses of fast crafts in waves.

2. The comparisons do reveal some characteristics about the performance of the linear and nonlinear techniques. In general, heave and pitch amplitudes are overpredicted by both numerical tools around the resonance frequencies. However, the nonlinear approach provides better predictions compared with experimental measurements than the pure linear theory. The different magnitudes of positive and negative amplitudes of large amplitude motions can be predicted by the nonlinear technique in the time domain.

3. Through the nonlinear theoretical and experimental investigations of the V-1 catamaran model for various forward speeds and wave amplitudes, it can be confirmed that the nonlinear effects become significant when the model speed and wave amplitudes increase. The peak values of large amplitude motions in heave and pitch modes measured around the resonance are smaller than those obtained from the small amplitude motion predictions.

Based on the experimental and comparative investigations, not only the underwater geometry but also form characteristics above the waterline of ship should be incorporated into the mathematical simulations for predicting the large amplitude motions of catamarans in waves. Through the experimental observations, the phenomena of cross-structure slamming of catamarans will be significantly effected by the forward speeds and incident wave amplitudes.

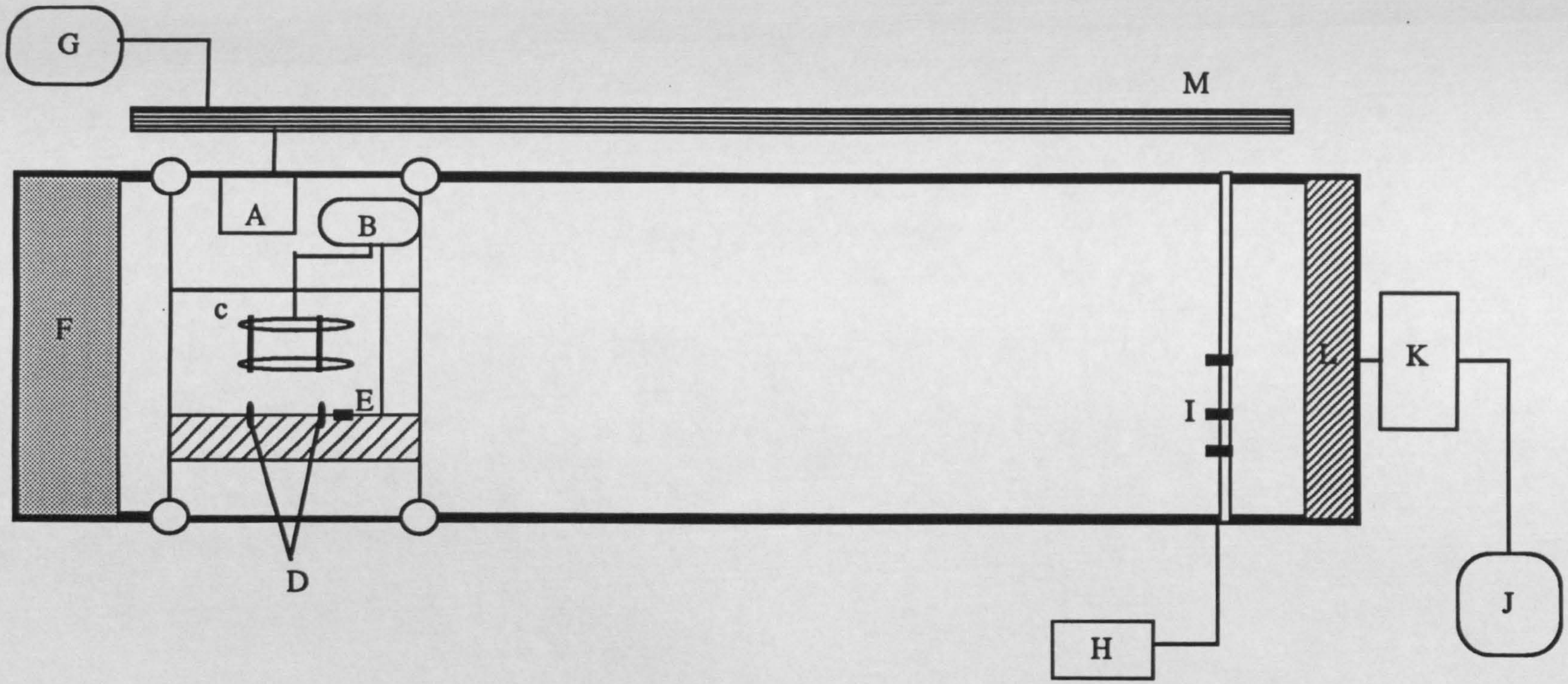

A: Control desk of Towing Carriage

B: Data-acquisition system

C: Catamaran model

D: Selspot system

E,I: Resistance type wave probes

F: Wave absorbing beach

G: Power control box

H: Chart-recorder

J: Dell-200 microcomputer(Digital-to-Analog converter)

K: Hydraulic unit

L: Wave maker

M: Current conductor rails

Figure 5.1: General Arrangement of Towing Tank

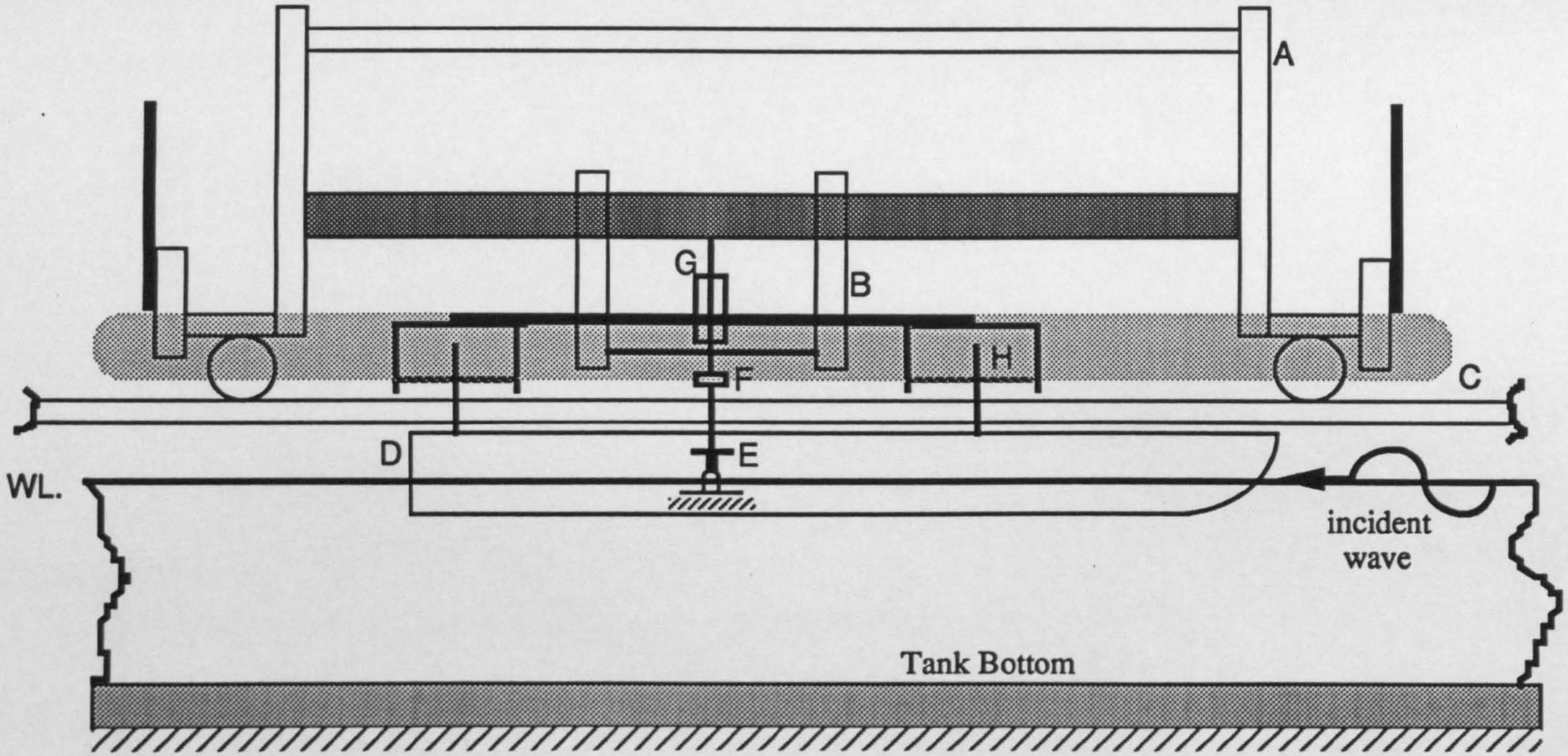

A: Main carriage

B: Measurement rig

C: Rail track

D: Catamaran model

E: Free pitch pivot

F: Force transducer

G: Towing post frame

H: Yaw restraint rod

Figure 5.2: Motion response measurement system on the Towing Carriage

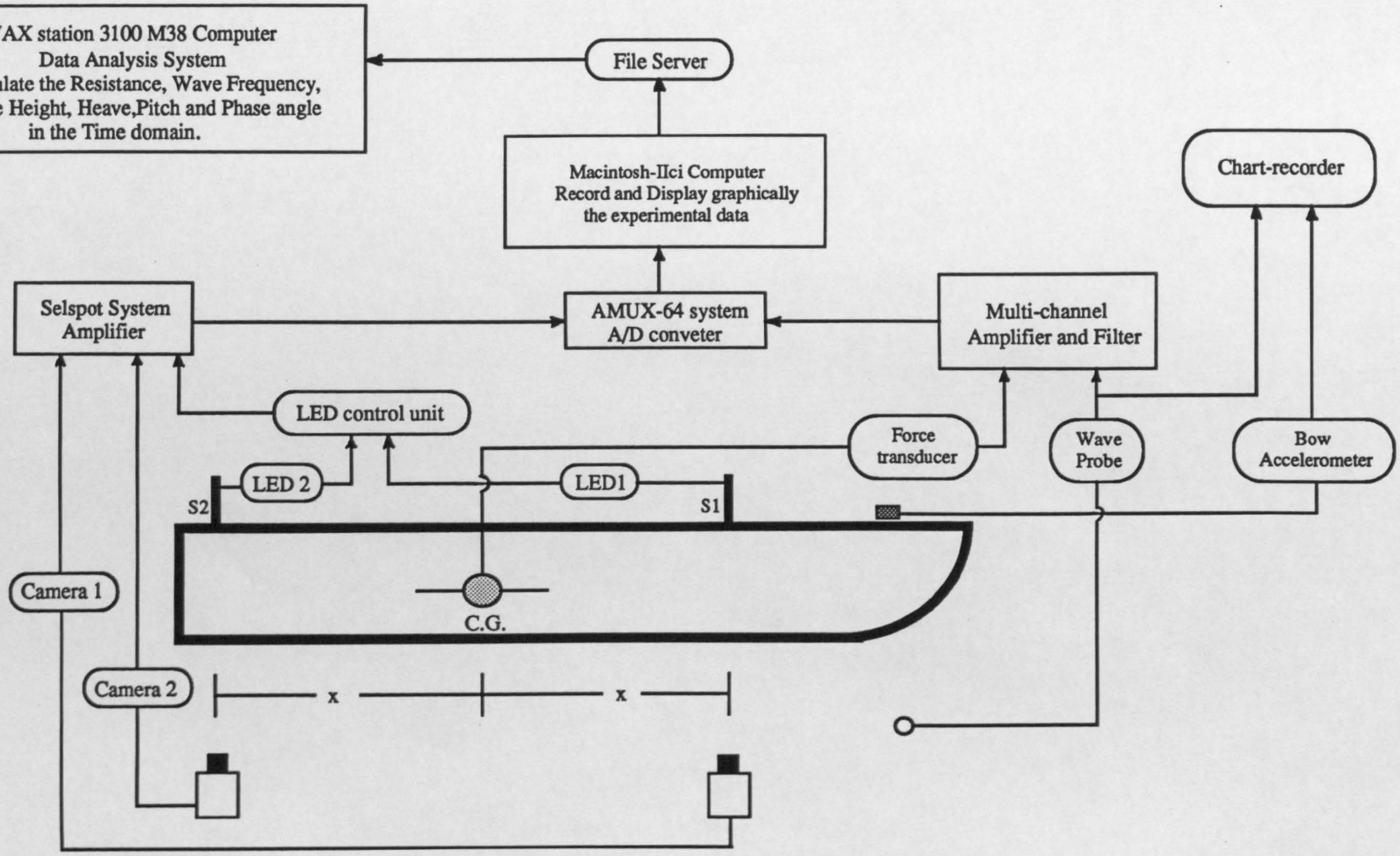

Figure 5.3: Block Diagram of the Data-acquisition System Setup

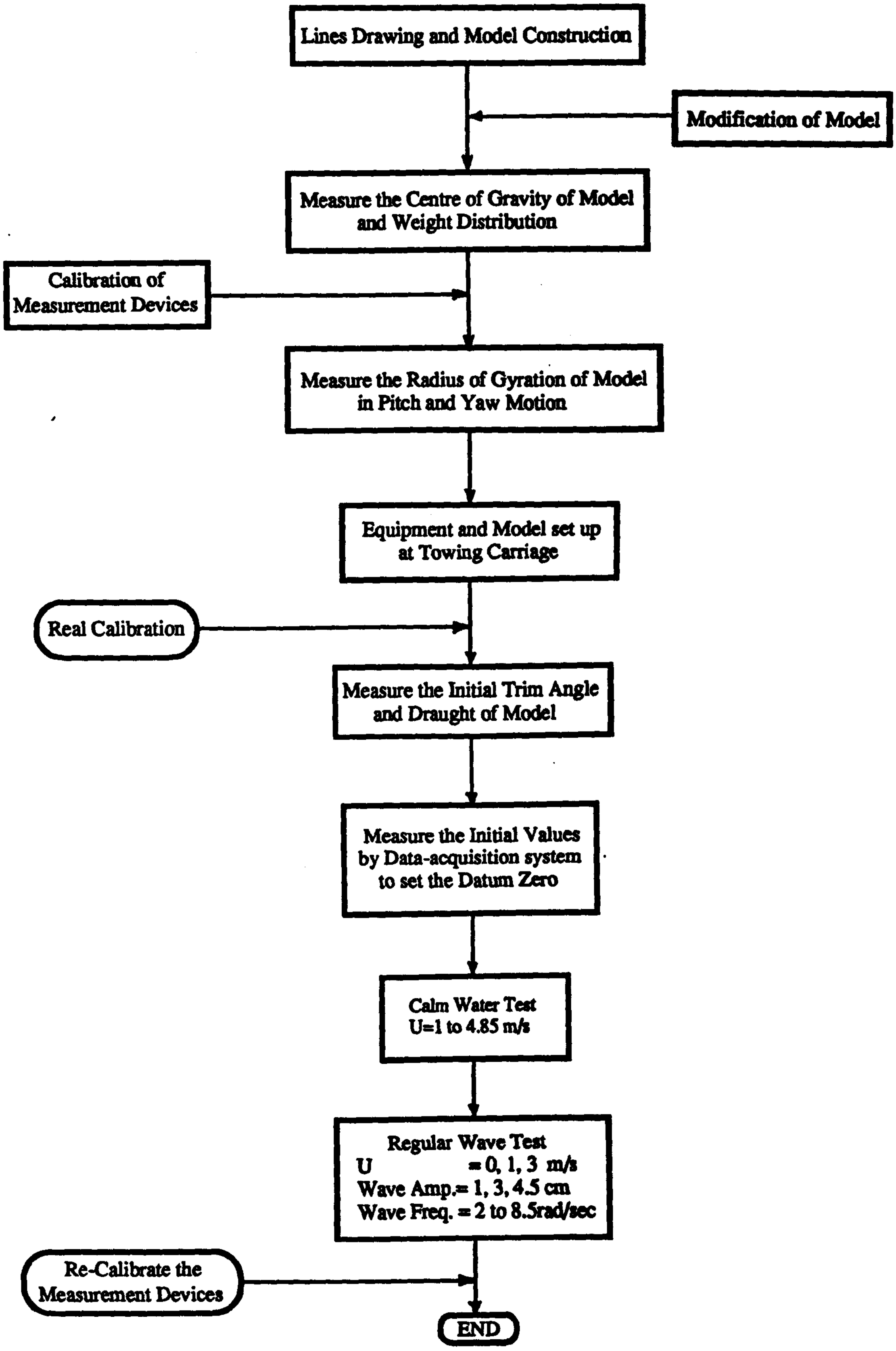

Figure 5.4: The Flowchart of Experiment

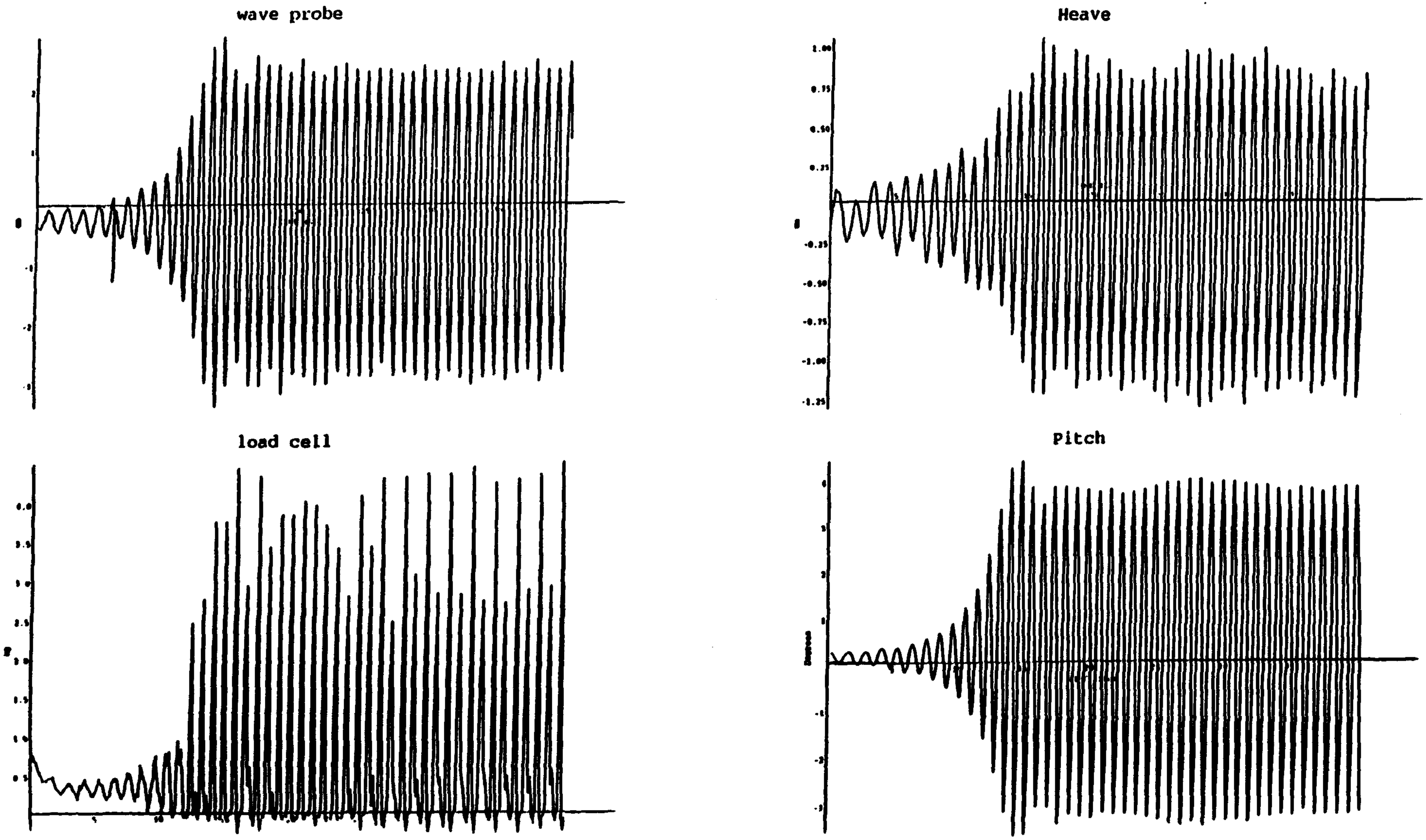

Figure 5.5 : The Sample Records of the Incident Wave and Motion Response Traces (Fn=0.226, $\zeta_a = 3.0cm$, $\omega_e = 5.0rad/sec$)

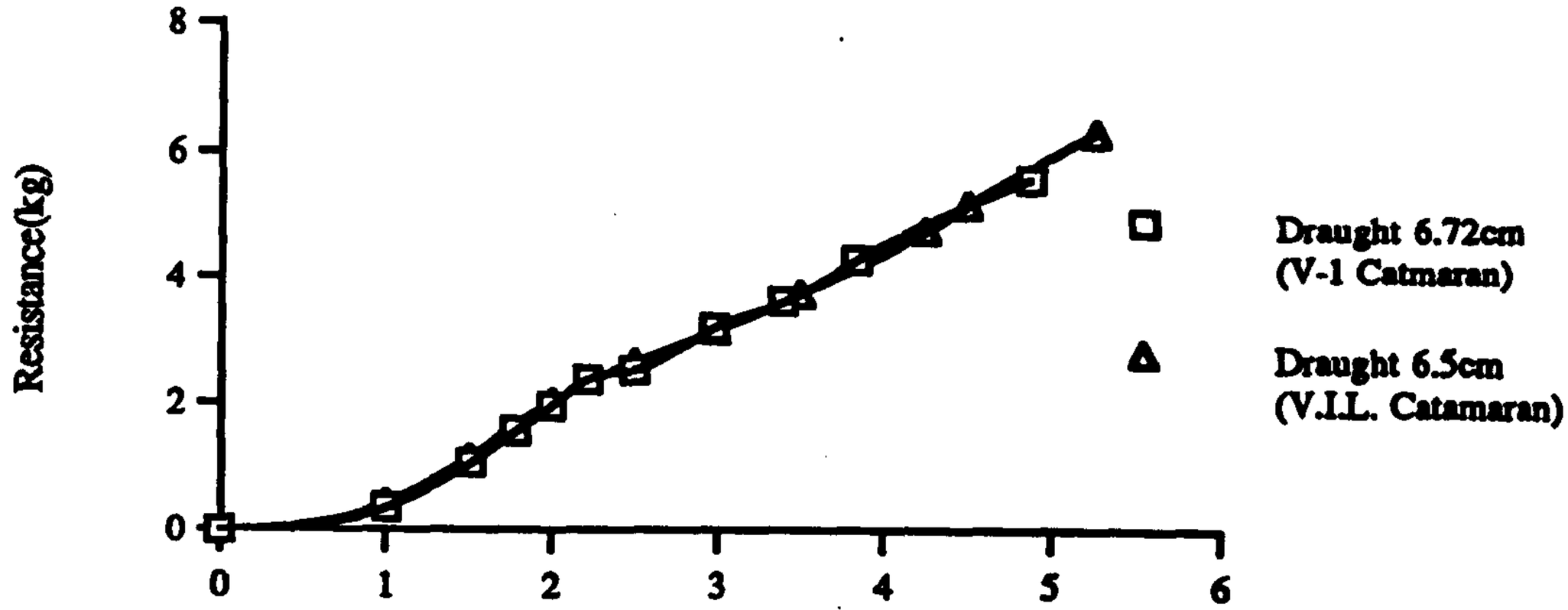

Figure 5.6: Resistance Measurements of the V-1 Catamaran

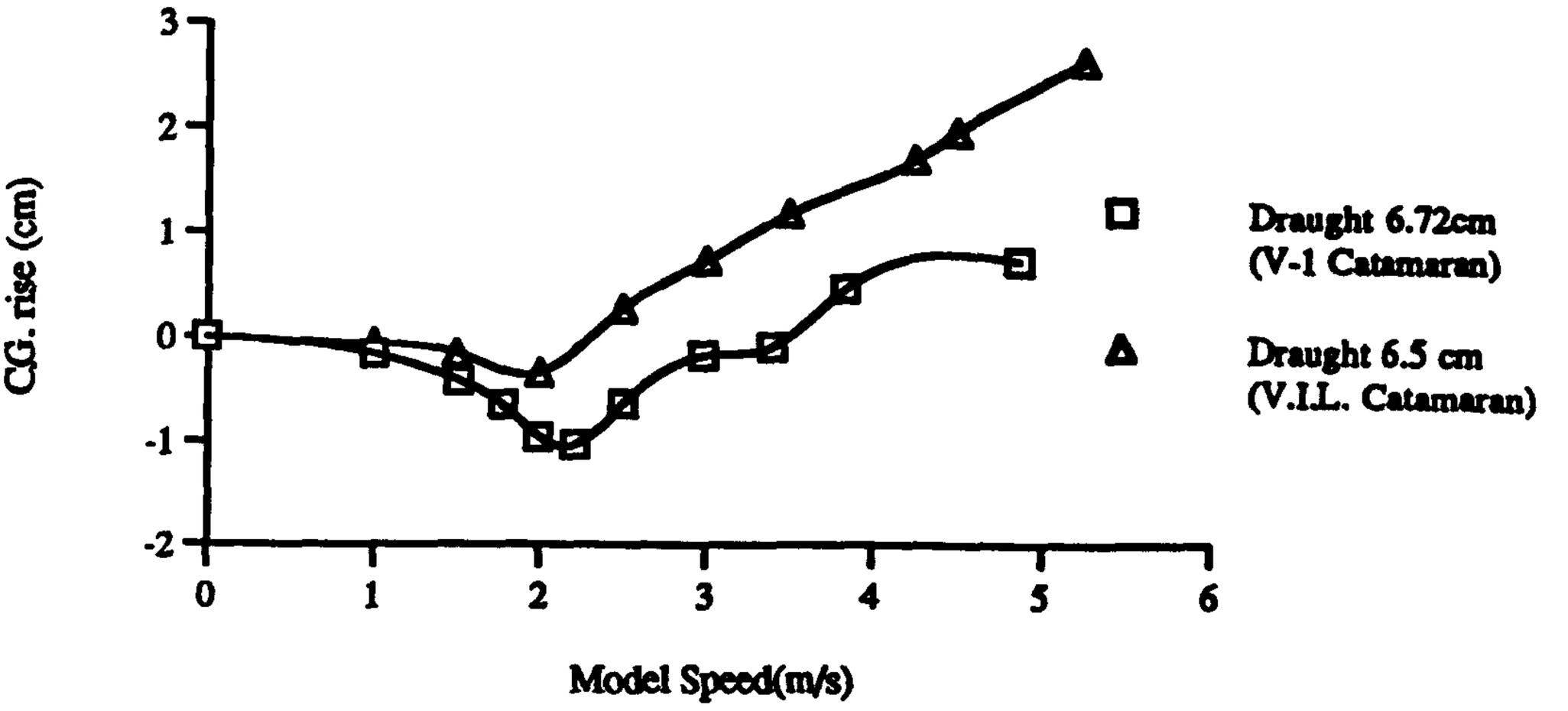

Figure 5.7: CG. rise Measurements of the V-1 Catamaran

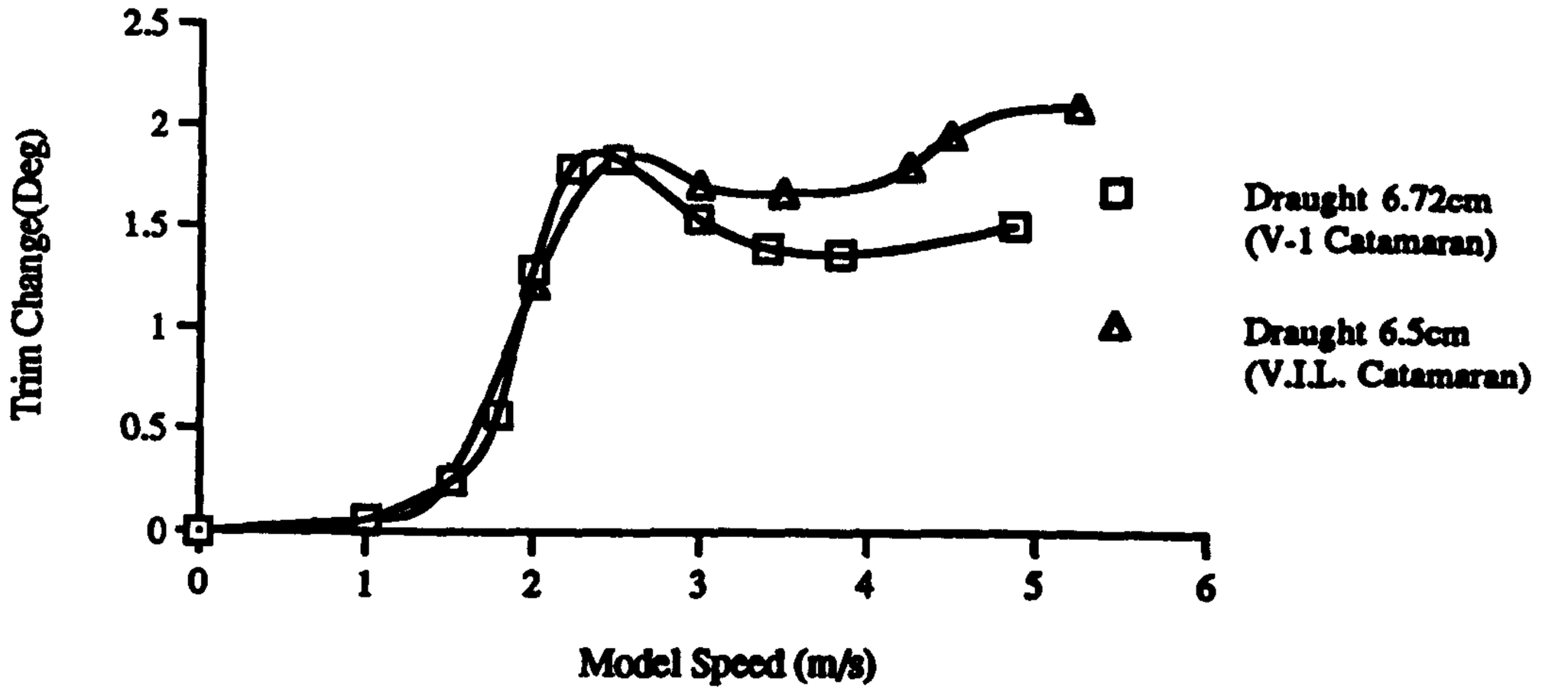

Figure 5.8: Trim Change Measurements of the V-1 Catamaran

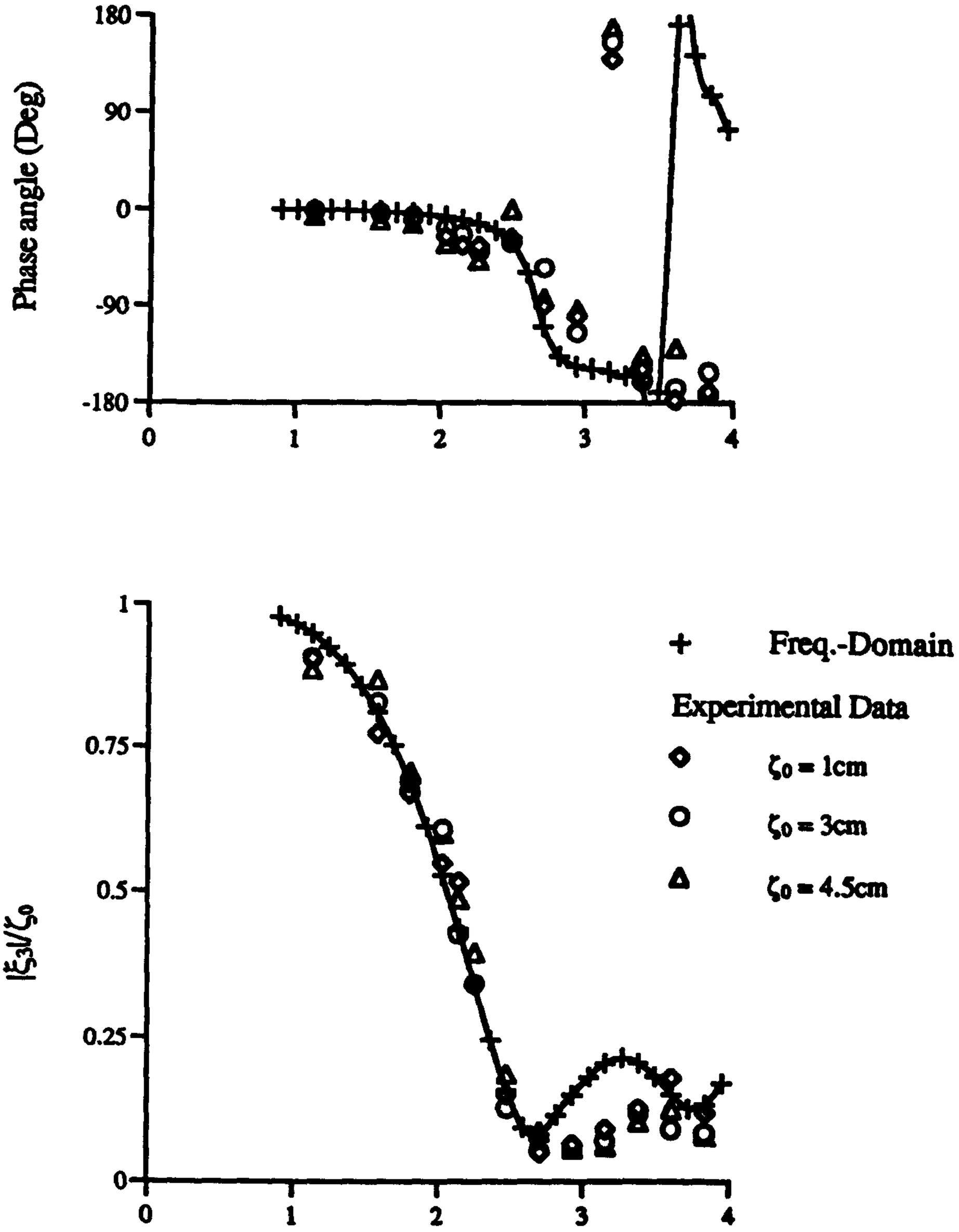

Figure 5.9: Experimental and Linear Theoretical Heave Motion Response of the V-1 Catamaran at F_n=0.0

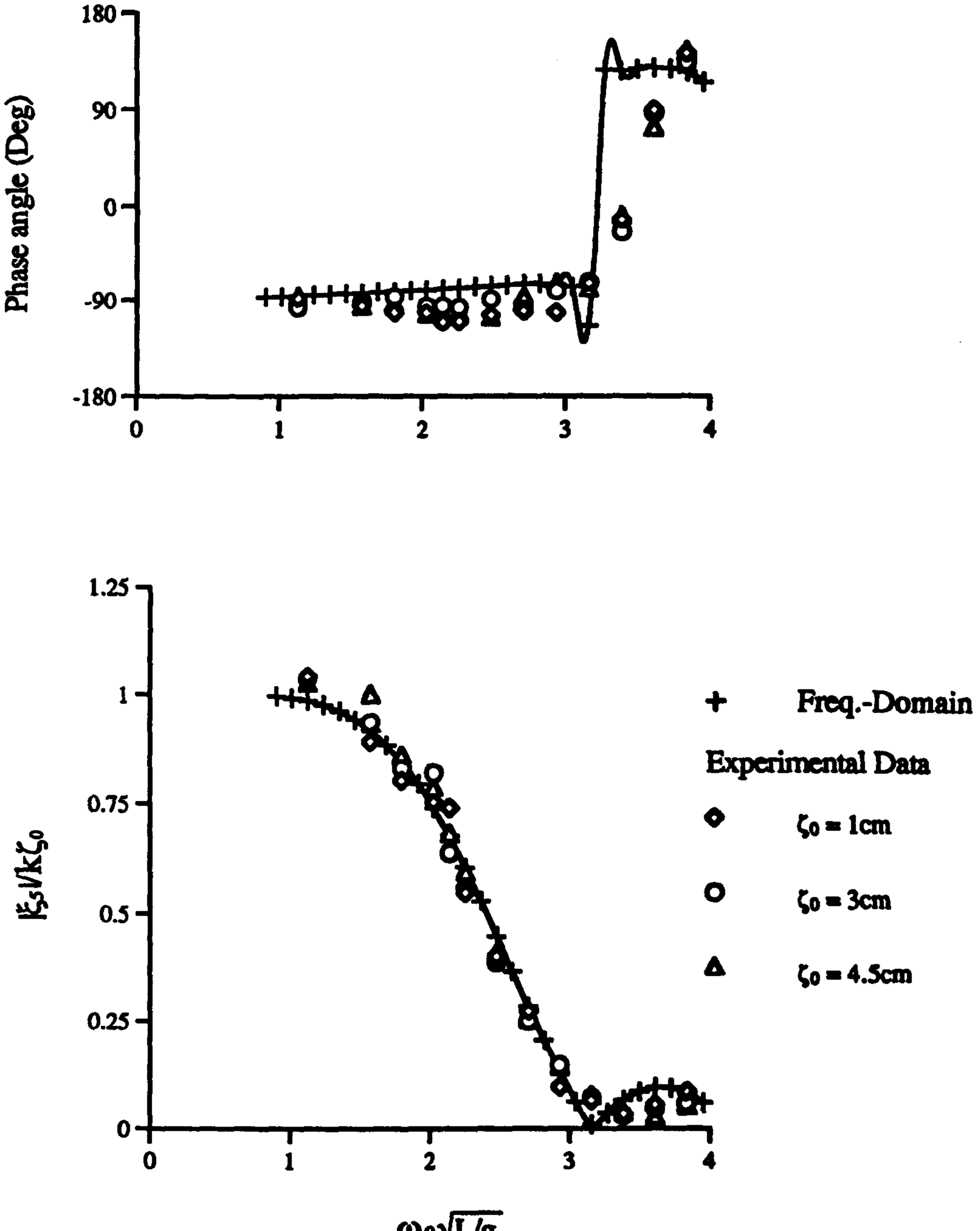

Figure 5.10: Experimental and Linear Theoretical Pitch Motion Response of the V-1 Catamaran at F_n=0.0

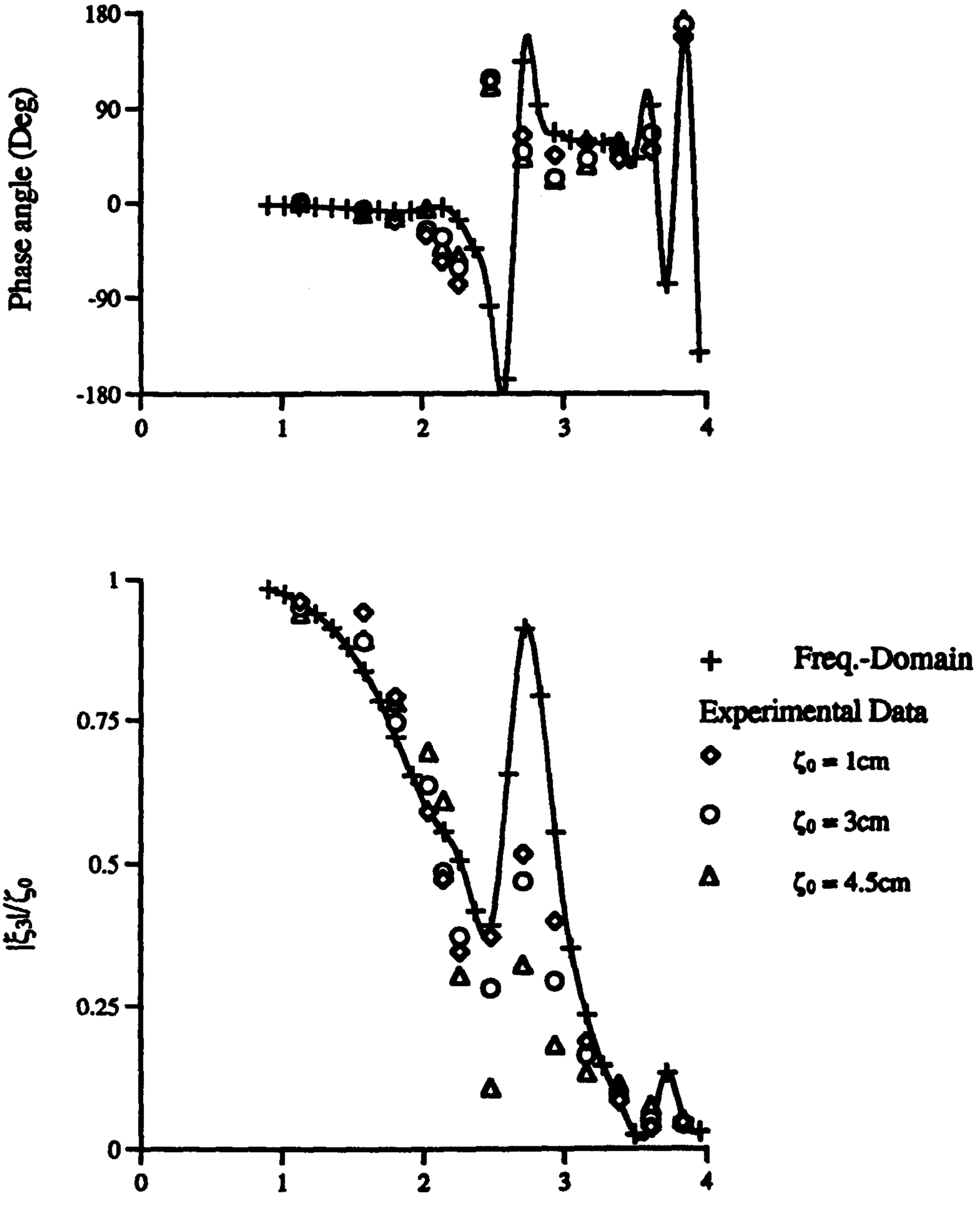

Figure 5.11: Experimental and Linear Theoretical Heave Motion Response of the V-1 Catamaran at Fn=0.226

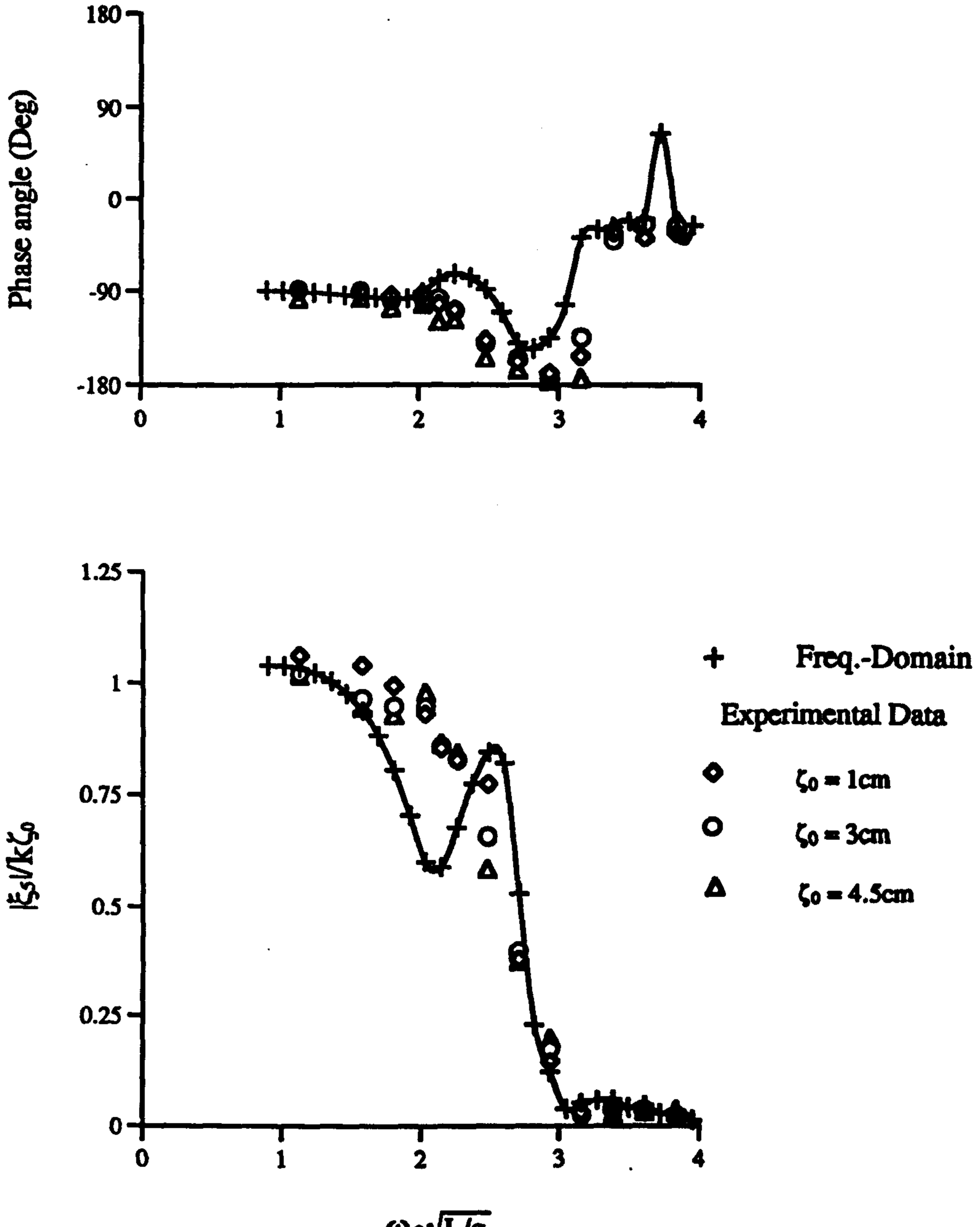

Figure 5.12: Experimental and Linear Theoretical Pitch Motion Response of V-1 Catamaran at Fn=0.226

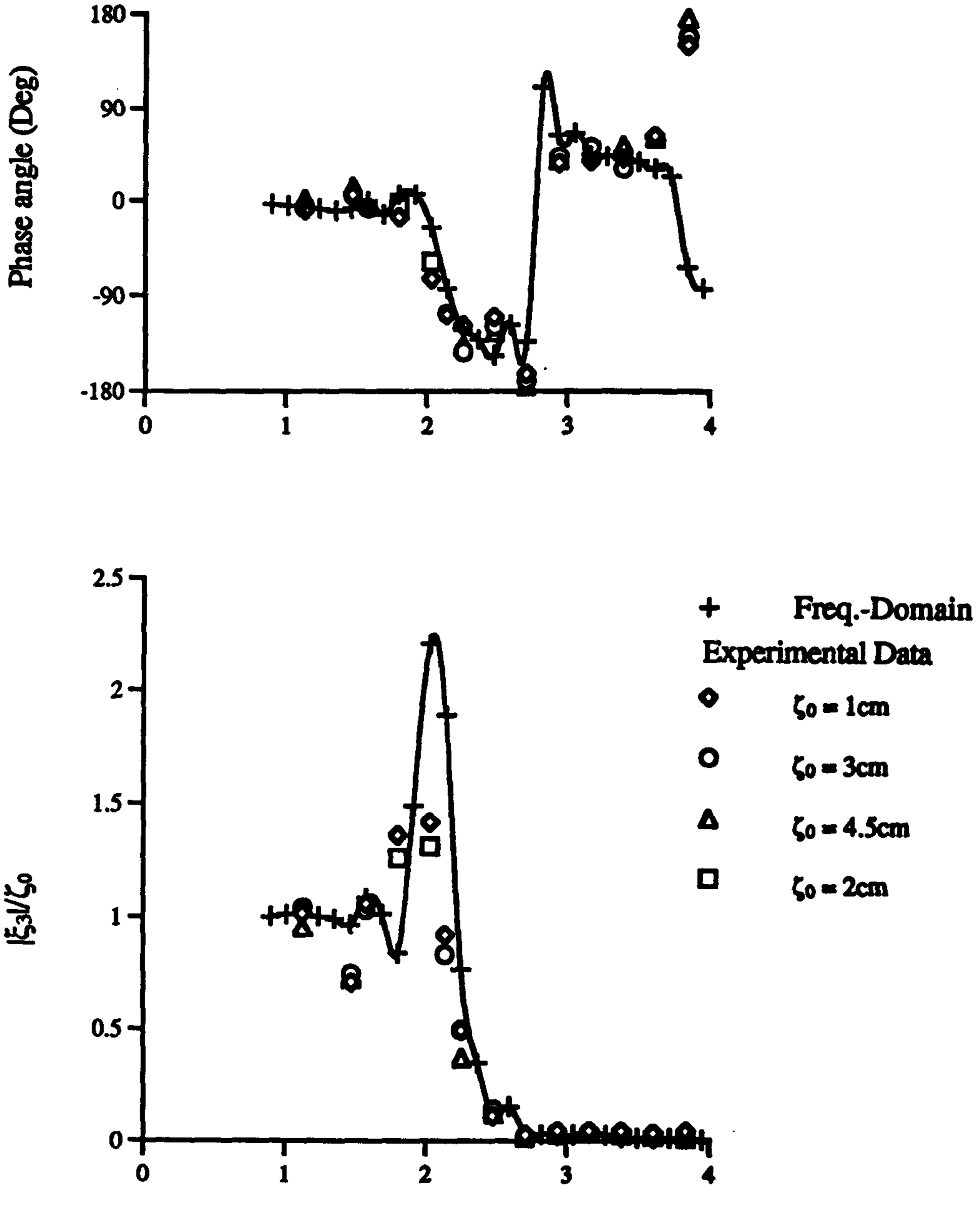

Figure 5.13: Experimental and Linear Theoretical Heave Motion Response of the V-1 Catamaran at F_n=0.677

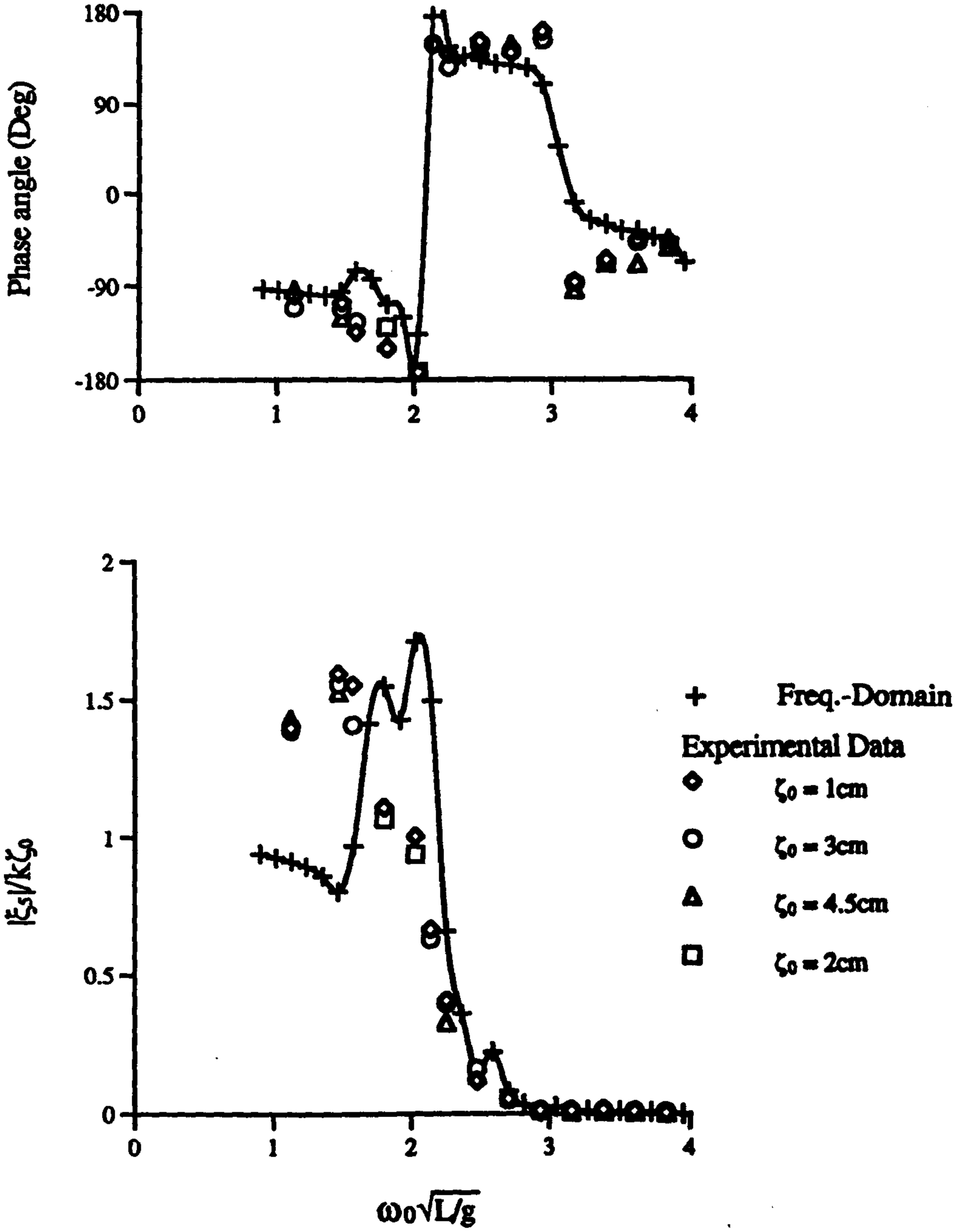

Figure 5.14: Experimental and Linear Theoretical Pitch Motion Response of the V-1 Catamaran at F_n=0.677

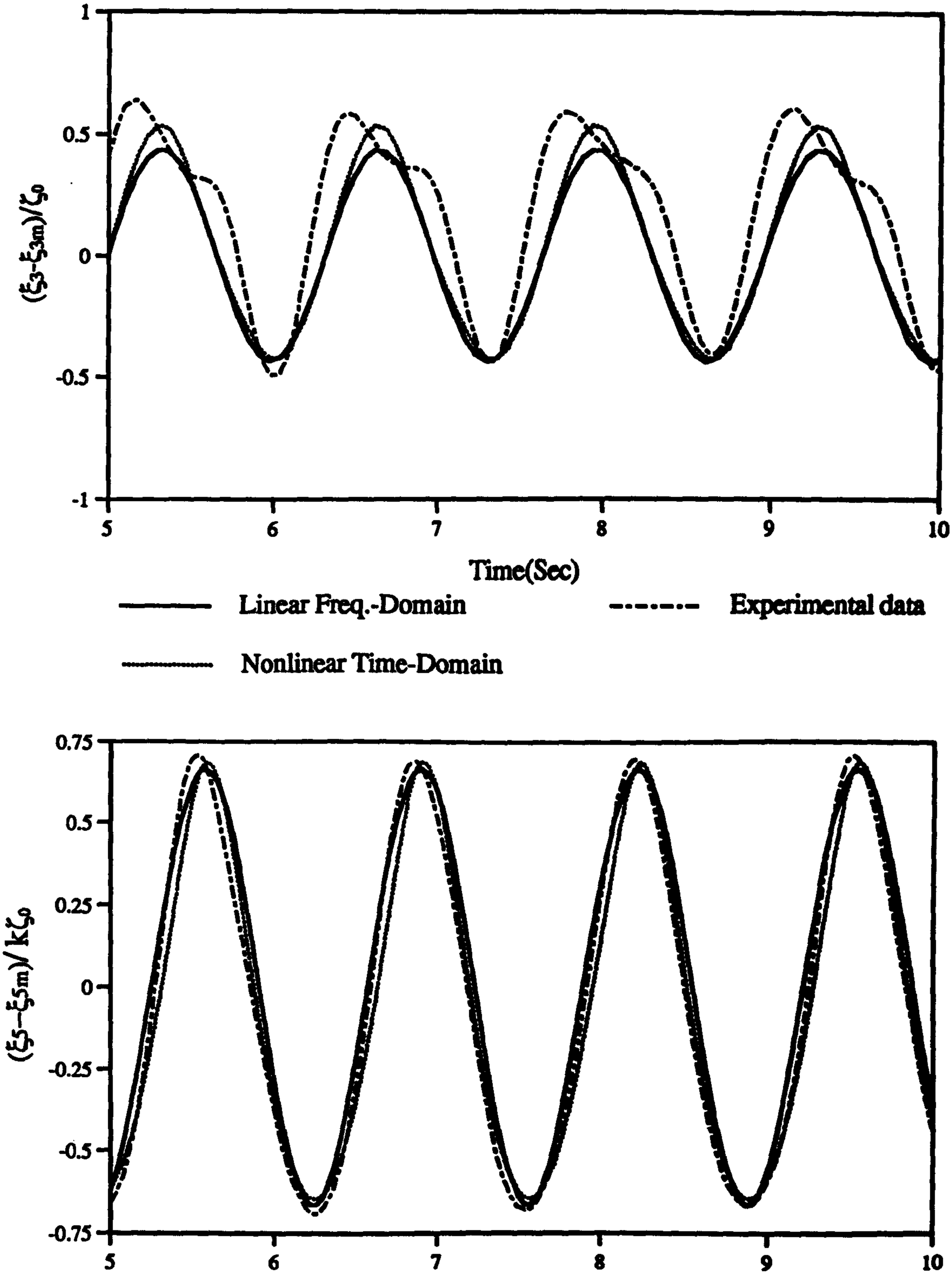

Figure 5.15 : Experimental and Theoretical Time Domain Histories for the Heave and Pitch Motions of V-1 Catamaran.
(Fn=0.00,ω_0=4.75 rad/sec,ζ_0=4.5cm)

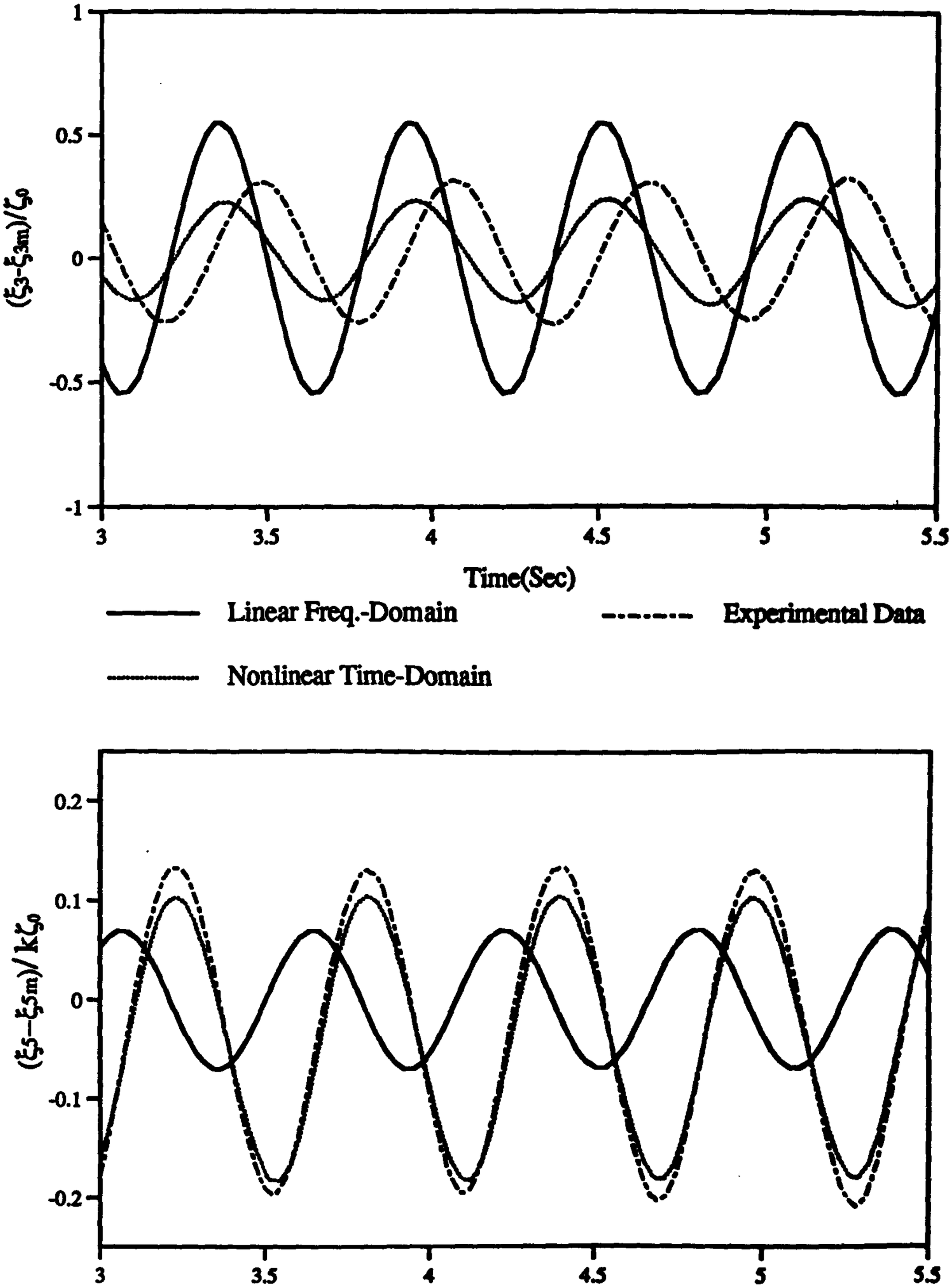

Figure 5.16 : Experimental and Theoretical Time Domain Histories for the Heave and Pitch Motions of V-1 Catamaran.
(Fn=0.226,ω_0=6.5 rad/sec,ζ_0=3.0cm)

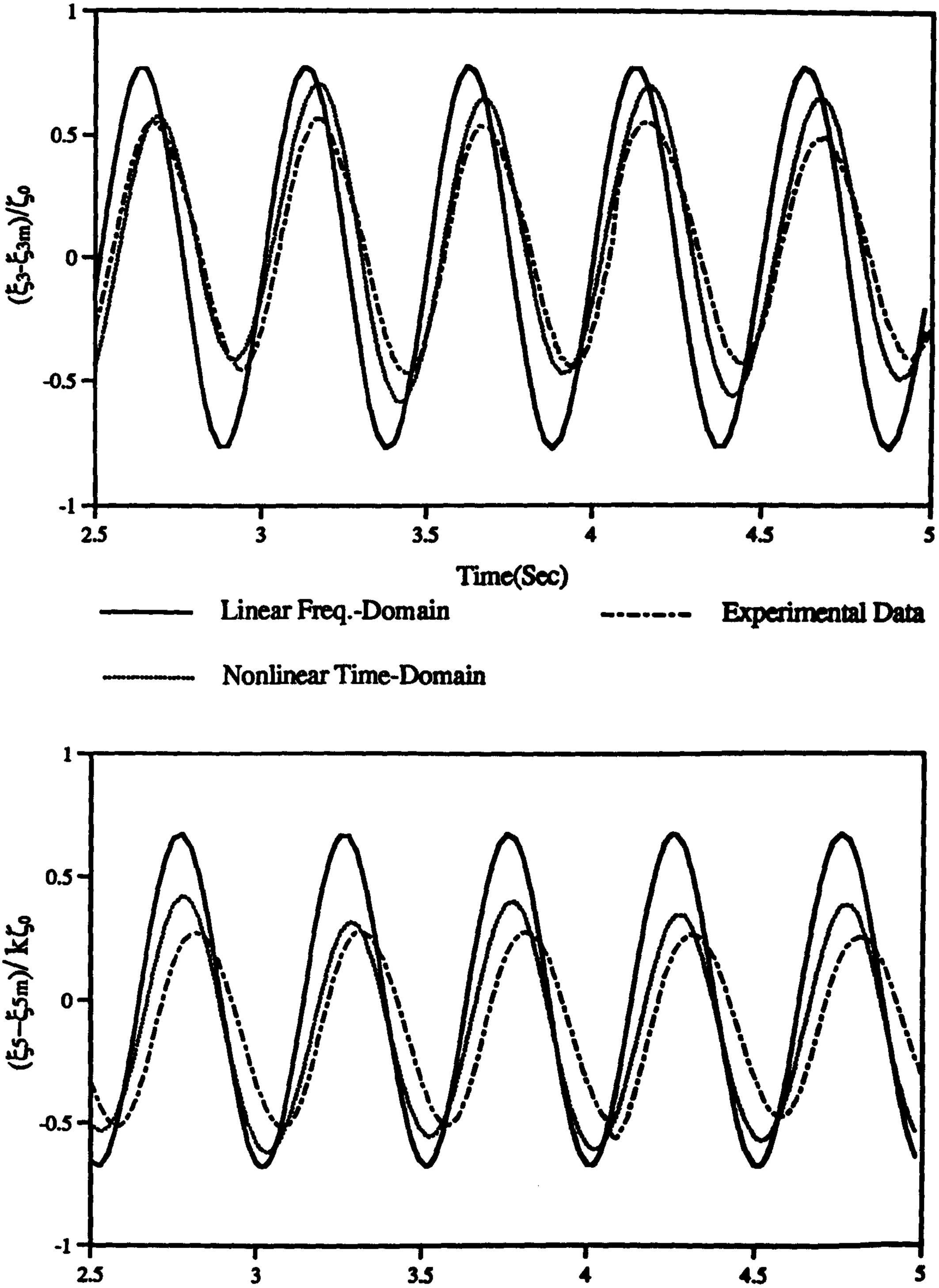

Figure 5.17 : Experimental and Theoretical Time Domain Histories for the Heave and Pitch Motions of V-1 Catamaran.
(Fn=0.677,ω_0=5.0 rad/sec,ζ_0=3.0cm)

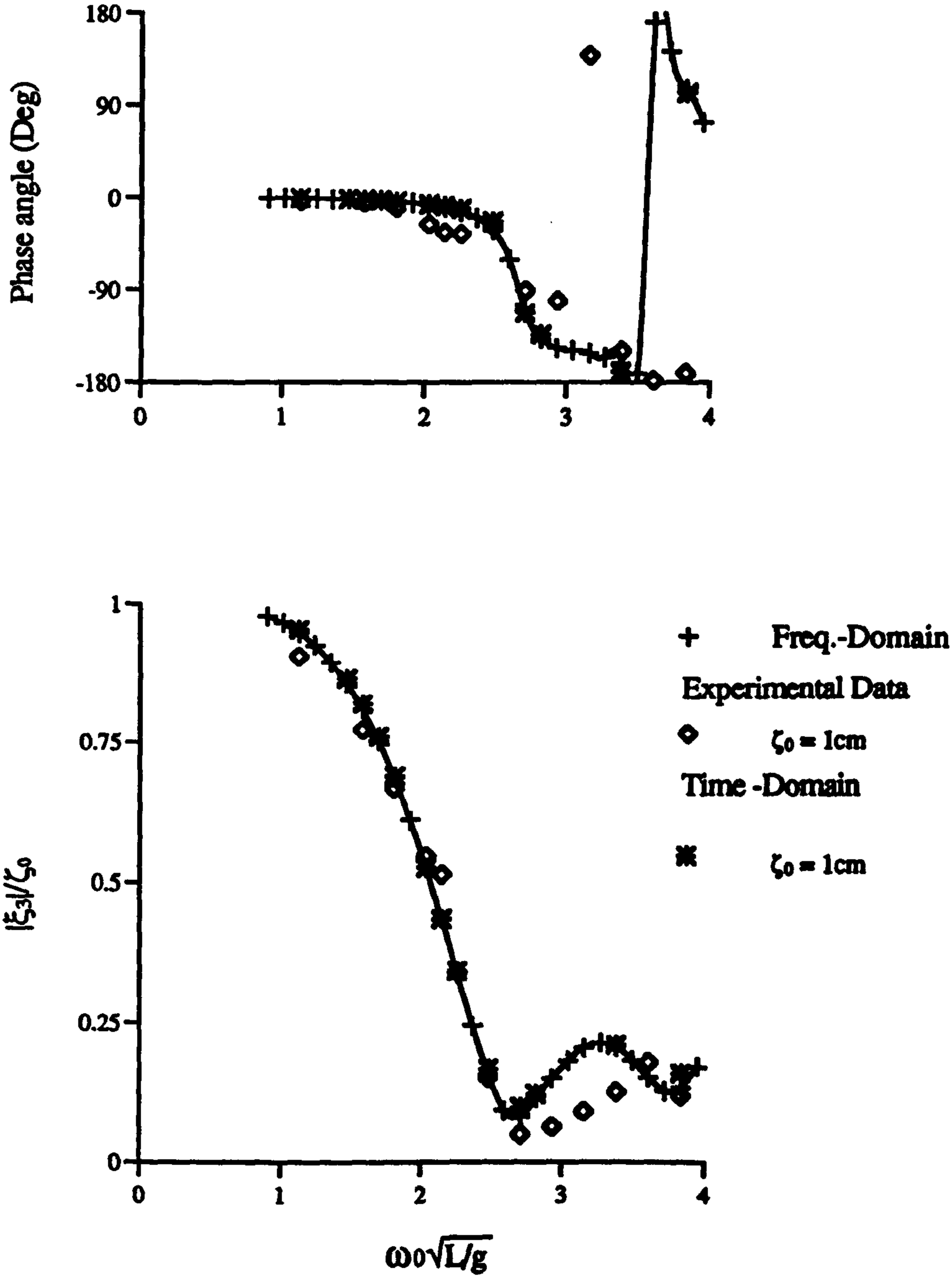

Figure 5.18: Experimental and Theoretical Heave Motion Response of the V-1 Catamaran at Fn=0.0(ζ_0 = 1cm)

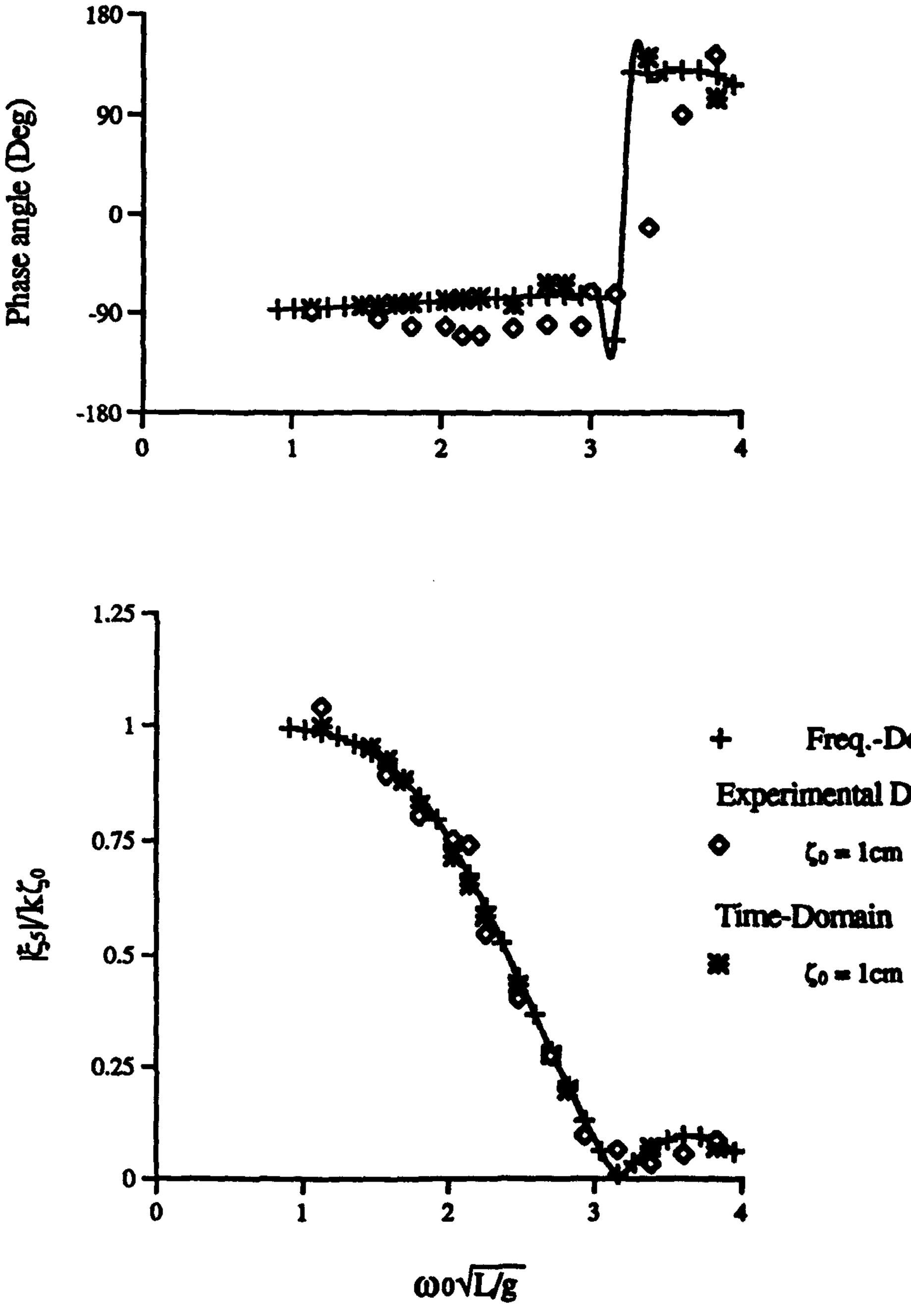

Figure 5.19 : Experimental and Theoretical Pitch Motion Response of the V-1 Catamaran at F_n=0.0 (ζ_0 = 1cm)

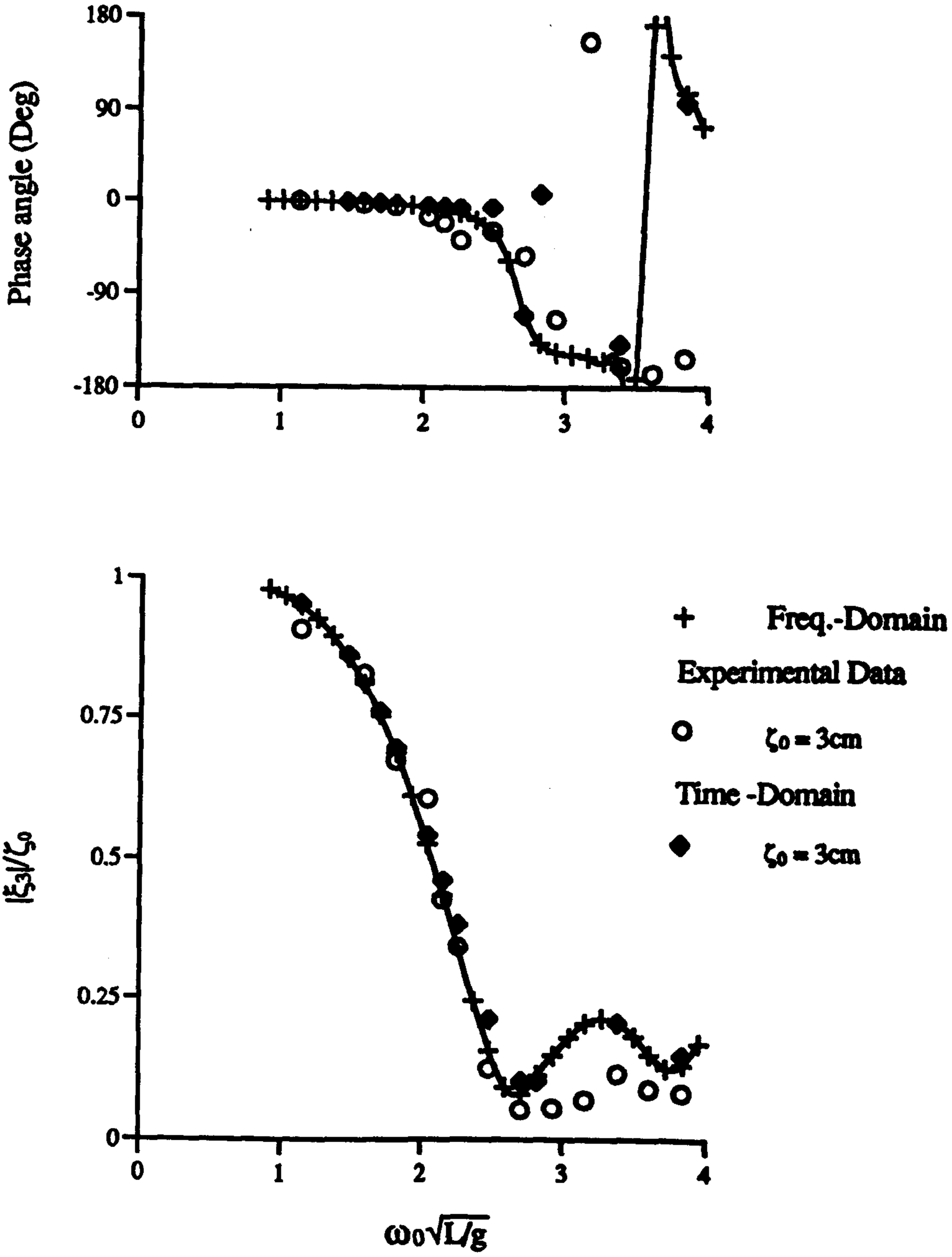

Figure 5.20: Experimental and Theoretical Heave Motion Response of the V-1 Catamaran at Fn=0.0 (ζ_0 = 3cm)

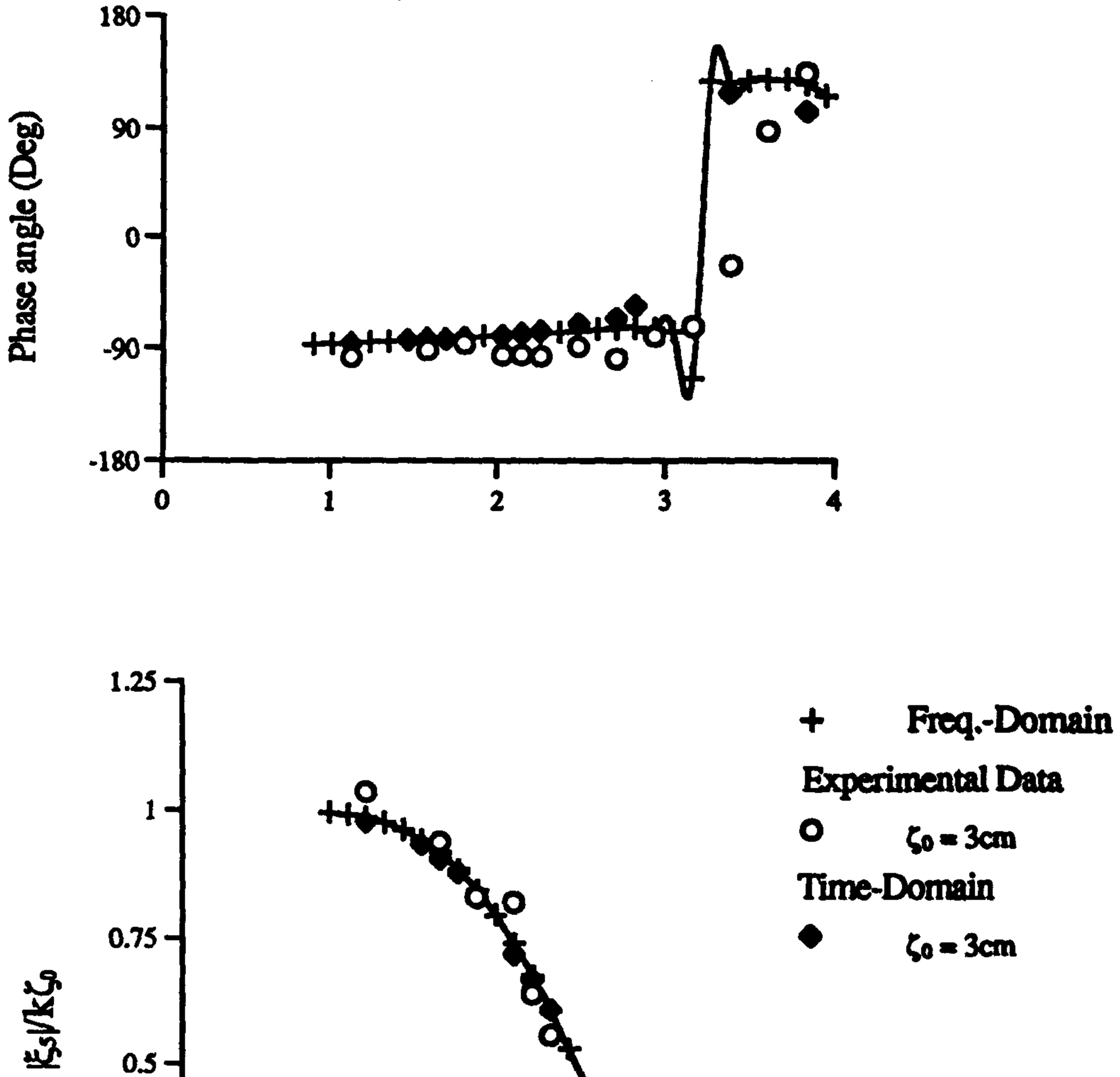

Figure 5.21: Experimental and Theoretical Pitch Motion Response of the V-1 Catamaran at F_n=0.0 (ζ_0 = 3cm)

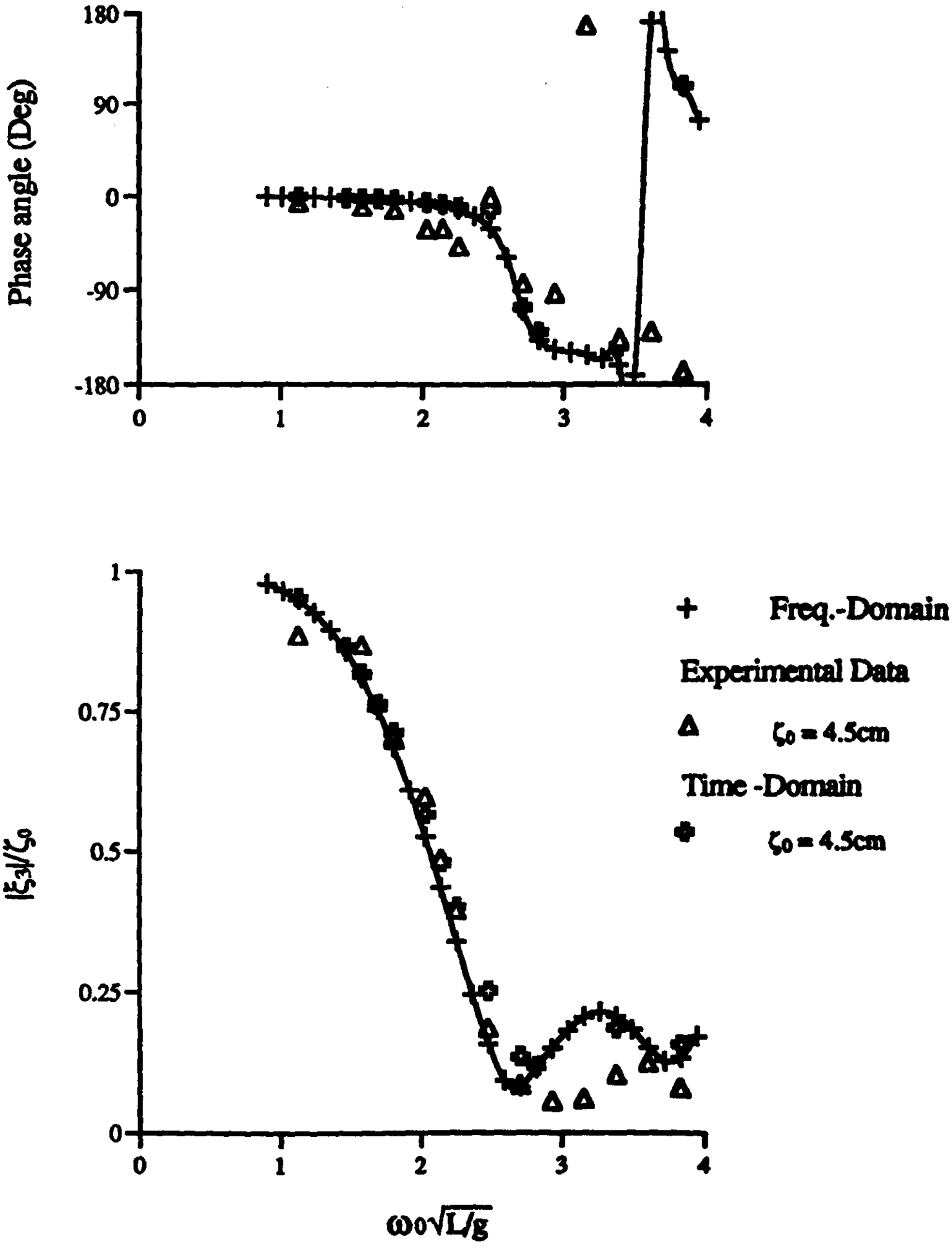

Figure 5.22: Experimental and Theoretical Heave Motion Response of V-1 Catamaran at Fn=0.0(ζ_0 = 4.5cm)

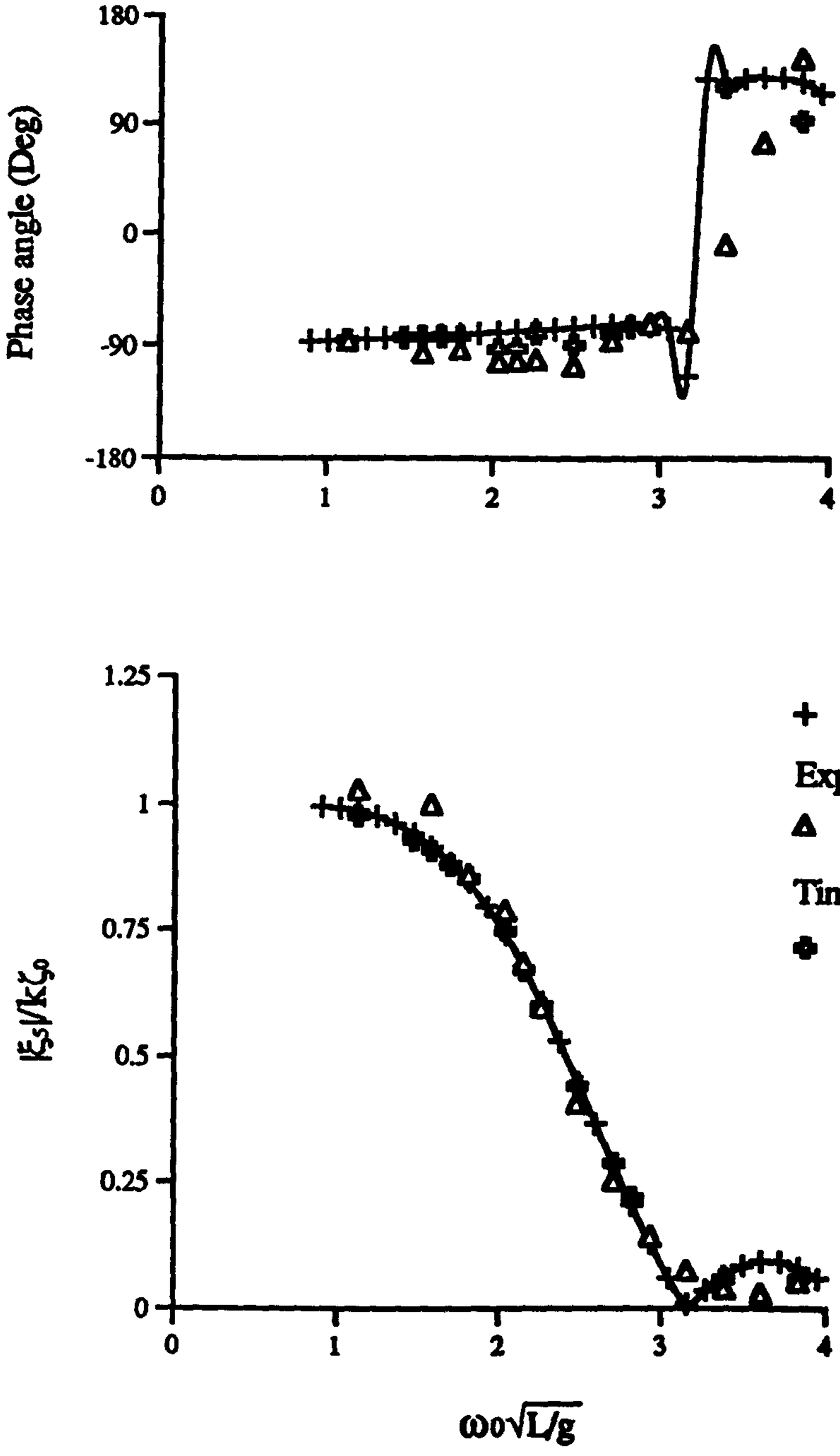

Figure 5.23: Experimental and Theoretical Pitch Motion Response of the V-1 Catamaran at F_n=0.0 (ζ_0 = 4.5cm)

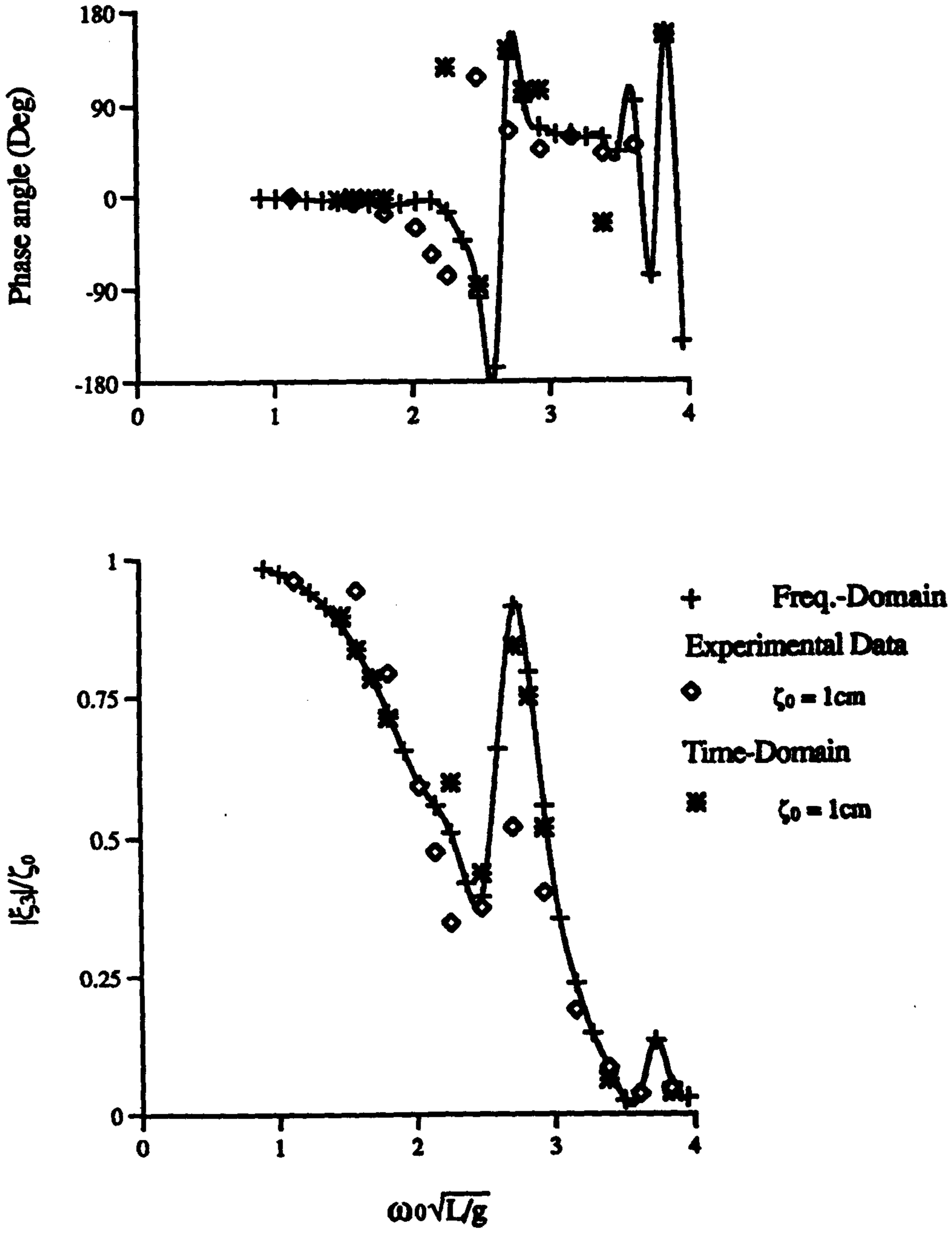

Figure 5.24 : Experimental and Theoretical Heave Motion Response of the V-1 Catamaran at Fn=0.226(ζ_0 = 1cm)

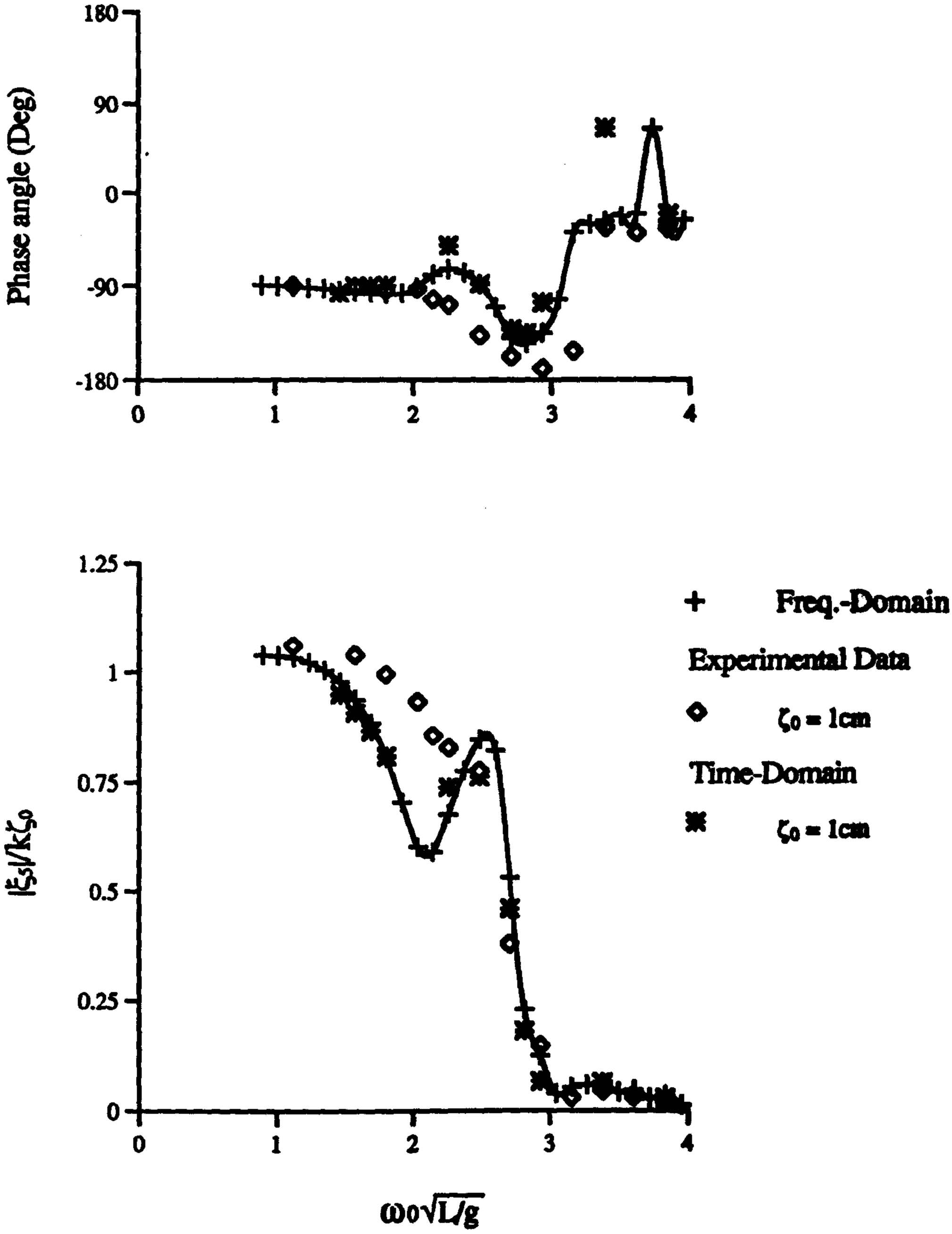

Figure 5.25 : Experimental and Theoretical Pitch Motion Response of the V-1 Catamaran at Fn=0.226(ζ_0 = 1cm)

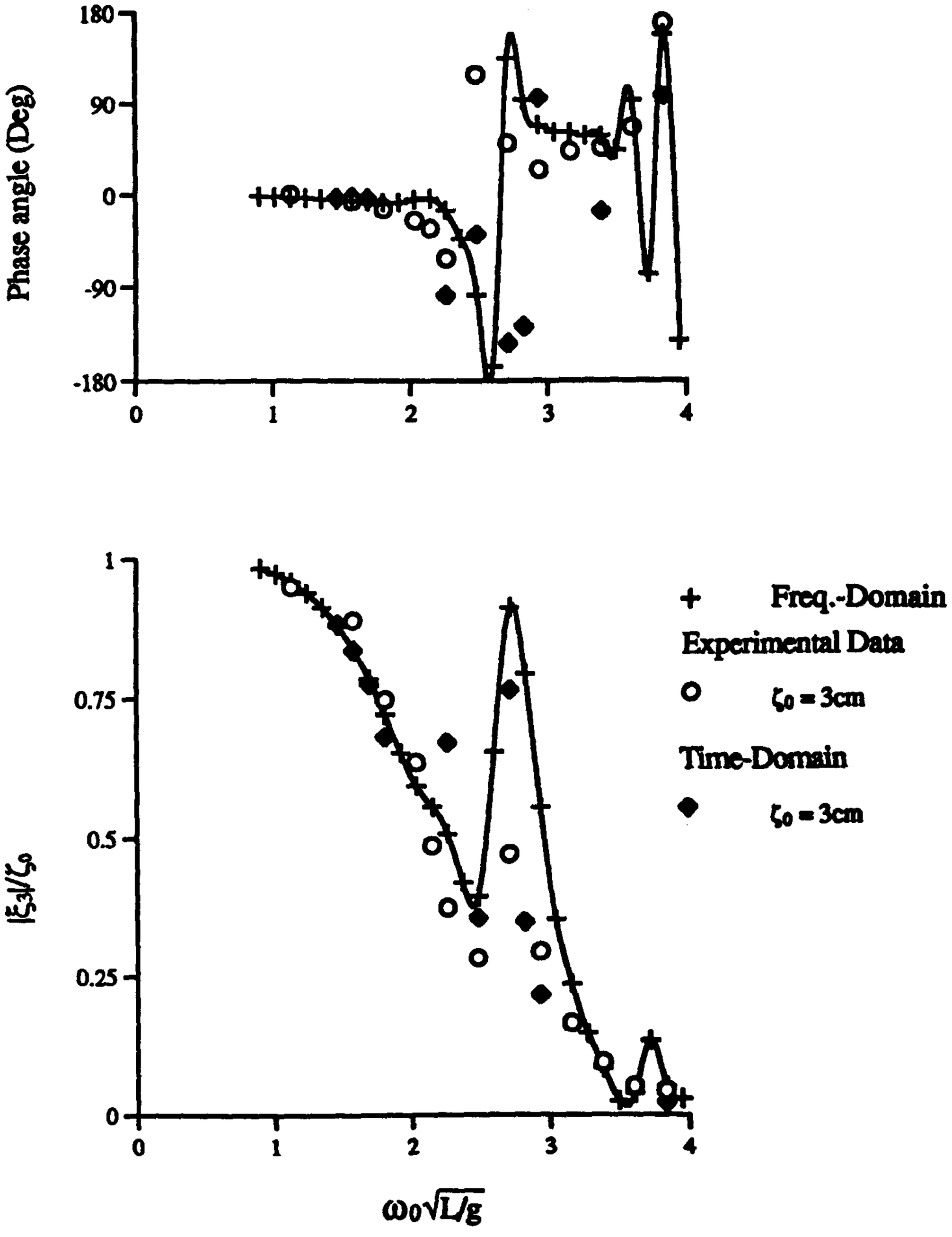

Figure 5.26: Experimental and Theoretical Heave Motion Response of the V-1 Catamaran at Fn=0.226(ζ_0 = 3cm)

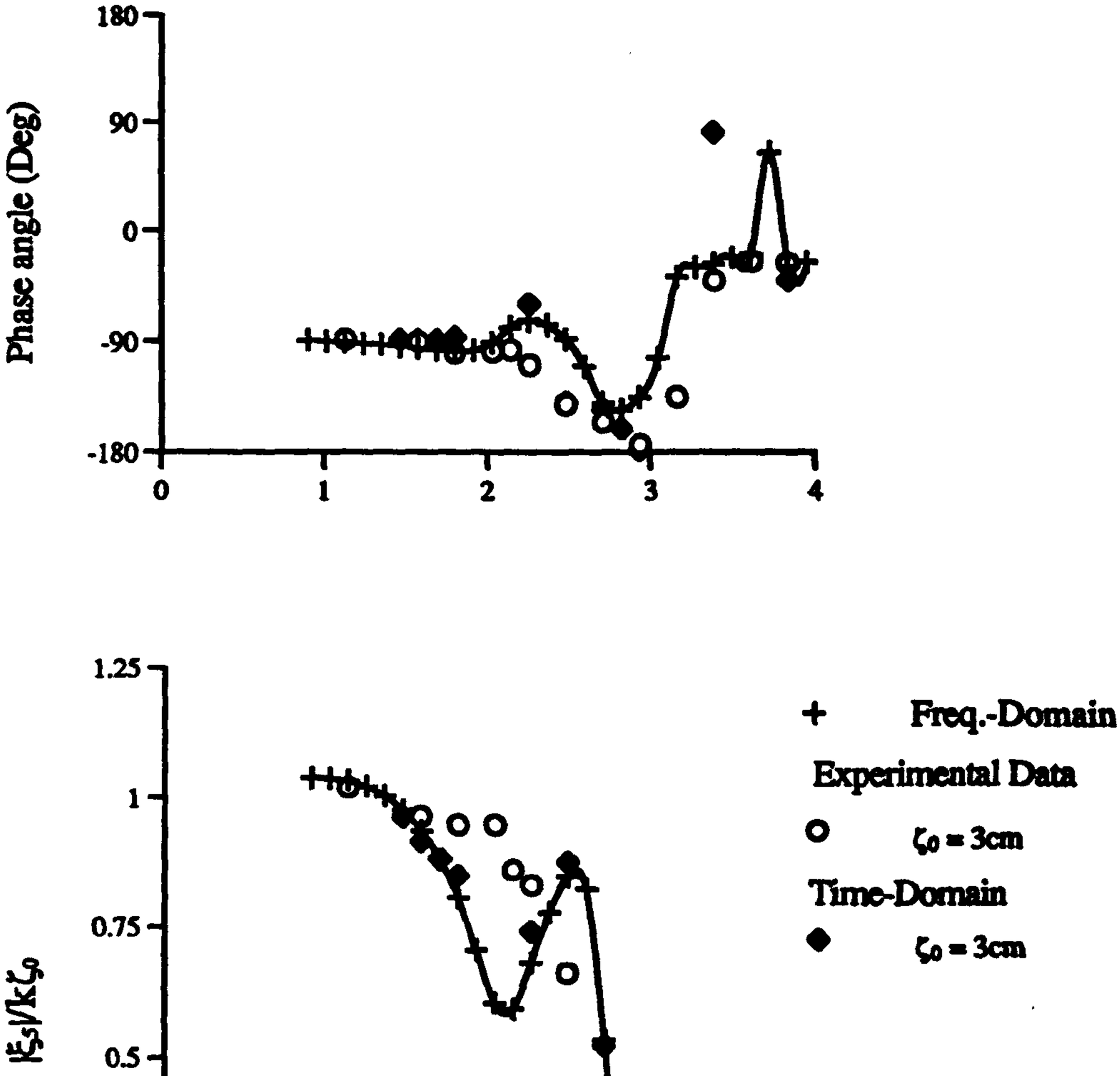

Figure 5.27 : Experimental and Theoretical Pitch Motion Response of the V-1 Catamaran at Fn=0.226(ζ_0 = 3cm)

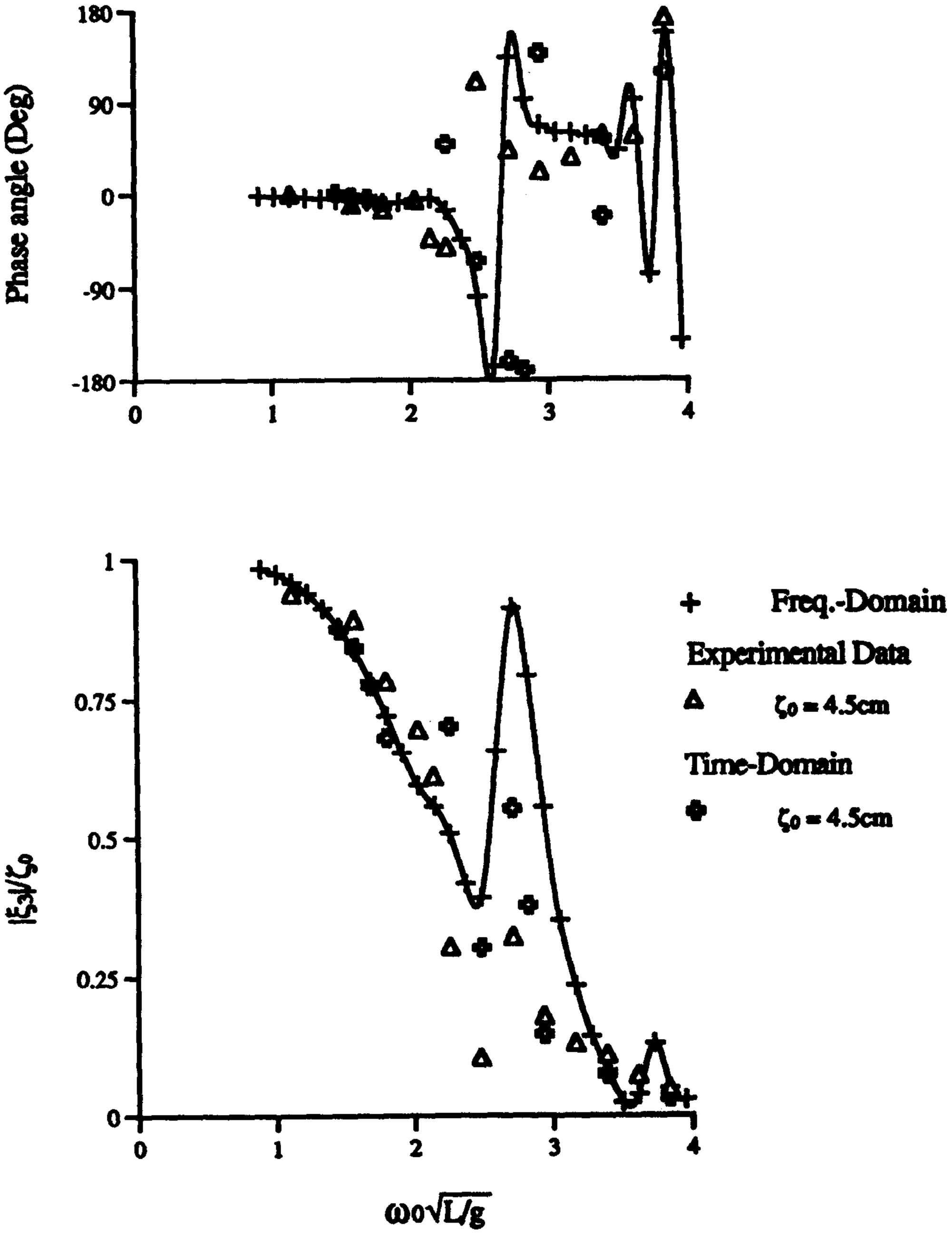

Figure 5.28: Experimental and Theoretical Heave Motion Response of the V-1 Catamaran at F_n=0.226(ζ_0 = 4.5cm)

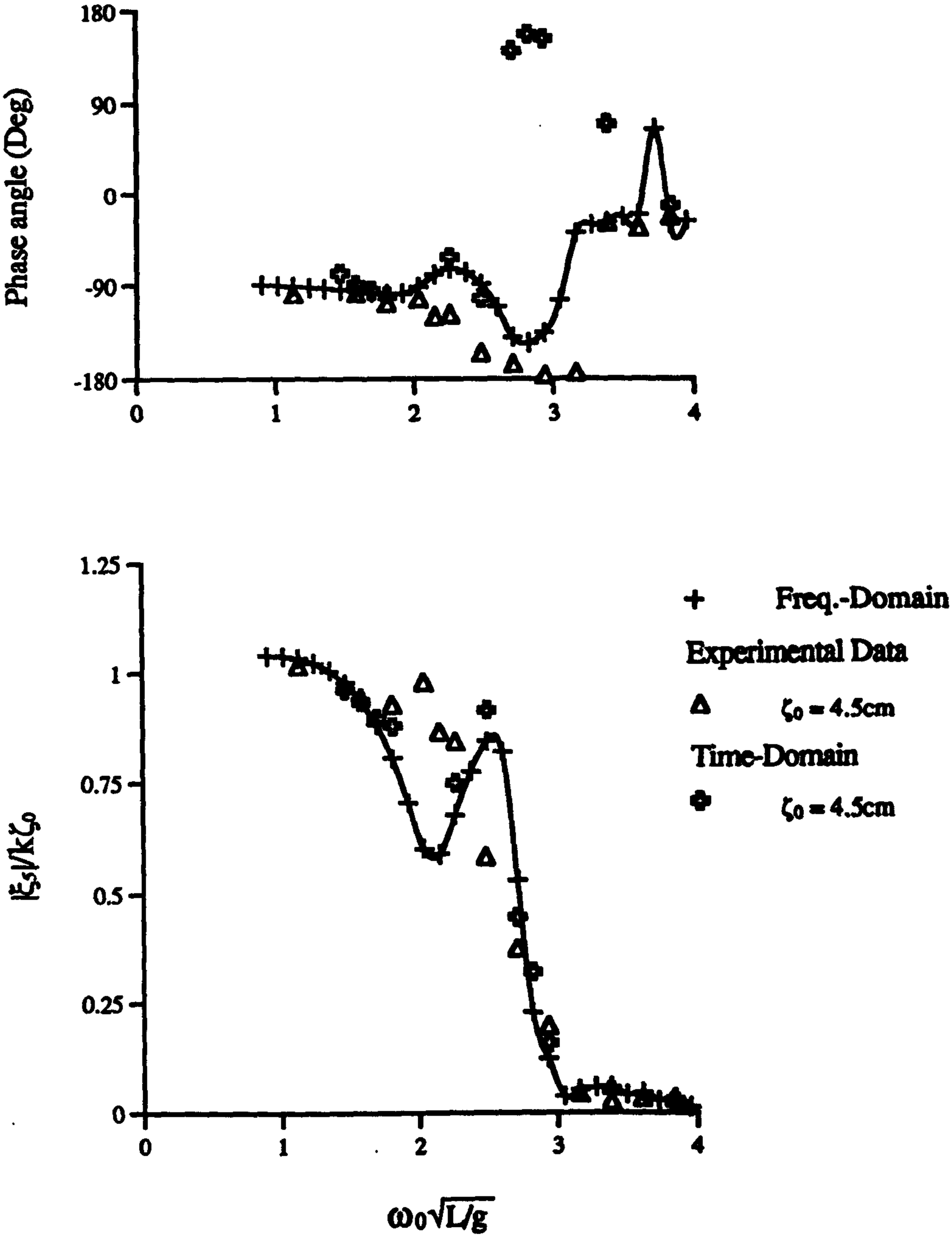

Figure 5.29 : Experimental and Theoretical Pitch Motion Response of the V-1 Catamaran at Fn=0.226(ζ_0 = 4.5cm)

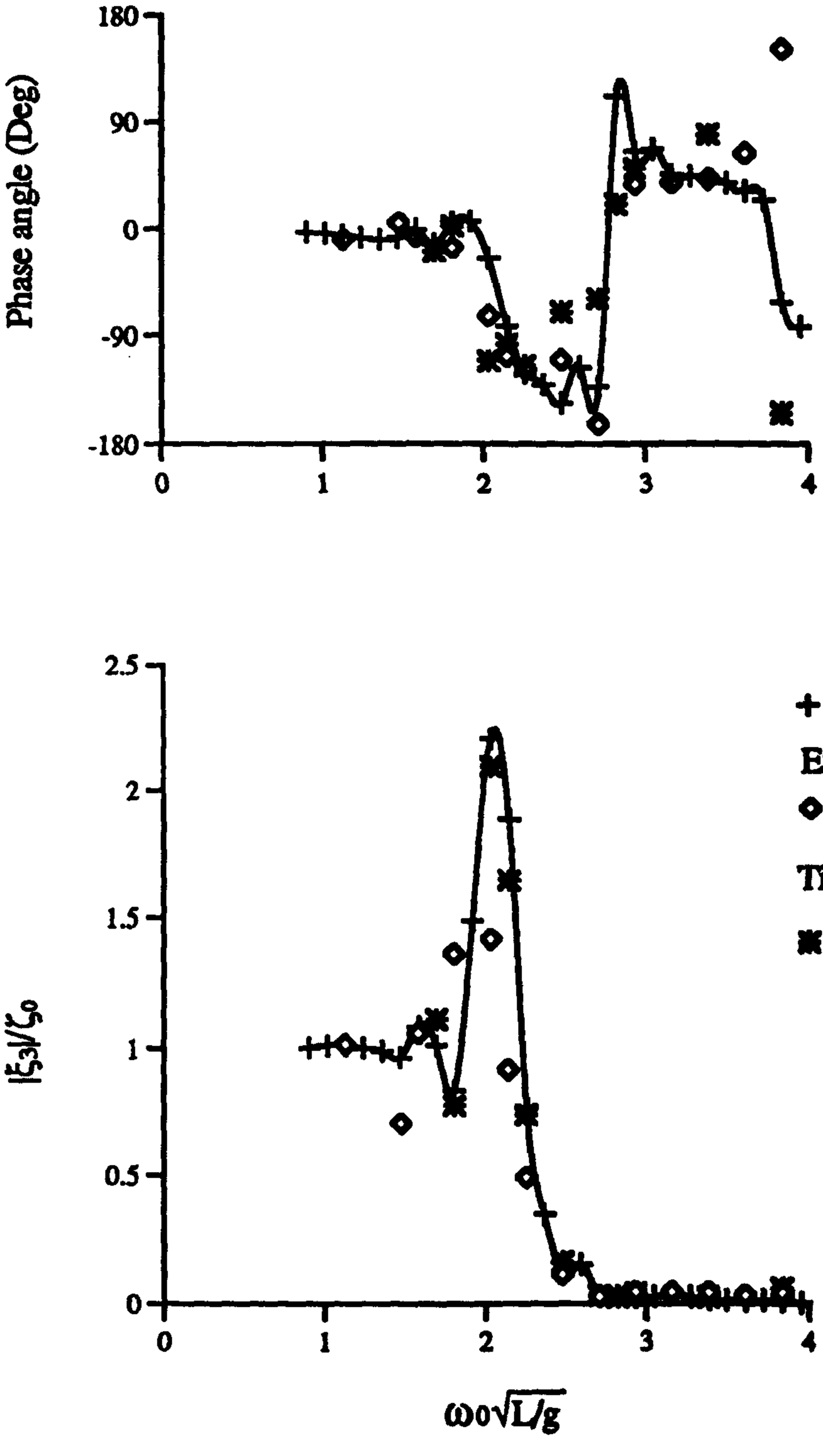

Figure 5.30 : Experimental and Theoretical Heave Motion Response of the V-1 Catamaran at F_n=0.677(ζ_0 = 1cm)

Figure 5.31 : Experimental and Theoretical Pitch Motion Response of the V-1 Catamaran at F_n=0.677(ζ_0 = 1cm)

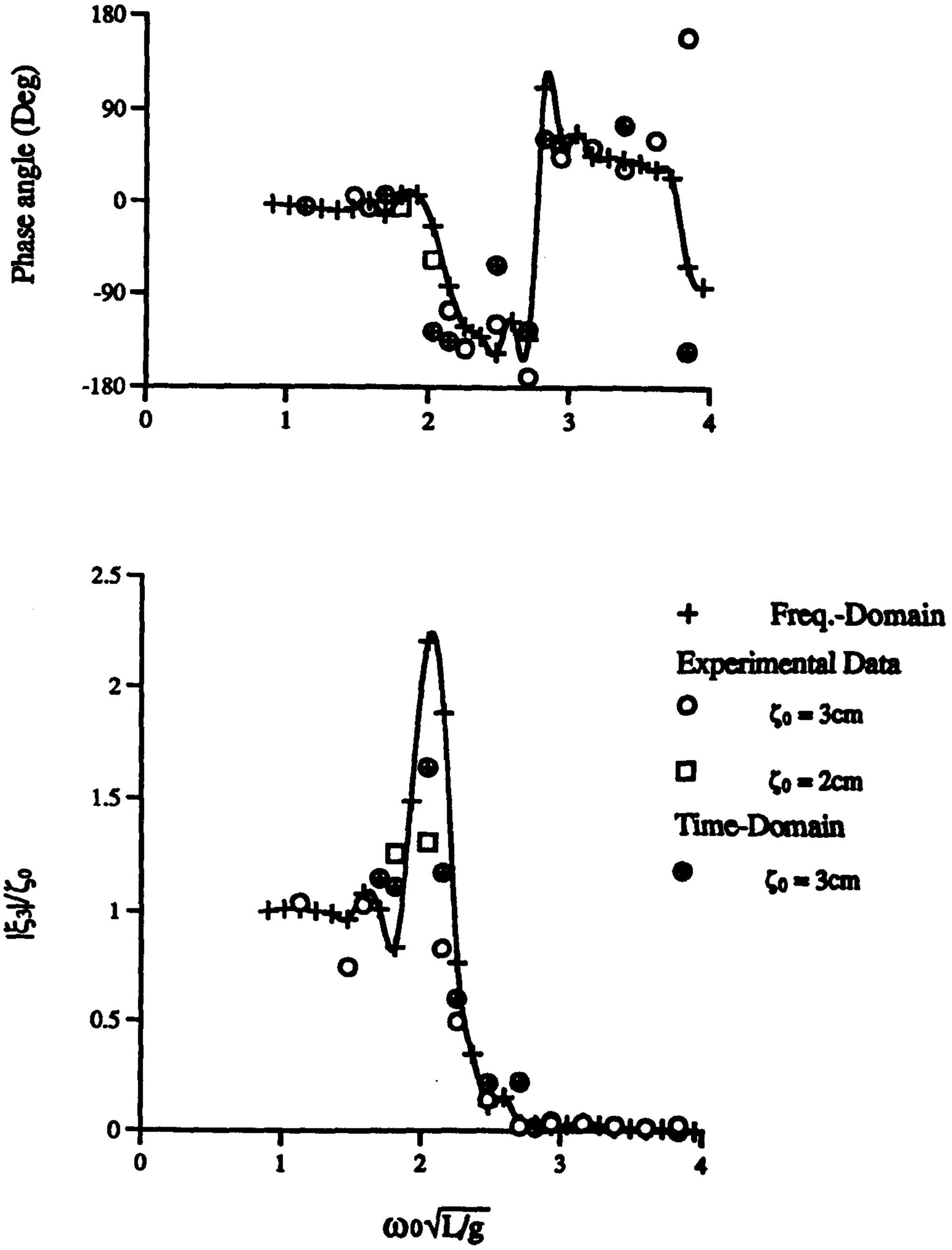

Figure 5.32: Experimental and Theoretical Heave Motion Response of the V-1 Catamaran at F_n=0.677(ζ_0 = 3cm)

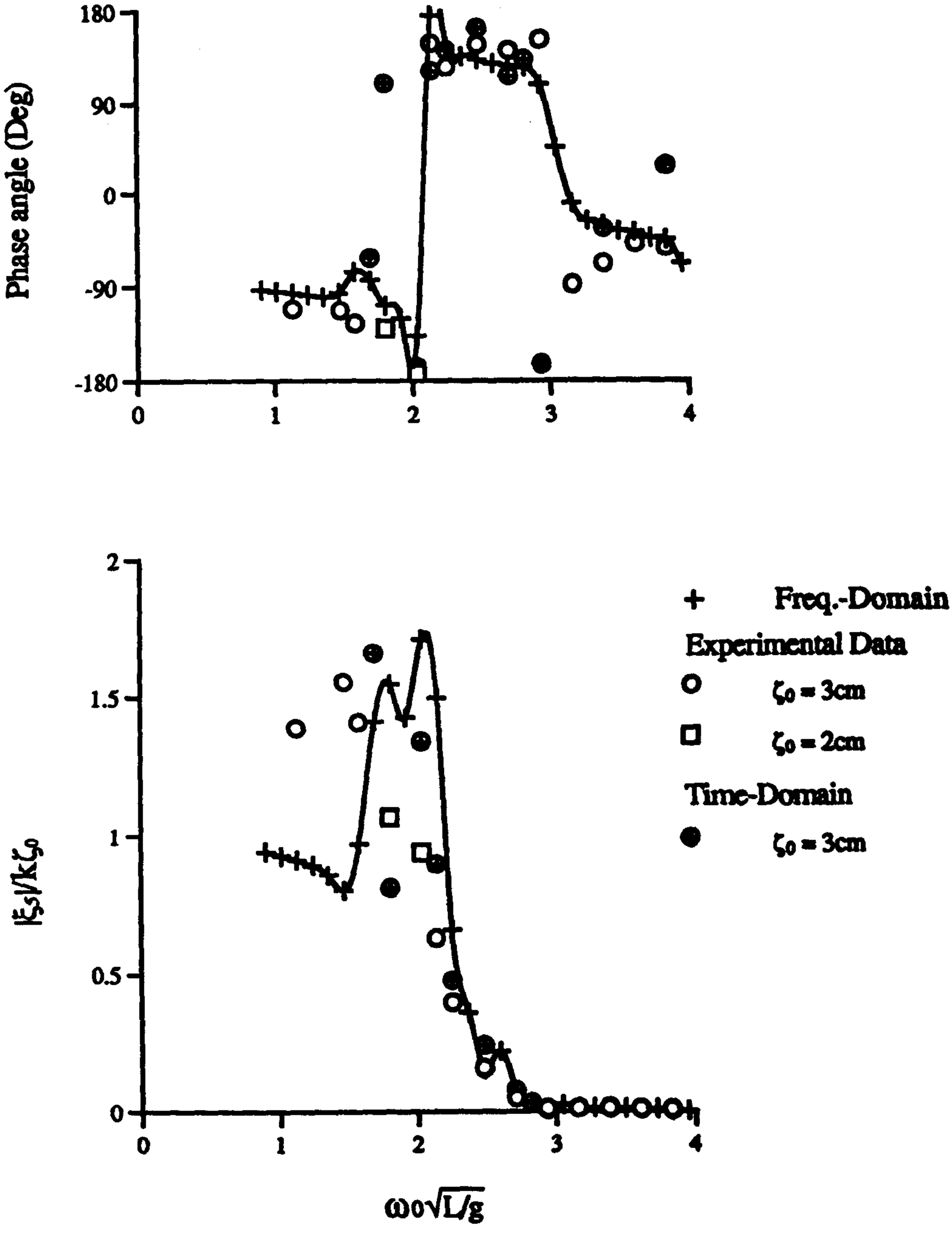

Figure 5.33: Experimental and Theoretical Pitch Motion Response of the V-1 Catamaran at Fn=0.677(ζ_0 = 3cm)

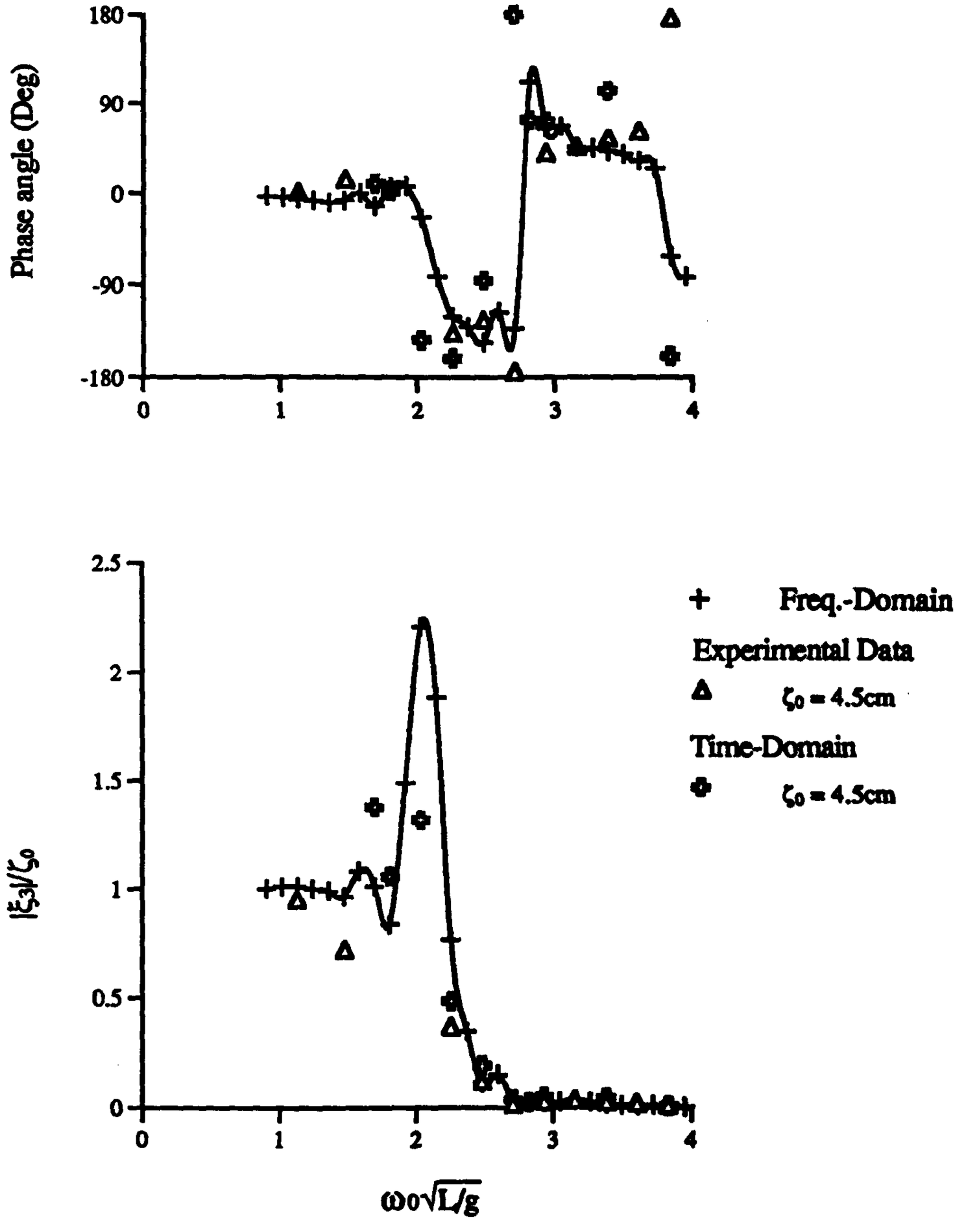

Figure 5.34: Experimental and Theoretical Heave Motion Response of the V-1 Catamaran at F_n=0.677(ζ_0 = 4.5cm)

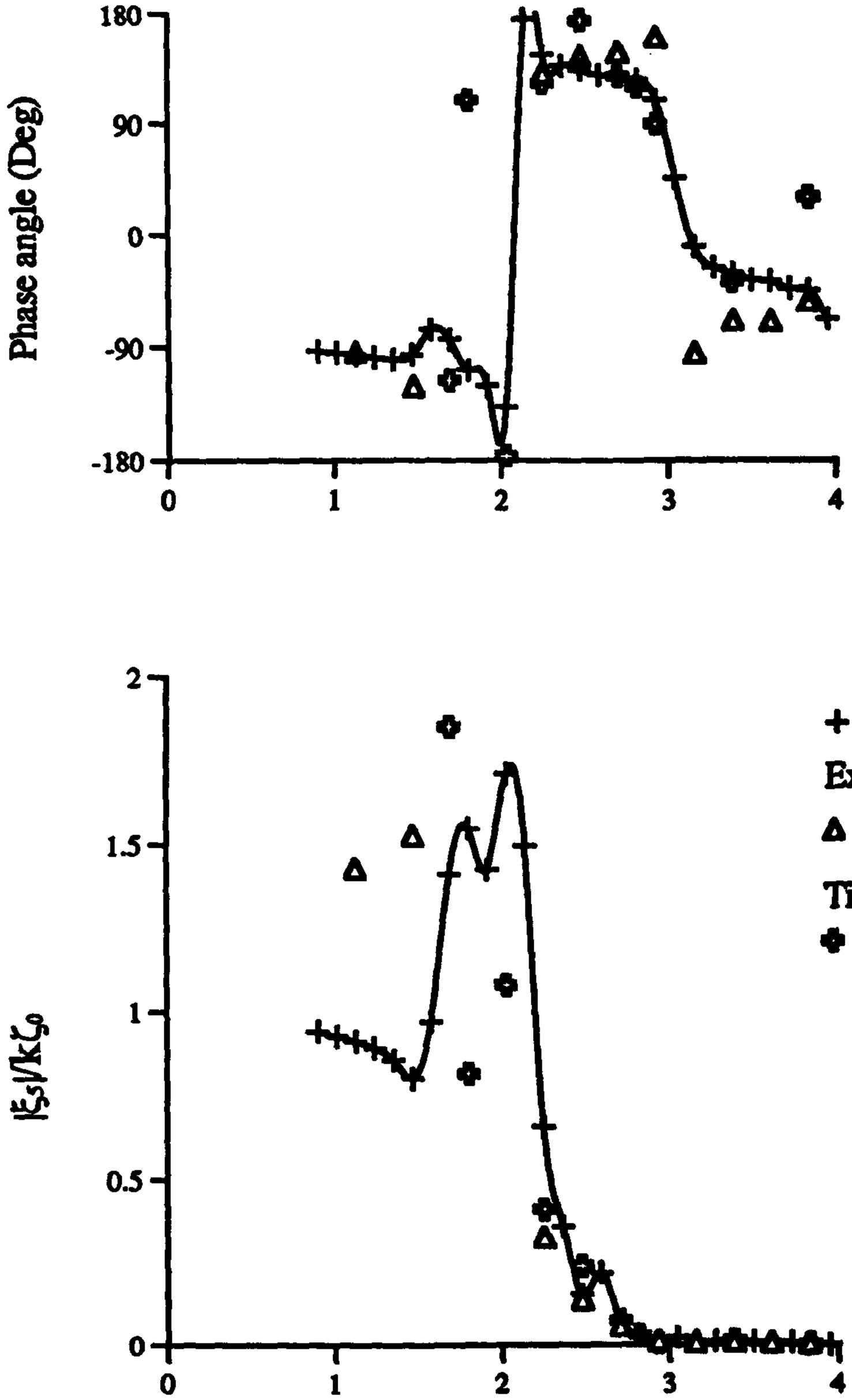

Figure 5.35: Experimental and Theoretical Pitch Motion Response of the V-1 Catamaran at F_n=0.677(ζ_0 = 4.5cm)

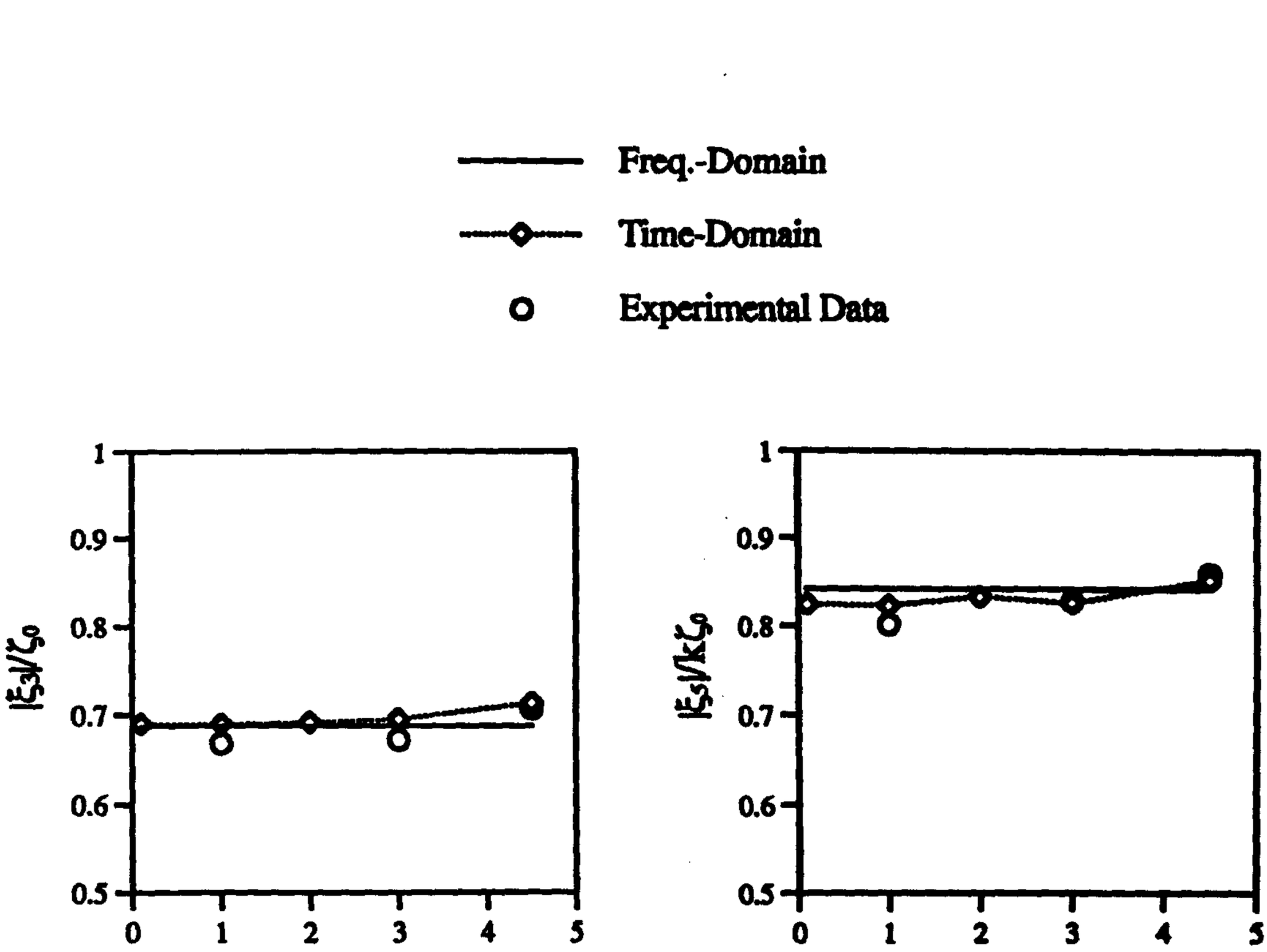

Figure 5.36: Nonlinearity of the Heave and Pitch Motions of V-1 Catamaran with Various Incident Wave Amplitudes. (Fn=0.00,ω_0=4.0 rad/sec)

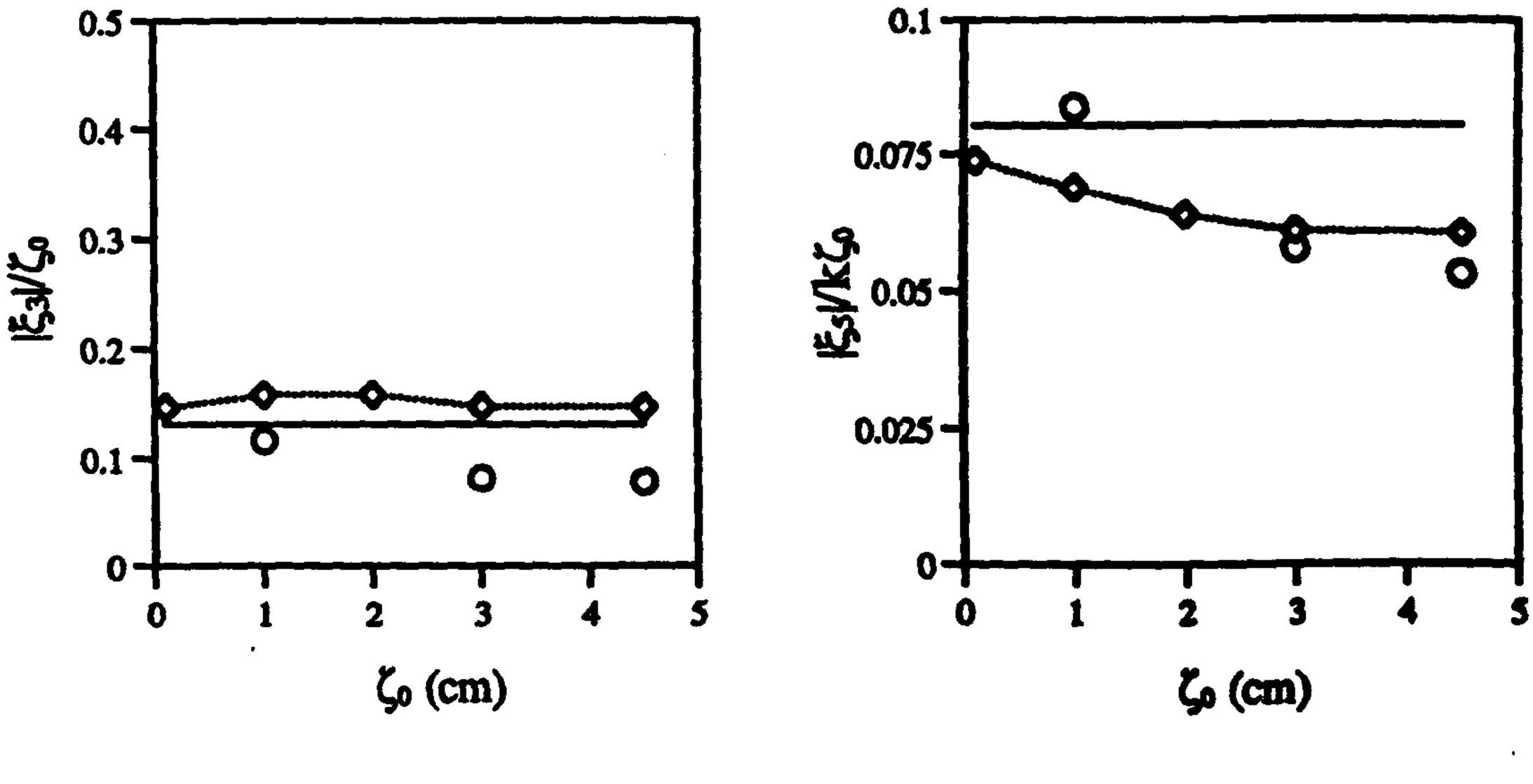

Figure 5.37 : Nonlinearity of the Heave and Pitch Motions of V-1 Catamaran with Various Incident Wave Amplitudes. (Fn=0.00,ω_0=8.5 rad/sec)

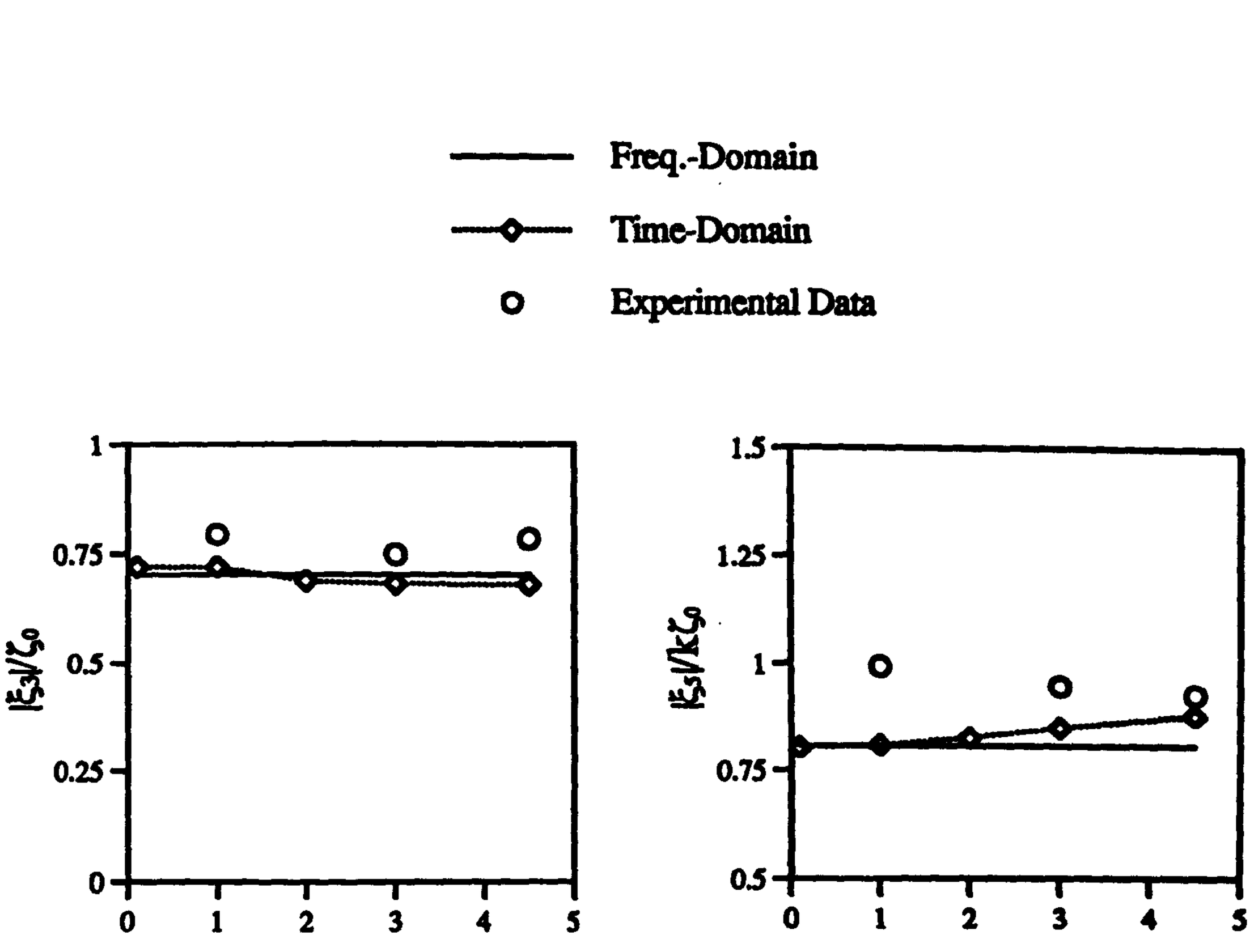

Figure 5.38 : Nonlinearity of the Heave and Pitch Motions of V-1 Catamaran with Various Incident Wave Amplitudes. (Fn=0.226,ω_0=4.0 rad/sec)

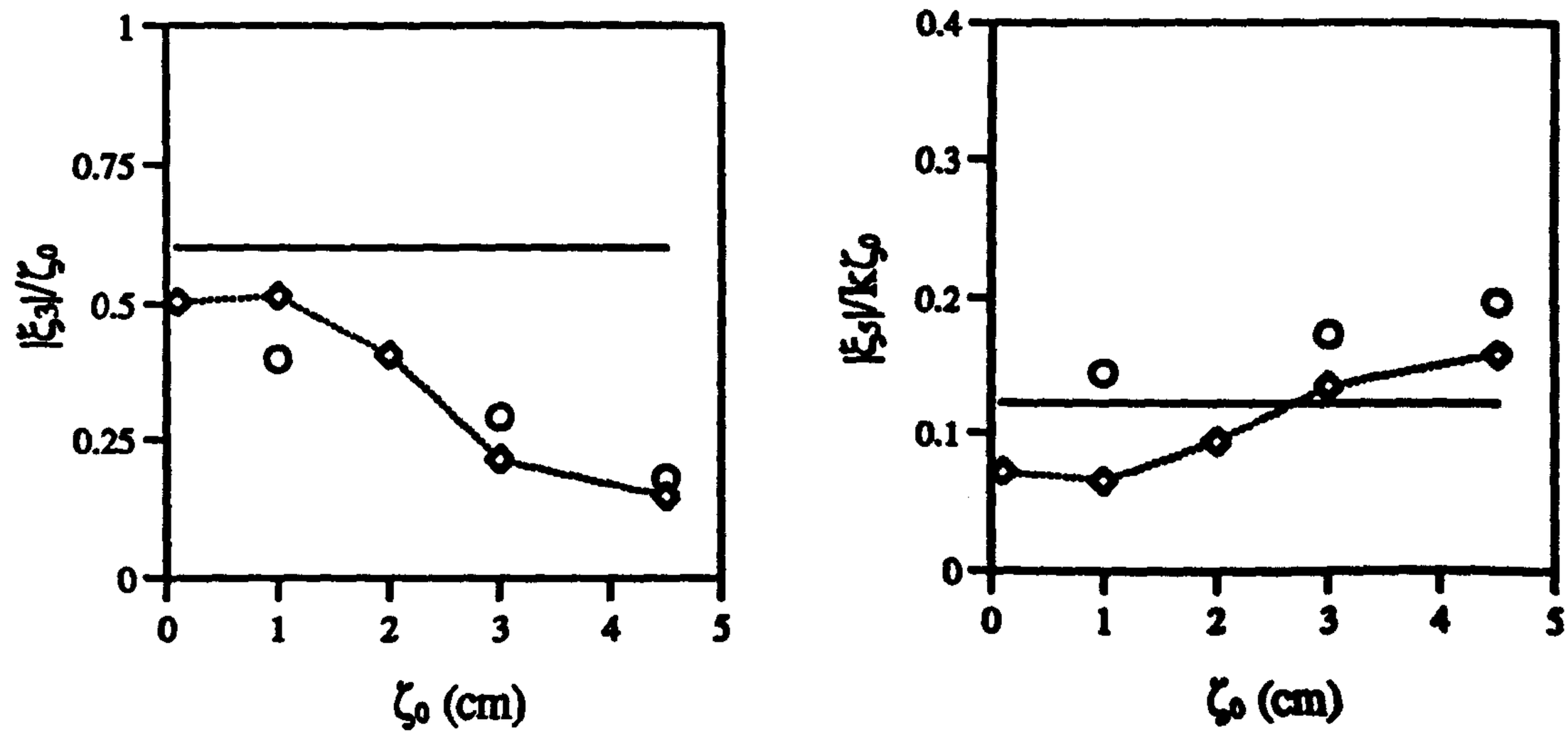

Figure 5.39 : Nonlinearity of the Heave and Pitch Motions of V-1 Catamaran with Various Incident Wave Amplitudes. (Fn=0.226,ω_0=6.5 rad/sec)

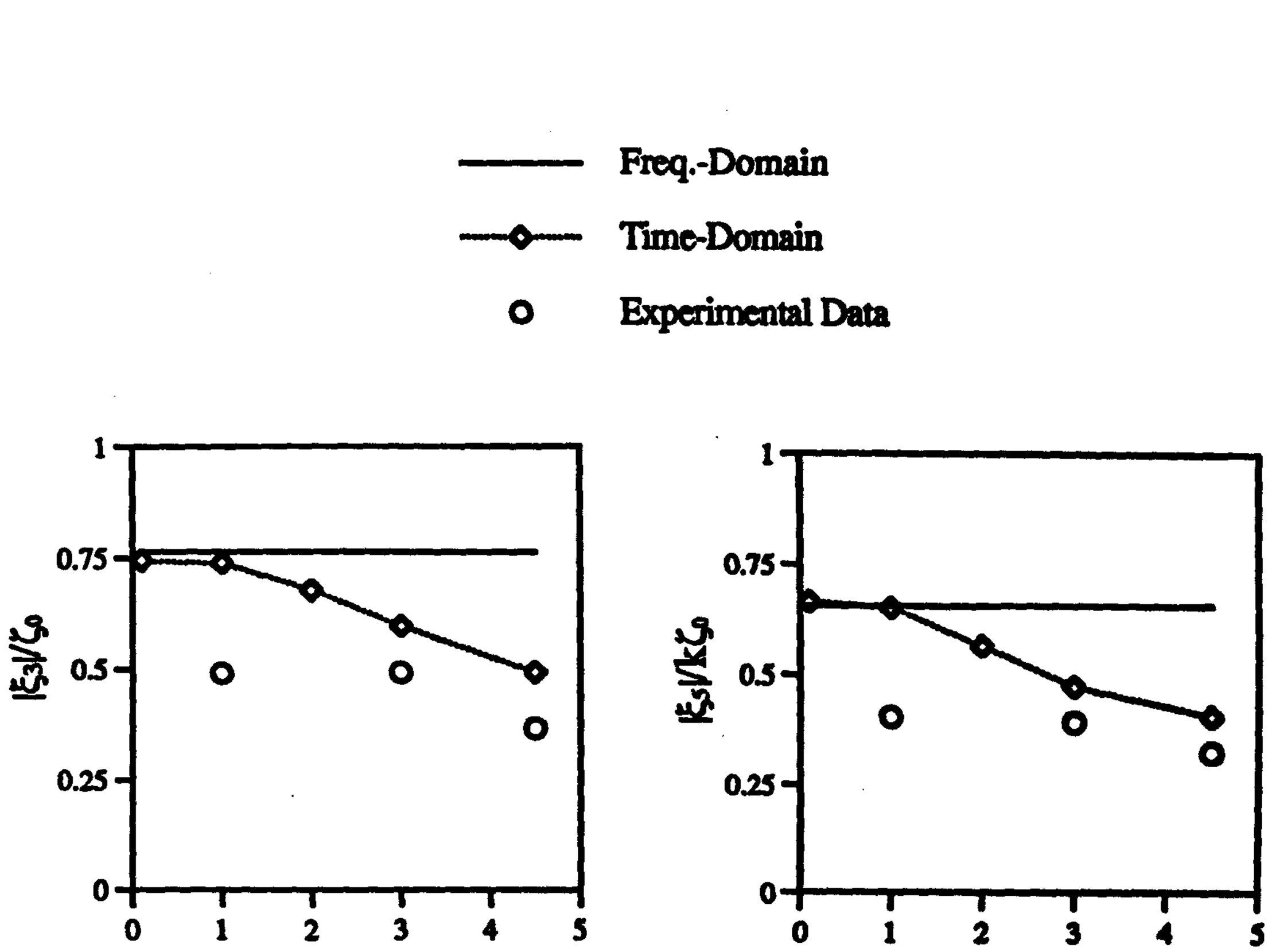

Figure 5.40 : Nonlinearity of the Heave and Pitch Motions of V-1 Catamaran with Various Incident Wave Amplitudes. (Fn=0.677,ω_0=5.0 rad/sec)

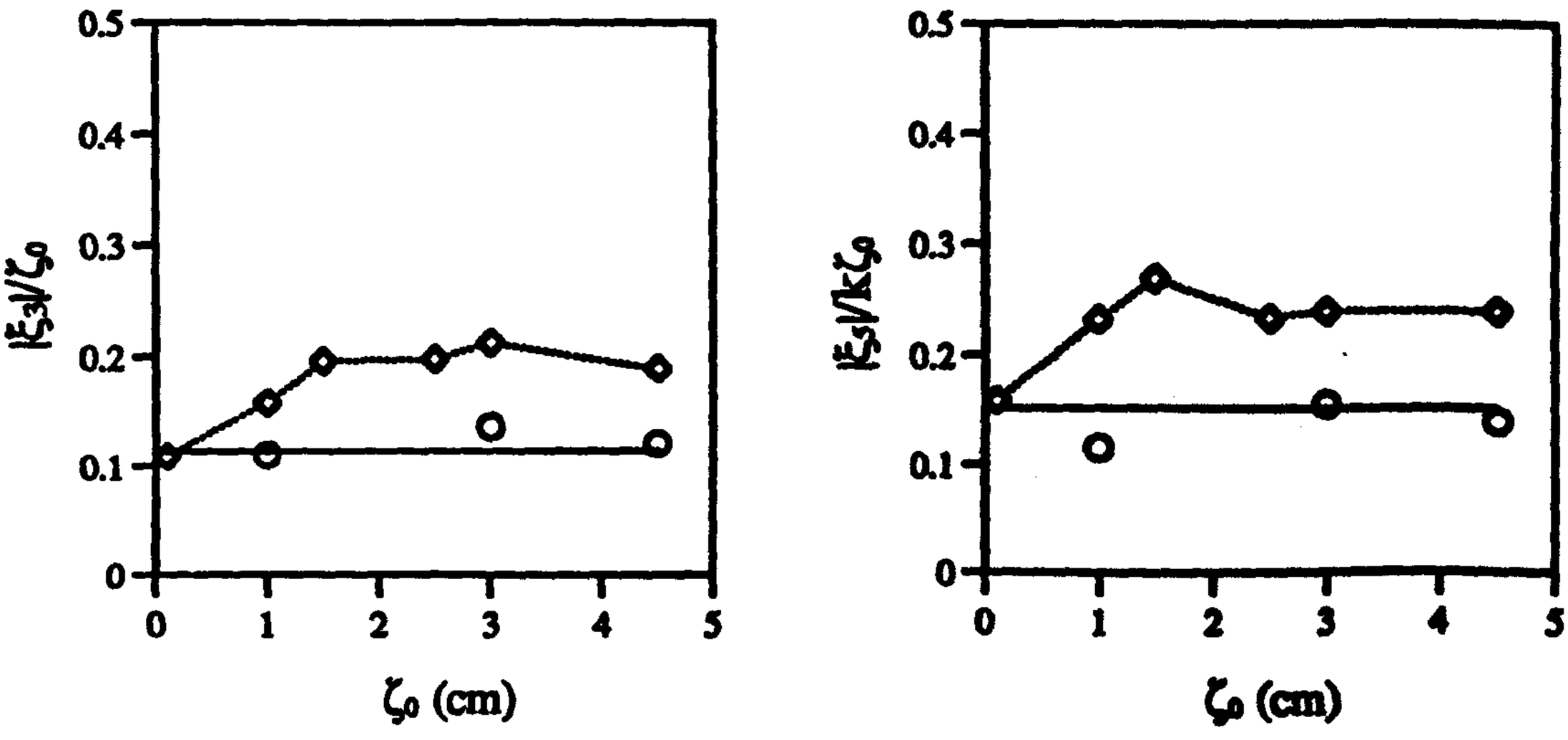

Figure 5.41 : Nonlinearity of the Heave and Pitch Motions of V-1 Catamaran with Various Incident Wave Amplitudes. (Fn=0.677,ω_0=5.5 rad/sec)

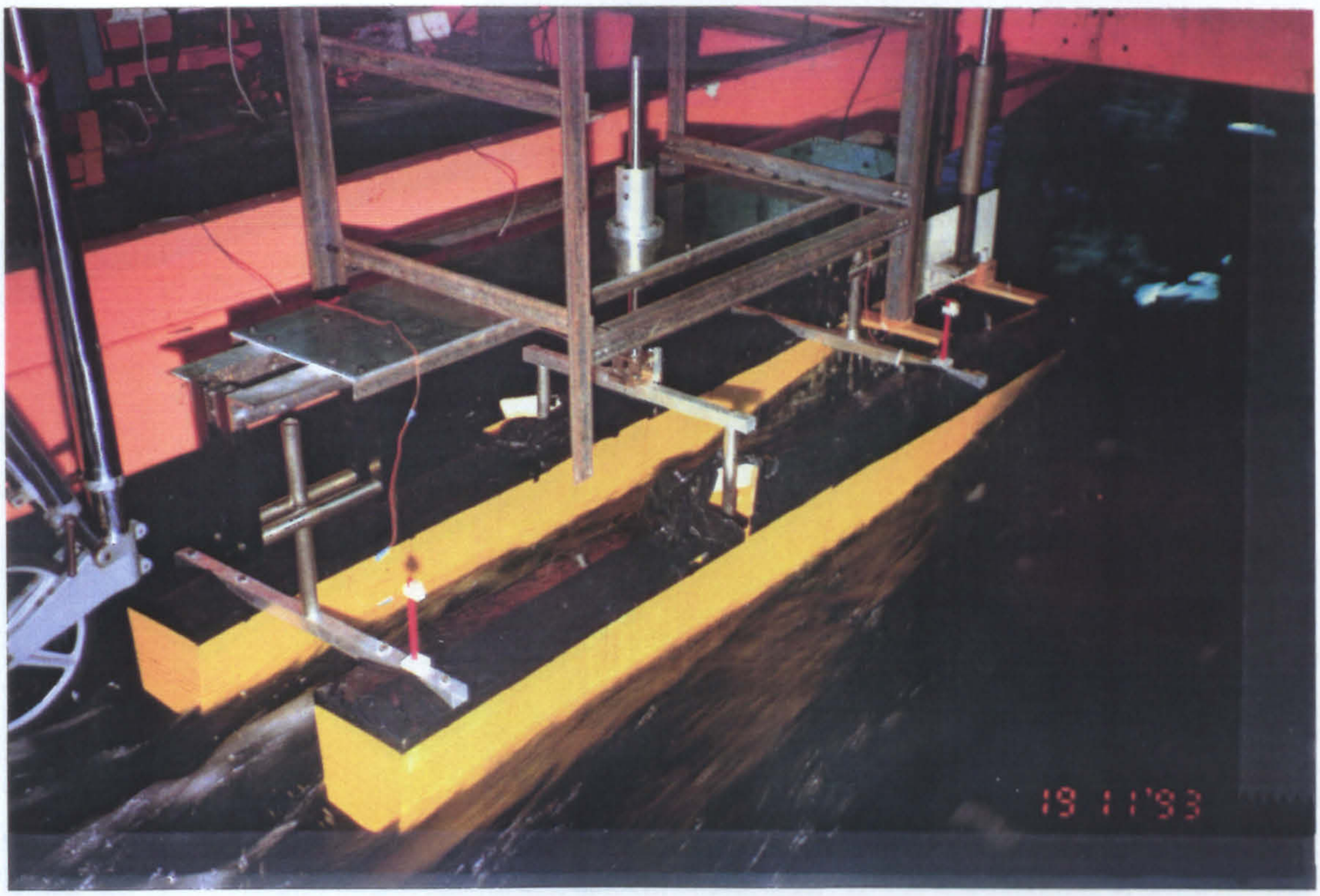

Figure 5.42 : The Behaviour of the Model Motion in Regular Wave Test:1/10
(Fn=0.677, $\zeta_0 = 3.0cm$, $\omega_0 = 4.75rad/\sec$)

Figure 5.43 : The Behaviour of the Model Motion in Regular Wave Test:2/10
(Fn=0.677, $\zeta_0 = 3.0cm$, $\omega_0 = 4.75rad/\sec$)

Figure 5.44 : The Behaviour of the Model Motion in Regular Wave Test:3/10
(Fn=0.677, $\zeta_0 = 3.0cm$, $\omega_0 = 4.75rad/\sec$)

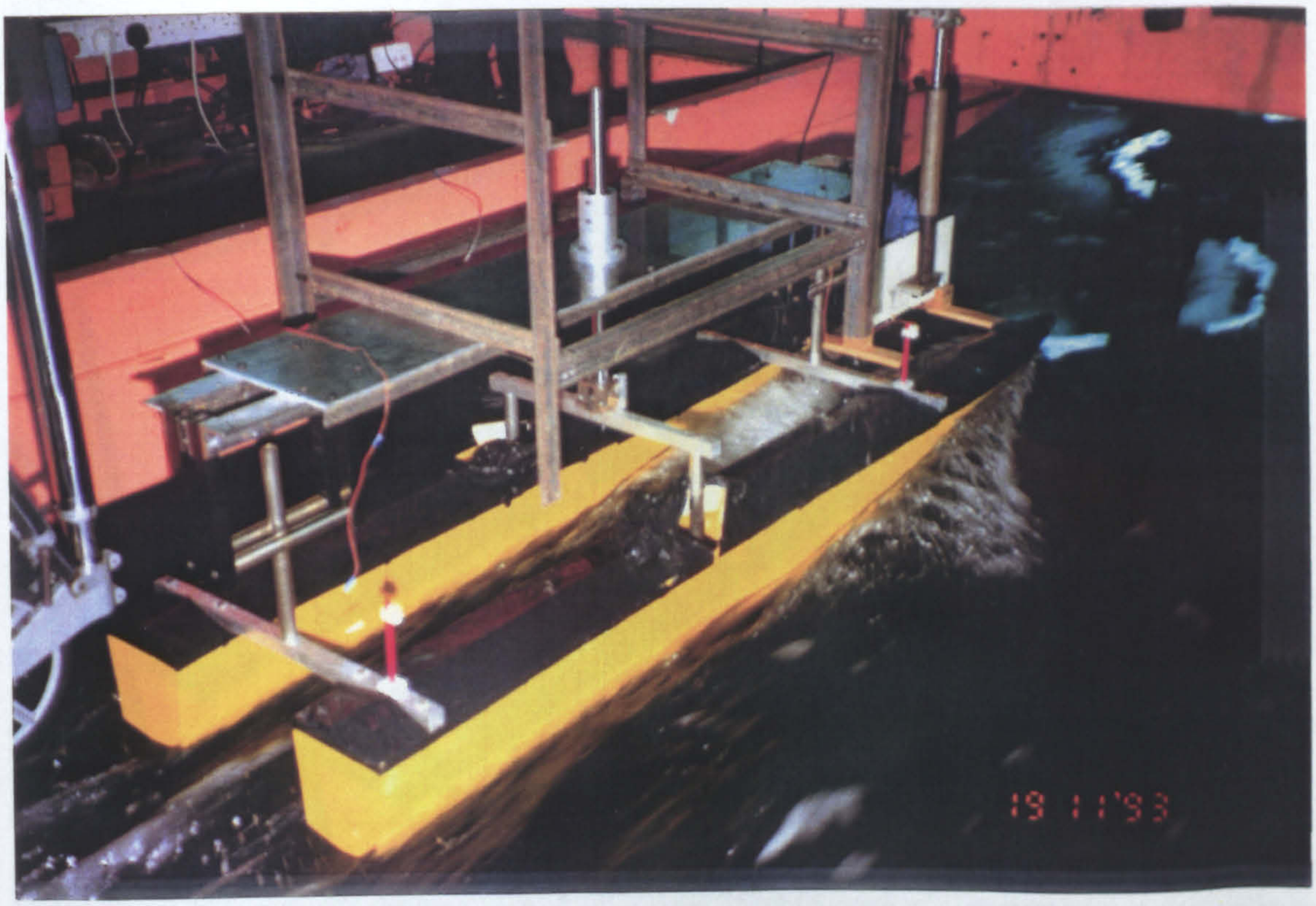

Figure 5.45 : The Behaviour of the Model Motion in Regular Wave Test:4/10
(Fn=0.677, $\zeta_0 = 3.0cm$, $\omega_0 = 4.75rad/\sec$)

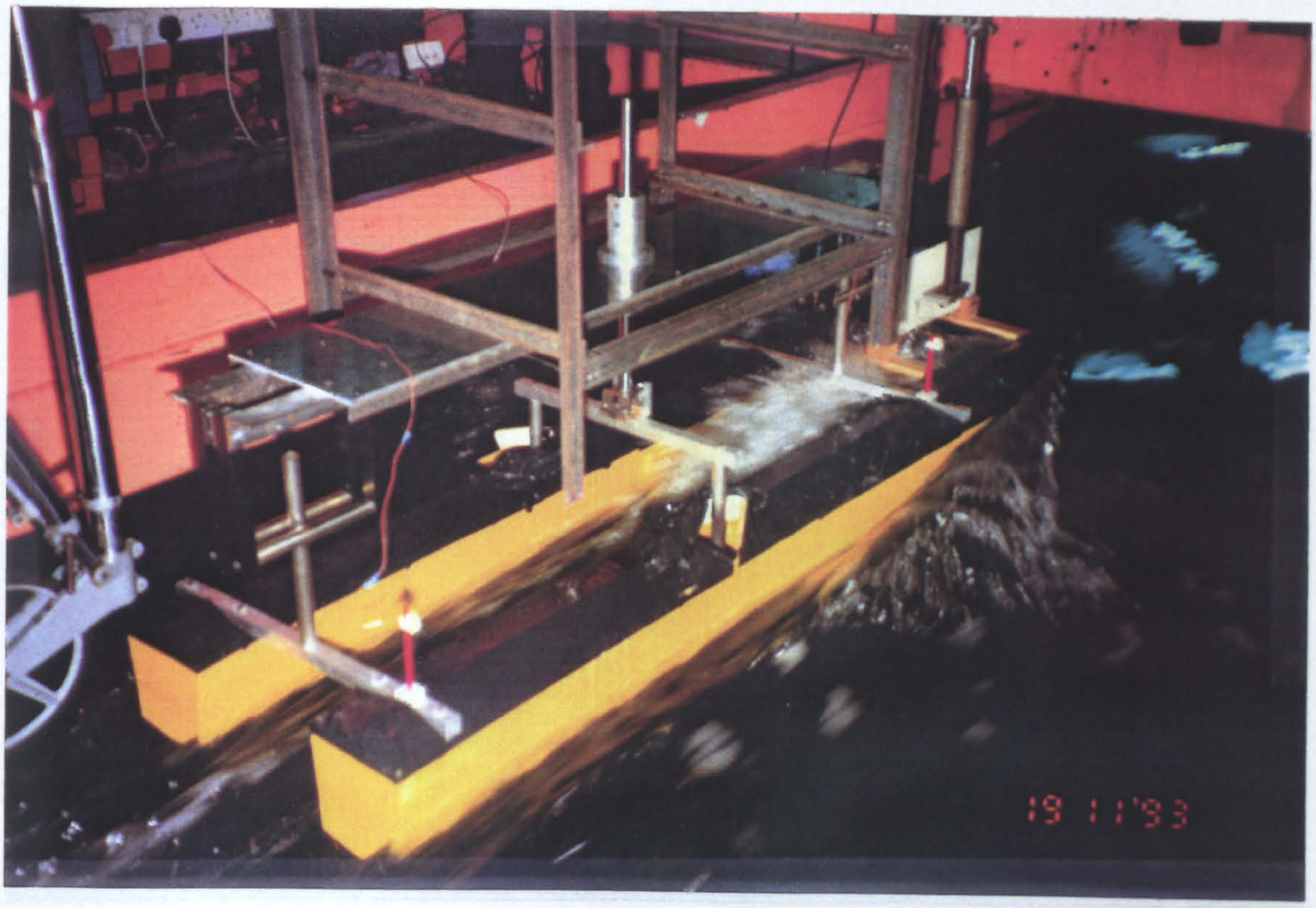

Figure 5.46 : The Behaviour of the Model Motion in Regular Wave Test:5/10
(Fn=0.677, $\zeta_o = 3.0cm$, $\omega_o = 4.75rad/\sec$)

Figure 5.47 : The Behaviour of the Model Motion in Regular Wave Test:6/10
(Fn=0.677, $\zeta_o = 3.0cm$, $\omega_o = 4.75rad/\sec$)

Figure 5.48 : The Behaviour of the Model Motion in Regular Wave Test:7/10 (Fn=0.677, $\zeta_0 = 3.0cm$, $\omega_0 = 4.75rad/\sec$)

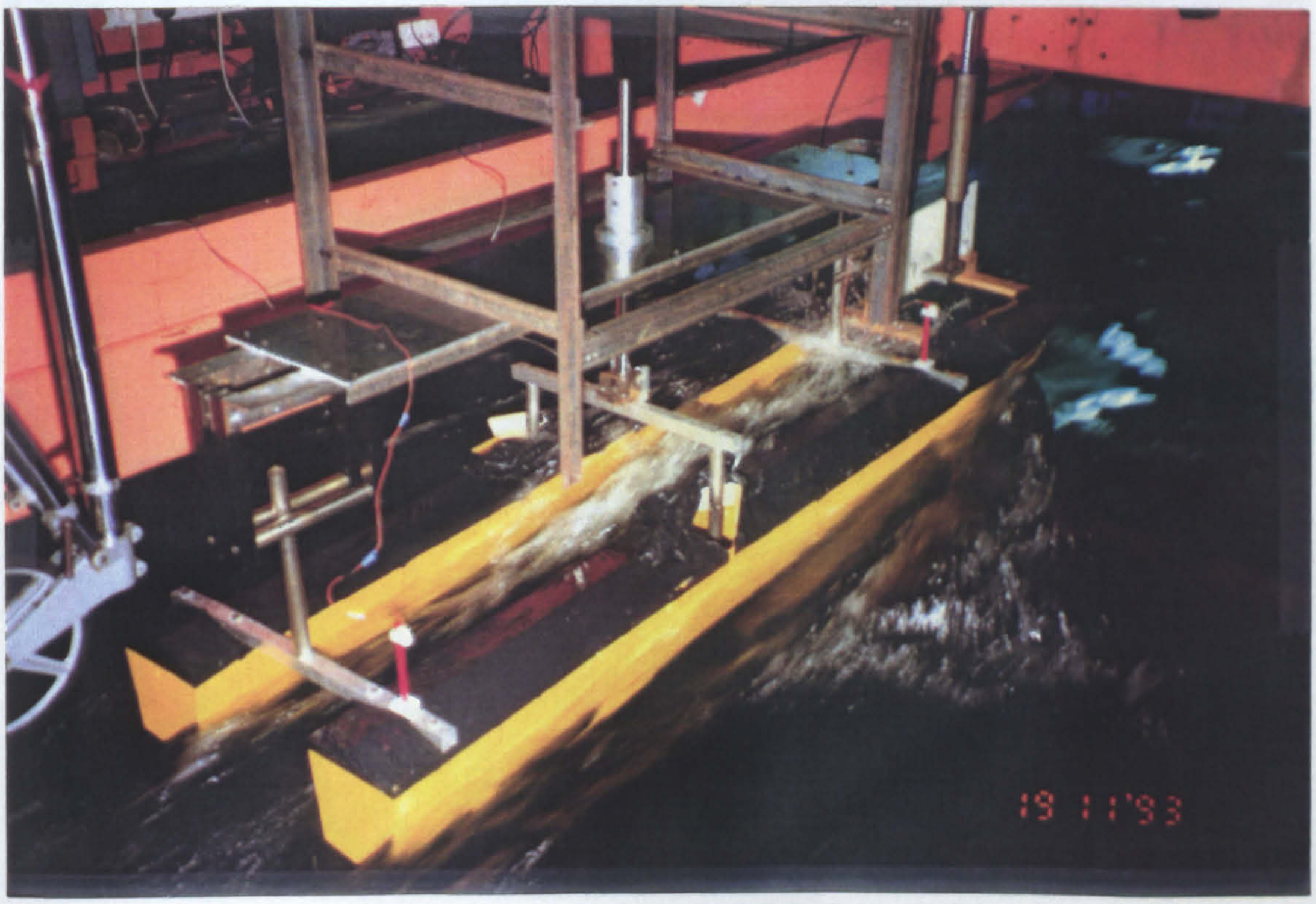

Figure 5.49 : The Behaviour of the Model Motion in Regular Wave Test:8/10 (Fn=0.677, $\zeta_0 = 3.0cm$, $\omega_0 = 4.75rad/\sec$)

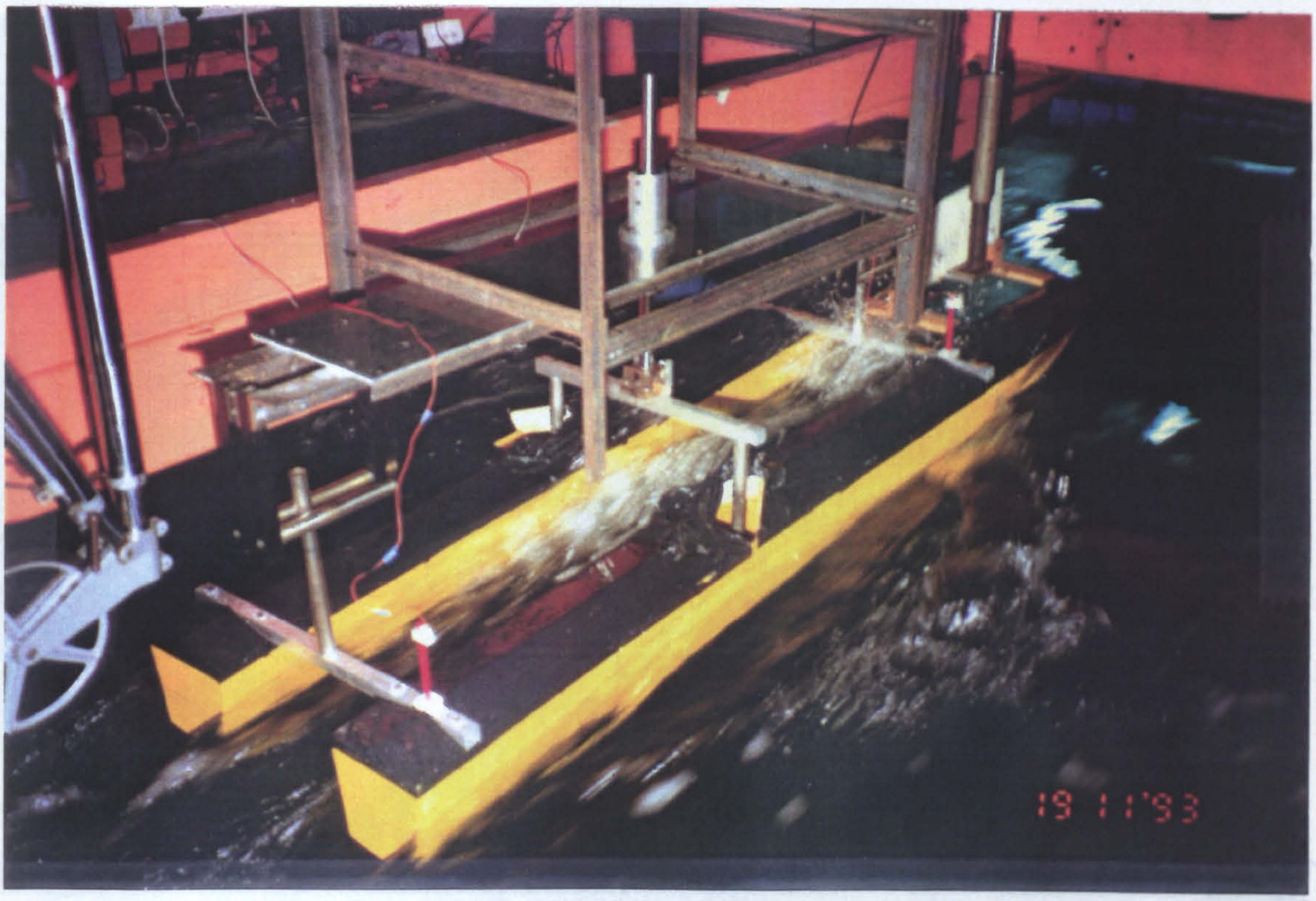

Figure 5.50 : The Behaviour of the Model Motion in Regular Wave Test:9/10
(Fn=0.677, $\zeta_0 = 3.0cm$, $\omega_0 = 4.75rad/\sec$)

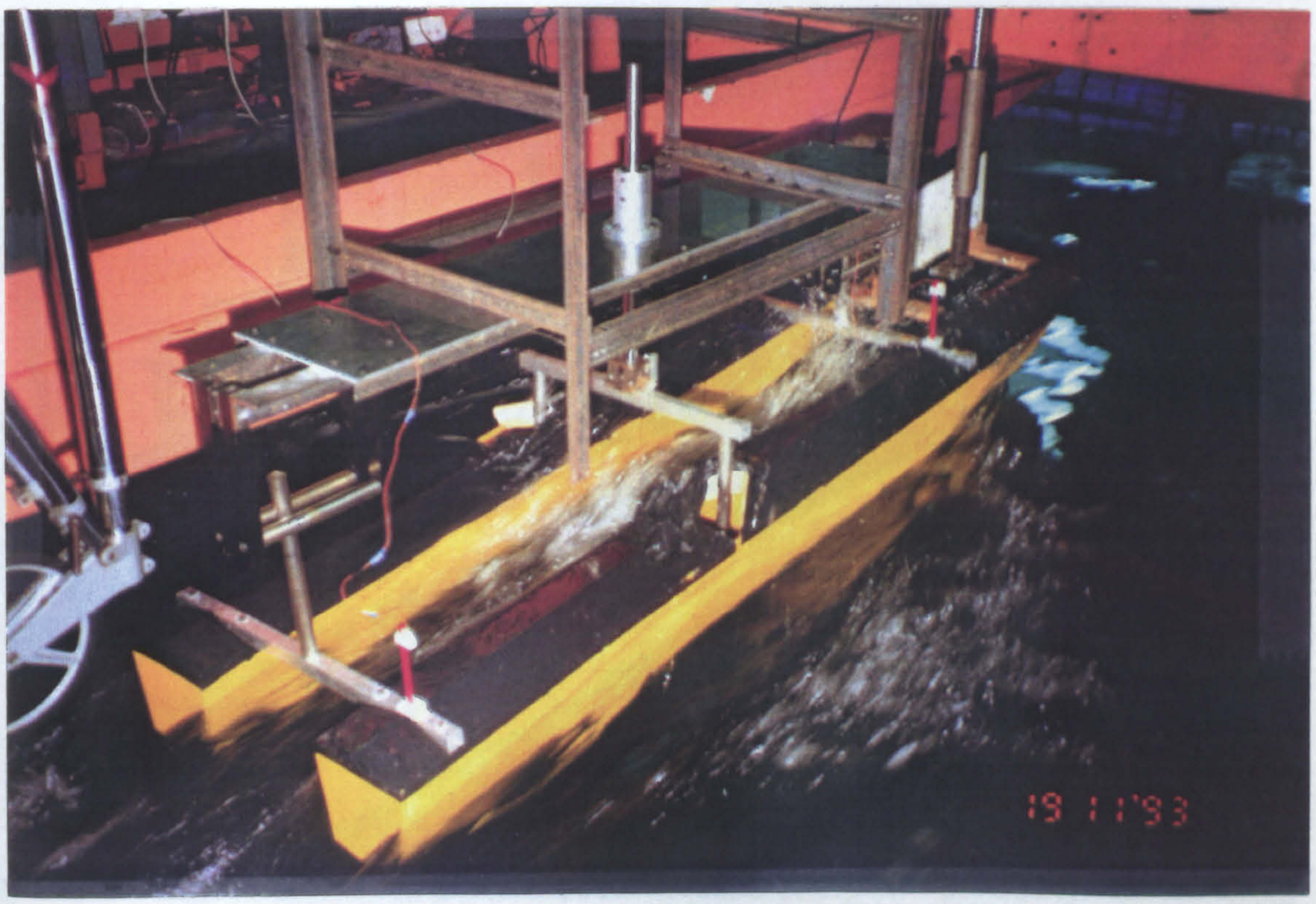

Figure 5.51 : The Behaviour of the Model Motion in Regular Wave Test:10/10
(Fn=0.677, $\zeta_0 = 3.0cm$, $\omega_0 = 4.75rad/\sec$)

Figure 5.52 : The Behaviour of the Model Motion in Regular Wave Test:1/2
(Fn=0.226, $\zeta_0 = 4.5cm$, $\omega_0 = 5.0rad/\sec$)

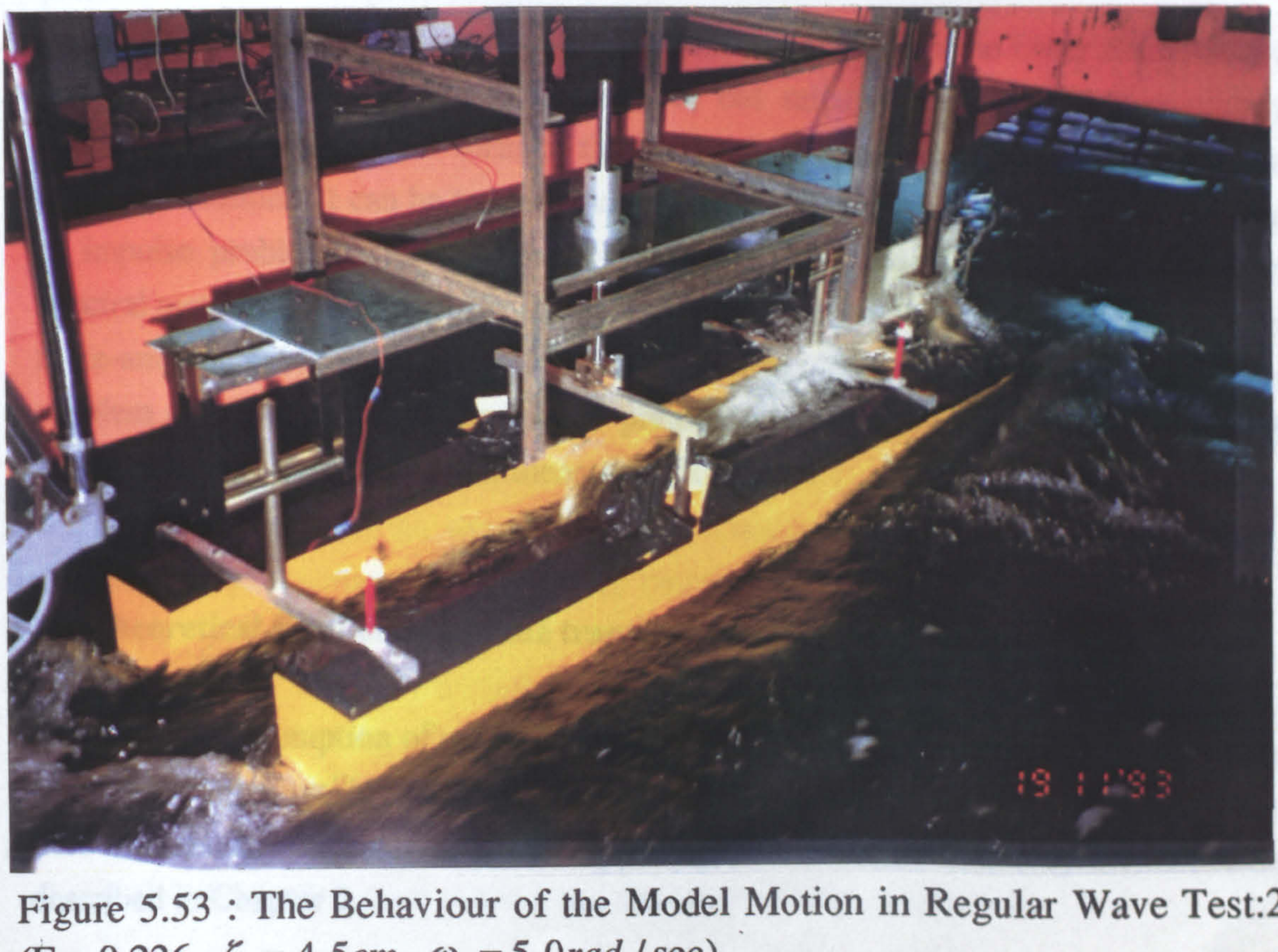

Figure 5.53 : The Behaviour of the Model Motion in Regular Wave Test:2/2
(Fn=0.226, $\zeta_0 = 4.5cm$, $\omega_0 = 5.0rad/\sec$)

CHAPTER 6
TRANSIENT MOTIONS OF TWO-DIMENSIONAL FLOATING BODIES

6.1 Introduction

The motion problem of a floating body on the free surface of fluid has been studied extensively in the frequency domain. It leads to the linear response that the body motion is small and strictly sinusoidal in time. Another more general approach for dealing with arbitrary motion is to formulate the problem in the time domain for solving the initial value problem.

The use of time domain analysis to predict the seakeeping characteristics of floating bodies has been increasing for the past several years. The solution for the time domain Green function is credited to Finkelstein(1957). Discussions of direct time domain solutions are presented by various authors such as Stoker(1957), Cummins(1962), Ogilvie(1964), and Wehausen(1967). As computational power has increased, it has become practical to study actual solutions and to investigate the computational advantages of time domain methods. Adachi and Ohmatsu(1979), Yeung(1982a), Newman(1985), Beck and Liapis(1987), Lin and Yue(1990) have successfully obtained results.

A more general and difficult class of motion problem than the linear theory is the one which retains the linearised free surface but satisfies the exact body boundary condition. The underwater form of the body can then change significantly over the course of motion. It can be treated numerically by advancing them in time as a series of impulse problems with new body shapes at each time step. In this Chapter, a spectral method which was first presented by Chapman (1979) is followed to solve the finite-amplitude initial value problem. Preliminary results for the linear radiation problem of two-dimensional bodies are presented and compared with those obtained from published experimental and theoretical data.

6.2 Theoretical formulation of the transient motion

Based on the assumption of potential flow theory, the problem of the transient motion of a rigid body travelling in waves can be formulated as the Laplace's equation in the fluid domain and the solution is determined by a set of initial-boundary conditions as described in Chapter 2.

If the body is slender and the wave slopes in the longitudinal direction are small, the three-dimensional boundary value problem can be approximated by a set of two-dimensional initial value problems. Furthermore, we assume that the free surface condition is linearised but still allow the motion amplitude to be finite. Then, the unsteady velocity potential $\tilde{\Phi}$ must satisfy the following initial-boundary conditions:

$$\tilde{\Phi}_{yy} + \tilde{\Phi}_{zz} = 0 \qquad \text{in } z < 0 \qquad (6.1)$$

$$\Phi_t + g\zeta = 0 \qquad \text{at } z=0 \qquad (6.2)$$

$$\zeta_t - \tilde{\Phi}_z = 0 \qquad \text{at } z=0 \qquad (6.3)$$

$$\tilde{\Phi}_n = \vec{V}_s(y,z,t)\cdot\vec{n} \qquad \text{on } S_B(y',z',t;x') \qquad (6.4)$$

$$\tilde{\Phi} = f_1(y,z;x) \qquad \text{when } t < 0 \qquad (6.5)$$

where $\vec{V}_s(y,z,t)$ is the local velocity of a point on the wetted body surface; $\vec{n}$ is a unit normal vector outward from the wetted body surface; $\tilde{\Phi}(y,z,t;x) = \tilde{\Phi}(x,y,z,t)$, the dependence of $\tilde{\Phi}$ on x is implicit but the effect will be included by through the body boundary condition. $f_1(y,z;x)$ is a given function at $t<0$. If the incident wave is present, the initial condition will be :

$$f_1(y,z;x) = \zeta_0\phi_0(p,t) \qquad \text{when } t = 0 \qquad (6.6)$$

where
ζ_0 is the incident wave amplitude.
$\phi_0(p,t)$ is the incident wave potential per unit amplitude.

To solve the finite-amplitude initial value problem, the free surface potential and elevation are represented by a spectral method and the body is modelled by the simple source distributions on the wetted hull and its negative image. The two-dimensional unsteady velocity potential is divided into three parts :

$$\tilde{\Phi}(p,t) = \phi_{fs}(p,t) + \phi_B(p,t) + \zeta_0\phi_0(p,t) \qquad (6.7)$$

where
$p = (y,z)$ is the field point.
$\phi_{fs}(p,t)$ is the contribution of the wave field alone and $\phi_{fs}(p,0) = 0$.

$\phi_B(p,t)$ is the contribution of the body source distribution.

The total effects of radiation and diffraction potential defined in Chapter 2 are equivalent to the sum of $\phi_B(p,t)$ and $\phi_S(p,t)$. However, this is not a one to one correspondence between the individual potentials.

6.2.1 Representation of the body

It will be shown from Green's theorem that the body potential $\phi_B(p,t)$ may be represented by a simple source distribution over the underwater surface of a floating body and its image. Similar technique described in Chapter 3 can be applied in here and the definition of fluid domain refers to figure 3.1. S_B is the surface of the body below the y axis. The y axis is divided into S_I interior to the body and S_F on either side. The lower half-plane, z<0, is divided into two regions: R exterior to the body and bounded by S_F, S_B and S_∞; and I interior to the body and bounded by S_I and S_B. Let the body potential in these two regions be $\phi_B^R(p,t)$ and $\phi_B^I(p,t)$.

The body potential must satisfy the impulse condition at the static waterline. Thus, the body potential, $\phi_B(p,t)$, may vanish on the free surface,

$$\phi_B(p,t)=0 \qquad p \text{ is on the } S_F \tag{6.8}$$

This condition can be satisfied by introducing an image system of negative sources in the half-plane, z>0. A two-dimensional Green's function which is defined as:

$$G(p;q) = \log(p-q) - \log(p-\bar{q}) \tag{6.9}$$

where

$p = y + iz$:field point
$q = \eta + i\zeta$:source point
$\bar{q} = \eta - i\zeta$:image source point

Based on the formulation of Green's theorem which detailed in Chapter 3, the body velocity potential in region R is represented by:

$$\int_{s_B}(\phi_B^R(q,t)\frac{\partial G(p;q)}{\partial n_q}-G(p;q)\frac{\partial \phi_B^R(q,t)}{\partial n_q})dl=\begin{Bmatrix}0\\-\pi\phi_B^R(p,t)\\-2\pi\phi_B^R(p,t)\end{Bmatrix}\quad\text{for}\quad\begin{matrix}p\notin R\\p\in S_B(t)\\p\in R\end{matrix}\qquad(6.10)$$

Also from the Green's theorem, the representations for the interior domain I can be obtained. Thus

$$\int_{s_B}(\phi_B^I(q,t)\frac{\partial G(p;q)}{\partial n_q}-G(p;q)\frac{\partial \phi_B^I(q,t)}{\partial n_q})dl=\begin{Bmatrix}0\\\pi\phi_B^I(p,t)\\2\pi\phi_B^I(p,t)\end{Bmatrix}\quad\text{for}\quad\begin{matrix}p\notin I\\p\in S_B(t)\\p\in I\end{matrix}\qquad(6.11)$$

Then from (6.10) and (6.11)

$$2\pi\phi_B^R(p,t)=\int_{s_B}(\phi_B^I(q,t)-\phi_B^R(q,t))\frac{\partial G(p;q)}{\partial n_q}dl+\int_{S_B}(\frac{\partial \phi_B^R(q,t)}{\partial n_q}-\frac{\partial \phi_B^I(q,t)}{\partial n_q})G(p;q)dl\qquad\text{for } p \text{ in R, on } S_B(t)\qquad(6.12)$$

Similarly,

$$2\pi\phi_B^I(p,t)=\int_{s_B}(\phi_B^I(q,t)-\phi_B^R(q,t))\frac{\partial G(p;q)}{\partial n_q}dl+\int_{s_B}(\frac{\partial \phi_B^R(q,t)}{\partial n_q}-\frac{\partial \phi_B^I(q,t)}{\partial n_q})G(p;q)dl\qquad\text{for } p \text{ in I}\qquad(6.13)$$

Thus, the potential over the entire lower half-plane is equivalent to a source distribution over S_B and a dipole distribution over S_B. Then

$$\mu(q,t)=\phi_B^I(q,t)-\phi_B^R(q,t)\qquad(6.14)$$

$$\sigma(q,t)=\frac{\partial \phi_B^R(q,t)}{\partial n_q}-\frac{\partial \phi_B^I(q,t)}{\partial n_q}\qquad(6.15)$$

where $\mu(q,t)$ and $\sigma(q,t)$ can be interpreted as the dipole strength and the source strength respectively. The most common assumption is that the potential is continuous across the body. It can be specified that

$$\phi_B^R(p,t)=\phi_B^I(p,t)\qquad\text{for } p \text{ on } S_B(t)\qquad(6.16)$$

This is equivalent to a source distribution of strength $\sigma(q,t)$ along S_B and its image is represented by Green's function defined in equation (6.9). The body component of the potential is of the form :

$$2\pi\phi_B(p,t) = \int_{S_B} \sigma(q,t)G(p;q)dl \qquad (6.17)$$

If we apply the body boundary condition in equation (6.4), then

$$\frac{\partial\phi_B}{\partial n_p} = -\frac{\partial(\phi_{fs}+\zeta_0\phi_0)}{\partial n_p} + \vec{V}_s \cdot n_p \qquad (6.18)$$

where

$$\vec{V}_s = (\dot{y}0(t), \dot{z}0(t)) + \dot{\theta}(t) \times (y_s(t) - y0(t), z_s(t) - z0(t))$$

The position of the body in space is defined by the coordinates of an origin fixed in the body $(y0(t), z0(t))$ and $\theta(t)$, the angle of rotation about the origin. $(y_s(t), z_s(t))$ is a point on the body surface.

The normal derivative of ϕ_B is with respect to the field point p and let the field point lie on the contour S_B. Then we get

$$\pi\sigma(p,t) + \int_{S_B} \sigma(q,t)\frac{\partial G(p;q)}{\partial n_p}dl = 2\pi\frac{\partial\phi_B(p,t)}{\partial n_p} \qquad \text{for } p \text{ on } S_B \qquad (6.19)$$

The first term in the left hand side of equation (6.19) ensures the isolation of singularity.

The numerical solution to the body problem posed involves first the determination of the source strength function $\sigma(q,t)$. Once the $\sigma(q,t)$ is known the velocity potential ϕ_B at any point in the fluid domain may be determined from equation (6.17).

For the large amplitude motion simulations, the portion of body surface under the static waterline at each time step is automatically divided into finite line segments. The body is represented by the simple source distribution on its surface with strength constant over each line segment and steady over each time step. The time interval Δt is made sufficiently small so that the body motion can be assumed impulsive. Any displacement of the body over a time interval is neglected.

6.2.2 Representation of the wave field

The representation of wave elevation field and its velocity potential by their spectral components allows the linearised free surface boundary conditions to be applied easily when adapting the free surface component of the flow into motion problem. It also aids to compute free surface induced pressures and velocities on the hull. The free surface $\zeta(y,t)$ can be described by

$$z-\zeta(y,t)=0 \tag{6.20}$$

The wave elevation $\zeta(y,t)$ and potential $\phi_{fs}(y,z,t)$ satisfy the kinematic and dynamic linearised free surface condition at z=0

$$\frac{\partial\zeta(y,t)}{\partial t}=\frac{\partial\phi_{fs}(y,0,t)}{\partial z} \tag{6.21}$$

$$\frac{\partial\phi_{fs}(y,0,t)}{\partial t}=-g\zeta(y,t) \tag{6.22}$$

where g denotes the acceleration of gravity. An arbitrary real continuous function $\zeta(y,t)$ defined over the z=0 plane can be written in the form

$$\zeta(y,t)=\int_0^\infty A(k,t)e^{iky}dk \tag{6.23}$$

where $A(k,t)$ is a complex vector which is a function of the wave number, k, and time, t, The elevation $\zeta(y,t)$ is taken to be the real part of the expression on the right hand side. It may be represented numerically by a finite summation of harmonics

$$\zeta(y,t)\equiv\sum_{n=1}^{n_w}A_n(t)e^{ik_ny}\Delta k_n \tag{6.24}$$

where k_n is the discrete wave number. This finite summation is an approximation to an infinite integral with an error which vanishes as the wave spacing Δk_n approaches zero and the maximum wave number k_{n_w}, which corresponds to the shortest wave length, approaches infinity.

Similarly if $\dot{\zeta}(y,t)$ is defined as the time derivative of $\zeta(y,t)$ due to free surface effects alone, that is the rate of change of $\zeta(y,t)$ in the absence of the hull, it may be

represented numerically by

$$\dot{\zeta}(y,t) \equiv \sum_{n=1}^{n_w} B_n(t)\omega_n e^{ik_n y}\Delta k_n \tag{6.25}$$

where ω_n is the discrete wave frequency and is defined by

$$\omega_n^2 = gk_n \tag{6.26}$$

The free surface potential can be derived :

$$\begin{aligned}\phi_{fs}(y,z,t) &= g\int_0^{\infty} B(k,t)\omega_n^{-1} e^{k(z+iy)}dk \\ &\equiv g\sum_{n=1}^{n_w} B_n(t)\omega_n^{-1} e^{k_n(z+iy)}\Delta k_n \end{aligned} \tag{6.27}$$

The distribution of values of k_n where $A_n(t)$ and $B_n(t)$ are specified is critical. The number of wave harmonics should be kept to minimum for practical computational time but the representation of wave field must be retained over the fluid boundaries and time interval of simulation.

The body and the free surface flow are assumed to be located in the neighbourhood of the origin of y-axis. It is assumed that the free surface components of the flow are periodic in space with periodic lengths $2\pi \cdot L_m$ in the y direction and periodic in time with a period of $2\pi \cdot T$. Then, the continuous form of k will be replaced by the discrete values :

$$k_n = n / L_m \qquad \text{n=1,2,3...} \tag{6.28}$$

$$k_n = \frac{n^2}{gT^2} \qquad \text{n=1,2,3...} \tag{6.29}$$

where L_m is the maximum distance from y-axis; T is the maximum time interval of simulation.

In the present case of a transient disturbance in an unbounded basin, the spacing of the discrete wave numbers and frequencies should be sufficiently small so that in the region of interest the wave field can be represented by a finite sum of harmonics. The wave lengths shorter than some minimum may be ignored in the numerical

representation. Equations (6.28) and (6.29) are applied in obtaining a k_n distribution satisfying the following requirements and the free surface flow representation must be valid :

(1) The maximum step sizes for k_n

$$k_{n+1} - k_n \leq L_m^{-1} \tag{6.30}$$

(2) The minimum upper bounds for k_n

$$k_n \geq l^{-1} \tag{6.31}$$

where l is the minimum characteristic length.

Then, the k_n can be defined as

$$k_n = \frac{n^2}{gT^2}, n = 1, \ldots n_B \tag{6.32}$$

$$k_n = k_{n-1} + L_m^{-1}, n = n_{B+1}, \ldots n_w \tag{6.33}$$

From equations (6.30) and (6.31), n_B and n_w can be determined :

$$n_{B+1}^2 - n_B^2 \geq \frac{gT^2}{L_m} \tag{6.34}$$

$$n_w^2 \geq \frac{gT^2}{l} \tag{6.35}$$

The actual choice of these three parameters L_m, T and l must be based on an understanding of the problem and the desired results. For general transient problems, L_m and l should depend on body dimensions. The free surface is represented by a pair of complex vectors, $A_n(t)$ and $B_n(t)$. The linearised free surface boundary conditions (6.21) and (6.22) can then be expressed by n_w pairs of simple differential equations by $A_n(t)$ and $B_n(t)$.

Compared with the physical representation of the free surface, the spectral representations show some advantages. One is that the wave spacing can be non-uniform with smaller spacing at the low wave numbers which correspond to the long

wave lengths. This increases the time interval of reflecting disturbance produced by the boundary over which the long wave lengths and therefore the solution remains valid. In a physical representation these long wave lengths are the first reflected from the boundary since they propagate the fastest. In addition, small body motion is a sufficient but not a necessary condition for a valid linearised free surface. The linear approximation can remain valid, if the body moves slowly, over large changes in the geometry of the submerged portion of the body which induce hydrostatic and hydrodynamic nonlinearities.

6.2.3 Body effect on the wave field

The transient problem is solved numerically by a series of small time steps. The wave field, as defined by the vectors $A_n(t)$ and $B_n(t)$ are available only for the current time step. When time is advanced from t to $t+\Delta t$, these vectors are updated as

$$A_n(t+\Delta t) = A_n(t)\cos(\omega_n \Delta t) + B_n(t)\sin(\omega_n \Delta t) + \Delta A_n^{Body} \tag{6.36}$$

$$B_n(t+\Delta t) = B_n(t)\cos(\omega_n \Delta t) - A_n(t)\sin(\omega_n \Delta t) \tag{6.37}$$

The terms of ΔA_n^{Body} are the contribution to the wave field from the body motion between t and $t+\Delta t$. The $B_n(t)$ vector represents the free surface potential and is changed a negligibly small amount over the time interval if Δt is sufficiently small.

The presence of the body induces a vertical velocity at the free surface which is included in the kinematic boundary condition through D(k,t) which represents the time rate of change in $A_n(t)$. The complex function D(k,t) can be obtained by expressing $\partial\phi_B / \partial z$ evaluated at the free surface in the integral form,

$$\left.\frac{\partial \phi_B}{\partial z}\right|_{z=0} = \mathrm{Re}\left\{\int_0^\infty D(k,t)e^{kiy}dk\right\} \tag{6.38}$$

For a simple source located at (y_B, z_B) and its negative image, the time rate of change of the elevation induced by the simple source is :

$$\left.\frac{\partial \phi_B}{\partial z}\right|_{z=0} = -2z_B / (z_B^2 + (y-y_B)^2) \tag{6.39}$$

and it can be expressed in the form as :

$$D(k,t) = 2e^{k(z_B - iy_B)} \tag{6.40}$$

Then integrating over the hull contour,

$$D(k,t) = 2\int_{S_B(t)} \frac{\sigma(q,t)}{2\pi} e^{k(z_B(t) - iy_B(t))} dl \tag{6.41}$$

where $\sigma(q,t)$ is the source strength which can be determined by the equation (6.19).

The change in $A_n(t)$ induced by the existence of body between t and $t+\Delta t$ may be represented in the form of the harmonics of ΔA_n^{Body}. From equations (6.21), (6.24) and (6.38), the change of the elevation induced by the body can be expressed as :

$$\Delta A_n^{Body} = D(k_n,t)\cdot \Delta t \tag{6.42}$$

6.2.4 Computation of hydrodynamic forces

The total hydrodynamic forces and moments are computed as follow :

$$F_i = -\iint_{S_B(t)} P n_j ds \tag{6.43}$$

From the Bernoulli's equation, the hydrodynamic pressure related to the free surface and body-induced velocity potential can be found in the translating coordinate system:

$$P = -\rho\left(\frac{\partial(\phi_{fs} + \zeta_0\phi_0)}{\partial t} + \frac{\partial\phi_B}{\partial t} + \frac{1}{2}(\vec{V}_B + \vec{V}_{fs})^2\right) \tag{6.44}$$

where

$$\vec{V}_B = \nabla\phi_B \tag{6.45}$$

$$\vec{V}_{fs} = \nabla(\phi_{fs} + \zeta_0\phi_0) \tag{6.46}$$

This pressure can be written with respect to the body-fixed frame as:

$$P = -\rho\left(\frac{D(\phi_{fs} + \zeta_0\phi_0)}{Dt} + \frac{D\phi_B}{Dt} - \frac{1}{2}(\vec{V}_s^2 - (\vec{V}_B + \vec{V}_{fs} - \vec{V}_s)^2)\right) \tag{6.47}$$

where $\frac{D}{Dt} = \frac{\partial}{\partial t} + \vec{V}_s \bullet \nabla$ denotes the time derivative in the body-fixed system. The pressure components due to the free surface and body are defined as:

$$p_{fs} = -\rho\frac{D(\phi_{fs} + \zeta_0\phi_0)}{Dt} \tag{6.48}$$

$$p_{BD} = -\rho\frac{D\phi_B}{Dt} \tag{6.49}$$

The body-induced pressure p_{BD} represents the time derivative of the potential at a body-fixed coordinate system. If the line segment of body remains submerged, it is unchanged in the body fixed system. Thus, the body fixed time derivative is then approximated by

$$\frac{D\phi_B(t_n)}{Dt} = \frac{\phi_B(t_n) - \phi_B(t_{n-1})}{t_n - t_{n-1}} \tag{6.50}$$

If the line segment has just been submerged over the latest time step so that Δt is not defined, then the time interval Δt^* since the midpoint passed the waterline is estimated from the depth and vertical velocity. The body-fixed time derivative is then approximated by:

$$\frac{D\phi_B(t_n)}{Dt} = \frac{\phi_B(t_n)}{\Delta t^*} \tag{6.51}$$

The calculation of quadratic term in equation (6.47) requires the tangential velocity induced by the body potential. Substitution of the nonlinear pressure shown in equation (6.47) into equation (6.43), the nonlinear hydrodynamic forces and moments can be obtained at each time step.

6.3 The radiation problem of two-dimensional bodies

Through the Fourier transform technique, the time domain method can be applied to investigate the linearised radiation problem which has been well developed in the

frequency domain. In this section, a transient response method has been used. Compared with the frequency domain method, the time domain technique is useful and effective in the reduction of total computation time with good accuracy. The numerical calculations were carried out with a submerged circular cylinder and a floating rectangle in the small amplitude motion region and were compared with those obtained from the published analytical theory and experimental data.

6.3.1 Relations between time- and frequency- domain descriptions

The general form for the hydrodynamic force vector, F(t), is generated by a vertical velocity, V(t), in the captive mode :

$$\vec{V}_S \bullet \vec{n} = V(t) n_3 \qquad t \geq 0 \qquad (6.52)$$

The solution of vertical force is the sum of an impulsive force induced by the hydrodynamic mass and the memory effects resulting from the free surface (Cummins, 1962; Wehausen, 1967; Chapman, 1981):

$$F(t) = F_{imp}\dot{V}(t) + \int_{-\infty}^{t} K(t-\tau)V(\tau)d\tau \qquad (6.53)$$

The constant vertical velocity $V(t)$ is chosen to be small to eliminate nonlinear effects for solving the linear radiation problem. Then, the resulting vertical force excluding the hydrostatic component is proportional to $V(t)$.

If the vertical velocity is further specified as a unit step function as follow :

$$\begin{aligned} V(t) &= 0 && t < 0 \\ V(t) &= -H(t) && t \geq 0 \end{aligned} \qquad (6.54)$$

for which the solution is

$$F(t) = -(F_{imp}\delta(t) + f(t)) \qquad (6.55)$$

where $\delta(t)$ is the Dirac delta function. The function $f(t)$ calculated in the captive mode is shown in figures 6.2 and 6.6 and can be represented by :

$$f(t) = \int_{0^+}^{\infty} K(\tau) d\tau \qquad t > 0 \qquad (6.56)$$

and the F_{imp} is defined by

$$F_{imp} = \rho \int_{s_B} dl \phi_B(p; 0^+) n_3(p) \qquad (6.57)$$

For the harmonic case,

$$\vec{V}_S \bullet \vec{n} = \cos(\omega t) n_3 \qquad (6.58)$$

Then, the force acting in the vertical direction is given by

$$F(t) = -\omega \sin(\omega t) F_{imp} - \int_{0^+}^{\infty} f(\tau) \omega \sin(\omega(t-\tau)) d\tau$$

$$= -\omega \sin(\omega t)[F_{imp} + \int_{0^+}^{\infty} f(\tau) \cos(\omega\tau) d\tau] + \omega \cos(\omega t)[\int_{0^+}^{\infty} f(\tau) \sin(\omega\tau) d\tau] \qquad (6.59)$$

The hydrodynamic force defined in the frequency domain for the harmonic motion is represented as :

$$F(t) = A_{33} \omega \sin(\omega t) - B_{33} \omega \cos(\omega t) \qquad (6.60)$$

Therefore,

$$\text{Added mass: } A_{33}(\omega_n) = -\left[F_{imp} + \int_{0^+}^{\infty} f(\tau) \cos(\omega_n \tau) d\tau \right] \qquad (6.61)$$

$$\text{Damping: } B_{33}(\omega_n) = -\left[\omega_n \int_{0^+}^{\infty} f(\tau) \sin(\omega_n \tau) d\tau \right] \qquad (6.62)$$

For fully linear problems at constant or zero forward speed, the time domain and frequency domain solutions are related by the Fourier transforms as shown in equations (6.61) and (6.62). However, if the body boundary condition is not applied on the mean position, the result is a kind of time-variant nonlinear system and the frequency and time domains are no longer simply related.

6.3.2 The radiation problem for a submerged circular cylinder in deep water

In order to validate the numerical method, an analytical solution given by Ogilvie(1963) of a fully submerged circular cylinder was compared with linear and nonlinear time domain analysis.

The linear time domain analysis is based on the acceleration body boundary condition in which the underwater body shape is fixed to solve the radiation problem. A computational advantage of the linear time domain analysis is that the coefficient matrix used to numerically solve the integral equation needs only be inverted once for a fixed underwater geometry. In the frequency domain calculation, the matrix must be inverted at each frequency. For a very large number of unknowns this leads to a large saving in computer time. The disadvantage of time domain analysis is that the solution must be time-stepped , which requires more computer time and memory than the frequency domain technique.

Using the acceleration body boundary condition, the time derivative of source strength, $\dot{\sigma}(p,t)$, relative to the body-fixed coordinate system is computed at the beginning of each time step from

$$\pi\dot{\sigma}(p,t)+\int_{s_B}\dot{\sigma}(q,t)\frac{\partial G(p;q)}{\partial n}dl=2\pi(-\bar{a}_{fs}\bullet\bar{n}+\bar{a}_s\bullet\bar{n}) \tag{6.63}$$

where $\bar{a}_{fs}$ is the free-surface induced acceleration which can be calculated from equation (6.27) at each time step. The $\bar{a}_s$ is the body acceleration at the body-fixed coordinate system. The source strength can be computed adequately by integrating its derivative in time:

$$\sigma(t+\Delta t)\cong\sigma(t)+\Delta t\dot{\sigma}(t) \tag{6.64}$$

Once the source strength $\sigma(t+\Delta t)$ is determined, the body velocity potential ϕ_B and free surface potential ϕ_{fs} can be obtained from equations (6.17) and (6.27) respectively.

Numerical computations were carried out for the submerged circular cylinder at **h/a**=2.0 where **h** is the non-dimensional distance from centre point of cylinder to the mean free surface and **a** is the radius of a unit circle. In this calculation, the parameters of transient problem were taken as: $L_m=4.0; l=0.2; T=26$ and $\Delta t=0.01$. Figure 6.2 shows the vertical transient forces calculated by the linear and nonlinear method in the

time domain. Both linear and nonlinear impulse forces F_{imp} are equal to -2.819651. The non-dimensional added mass and damping coefficients in heave mode are shown in figures 6.3 and 6.4 as a function of ka where k is the wave number. Excellent agreement is found with values measured from the curves of Ogilvie's (1963) analytical solutions.

In the nonlinear time domain method, the body boundary condition is satisfied on the instantaneous wetted surface of the body, while the linearised free surface boundary condition is retained. Therefore, this numerical method can provide more accurate predictions when the large amplitude motion responses occur.

6.3.3 The forced motions of a floating rectangle

The hydrodynamic forces acting on a floating rectangle in the captive mode were calculated by using the nonlinear time domain method. This rectangle has a non-dimensional width of 2.0, a height of 1.0 and a draught 0.5 as shown in figure 6.5. The parameters of transient problem defined in section 6.2.2 were chosen as: $L_m = 2.5; l = 0.25; T = 26$ and $\Delta t = 0.01$. Figure 6.6 is the vertical force induced by the velocity step function in the time history. The impulse force F_{imp} is equal to -2.1109 when twenty body segments are used. Figures 6.7 and 6.8 show the non-dimensional added mass and radiation damping curves as a function of non-dimensional wave frequencies. The numerical predictions were compared with the experimental results published by Vugts (1968). There are some discrepancies observed between the numerical calculations obtained from the transient theory and published experimental measurements. Generally speaking, better predictions are found in added mass curve than in damping curve. The numerical results show a slight overprediction of the damping coefficients for the forced heave motions of a floating rectangle. Some deviations are observed in the hydrodynamic coefficient curves at high frequency region as shown in figures 6.7 and 6.8. In the time histories of the vertical force induced by the velocity step function, an unsteady oscillating curve has been found after time=8 as shown in figure 6.6. Such numerical instability was not reported by Chapman (1979) in the calculation of the same forced motions of the floating rectangle. However, the irregular frequencies have been observed in the linear frequency domain calculation as well as in the time domain analysis by Adachi & Ohmatsu (1979) and Beck & Liapis (1987) in the solutions of the motion problem of floating bodies by using the Green function method. The irregular frequencies are a set of discrete frequencies at which the numerical solutions are singular. Recalling that

Fourier transform of a sinusoidal wave in the time domain is the Delta function in the frequency domain. The discrepancies observed in this study may be as results of the irregular frequencies in calculating the motion of a floating body.

6.4 Conclusions

Based on the slender body approximation, the three-dimensional boundary value problem has been reduced to a set of two-dimensional initial value problem. A nonlinear method for solving the transient motion problem of two-dimensional bodies has been formulated. The free surface is linearised but the exact body boundary condition permits large amplitude motions.

The combined simple body source and spectral representations of the free surface have been applied to solve the transient motion problem instead of using the time domain Green function technique. This novel treatment for studying such unsteady free surface problems is first proposed by Chapman (1979). The free surface potential which satisfies linearised free surface condition can be approximated in deep water by a finite summation of harmonics. The careful choice of wave number and frequency distribution has been presented in order to minimise the computational time but still retain the representation of wave field. In this way, an initial value problem can be advanced in small time steps and solved by using the impulse theory.

In the preliminary research stage, the nonlinear numerical model has been validated by the results of linear hydrodynamic coefficients of two-dimensional bodies obtained from the published theoretical and experimental data. The relations between time- and frequency- domain results are related through the Fourier transform technique in the case of linear theory. For a submerged circular cylinder, the numerical calculations for hydrodynamic coefficients in heave mode are in very good agreement with the analytical solutions given by Ogilvie (1963). There are some numerical difficulties occurred in predicting the hydrodynamic forces of the forced motions of the floating rectangle. Some unsteady oscillations of the vertical forces have been observed in the time histories. The numerical calculations for the radiation damping coefficients are higher than the experimental measurements reported by Vugts (1968).

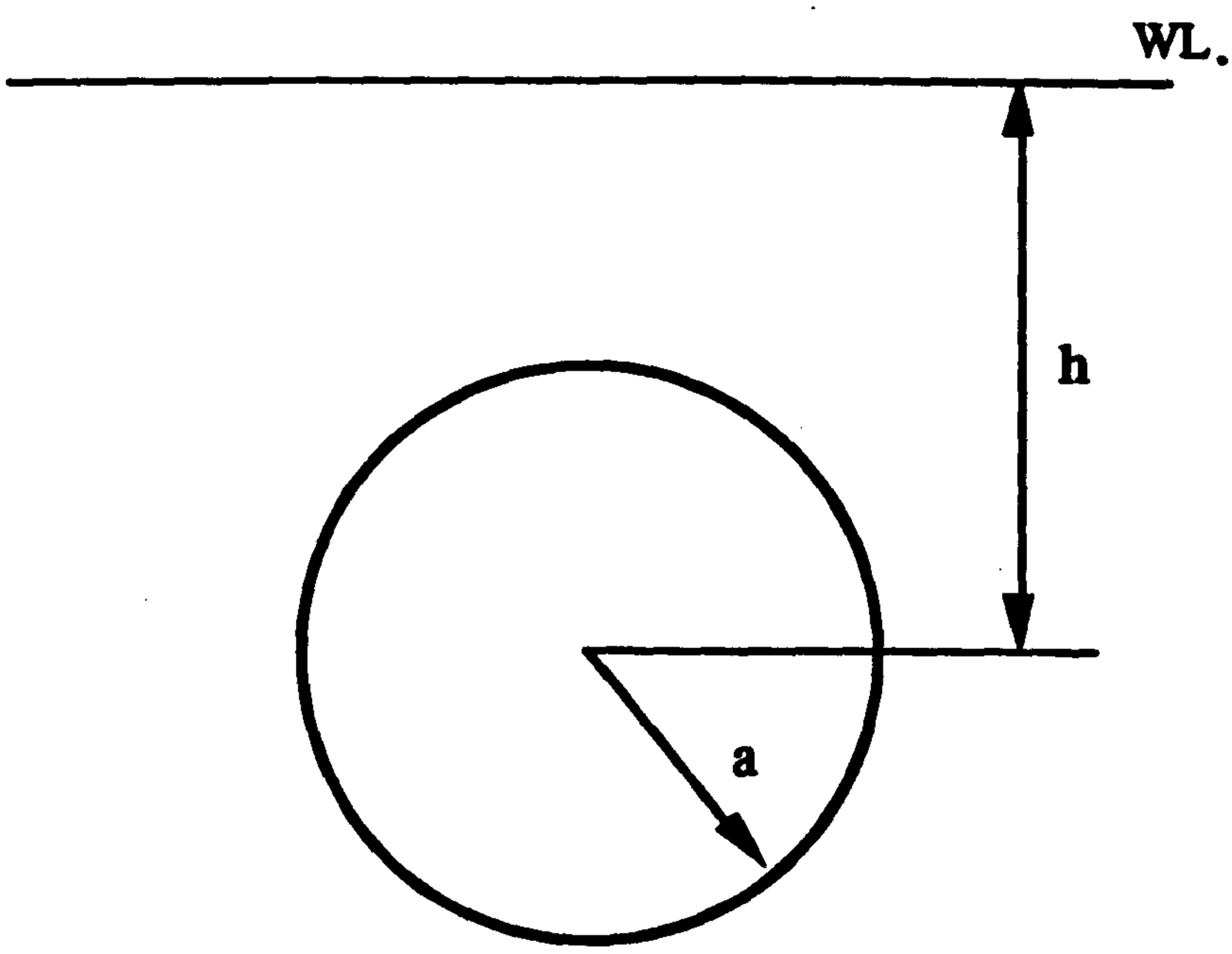

Figure 6.1: Sketch of a circular cylinder

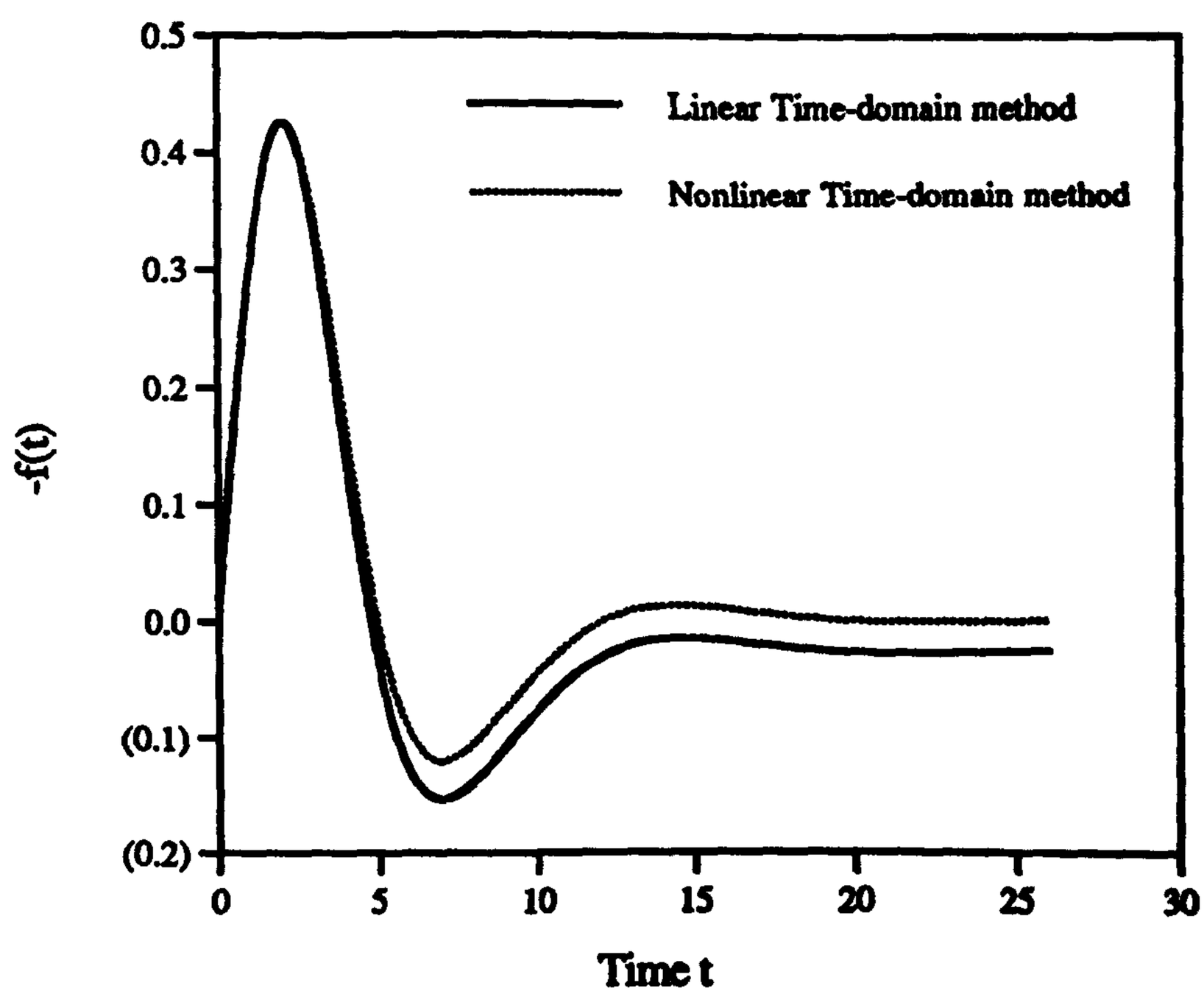

Figure 6.2: Vertical force induced by the velocity step function for a submerged circular cylinder

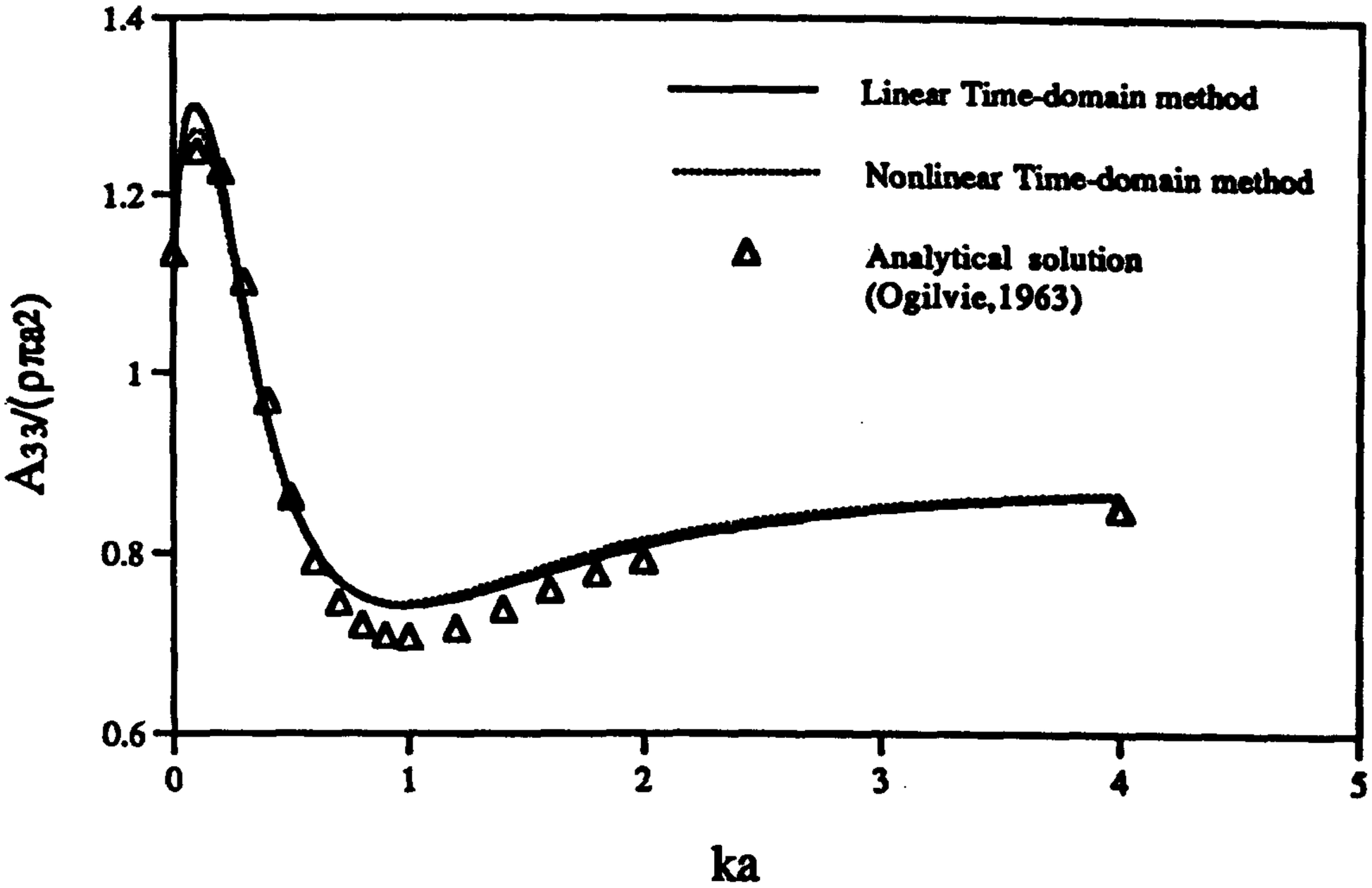

Figure 6.3: Heave added mass for a submerged circular cylinder (h/a=2.0)

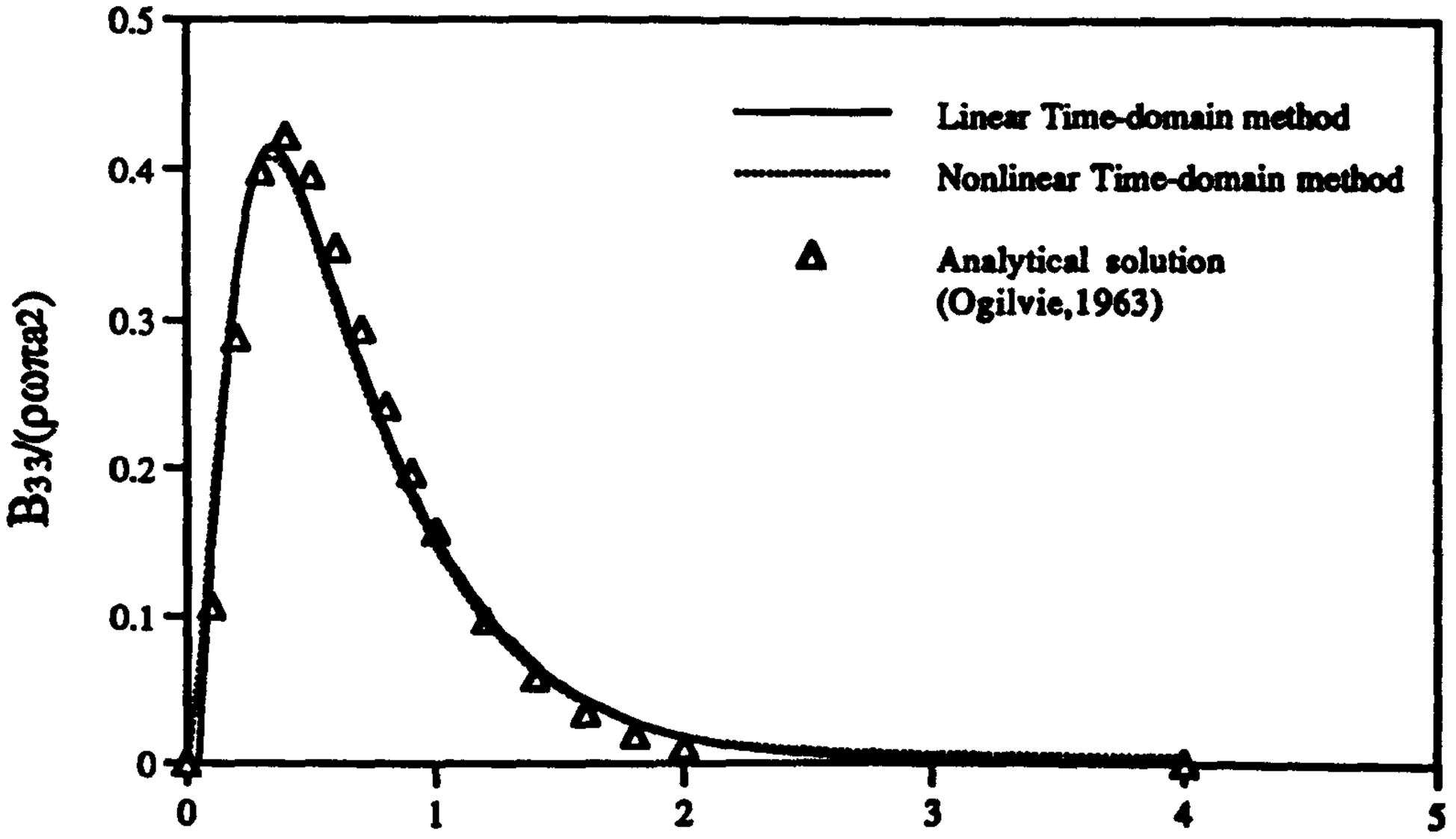

Figure 6.4: Heave radiation damping for a submerged circular cylinder (h/a=2.0)

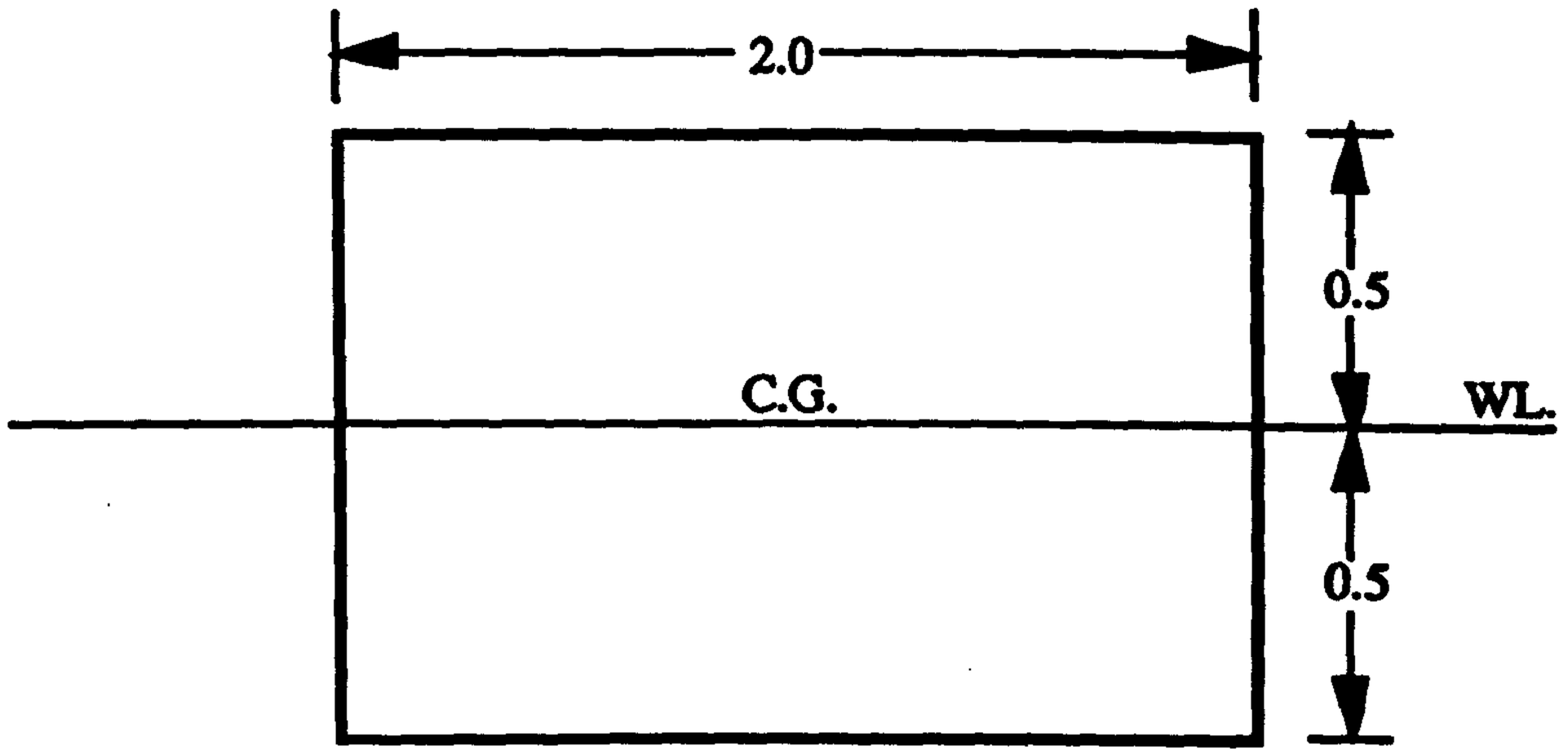

Figure 6.5: Sketch of a floating rectangle

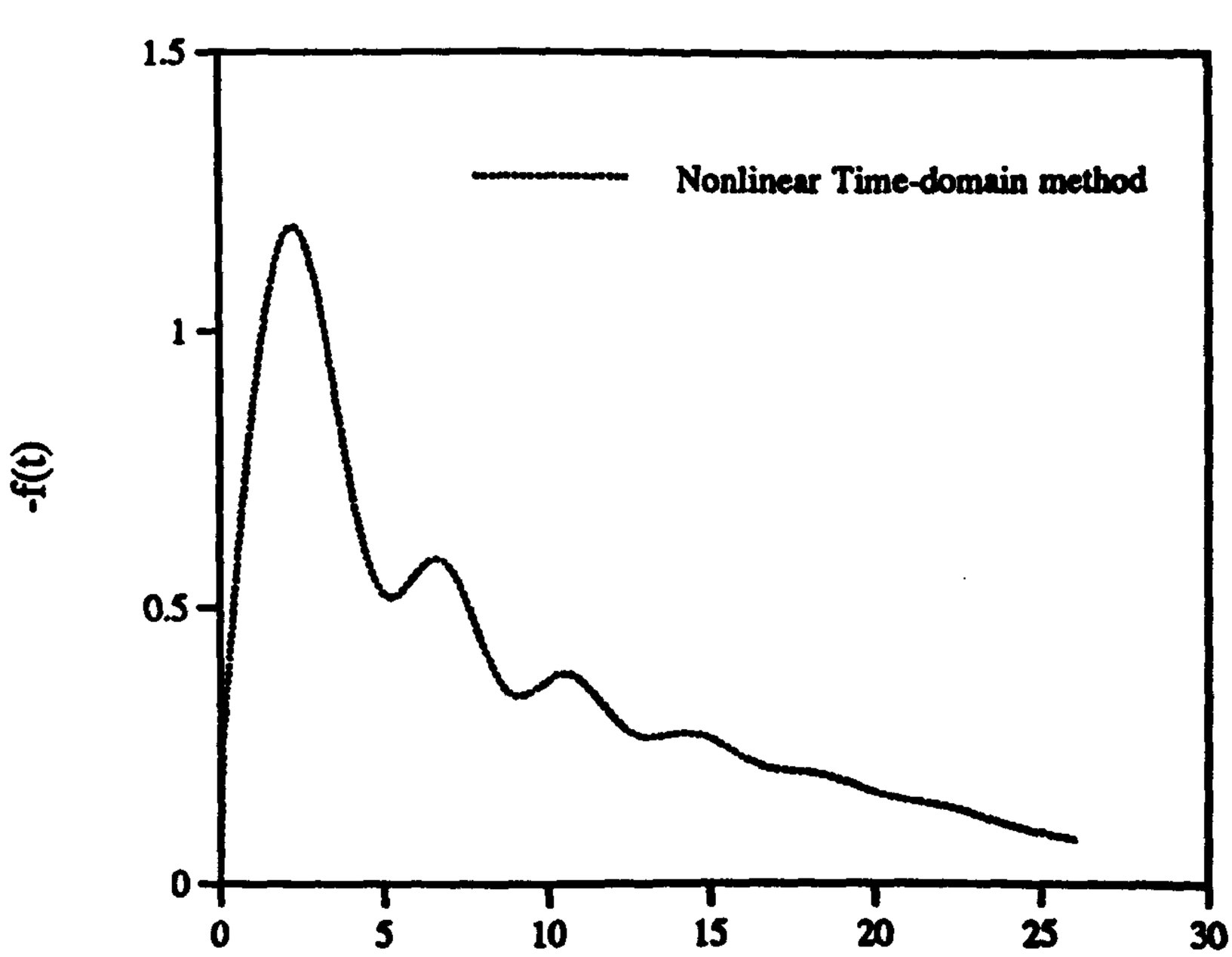

Figure 6.6: Vertical force induced by the velocity step function for a floating rectangle

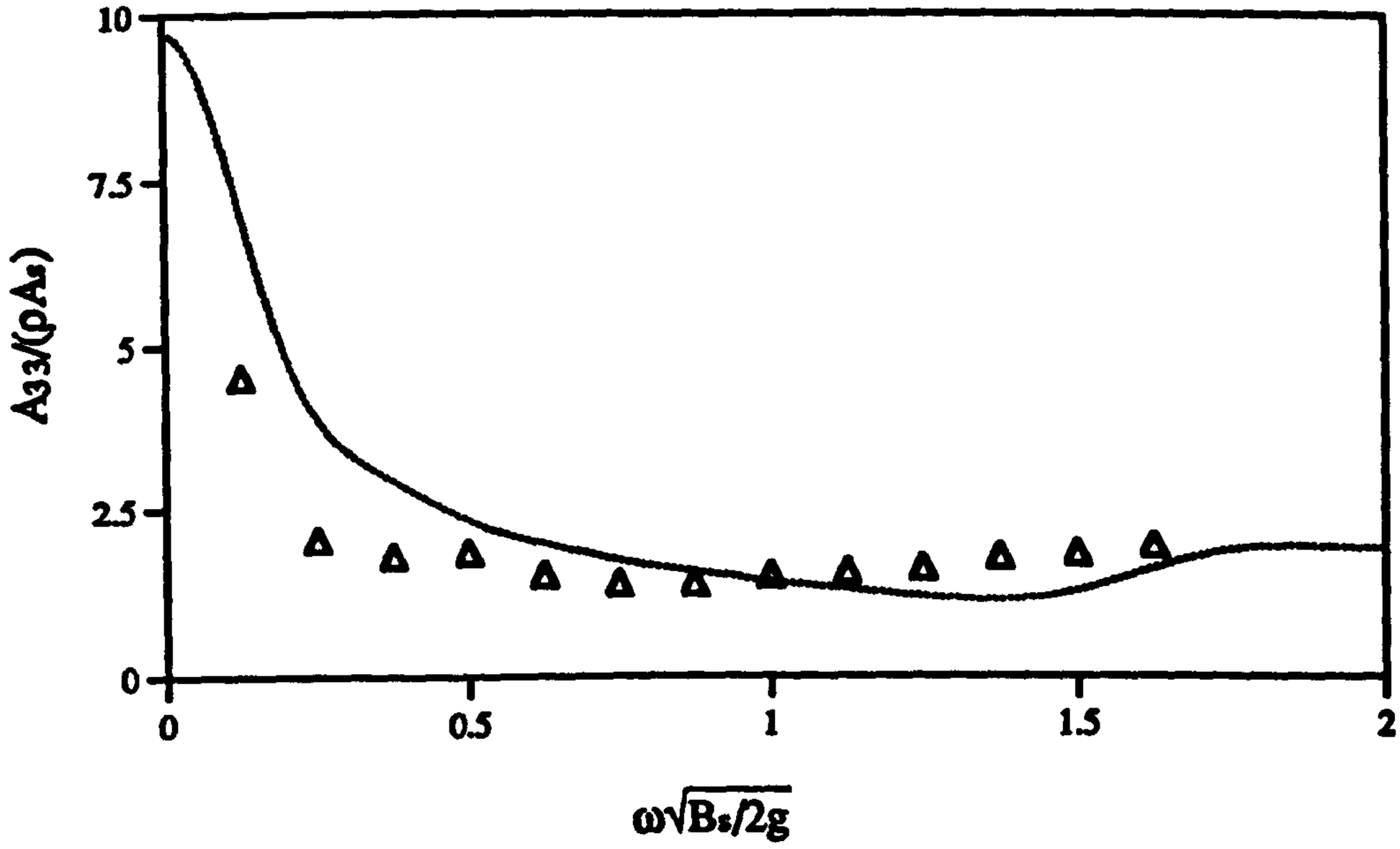

Figure 6.7: Added mass coeffiecient of a floating rectangle in heaving

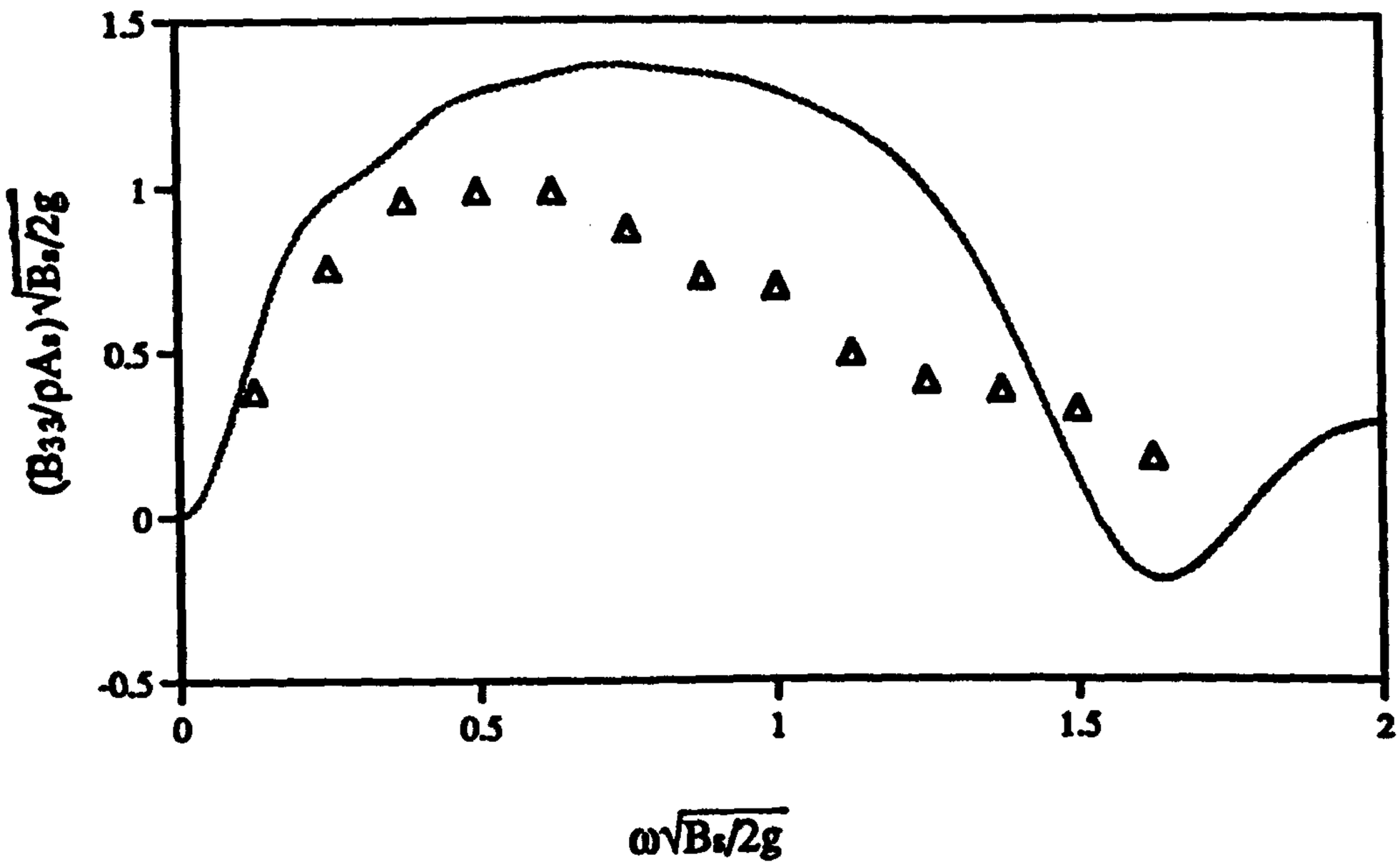

Figure 6.8: Damping coeffiecient of a floating rectangle in heaving

CHAPTER 7
CONCLUDING REMARKS

A theoretical formulation for the motion problem of a catamaran travelling in waves has been presented. The solution of the governing equation is determined by the initial-boundary conditions of the potential flow. The nonlinear free surface condition and the body boundary condition on an unsteady body surface make the problem unamenable to obtain analytical or numerical solutions. By using the perturbation analysis, these two conditions can be transformed from the exact surfaces to the undisturbed free surface and mean wetted body surface. Assuming that the steady perturbation potential can be neglected in the linearised free surface condition for the unsteady flow, a linearised free surface condition can be defined in terms of the forward speed and the frequency of oscillation. If the body is thin and slender or the mean forward speed is low, the linearised body boundary condition is reduced to a simple forward speed correction on the pitch and yaw motions. In order to solve the arbitrary motions, the position and velocity of the system must be specified for the initial value problem. If the motion of a body is considered in the steady-state oscillation, the initial-boundary value problem is further simplified to the boundary value problem because all transients will die out.

The small amplitude motion problem of catamarans in waves has been formulated in the frequency domain by means of the two-dimensional Green function integral equation method. Based on the assumptions of slender body and high frequency oscillatory motions, the unsteady velocity potential due to incident, diffracted and radiated wave systems have been represented by distributing the two-dimensional pulsating sources along the underwater surface of a floating body and its image. Numerical computations for three catamarans (ASR5061, Marintek and V-1 catamarans) travelling in the oblique waves have been carried out to compare with experimental measurements. The numerical predictions and experimental data at the low forward speed region correlated well. When the forward speed increases, the numerical results gave a gross overprediction of the motion responses at the resonance frequencies and the theoretically predicted position of resonance was slightly higher than the values obtained from experimental measurements. Generally better predictions were obtained in heave motions than in pitch motions when the linear frequency domain technique was used. In the case of V-1 catamaran, the negative added mass and a set of discrete characteristic frequencies due to the effects of interaction between twin hulls have been observed in the calculated hydrodynamic coefficient curves. The calculated cross coupled hydrodynamic coefficients well satisfied the Timman-

Newman's (1962) symmetry relationships at the zero speed condition. Through the theoretical and experimental investigations, it became clear that the resonance positions of motion response curves in heave and pitch modes shift toward the lower wave frequency region and the magnitudes of motion responses at resonance frequencies increase when the forward speed increases.

A nonlinear strip method has been developed to predict the large amplitude motions of catamarans in regular waves. In the method, it is inherently assumed that the motion response is a kind of steady-state oscillation. The time-varying hydrodynamic forces are retrieved from a hydrodynamic database which is generated by using the linear frequency domain technique. The large variation of hydrodynamic coefficient curves has been observed in the shallow draught region for the V-1 catamaran. The coupled equations of motion for heave and pitch modes have been solved in the time domain by using the Runge-Kutta method. In order to overcome the numerical divergence problem, a ramp function and results obtained from the linear frequency domain method have been introduced to initialise the system. Validation studies have been carried out by comparing the results obtained from the linear theory with those obtained from the nonlinear theory with a small incident wave amplitude. The motion amplitude and phase angle of V-1 catamaran in the head sea condition obtained from both numerical methods have a perfect match.

The nonlinear effects of large amplitude motions of the V-1 catamaran in the head sea conditions have been investigated by using the results obtained from the quasi-nonlinear time domain technique and by a series of systematical experiments carried out in the Towing Tank of the Hydrodynamics Laboratory at the University of Glasgow. A post-towing measurement system has been designed and tested. It shows that this experimental setup is a very suitable system to investigate the motion responses of fast crafts travelling in waves. Based on the comparative studies, it can be concluded that the nonlinear time domain method can provide more reasonable predictions for the large amplitude motions of catamarans than the linear frequency domain method. Generally, the theoretical results obtained from the linear frequency domain and nonlinear time domain methods show a gross overprediction of the resonance values of motion responses. It is concluded that the nonlinear effects are significant when the model speed and wave amplitudes increase. The peak values of large amplitude motions around the resonance as obtained from the nonlinear time domain predictions as well as from measurements are smaller than those obtained from the linear theory. When the large amplitude motions of V-1 catamaran occur, the positive and negative amplitudes observed from experimental measurements and

nonlinear time domain simulations are of different magnitudes in the time histories. Through the experimental observations, it can be concluded that the impact phenomena of V-1 catamaran will be significantly effected by the forward speed and incident wave amplitude. Some parametric studies on the effects caused by the nonlinear terms for the V-1 catamaran configuration have been carried out by comparing the motion time histories obtained from different numerical models. In these selected test conditions, it became clear that the nonlinear motions are controlled by the hydrodynamic coefficients and wave exciting forces in the low forward speed region and by the hydrostatic forces in the high forward speed region.

Through the slender body approximation, the three-dimensional potential flow problem has been reduced to a set of two-dimensional initial value problem. The solution of the two-dimensional transient motion problem has been constructed by means of a spectral representation for the wave field and a distribution of simple sources on the instantaneous wetted body surface. In the free surface wave field, the free surface potential which satisfies linearised free surface condition is approximated by a finite summation of harmonics. The wave field is updated by the contribution of the body motion when time is advanced. The relationships between solutions obtained from the time and frequency domain methods have been formulated by using the Fourier transform technique. The numerical computations for the fully submerged circular cylinder in deep water have been carried out by using linear and nonlinear time domain programs. Comparisons display an excellent agreement between the calculated hydrodynamic coefficients and the analytical solutions given by Ogilvie (1963). For a floating rectangle, some unsteady oscillations of the calculated vertical forces have been found in the time histories. The linear damping coefficients obtained from theoretical calculations are higher than those obtained from the experimental measurements reported by Vugts (1968).

Recommendation for future work

The quasi-nonlinear time domain technique has been shown to provide more reasonable predictions for the large amplitude motions of catamarans travelling in waves than the linear frequency domain theory. The predictions will be improved by incorporating the viscous damping into the time domain simulations. This time domain motion program has provided a good basis for further investigations regarding of slamming load, deck wetness and control fin analysis of catamarans. However, the nonlinear strip method is a kind of practical tool to investigate the large amplitude

motion problem. Although the spectral method requires more computer time and memory than the frequency domain technique, it is a powerful tool to solve the finite-amplitude initial value problem. It is very worthwhile to devote continuous efforts in this line of research. These efforts should include the elimination of the numerical instability in the case of the floating body motion solution and the predictions of the large amplitude motions of a catamaran travelling in waves by using the slender body approximation method.

REFERENCES

Adachi, H. & Ohmatsu, S. (1979)
"On the Influence of Irregular Frequencies in the Integral Equation Solutions of the Time-Dependent Free Surface Problems", Journal of Soc. Naval Arch., Japan, Vol.146, pp.119-28.

Arthur, E. K. (1988)
"Time Domain Simulation of SWATH Ship Motions", M.Sc. Thesis, Department of Naval Architecture and Ocean Engineering, University of Glasgow.

Atlar, M. (1981)
"A Study of the Frank Close-Fit Method; Theory, Application and Comparison with Other Methods", NAOE-HL-81-09, Department of Naval Architecture and Ocean Engineering, University of Glasgow.

Atlar, M. (1986)
"SWATH Wave Load Program, Method of Solution for Five Degrees of Freedom Coupled Equations of a SWATH Ship", NAOE-86-36, Department of Naval Architecture and Ocean Engineering, University of Glasgow.

Beck, R. F. (1994)
"Time-Domain Computations for Floating Bodies", Applied Ocean Research, 16, pp.267-282.

Beck, R. F. & Liapis, S. J. (1987)
"Transient Motions of Floating Bodies at Zero Forward Speed", Journal of Ship Research, Vol.31. No.3, pp.164-76.

Borresen, R. and Tellsgard, F. (1980)
"Time History Simulation of Vertical Motions and Loads on Ships in Regular, Head Waves of Large Amplitude", Norwegian Maritime Research, No.3.

Chan, H. S. (1990)
"A Three-dimensional Technique for Predicting First and Second Order Hydrodynamic Forces on a Marine Vehicle Advancing in Waves", Ph.D. Thesis, Department of Naval Architecture and Ocean Engineering, University of Glasgow, August.

Chan, H. S. (1993)
"Prediction of Motion and Wave loads of Twin-hull Ships", Marine Structures, 6, pp.75-102.

Chapman, R. B. (1975)
"Numerical Solution for Hydrodynamic Forces on a Surface - Piercing Plate Oscillating in Yaw and Sway", Proc. of the 1st International Conference on Numerical Ship Hydrodynamics, DTNSRDC, Maryland, pp.333-350.

Chapman, R. B. (1976)
"Free-Surface Effects for Yawed Surface-Piercing Plates", Journal of Ship Research, Vol.20, No.3, pp.125-136.

Chapman, R. B. (1977)
"Survey of Numerical Solutions for Ship Free-Surface Problem", Proc. of the 2nd International Conference on Numerical Ship Hydrodynamics, Berkeley, pp. 5-16.

Chapman, R. B. (1979)
"Large Amplitude Transient Motion of Two Dimensional Floating Bodies", Journal of Ship Research, Vol.23, No.1, March, pp. 20-31

Chapman, R. B. (1981)
"Time-Domain Method for Computing Forces and Moments Acting on Three-Dimensional Surface-Piercing Ship Hulls with Forward Speed", Proc. of the 3rd International Conference on Numerical Ship Hydrodynamics, Paris, pp.237-247.

Chiu, F. and Fujino, M. (1991)
"Nonlinear Prediction of Vertical Motions of a Fishing Vessel in Head Sea", Journal of Ship Research, Vol.35, No.1, pp.32-39.

Corlett, E. C. B. (1969)
"Twin Hull Ship", Quarterly Trans. of RINA, Vol.111, No.4, pp.401-438.

Cummins, W. E. (1962)
"The Impulse Response Function and Ship Motions", Schiffstechnik, 9, pp.101-9.

Elsimillawy, N. and Miller, N. S. (1986)
"Time Simulation of Ship Motions : A Guide to the Factors Degrading Dynamic Stability", Transactions of SNAME, Vol.94, pp.215-240.

Everest, J. T. (1968)
"Some Research on the Hydrodynamics of Catamarans and Multi-Hulled Vessels in Calm Water", Trans. North-East Coast Institution of Engineers and Shipbuilders, 84, pp. 129-148.

Faltinsen, O. (1977)
"Numerical Solution of Transient Nonlinear Free-Surface Motion Outside or Inside Moving Bodies", Proc. of the 2nd International Conference on Numerical Ship Hydrodynamics, Berkeley, pp. 347-357.

Faltinsen, O., Hoff, J. R., Kvalsvold, J. and Zhao, R. (1992)
"Global Loads on High-speed Catamarans", Proc. of the 5th International Symp. on Practical Design of Ships and Mobile Units", University of Newcastle-upon-Tyne, U.K., pp.1360-1373.

Fang, C. C. and Wang, C. T. (1990)
"A Preliminary Study of the Flap Effect on the Motions of Planing Boat with Variable Width in Regular waves", Journal of SNAME, R.O.C., Vol.9, No.2, pp.91-99.

Fang, C. C. (1994)
"Experimental Investigation of Large Amplitude Motions of a Catamaran in Waves", NAOE-94-15, Department of Naval Architecture and Ocean Engineering, University of Glasgow.

Fang, C. C. , Chan, H. S. and Incecik, A. (1996)
"Investigation of Motions of Catamarans in Regular Waves - 1", Ocean Engineering, Vol.23, No.1, pp.89-105.

Fang, M. C., Lee, M. L. and Lee, C. K. (1993)
"Time History Simulation of Water Shipping on Ship in Large Longitudinal Waves", Journal of Ship Research, Vol.37, No.2, pp.126-137.

Fang, M. C. and Her, S. S. (1995)
"The Nonlinear SWATH Ship Motion in Large Longitudinal Waves", International Shipbuilding Progress, Vol.42, No.431, September, pp.197-220.

Finklestein, A. (1957)
"The Initial Value Problem for Transient Water Wave", Communications on Pure and Applied Mathematics., Vol.10, pp 511-522.

Frank, W. (1967)
"On the Oscillation of Cylinders In or Below the Free Surface of Deep Fluids", NSRDC, Report 2375, October.

Froude, W. (1861)
"On the Rolling of Ships", Transactions of INA, Vol.2, pp.180-229.

Fridsma, G. (1969)
"A Systematic Study of the Rough-Water Performance of Planing Boats", Davidson Lab. SIT Rept. R-1275.

Fujino, M. and Yoon, B. S. (1986)
"A Practical Method of Estimating Ship Motions and Wave Loads in Large Amplitude Waves" , International Shipbuilding Progress, Vol.33, No.385, pp.159-172.

Greenhow, M. (1987)
"Wedge Entry into Initially Calm Water", Applied Ocean Research, Vol.9, No.4, pp.214-223.

Hadler, J., B., Lee, C. M., Birmingham, J., T. and Jones, H. D. (1974)
"Ocean Catamaran Seakeeping Design, Based on the Experiences of USNS Hayes", Transactions of SNAME, Vol.82, pp.126-161.

Haskind, M. D. (1946)
"The Hydrodynamic Theory of Heaving and Pitching of a Ship", Translated in SNAME Tech. & Res. Bull. No.1-12, 1953.

Hudson, D. A., Price, W. G. and Temarel, P. (1995)
"Seakeeping Performance of High Speed Displacement Craft", Proc. of the 3rd International Conference on Fast Sea Transportation, Lubeck-Travemunde, Germany,September. pp.877-892.

Incecik, A., Morrison, B. F. and Rodgers, A.J. (1991)
"Experimental Investigation of Resistance and Seakeeping Characteristics of a Catamaran Design", Proc. of the 1st International Conference on Fast Sea Transportation, Norway, pp.239-258.

Insel, M. and Molland, A. F. (1991)
"An Investigation into the Resistance Components of High Speed Displacement Catamarans", Transactions of RINA, pp.1-20.

Kim, C. H., Chou, F. S. and Tien, D. (1980)
"Motions and Hydrodynamic Loads of a Ship Advancing in Oblique Waves", Transactions of SNAME, Vol.88, pp.225-256.

Korvin-Kroukovsky, B., V. (1955)
"Investigation of Ship Motions in Regular Waves", Transactions of SNAME, Vol.63, pp. 386-435.

Kring, D. and Sclavounos, P. D. (1991)
"A New Method for Analyzing the Seakeeping of Multi-Hull Ships",Proc. of the 1st International Conference on Fast Sea Transportation, Norway, pp.429-444.

Krylov, A. N. (1896)
"A New Theory of Pitching of Ships on Waves and of Stress Produced by This Motion", Transactions of INA, Vol.37, pp.326-368.

Lee, C. M., Jones, H. D. and Bedel, J. W. (1971)
"Added Mass and Damping Coefficients of Heaving Twin Cylinders in a Free Surface", NSRDC Report 3695.

Lee, C. M., Jones, H. D. and Curphey, R. M. (1973)
"Prediction of Motion and Hydrodynamic Loads of Catamarans", Marine Technology, Vol.10, No.4, pp.392-405.

Lewis, F. M. (1929)
"The Inertia of Water Surrounding a Vibrating Ship", Transactions of SNAME, Vol.37, pp.1-20.

Lin, W. M., Newman, J. N. and Yue, D. K. P. (1984)
"Nonlinear Forced Motions of Floating Bodies", Proc. of the 15th Symp. on Naval Hydrodynamics, Hamburg, Germany, pp.33-49.

Lin, W. M. and Yue, D. K. P. (1990)
"Numerical Solutions for Large Amplitude Ship Motions in the Time Domain", Proc. of the 18th Symp. on Naval Hydrodynamics, Ann Arbor, MI, pp.41-66.

Lloyd, A. R. J. M. (1989)
Seakeeping: Ship Behaviour in Rough Weather, Ellis Horwood Limited.

Loeser, D. J., Yue, D. K. P. and Salvesen, N. (1982)
"Slender-Body Calculations of Large-Amplitude Ship Motions", Proc. of the 14th Symp. on Naval Hydrodynamics, Ann Arbor, pp.383-414.

Maskell, S. J. and Ursell, F. (1970)
"The Transient Motion of a Floating Body", Journal of Fluid Mechanics, Vol.44, Part 2, pp.303-313.

Michel, W. H. (1961)
"The Sea-Going Catamaran Ship, Its Features and Its Feasibility", International Shipbuilding Progress, Vol.8, No.85, September, pp.390-401.

Newman, J. N. (1985)
"Transient Axisymmetric Motion of a Floating Cylinder", Journal of Fluid Mechanics, Vol.157, pp.17-33.

Newman, J. N. and Tuck, E. O. (1964)
"Current Progress in the Slender-Body Theory of Ship Motions", Proc. of the 5th Symp. on Naval Hydrodynamics, ACR-112, pp.129-167.

Ogilvie, T. F. (1963)
"First- and Second- Order Forces on a Cylinder Submerged Under a Free Surface", Journal of Fluid Mechanics, 16, pp.451-72.

Ogilvie, T. F. (1964)
"Recent Progress Toward the Understanding and Prediction of Ship Motions", Proc. of the 5th Symp. on Naval Hydrodynamics, Office of Naval Research, Washington DC, pp.3-128.

Ogilvie, T. F. and Tuck, E. O. (1969)
"A Rational Strip Theory for Ship Motions", Part 1, Report No.013, Dept. NAME, University of Michigan.

Ohkusu, M. (1969)
"On the Heaving Motion of Two Circular Cylinders on the Surface of a Fluid", Report of Research Institute for Applied Mechanics, Kyushu University, Vol.17, No.58

Ohkusu, M. and Wen, G. (1995)
"Seakeeping of a High Speed Catamaran in Oblique Seas", Trans. of the West-Japan Society of Naval Architects, No.89, pp.55-66.

Oving, A. J. (1985)
"Semi-Planing Catamarans: Study of Resistance and Resistance Prediction", Report of Martime Techniek TH Delf, August.

Press, W. H., Teukolsky, S. A.,Vetterling, W. T. and Flannery, B. P. (1992)
Numerical Recipies in Fortran, 2nd Edition, Cambridge University Press.

Salvesen, N., Tuck, E. O. and Faltinsen, O. (1970)
"Ship Motions and Sea Loads", Transactions of SNAME, Vol.78, pp.250-287.

Salvesen, N. (1981)
"Five Years of Numerical Naval Ship Hydrodynamics at DTNSRDC", Journal of Ship Research, Vol.25, No.4, pp.219-235.

Salvesen, N. (1982)
"Nonlinear Large Amplitude Low-Frequency Ship-Motions", United States Naval Academy, Division of Engineering and Weapons, Hydrodynamics Laboratory Report EW-10-82.

Sommerfeld, A. (1949)
Partial Differential Equations in Physics, Academic Press Inc.

Stevens, M.J. and Crago, W. A. (1966)
"Comparative Tests in Waves at Three Experimental Establishments Using the Same Model", Proc. of the 11th International Towing Tank Conference, Tokyo, pp.332-342.

Stoker, J. J. (1957)
Water Waves, Interscience publishers, New York.

Takagi, K. (1986)
"Calculations of the Hydrodynamic Forces Acting upon a Ship with Large Amplitude Motions", Journal of Soc. Naval Arch., Japan, Vol.160, pp.131-140.

Tasai, F. and Koterayama, W. (1973)
"On the Non-Linear Hydrodynamic Forces for Heaving Circular Cylinder on a Free Surface", Trans. of the West-Japan Society of Naval Architects, No.46, pp.91-108.

Taylor, R. E. and Hu, C. S. (1991)
"Multipole Expansions for Wave Diffraction and Radiation in Deep Water", Ocean Engineering, Vol.18, No.3, pp.191-224.

Timman, R. and Newman, J. N. (1962)
"The Coupled Damping Coefficients of a Symmetric Ship", Journal of Ship Research, Vol.5, pp.1-7.

Ursell, F. (1949)
"On the Heaving Motion of a Circular Cylinder on the Surface of a Fluid", Quart. Journal of Mech. Appl. Math. Vol.2, pp.218-231.

Ursell, F. (1962)
"Slender Oscillating Ships at Zero Forward Speed", Journal of Fluid Mechanics, Vol.19, pp.496-516.

Vinje, T. & Brevig, P. (1981)
"Nonlinear Ship Motions", Proc. of the 3rd International Conference on Numerical Ship hydrodynamics, Paris, France, pp.257-68.

Vugts, J. H. (1968)
"The Hydrodynamic Coefficients for Swaying, Heaving, and Rolling Cylinders in a Free Surface", International Shipbuilding Progress, Vol.15, No.167, pp.251-276.

Wang, S. and Wahab, R. (1971)
"Heaving Oscillation of Twin Cylinders in a Free Surface", Journal of Ship Research, Vol.15, No.1, pp.33-48.

Wahab, R., Pritchett, C. and Ruth, L. C. (1971)
"On the behaviour of the ASR Catamaran in Waves", Marine Technology, 8, pp.334-360.

Wehausen, J., V. and Laitone, E. V. (1960)
Surface Waves, Handbuch Der Physik, Band IX, Springer-Verlag, Berlin, pp.446-478.

Wehausen, J. V. (1967)
"Initial Value Problem for the Motion in an Undulating Sea of a Body with Fixed Equilibrium Position", Journal of Eng. Maths., 1, pp.1-19.

Wehausen, J. V. (1971)
"The Motion of Floating Bodies", Annual Review of Fluid Mechanics, Vol.3, pp.237-268.

Yeung, R. W. (1982a)
"The Transient Heaving Motion of Floating Cylinders", Journal of Eng. Maths., 16, pp.97-119.

Yeung, R. W. (1982b)
"Numerical Methods in Free-Surface Flows", Annual Review of Fluid Mechanics, Vol.14, pp.395-442.

Yeung, R.W. and Kim, S. H. (1981)
"Radiation Forces on Ships with Forward Speed" Proc. of the 3rd International Conference on Numerical Ship Hydrodynamics, Paris, pp.VII-4-1-4-17.

Yim, B. (1971)
"Investigation of Gravity and Ventilation Effects in Water Entry of Thin Foils", Nonsteady Flows of Water at High Speeds, Proc. of Symposium IUTAM, Leningrad, U.S.S.R..

Zarnick, E. E. (1978)
"A Nonlinear Mathematical Model of Motions of a Planing Boat in Regular Waves",
DTNSRDC 78/032.

APPENDIX

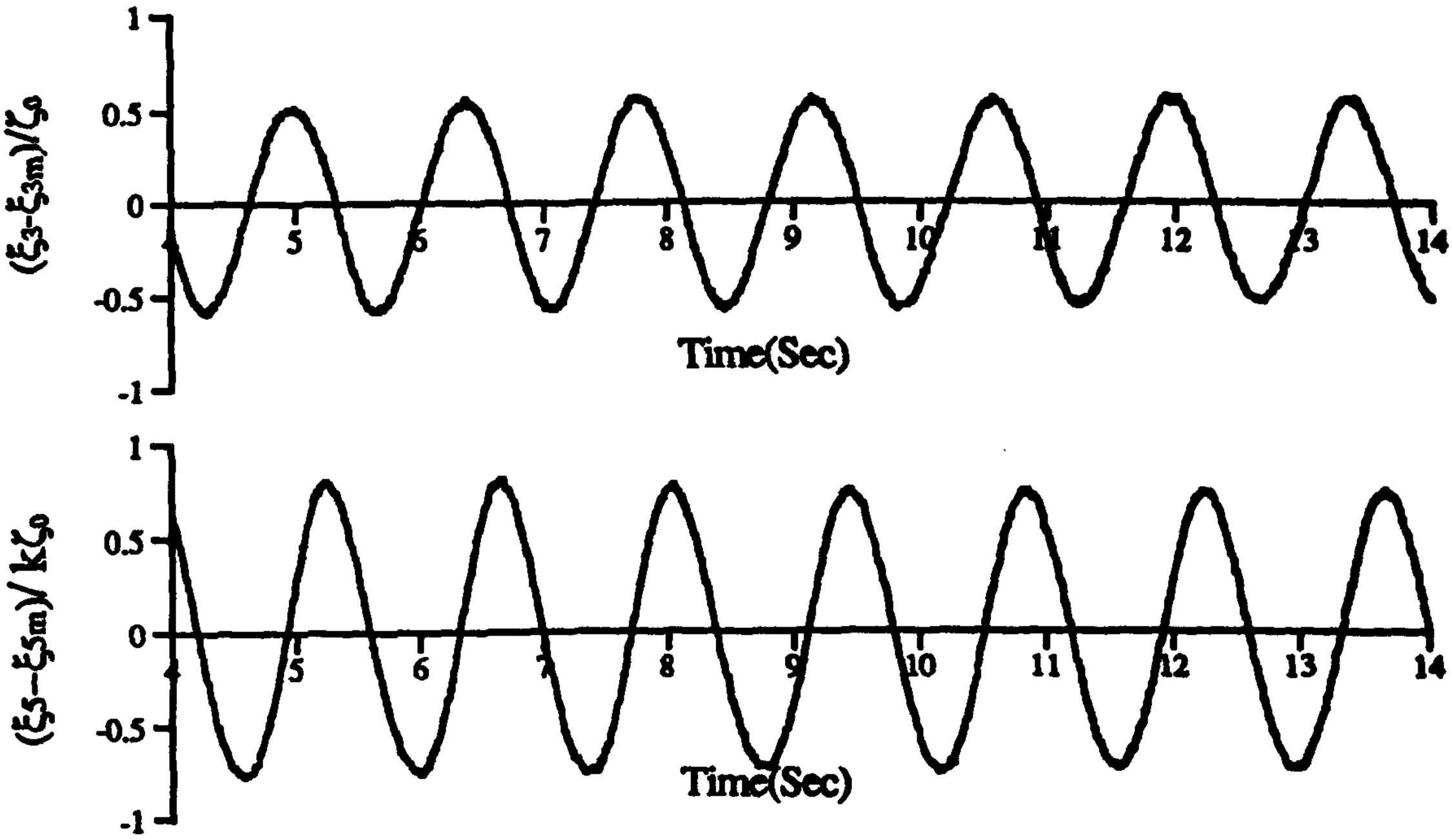

Figure A.1 : Experimental Records for the Heave and Pitch Motions of V-1 Catamaran.(Fn=0.00,ζ_0=1.0cm,ω_0=4.5 rad/sec)

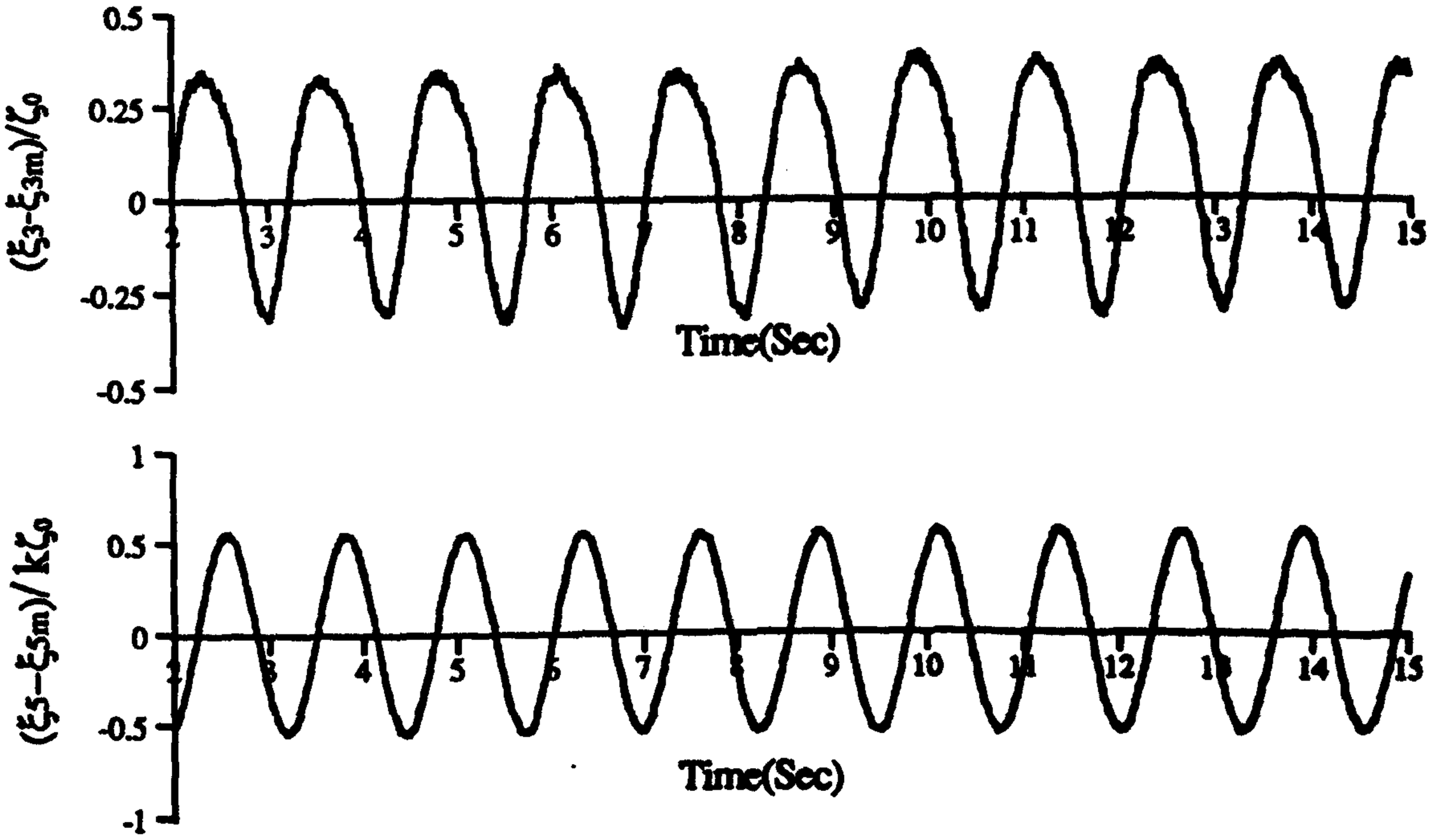

Figure A.2 : Experimental Records for the Heave and Pitch Motions of V-1 Catamaran.(Fn=0.00,ζ_0=1.0cm,ω_0=5.0 rad/sec)

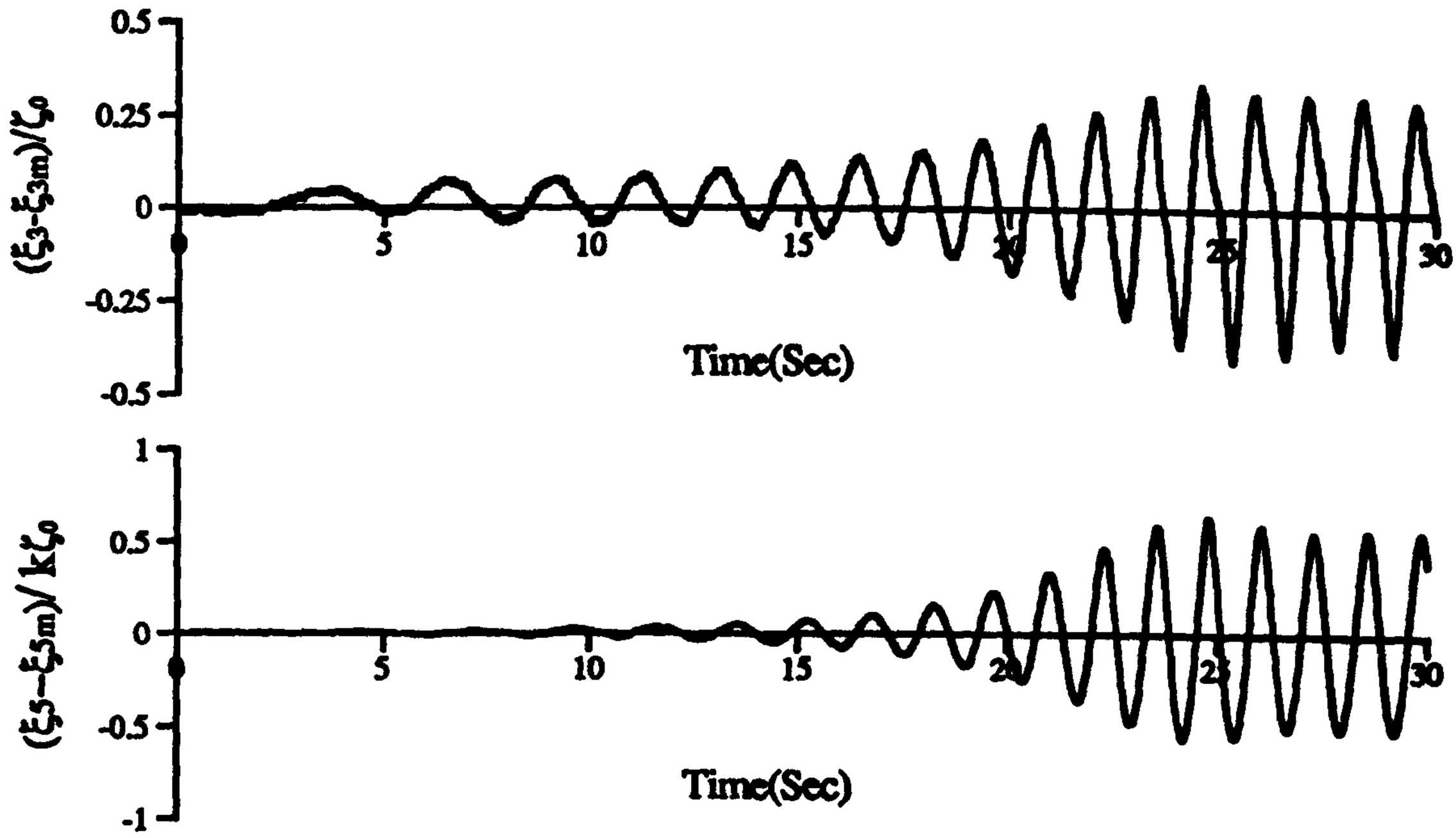

Figure A.3 : Experimental Records for the Heave and Pitch Motions of V-1 Catamaran.(Fn=0.00,ζ_0=3.0cm,ω_0=5.0 rad/sec)

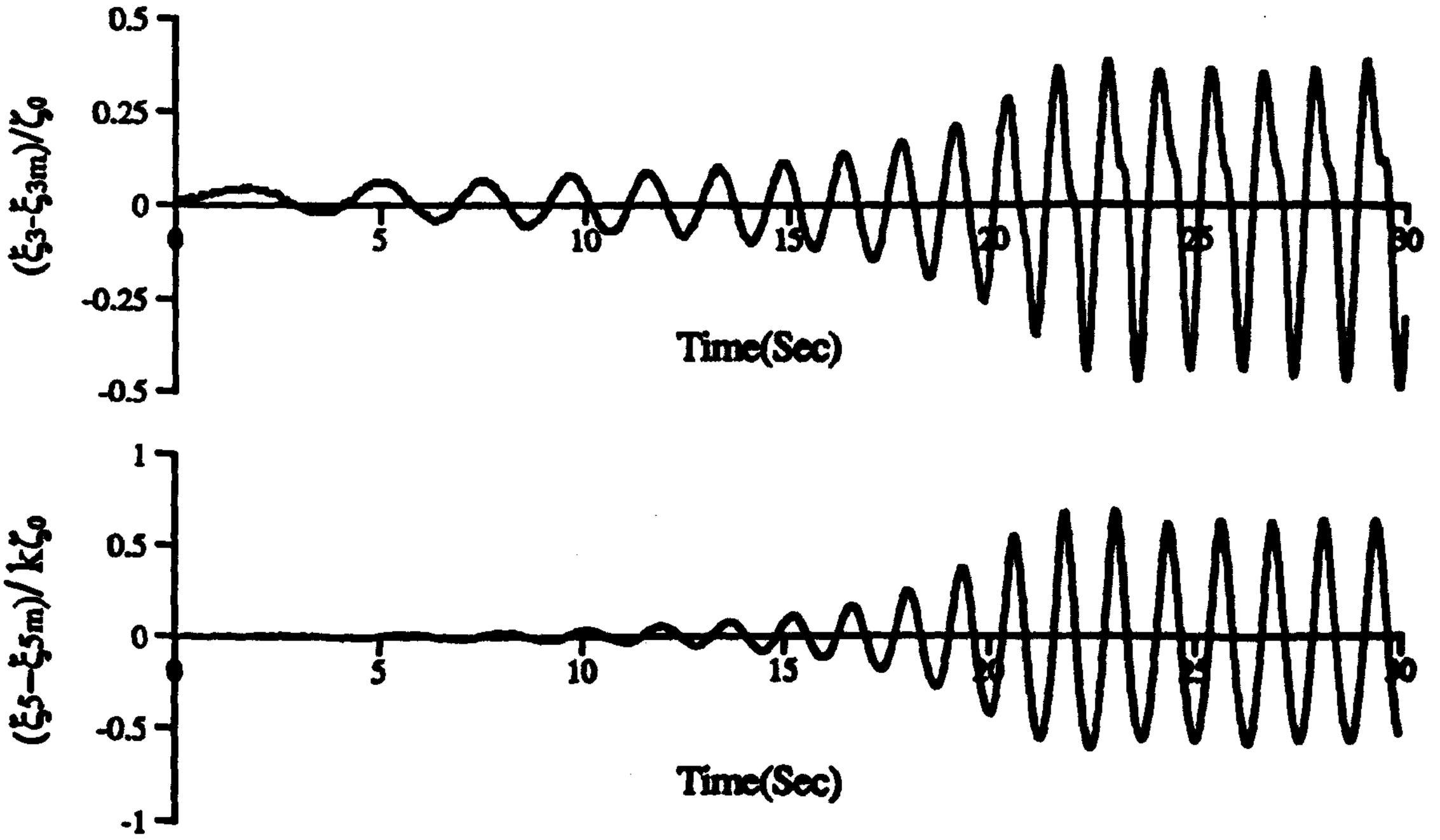

Figure A.4 : Experimental Records for the Heave and Pitch Motions of V-1 Catamaran.(Fn=0.00,ζ_0=4.5cm,ω_0=5.0 rad/sec)

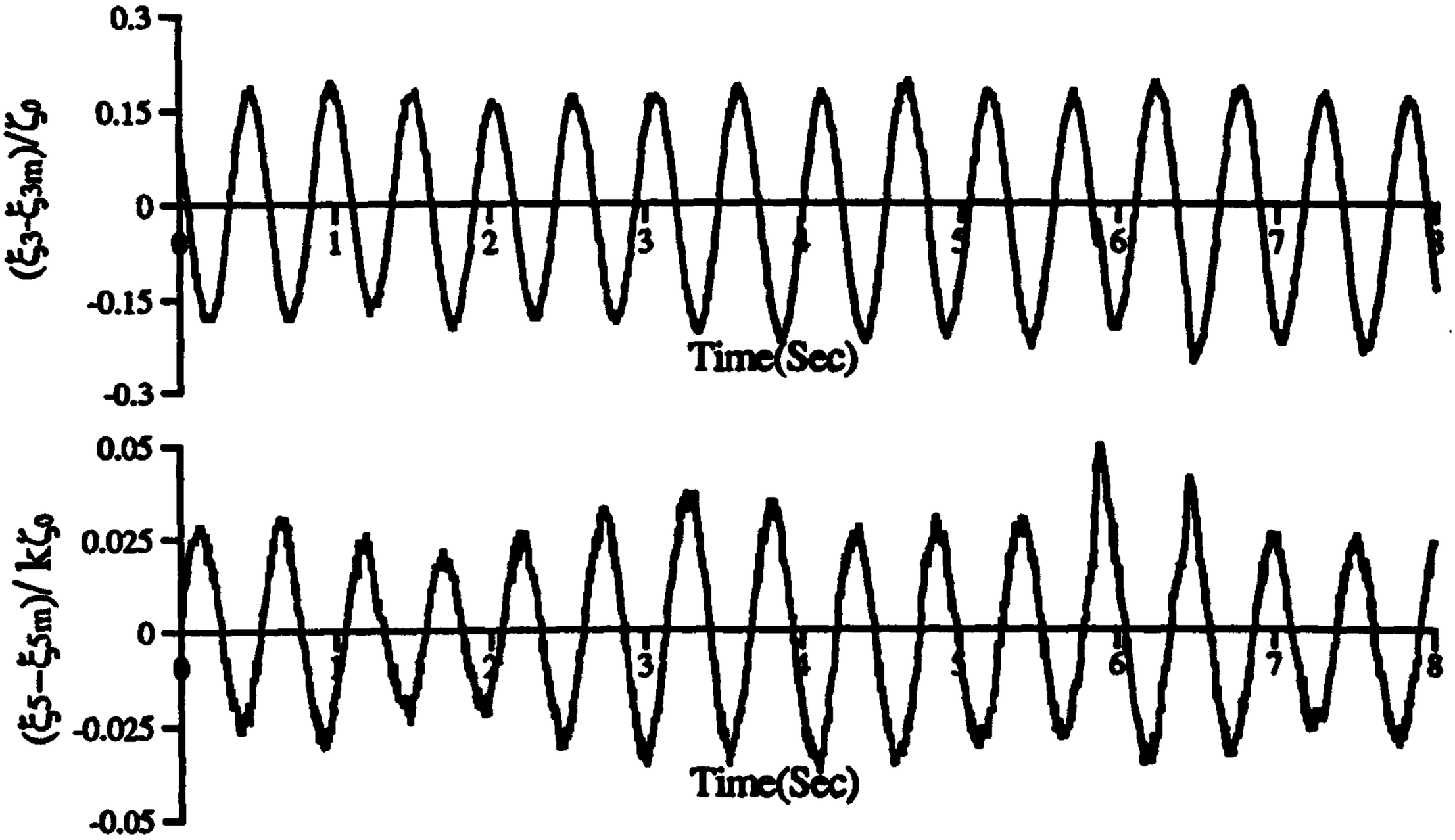

Figure A.5 : Experimental Records for the Heave and Pitch Motions of V-1 Catamaran.(Fn=0.226,ζ_0=1.0cm,ω_0=7.0 rad/sec)

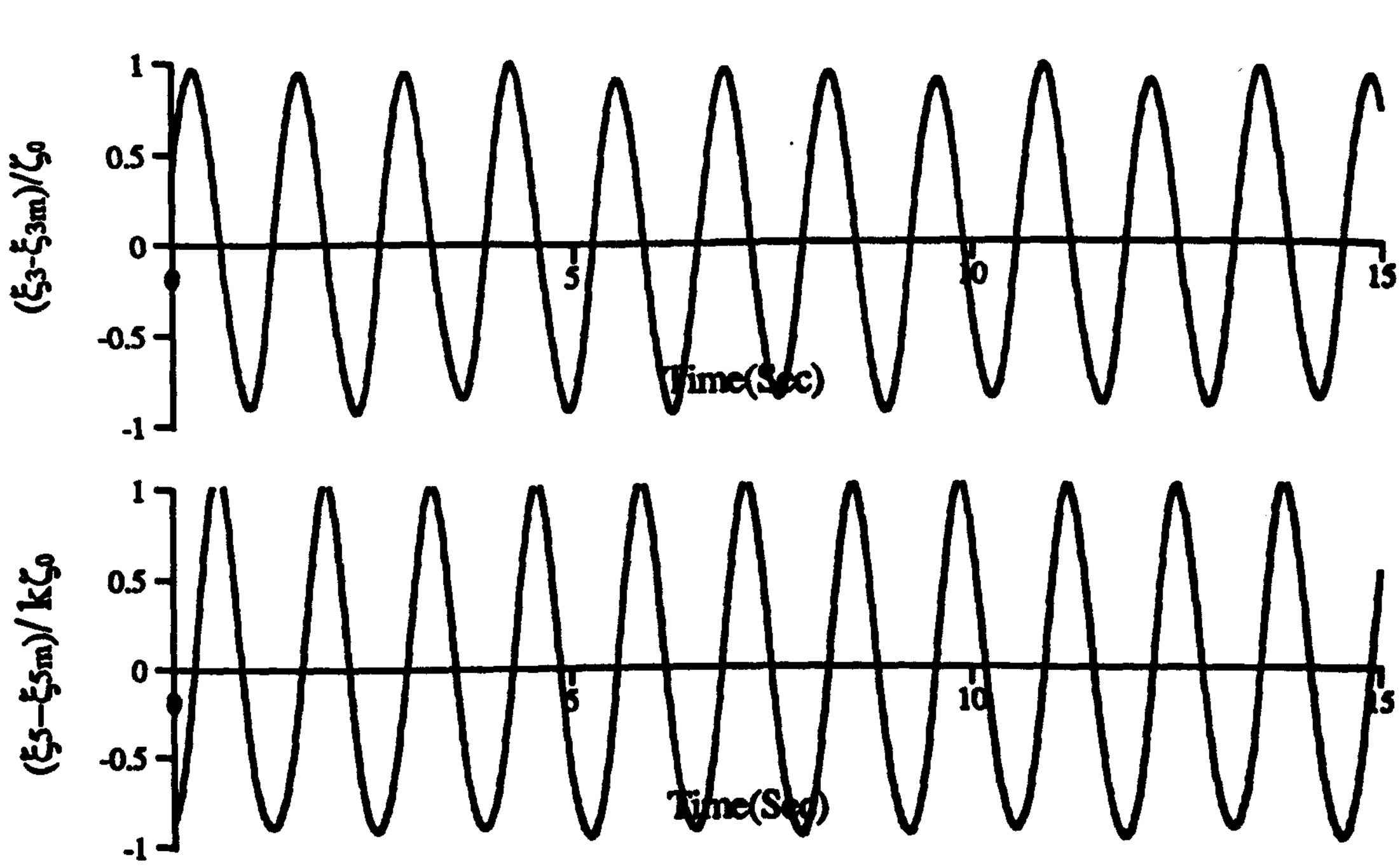

Figure A.6 : Experimental Records for the Heave and Pitch Motions of V-1 Catamaran.(Fn=0.226,ζ_0=4.5cm,ω_0=3.5 rad/sec)

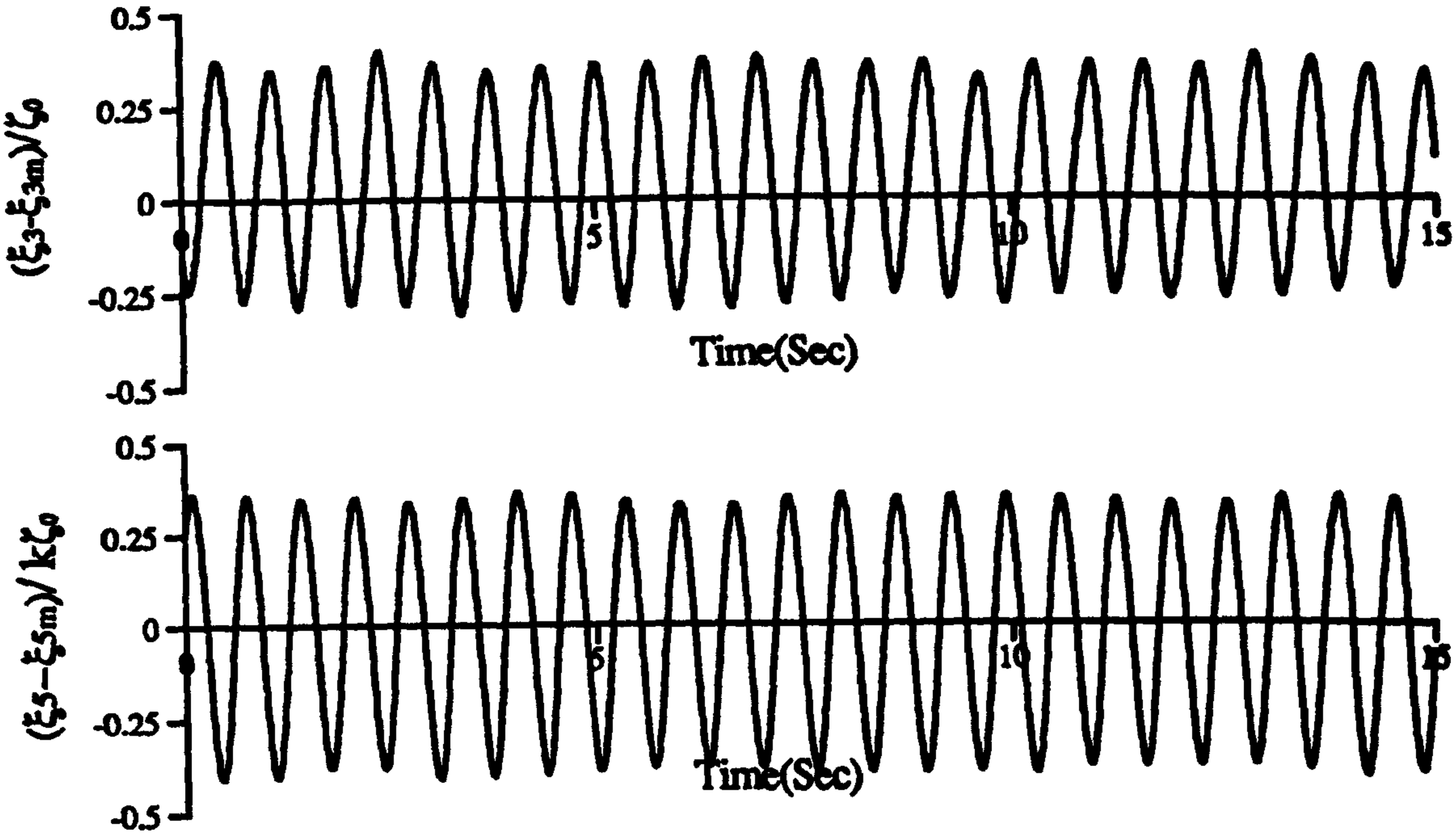

Figure A.7 : Experimental Records for the Heave and Pitch Motions of V-1 Catamaran.(Fn=0.226,ζ_0=4.5cm,ω_0=6.0 rad/sec)

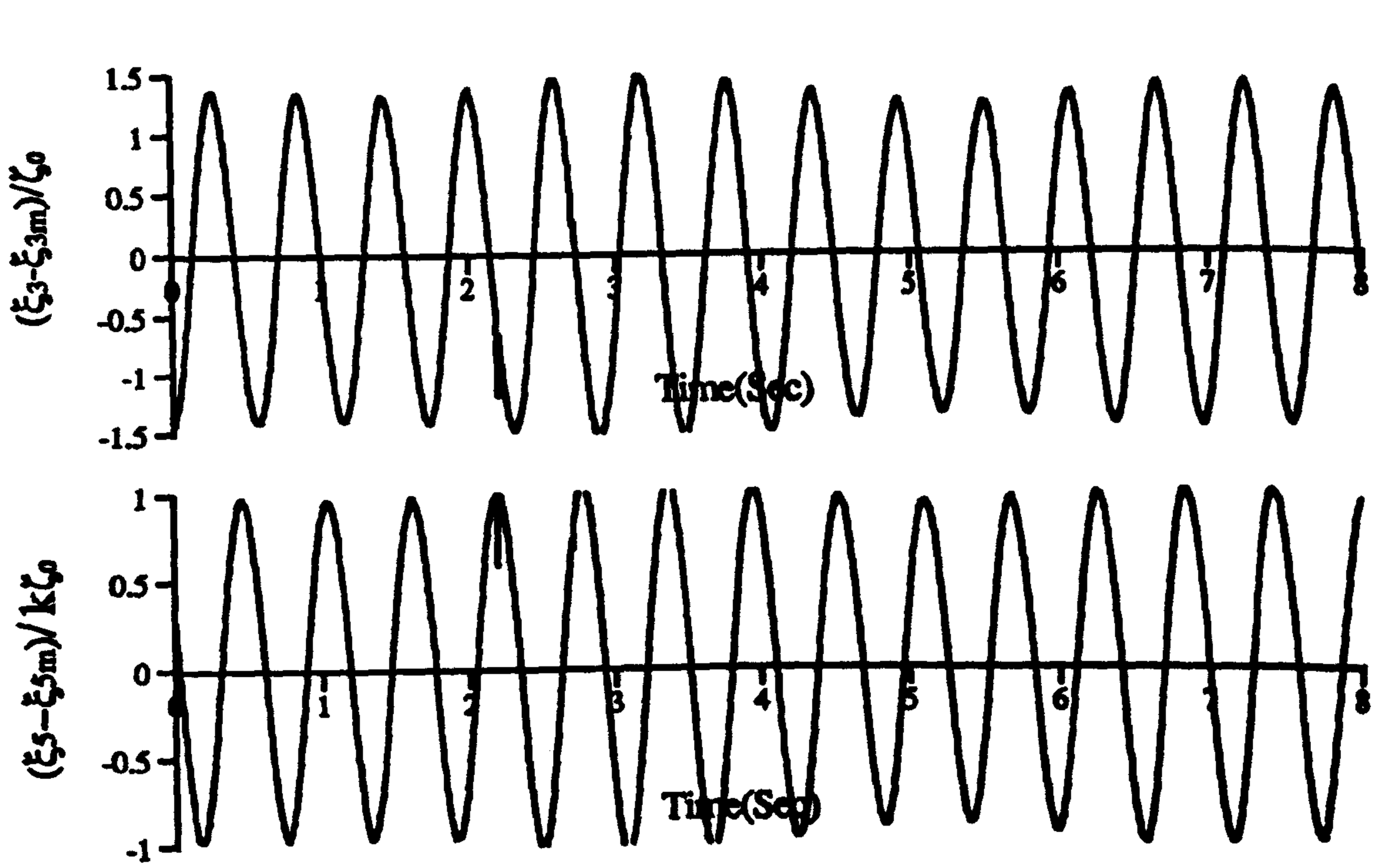

Figure A.8 : Experimental Records for the Heave and Pitch Motions of V-1 Catamaran.(Fn=0.677,ζ_0=1.0cm,ω_0=4.5 rad/sec)

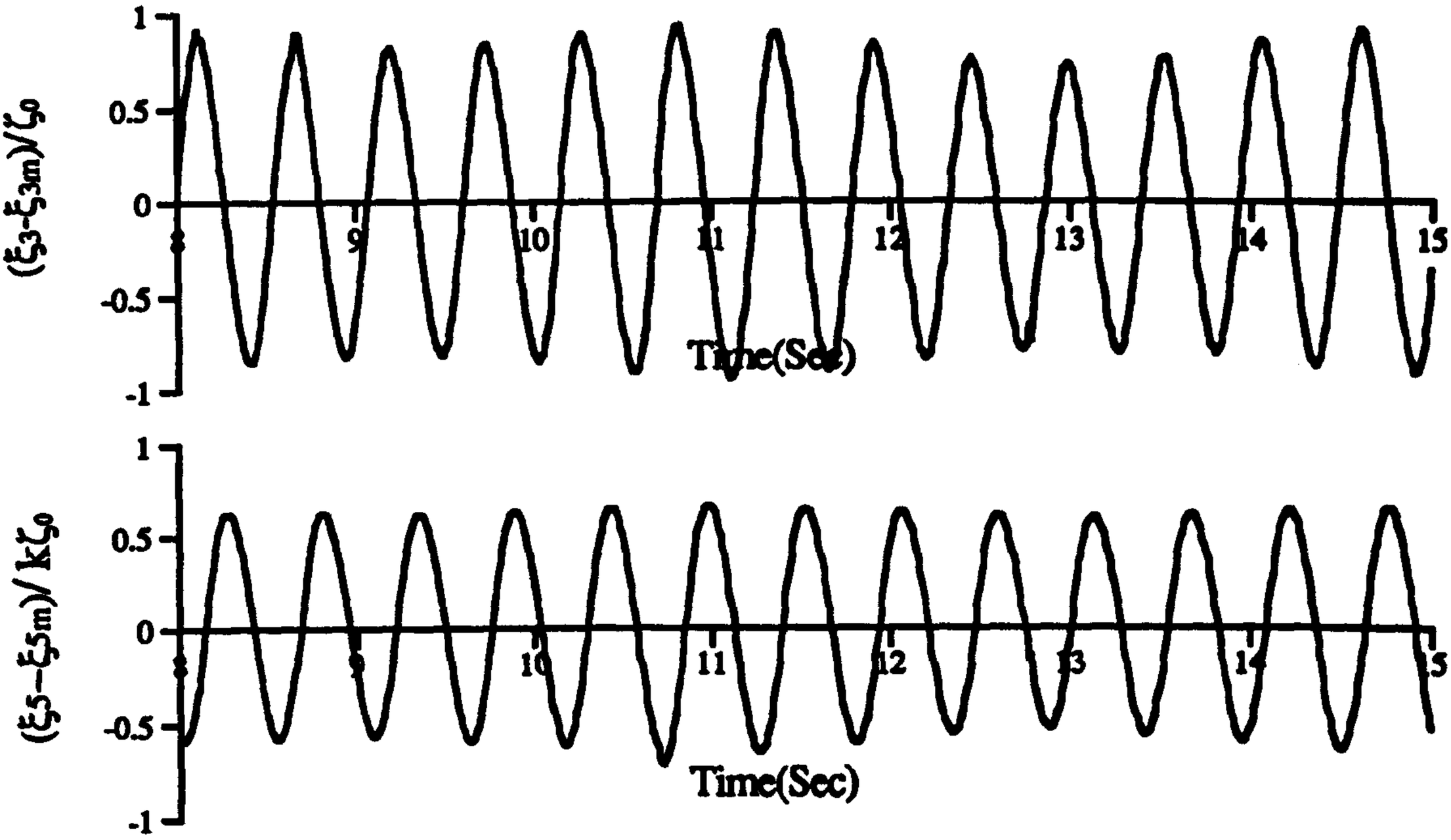

Figure A.9 : Experimental Records for the Heave and Pitch Motions of V-1 Catamaran.(Fn=0.677,ζ_0=3.0cm,ω_0=4.75 rad/sec)

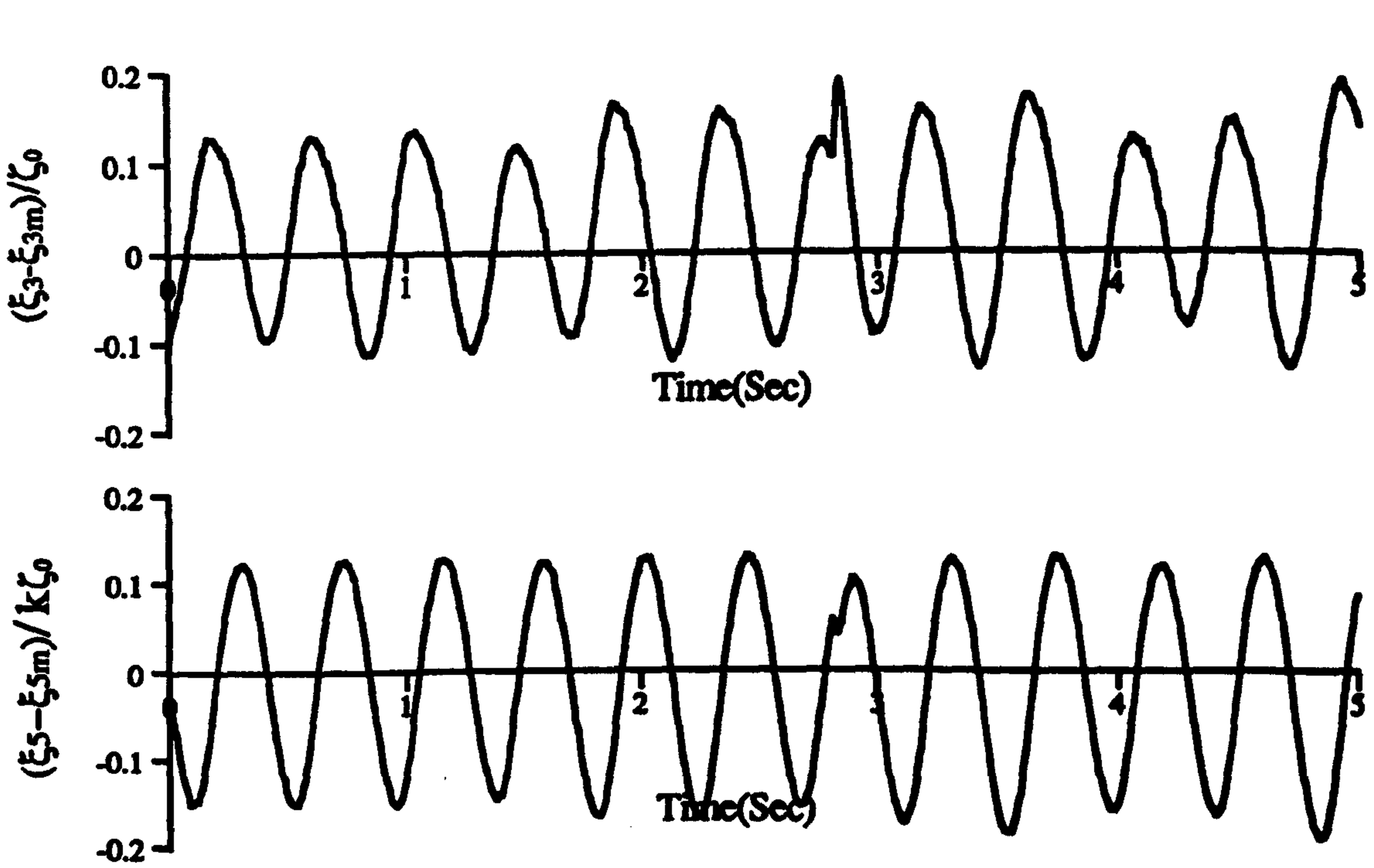

Figure A.10 : Experimental Records for the Heave and Pitch Motions of V-1 Catamaran.(Fn=0.677,ζ_0=4.5cm,ω_0=5.5 rad/sec)